Universidad de Oviedo
Universidá d'Uviéu
University of Oviedo

Programa de Doctorado en Materiales

Mejora del comportamiento en servicio de fundiciones blancas altamente aleadas mediante la optimización microestructural y el análisis de diferentes tratamientos térmicos.

TESIS DOCTORAL

Alejandro González Pociño

Junio 2021

Universidad de Oviedo

Universidá d'Uviéu

University of Oviedo

Programa de Doctorado en Materiales

Mejora del comportamiento en servicio de fundiciones blancas altamente aleadas mediante la optimización microestructural y el análisis de diferentes tratamientos térmicos.

TESIS DOCTORAL

Director de tesis

Dr. D. José Florentino Álvarez Antolín

Universidad de Oviedo
Universidá d'Uviéu
University of Oviedo

RESUMEN DEL CONTENIDO DE TESIS DOCTORAL

1.- Título de la Tesis	
Español: Mejora del comportamiento en servicio de fundiciones blancas altamente aleadas mediante la optimización microestructural y el análisis de diferentes tratamientos térmicos.	Inglés: Improvement of the in-service behavior of High Chromium White Cast Irons through microstructural optimization and the analysis of different heat treatments

2.- Autor	
Nombre: Alejandro González Pociño	DNI:
Programa de Doctorado: Materiales	
Órgano responsable: Comisión Académica Programa de Doctorado en Materiales	

RESUMEN (en español)

Las fundiciones blancas altamente aleadas en cromo son ampliamente utilizadas en minería, en operaciones de trituración y molienda, industrias cementeras, maquinaria de obra civil, etc. En estas aleaciones se busca un excelente comportamiento al desgaste erosivo y al desgaste abrasivo, además, se requiere de cierta tenacidad para resistir el impacto de bolas de molino, rocas o minerales, siendo este un objetivo secundario, el cual no puede bajo ningún concepto mermar la resistencia al desgaste requerida. Se estudian dos calidades de estas aleaciones, una con 18% en cromo y otra con 25% en este mismo elemento. La metodología utilizada para estudiar la influencia de estos factores se basa en el Diseño de Experimentos. Con esta técnica se estudian factores relacionados con tratamientos térmicos y termoquímicos, a distintos niveles, siendo éstos los valores que pueden tomar dichos factores. Lo que se obtiene con esta técnica son los factores que tienen un efecto significativo sobre la función respuesta del material, como es por ejemplo la dureza, la resistencia al desgaste, la tenacidad, etc. Una vez obtenidos los factores que influyen significativamente en las propiedades del material, se analiza la correlación que existe con la microestructura, haciendo una amplia discusión acerca de la optimización microestructural de este tipo de aleaciones para mejorar su comportamiento en servicio.

RESUMEN (en Inglés)

White cast irons, highly alloyed in chromium, are widely used in mining, in crushing and grinding operations, cement industries, civil engineering machinery, etc. In these alloys, an excellent behavior to erosive wear and abrasive wear is sought, in addition, a certain tenacity is required to resist the impact of mill balls, rocks or minerals, this being a secondary objective, which cannot under any circumstances diminish the required wear resistance. Two qualities of these alloys are studied, one with 18% in chromium and the other with 25% in this same element. The methodology used to study the influence of these factors is based on the Design of Experiments. With this technique, factors related to thermal and thermochemical treatments are studied, at different levels, these being the values that these factors can take. What is obtained with this technique are the factors that have a significant effect on the response function of the material, such as hardness, wear resistance, toughness, etc. Once the factors that significantly influence the properties of the material have been obtained, the correlation that exists with the microstructure is analyzed, making a broad discussion about the microstructural optimization of this type of alloys to improve their performance in service.

SR. PRESIDENTE DE LA COMISIÓN ACADÉMICA DEL PROGRAMA DE DOCTORADO EN MATERIALES

Universidad de Oviedo
Universidá d'Uviéu
University of Oviedo

FORMULARIO RESUMEN DE TESIS POR COMPENDIO

1.- Datos personales solicitante	
Apellidos: González Pociño	Nombre: Alejandro

Curso de inicio de los estudios de doctorado	16/17

	SI	NO
Acompaña acreditación por el Director de la Tesis de la aportación significativa del doctorando	X	
Acompaña memoria que incluye		
Introducción justificativa de la unidad temática y objetivos	X	
Copia completa de los trabajos *	X	
Resultados/discusión y conclusiones	X	
Informe con el factor de impacto de las publicaciones	X	
Se acompaña aceptación de todos y cada uno de los coautores a presentar el trabajo como tesis por compendio	X	
Se acompaña renuncia de todos y cada uno de los coautores a presentar el trabajo como parte de otra tesis de compendio	X	

* Ha de constar el nombre y adscripción del autor y de todos los coautores asi como la referencia completa de la revista o editorial en la que los trabajos hayan sido publicados o aceptados en cuyo caso se aportará justificante de la aceptación por parte de la revista o editorial

FOR-MAT-VOA-033

Artículos, Capítulos, Trabajos

Trabajo, Artículo 1

Titulo (o título abreviado)	Erosive wear resistance regarding different destabilization heat treatments of austenite in high chromium white cast iron, alloyed with Mo.
Fecha de publicación	07-Mayo-2019
Fecha de aceptación	05-Mayo-2019
Inclusión en Science Citation Index o bases relacionadas por la CNEAI (indíquese)	METALLURGY & METALLURGICAL ENGINEERING
Factor de impacto	2.244 (Q1)

Coautor2 x Doctor □ No doctor . Indique nombre y apellidos	Florentino Álvarez Antolín
Coautor3 x Doctor □ No doctor . Indique nombre y apellidos	Juan Asensio Lozano

Universidad de Oviedo
Universidá d'Uviéu
University of Oviedo

Trabajo, Artículo 2

Titulo (o título abreviado)	Influence of thermal parameters related to destabilization treatments on erosive wear resistance and microstructural variation of white cast iron containing 18% Cr. application of design of experiments and Rietveld structural analysis.
Fecha de publicación	05-Octubre-2019
Fecha de aceptación	04-Octubre-2019
Inclusión en Science Citation Index o bases relacionadas por la CNEAI (indíquese)	MATERIALS SCIENCE, MULTIDISCIPLINARY
Factor de impacto	3.424 (Q2)

Coautor2 x Doctor □ No doctor . Indique nombre y apellidos	Florentino Álvarez Antolín
Coautor3 x Doctor □ No doctor . Indique nombre y apellidos	Juan Asensio Lozano

Trabajo, Artículo 3

Titulo (o título abreviado)	Optimization, by means of a design of experiments, of heat processes to increase the erosive wear resistance of white hypoeutectic cast irons alloyed with Cr and Mo.
Fecha de publicación	02-Abril-2019
Fecha de aceptación	29-Marzo-2019
Inclusión en Science Citation Index o bases relacionadas por la CNEAI (indíquese)	METALLURGY & METALLURGICAL ENGINEERING
Factor de impacto	2.244 (Q1)

Coautor2 x Doctor □ No doctor . Indique nombre y apellidos	Florentino Álvarez Antolín
Coautor3 x Doctor □ No doctor . Indique nombre y apellidos	Juan Asensio Lozano

Trabajo, Artículo 4

Titulo (o título abreviado)	Optimization of thermal processes applied to hypoeutectic white cast iron containing 25% Cr aimed at increasing erosive wear resistance.
Fecha de publicación	09-Marzo-2020
Fecha de aceptación	06-Marzo-2020
Inclusión en Science Citation Index o bases relacionadas por la CNEAI (indíquese)	METALLURGY & METALLURGICAL ENGINEERING
Factor de impacto	2.244 (Q1)

Coautor2 x Doctor □ No doctor . Indique nombre y apellidos	Florentino Álvarez Antolín
Coautor3 x Doctor □ No doctor . Indique nombre y apellidos	Juan Asensio Lozano

Universidad de Oviedo
Universidá d'Uviéu
University of Oviedo

Trabajo, Artículo 5

Titulo (o título abreviado)	Influence of thermal processing factors, linked to the destabilisation of austenite, on the microstructural variation of a white cast iron containing 25% Cr and 0.6% Mo.
Fecha de publicación	23-Junio-2020
Fecha de aceptación	21-Junio-2020
Inclusión en Science Citation Index o bases relacionadas por la CNEAI (indíquese)	METALLURGY & METALLURGICAL ENGINEERING
Factor de impacto	2.244 (Q1)

Coautor2 x Doctor □ No doctor . Indique nombre y apellidos	Florentino Álvarez Antolín
Coautor3 x Doctor □ No doctor . Indique nombre y apellidos	Juan Asensio Lozano
Coautor4 x Doctor □ No doctor . Indique nombre y apellidos	Hugo Álvarez Pérez

Trabajo, Artículo 6

Titulo (o título abreviado)	The joint effects of nitriding and parameters related to the destabilisation of austenite on wear resistance in white cast iron with 25% Cr.
Fecha de publicación	04-Enero-2021
Fecha de aceptación	30-Diciembre-2020
Inclusión en Science Citation Index o bases relacionadas por la CNEAI (indíquese)	METALLURGY & METALLURGICAL ENGINEERING
Factor de impacto	2.244 (Q1)

Coautor2 x Doctor □ No doctor . Indique nombre y apellidos	Florentino Álvarez Antolín
Coautor3 x Doctor □ No doctor . Indique nombre y apellidos	Juan Asensio Lozano

Trabajo, Artículo 7

Titulo (o título abreviado)	Improvement of impact toughness and abrasion resistance of a 3C-25Cr-0.5Mo alloy using a design of experiment statistical technique: microstructural correlations after heat treatments.
Fecha de publicación	06-Abril-2021
Fecha de aceptación	02-Abril-2021
Inclusión en Science Citation Index o bases relacionadas por la CNEAI (indíquese)	METALLURGY & METALLURGICAL ENGINEERING
Factor de impacto	2.244 (Q1)

Coautor2 x Doctor □ No doctor . Indique nombre y apellidos	Florentino Álvarez Antolín
Coautor3 x Doctor □ No doctor . Indique nombre y apellidos	Juan Asensio Lozano
Coautor4 x Doctor □ No doctor . Indique nombre y apellidos	Ana García Diez

Universidad de Oviedo
Universidá d'Uviéu
University of Oviedo

Trabajo, Artículo 8

Titulo (o título abreviado)	Evaluation of Hardness, Sliding Wear and Strength of a Hypoeutectic White Iron with 25%Cr after Heat Treatments
Fecha de publicación	
Fecha de aceptación	07-Junio-2021
Inclusión en Science Citation Index o bases relacionadas por la CNEAI (indíquese)	METALLURGY & METALLURGICAL ENGINEERING
Factor de impacto	2.244 (Q1)

Coautor2 x Doctor □ No doctor . Indique nombre y apellidos	Juan Asensio Lozano
Coautor3 x Doctor □ No doctor . Indique nombre y apellidos	Florentino Álvarez Antolín
Coautor4 x Doctor □ No doctor . Indique nombre y apellidos	Ana García Diez

En caso de compendio de un número de artículos superior a seis, se incorporarán hojas suplementarias conforme a este modelo

Agradecimientos

A José Florentino Álvarez Antolín y a Juan Asensio Lozano, por su dedicación para explicarme y ayudarme en todas las ocasiones en las que les he requerido para la realización de esta Tesis Doctoral y por enseñarme que con esfuerzo y sacrificio todo es posible. También les quiero agradecer, en lo personal, su comprensión y su hombro en momentos complicados durante la realización de este trabajo.

A todos los compañeros que han colaborado de una forma u otra con el desarrollo de esta investigación.

A mi familia, pareja y amigos por estar a mi lado y apoyarme en todo momento,

Gracias.

Dedicado a mi tío Javi, que aunque no haya podido disfrutar conmigo de este momento, siempre estará en mi memoria.

INDICE

RESUMEN

Las fundiciones blancas altamente aleadas en cromo son ampliamente utilizadas en minería, en operaciones de trituración y molienda, industrias cementeras, maquinaria de obra civil, etc. En estas aleaciones se busca un excelente comportamiento al desgaste erosivo y al desgaste abrasivo, además, se requiere de cierta tenacidad para resistir el impacto de bolas de molino, rocas o minerales, siendo este un objetivo secundario, el cual no puede bajo ningún concepto mermar la resistencia al desgaste requerida. Se estudian dos calidades de estas aleaciones, una con 18% en cromo y otra con 25% en este mismo elemento. La metodología utilizada para estudiar la influencia de estos factores se basa en el Diseño de Experimentos.

Con esta técnica se estudian factores relacionados con tratamientos térmicos y termoquímicos, a distintos niveles, siendo éstos los valores que pueden tomar dichos factores. Lo que se obtiene con esta técnica son los factores que tienen un efecto significativo sobre la función respuesta del material, como es por ejemplo la dureza, la resistencia al desgaste, la tenacidad, etc. Una vez obtenidos los factores que influyen significativamente en las propiedades del material, se analiza la correlación que existe con la microestructura, haciendo una amplia discusión acerca de la optimización microestructural de este tipo de aleaciones para mejorar su comportamiento en servicio.

1. INTRODUCCIÓN

1.1- Principales usos. Comportamiento al desgaste.

Las fundiciones blancas altamente aleadas en Cromo son ampliamente utilizadas debido al alto rango de propiedades mecánicas que pueden ser obtenidas tras la realización de diferentes tratamientos térmicos, modificando su microestructura. Para muchos usuarios, las fundiciones férreas de alto Cr tienen elevada tenacidad respecto a otras fundiciones blancas, además de un excelente comportamiento al desgaste abrasivo y erosivo. Sin embargo, obtener la microestructura adecuada para tales propiedades no es una tarea sencilla y esto explica por qué se han dedicado y se siguen dedicando muchas investigaciones para mejorar esta familia particular de fundiciones. Debido a que su uso por excelencia es debido a su comportamiento al desgaste, en este estudio se harán diversos ensayos para analizar dicho comportamiento.

Los procesos de desgaste se pueden clasificar como desgaste abrasivo de dos o tres cuerpos y por su aplicación de bajo o alto esfuerzo. Los desgastes típicos son el de abrasión, erosivo (impacto) y abrasión combinado con corrosión.

La tabla 1 esquematiza los distintos tipos de desgaste señalados anteriormente.

Tabla 1. Clasificación general de ensayos de desgaste

Tipos de Desgaste	Como desgasta	Manifestación
Impacto-Abrasión	Repetición de impactos + abrasión	No existe modelo único
Gouging	Grandes partículas abrasivas, esfuerzo extremo	Surcos profundos, gran deformación
Alto esfuerzo	Esfuerzo suficiente para romper las partículas abrasivas	Altas tasas de desgaste, marcas de rayado visibles
Bajo esfuerzo	Esfuerzo que no rompe las partículas abrasivas	Bajas tasas de desgaste, rayado menos marcado
Corrosión-Abrasión	Corrosión + Abrasión	Varias; marcas de corrosión aceleradas

El desgaste a abrasión es una forma de desgaste que depende en su totalidad de las partículas duras. Por otro lado, esas partículas actúan como concentradores de tensiones que conducen a deformaciones severas con cargas relativamente bajas. En la industria, estos procesos vienen detallados en la Figura 1 [1]. El proceso básico de trituración lo componen la roca y la fundición, y aunque la fundición sale a priori victoriosa, las sucesivas acciones de abrasión, golpes, etc., llevan a cabo un proceso de fatiga del material que finalmente conduce a la fractura.

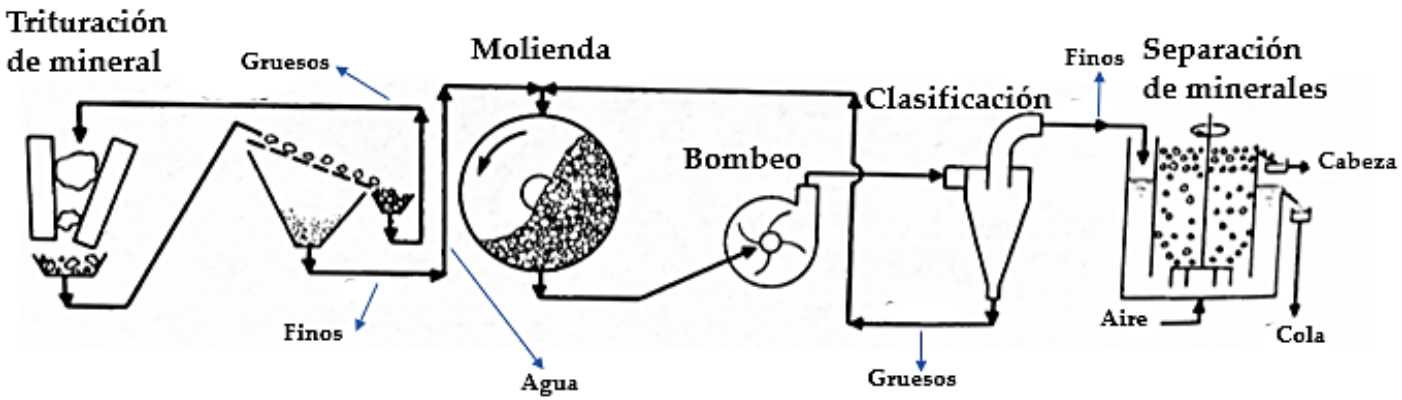

Tipo de desgaste	**1-** Gauging (partículas grandes actúan como abrasivo) **2-** Bajo esfuerzo	**1-** Bajo esfuerzo **2-** Gouging **3-** Abrasión-corrosión. a) Gruesos b) Finos	**1-** Alto esfuerzo **2-** Gouging **3-** Abrasión-corrosión.	**1-** Bajo esfuerzo **2-** Abrasión-corrosión.	**1-** Bajo esfuerzo **2-** Abrasión-corrosión.	**1-** Bajo esfuerzo **2-** Abrasión-corrosión.
Material recomendado	Acero al Mn, *Fundición Blanca martensítica.*	Acero al Mn, *Fundición Blanca martensítica*. Acero martensítico, aceros inoxidables	Acero con bajo Mn, *Fundición Blanca martensítica*, Acero perlítico, Acero martensítico.	*Fundición Blanca martensítica*	*Fundición Blanca martensítica*, cerámicos	*Fundición Blanca martensítica*, cerámicos.

Figura 1. Diagrama de flujo típico en industria de procesamiento y molienda de minerales, cementeras, etc., y con distintos tipos de desgaste

Como se puede apreciar, las fundiciones blancas altamente aleadas con matriz martensítica son muy utilizadas en este tipo de industria en ambientes agresivos, donde sea prioritario una elevada resistencia al desgaste erosivo y abrasivo [2], siendo este un requisito prioritario por ejemplo, en las industrias mineras destinadas al procesamiento de minerales [3,4], cementeras y centrales térmicas, o en el bombeo de los lodos generados en estas industrias [4-6].

Son varios los ensayos de laboratorio existentes para evaluar distintos comportamientos frente al desgaste de este tipo de materiales. En la Figura 2 [1] se muestran los más comunes.

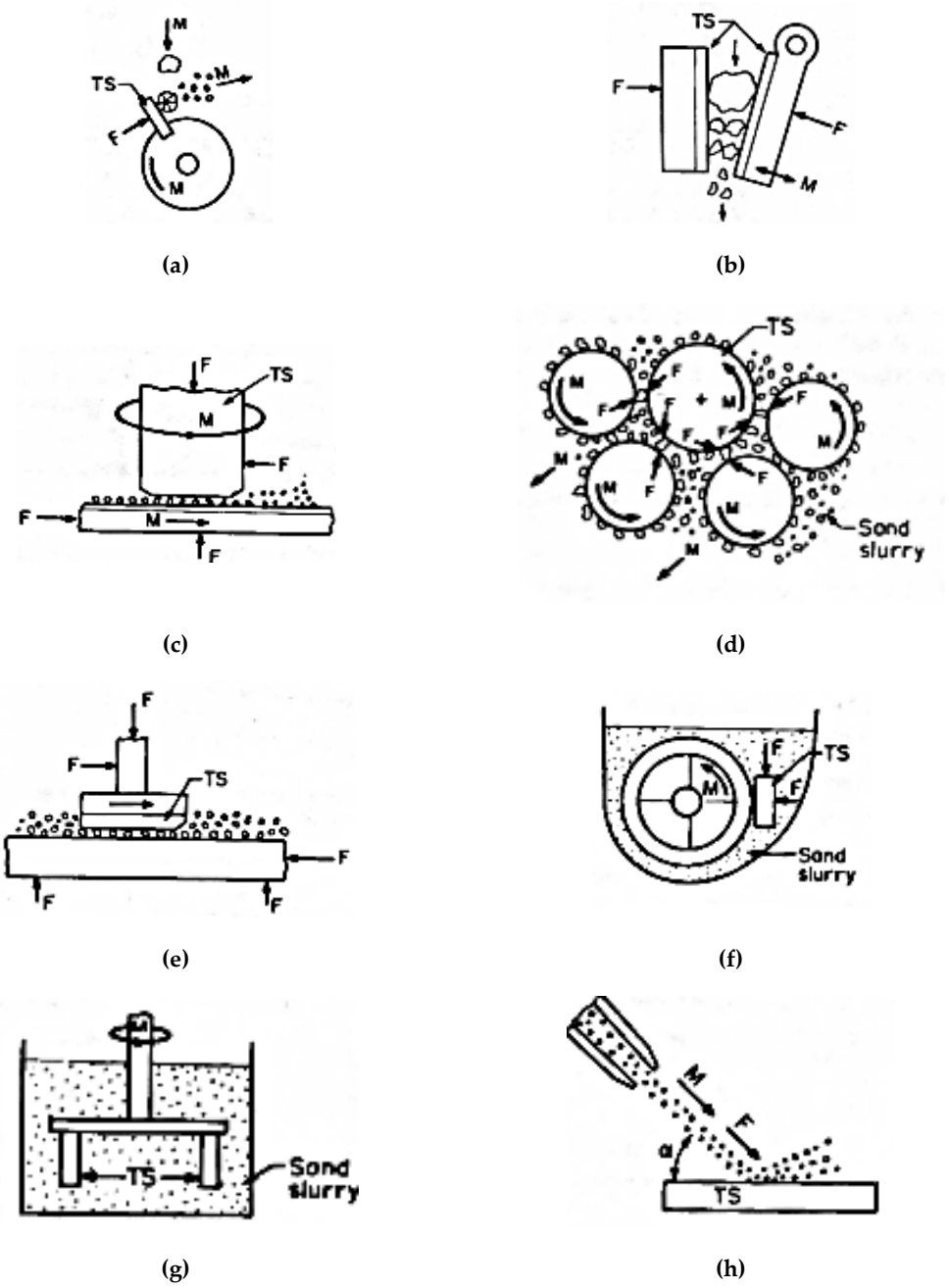

Figura 2. Ensayos de laboratorio más habituales para determinar la resistencia al desgaste erosivo y abrasivo de un material. **(a)** Pulverizador de impacto; **(b)** trituradora de compresión; **(c)** pin on disk; **(d)** molino de bolas; **(e)** ensayo de vaivén; **(f)** desgaste de rueda; **(g)** desgaste por agitación; **(h)** desgaste por chorro de arena.

Los ensayos más utilizados, junto con sus respectivas variantes para caracterizar materiales en cuanto a la resistencia al desgaste abrasivo son los que se detallan en la Figura 3 [7].

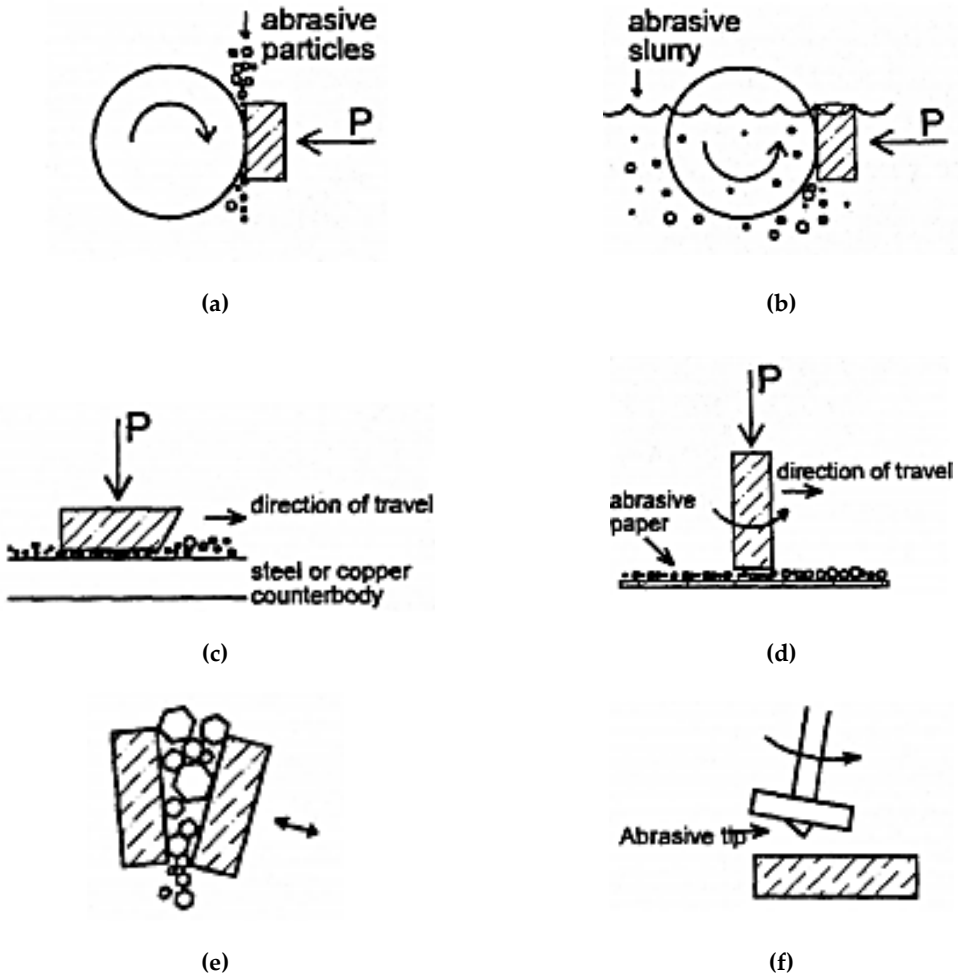

Figura 3. **Bajo esfuerzo:** **(a)** desgaste de rueda seca; **(b)** desgaste de rueda húmeda; **Alto esfuerzo:** **(c)** ensayo de vaivén; **(d)** pin on disk; **Gauging:** **(e)** trituradora de mandíbulas; **(f)** desgaste de rueda; **(g)** péndulo con punta abrasiva.

1.2- Efectos del Cromo en las aleaciones férreas

Para entrar en detalle en este tipo de fundiciones férreas, resulta imprescindible comprender los efectos que tiene sobre la fundición el elemento aleante de mayor peso, que es en este caso el Cr. Su efecto sobre las temperaturas críticas de transformaciones alotrópicas del Fe, en este caso sobre los puntos de transformación de Fe(δ) en Fe(ɤ), temperatura crítica A_4, y de Fe(ɤ) en Fe(α), temperatura crítica A_3 es muy relevante. El Cr amplía la estabilidad de la fase Fe(δ), haciendo que durante el enfriamiento su transformación en fase Fe(ɤ) pueda aparecer a menores temperaturas cuanto mayor sea el porcentaje en Cr. En la transformación de fase Fe(δ) a fase Fe(ɤ), el Cr es siempre alfágeno. Por otra parte, para la transformación de la fase Fe(ɤ) en fase Fe(α), los contenidos en Cr menores del 7% hacen de este elemento un elemento gammágeno, mientras que para contenidos mayores al 7% es siempre alfágeno.

También afecta a la templabilidad de la austenita, haciéndola más reacia a su transformación en un enfriamiento continuo, además de deprimir la temperatura de inicio de transformación martensítica (Ms), lo que da lugar a la presencia de cierta cantidad de austenita no transformada o retenida a temperatura ambiente.

1.2.1- Diagrama de equilibrio Cr-C.

Los carburos que según el diagrama de equilibrio Cr-C pueden aparecer serían los siguientes tres tipos: Cr_7C_3, $Cr_{23}C_6$ y Cr_3C_2. Los dos primeros son los que más aparecen en las fundiciones sometidas a estudio, siendo más habitual si cabe, el primero.

En el diagrama Cr-C (Figura 4), se puede observar la existencia de tres reacciones peritécticas.

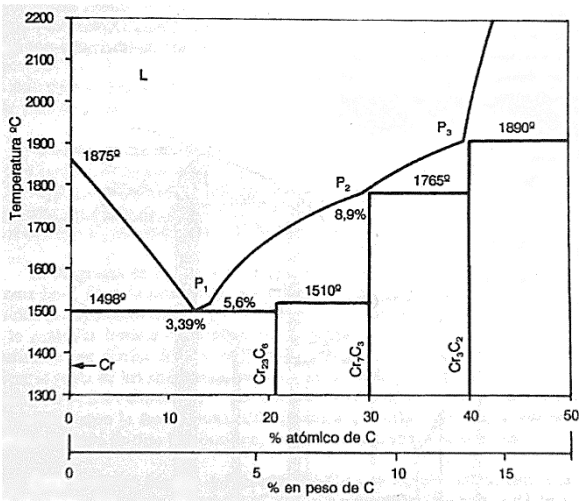

Figura 4. Diagrama Cr-C

La más sencilla de ver en el diagrama es la peritéctica que se produce a la temperatura de 1510°C, en la que se forma el carburo $Cr_{23}C_6$ a partir de la corrosión del carburo Cr_7C_3 por parte del líquido de 5,6%C. En este diagrama se observa también una reacción eutéctica a 1498°C donde el líquido de 3,39%C da lugar al carburo $Cr_{23}C_6$ y a una solución sólida de C en Cr.

Si se observa ahora el diagrama Fe-Cr de la Figura 5, cualquiera que sea el porcentaje de Cr en el Fe da lugar a una solidificación del líquido en la solución sólida α. También se observa el carácter gammágeno del Cr hasta contenidos del 7%, viendo como disminuye la temperatura de transformación de γ en α, siendo alfágeno como se ha mencionado anteriormente para contenidos superiores a este porcentaje.

1.2.2- Diagrama de equilibrio Fe-Cr.

El diagrama de la Figura 5 muestra la influencia del Cr en las transformaciones de fase que experimentan las variedades alotrópicas del Fe.

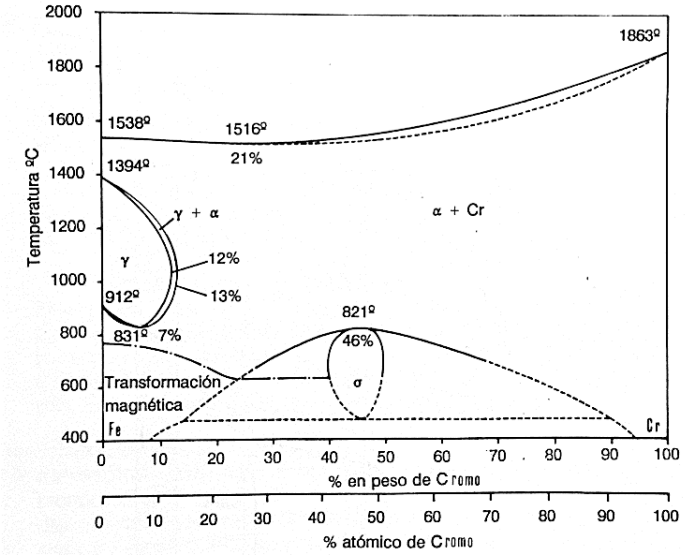

Figura 5. Diagrama Fe-Cr

El Fe presenta, como se sabe tres variedades alotrópicas (δ, ɤ y α). El Fe(δ) solidifica a 1538°C, siendo su celda elemental cúbica centrada en el cuerpo. La siguiente transformación es la del Fe(δ) en Fe(ɤ) (denominada habitualmente austenita), cuya celda elemental es cúbica centrada en las caras y ocurre a 1394°C. La última transformación de austenita a Fe(α) ocurre a 912°C, siendo su celda elemental cúbica centrada en el cuerpo, pero con un menor parámetro de celda que la variedad alotrópica de Fe(δ).

El Cr amplía la estabilidad del Fe(δ), ocurriendo la transformación de esta variedad alotrópica en Fe(ɤ) a una temperatura menor cuanto mayor sea el contenido en Cr. En este caso el Cr es siempre alfágeno.

Como se ha mencionado anteriormente, para la siguiente transformación, que se corresponde con la de Fe(ɤ) a Fe(α), el Cr se comporta como gammágeno para contenidos menores al 7%, pues se observa cómo disminuye de forma más rápida la línea de temperatura A_3 de lo que lo hace la línea de temperatura A_4 -temperatura de transformación de Fe(δ) a Fe(ɤ)-.

Se pueden observar también en el diagrama tres zonas dentro del bucle gamma o austenítico. La primera zona es la que tiene porcentajes en Cr menores del 12%, los cuales podrían ser plenamente austenizados. La segunda es la que está comprendida entre el 12% y el 13% de Cr. En esta zona la aleación no puede ser completamente austenizada, sino que tendrá una estructura mixta α + ɤ. La tercera y última zona sería la que tiene más de un 13% en Cr. En esta zona del diagrama, los ferrocromos mantienen la estructura primaria de solidificación Fe(δ) a temperatura ambiente.

En la parte inferior del diagrama, se puede observar un bucle de fase σ que puede aparecer con contenidos de aproximadamente 45%Cr, como un compuesto intermetálico tetragonal que precipita en las juntas de grano de la fase δ a la que confiere mucha fragilidad dada la complejidad de su distribución atómica, la cual involucra un gran número de enlaces metálicos fuertemente direccionales, causando la marcada rigidez de la celda cristalina y, de esta forma, su nula capacidad de deformación. Este intermetálico solo aparece tras miles de horas a 550°C, pues sus curvas de transformación están muy alejadas del origen de tiempos, por lo que no tiene mucho

interés práctico. Además, en el caso de aparecer, pueden ser redisueltas en poco tiempo mediante calentamientos a temperaturas superiores a 900°C.

1.2.3- Diagrama ternario Fe-C-Cr.

Después de los efectos del Cr, el carácter gammágeno del C y su posibilidad para formar carburos se pueden ver una serie de consecuencias. En este diagrama, los límites del bucle Fe(ɤ) (12%) y los del bucle Fe(δ + ɤ) (13%) vistos en el diagrama binario Fe-Cr, se desplazan hacia mayores contenidos en Cr a medida que aumenta el porcentaje en C. Al incrementarse el porcentaje en C, se produce también un ensanchamiento del bucle Fe(δ + ɤ), siendo máximo para contenidos de 0,6%C aproximadamente, como se puede visualizar en la Figura 6.

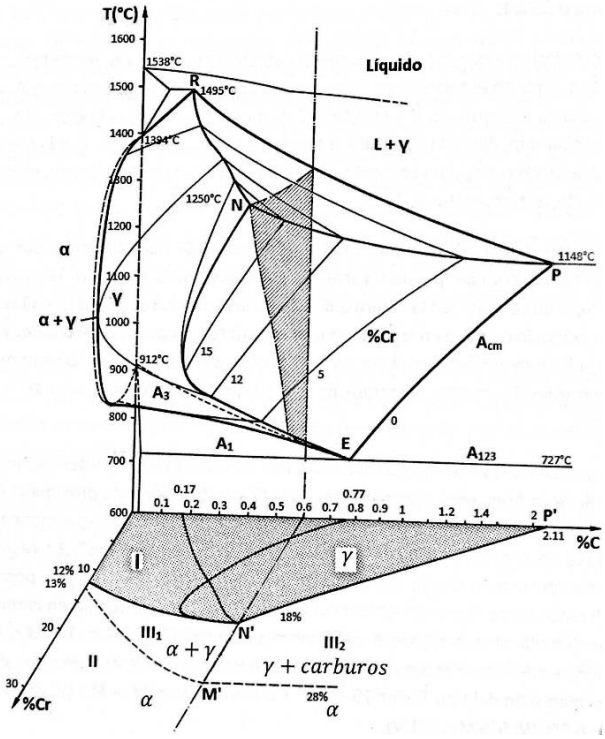

Figura 6. Modificación del bucle de la austenita con los porcentajes de C y Cr.

El bucle gamma en este punto presenta su máximo vertical para contenidos de 18%Cr, es decir, es el límite donde estas aleaciones pueden ser austenizadas completamente durante el calentamiento. De la misma manera, el bucle (α + ɤ) presenta su máximo vertical en el 28%Cr. A partir de ahí, la aleación es completamente ferrítica sea cual sea el porcentaje en C.

Cuando la cantidad de C supera el 0,6%, este elemento influye de tres maneras significativas:

1. La primera es la influencia sobre los límites de saturación de C en la austenita. De esta manera, si el Fe(ɤ) contiene átomos de Cr en solución sólida de sustitución, además de los propios de C en solución sólida de inserción octaédrica (o con menos probabilidad tetraédrica), el contenido máximo de C (punto P) que soporta la austenita decrece al aumentar el contenido en Cr. Además de desplazarse dicho punto hacia contenidos menores en C, también lo hace hacia temperaturas mayores con el aumento del contenido en Cr, ya que el Cr cristaliza en un sistema distinto al Fe(ɤ) y lo distorsiona. Esta distorsión dificulta la solución sólida de C en la austenita y

requiere de mayor temperatura para poder hacerlo, pues es la manera que tiene la red de la austenita para dilatarse.

2. La segunda es la influencia sobre la precipitación de carburos proeutectoides (curva A_{cm}) de tipo cementítico Kc, ya que estos $C(Fe,Cr)_3$, son más estables que la Fe_3C y por tanto, precipitarán a partir de la austenita a temperaturas más altas.

3. La tercera es la influencia sobre la composición y temperaturas de la transformación eutectoide, estando localizadas a medida que aumenta el porcentaje en Cr (hasta el 15%), cada vez a composiciones más bajas en C y a mayor temperatura, como puede verse en el diagrama de la Figura 7. Como el punto eutectoide es el punto de unión entre la línea A_3 y la A_{cm}, es normal que cada vez esté a temperaturas más altas por la segunda influencia ya comentada, sumada al carácter alfágeno del Cr cuando supera el 7%. El campo Fe(ɤ) queda reducido a un punto, para 18%Cr y 0,6%C.

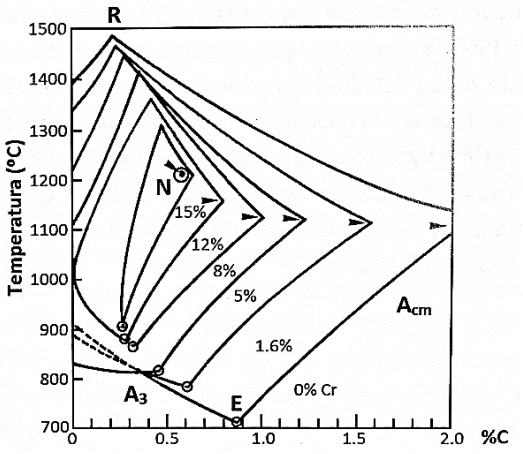

Figura 7. Campo de Fe(ɤ) según porcentajes de C y Cr.

El solape del diagrama de la Figura 4 con el diagrama de la Figura 5, compone el diagrama Fe-C-Cr de la Figura 8, que es el que permite estudiar con profundidad las reacciones que ocurren en las fundiciones que se estudian. En este diagrama se van a explicar las reacciones eutécticas, peritécticas e invariantes (peritécticas ternarias de segunda clase) que existen para temperaturas y composiciones dadas. Como es sabido, por tratarse de tres elementos en el mismo diagrama, las eutécticas binarias tendrán un grado de libertad, por lo que no ocurrirán de manera instantánea y a la misma temperatura. En cuanto a las reacciones invariantes, aparecen tres a medida que disminuye la temperatura:

- A 1415°C, aparece representada bajo el punto G, con un contenido en Cr de aproximadamente el 60% la reacción peritéctica siguiente:

$$Liq + M_{23}C_6 \rightarrow \alpha + M_7C_3$$

- A 1275°C, aparece representada bajo el punto H, con un contenido en Cr de aproximadamente el 35% la reacción peritéctica siguiente:

$Liq + M_7C_3 \rightarrow \gamma + M_7C_3$

- A 1160°C, aparece representada bajo el punto K, con un contenido en Cr de aproximadamente el 15% la reacción peritéctica siguiente:

$Liq + M_7C_3 \rightarrow \gamma + M_3C$

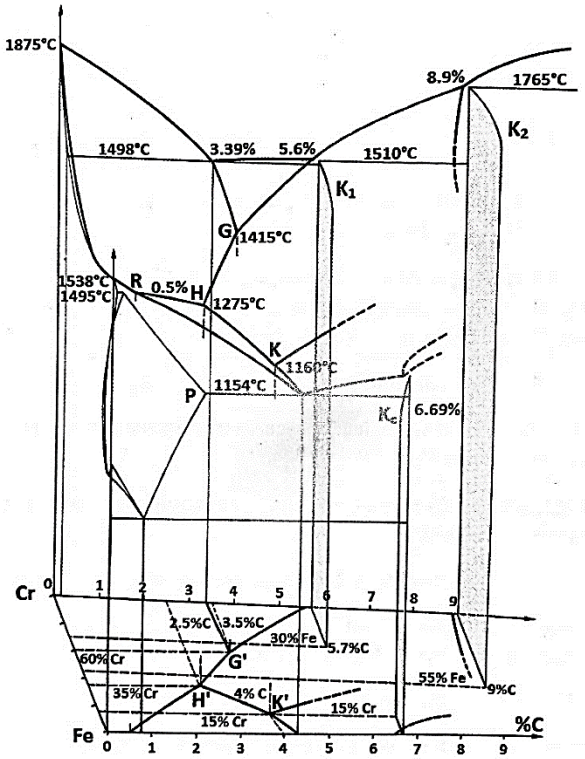

Figura 8. Diagrama ternario Fe-C-Cr

Por otro lado, la reacción peritéctica binarias para tener en cuenta, es la de formación del carburo $M_{23}C_6$, que ocurre a 1510°C.

$Liq_{(5,6\%C)} + Cr_7C_3 \rightarrow Cr_{23}C_6$

Liq + $\alpha \rightarrow \gamma$; correspondiente al segmento RH en el diagrama ternario.

Finalmente, se expondrán las reacciones eutécticas binarias que tienen lugar:

- Para porcentajes en Cr comprendidos entre el 35% y el 60% aparece la eutéctica GH:

$Liq \rightarrow \alpha + M_7C_3$ (carburos denominados K_2).

- Para porcentajes comprendidos entre el 15% y el 35% de Cr, aparece la eutéctica HK:

$Liq \rightarrow \gamma + M_7C_3$ *ó* K_2

- Por último, la eutéctica que comprende los contenidos menores del 15% Cr sería la unión de K con lo que sería la eutéctica en el diagrama Fe-C metaestable: $Liq \rightarrow \gamma + M_3C$

(denominados Kc, carburos mixtos de tipo cementítico en la que parte de los átomos de Fe pueden estar sustituidos por átomos de Cr).

Cabe resaltar en cuanto a propiedades anti desgaste, que los carburos que se forman a partir de la eutéctica HK en las fundiciones con 18% y 25%Cr son de muy alta dureza, como se detallará en el siguiente apartado.

Si se proyecta en planta las líneas de las peritécticas y eutécticas binarias, juntos con los puntos de las peritécticas ternarias de segunda clase, se obtiene el diagrama de la Figura 9, que es más sencillo a la hora de interpretar la microestructura resultante con los porcentajes de C y de Cr.

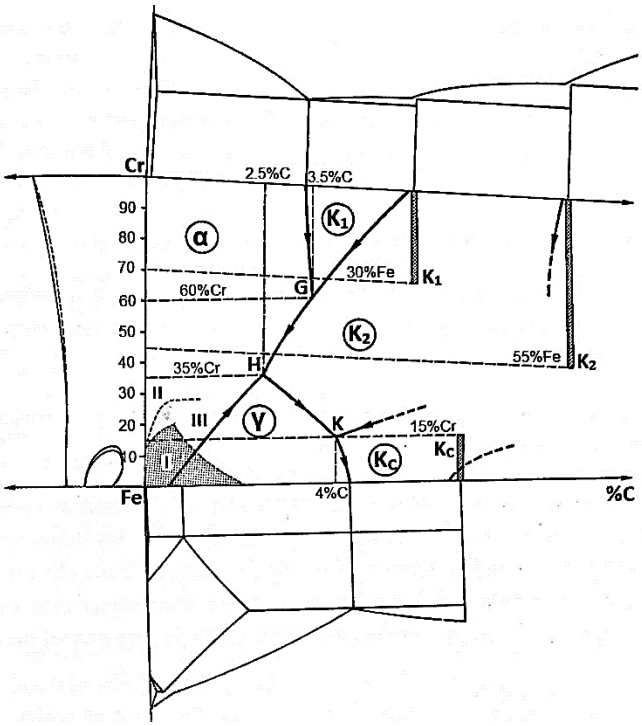

Figura 9. Diagrama ternario en dos dimensiones para facilitar su visualización.

Hay que señalar que no todos estos carburos se forman por cristalización primaria durante la solidificación, sino que pueden aparecer como resultado de precipitación en el estado sólido como ocurre con la cementita terciaria en los aceros de bajo carbono, por ejemplo.

1.3- Microestructura y propiedades mecánicas de los distintos carburos.

1.3.1- Morfología detallada de los distintos carburos.

Carburo mixto M_3C (principalmente asociado al Fe): la morfología básica de este carburo es la misma, ya esté formado durante la solidificación eutéctica (hipoeutécticas y eutécticas) o durante la solidificación primaria (hipereutécticas). La morfología de este carburo mostrada en la Figura 10 [8,9] es a menudo descrita como un compuesto de estructuras delgadas en forma de placas, que pueden parecer compactas o estar plagadas de agujeros. La continuidad de estas delgadas estructuras en forma de placa es una de las principales alteraciones microestructurales en el tipo M_3C. Cuando estos carburos precipitan en estado sólido, lo suele hacer en su forma más común junto con ferrita, como es el caso de la perlita.

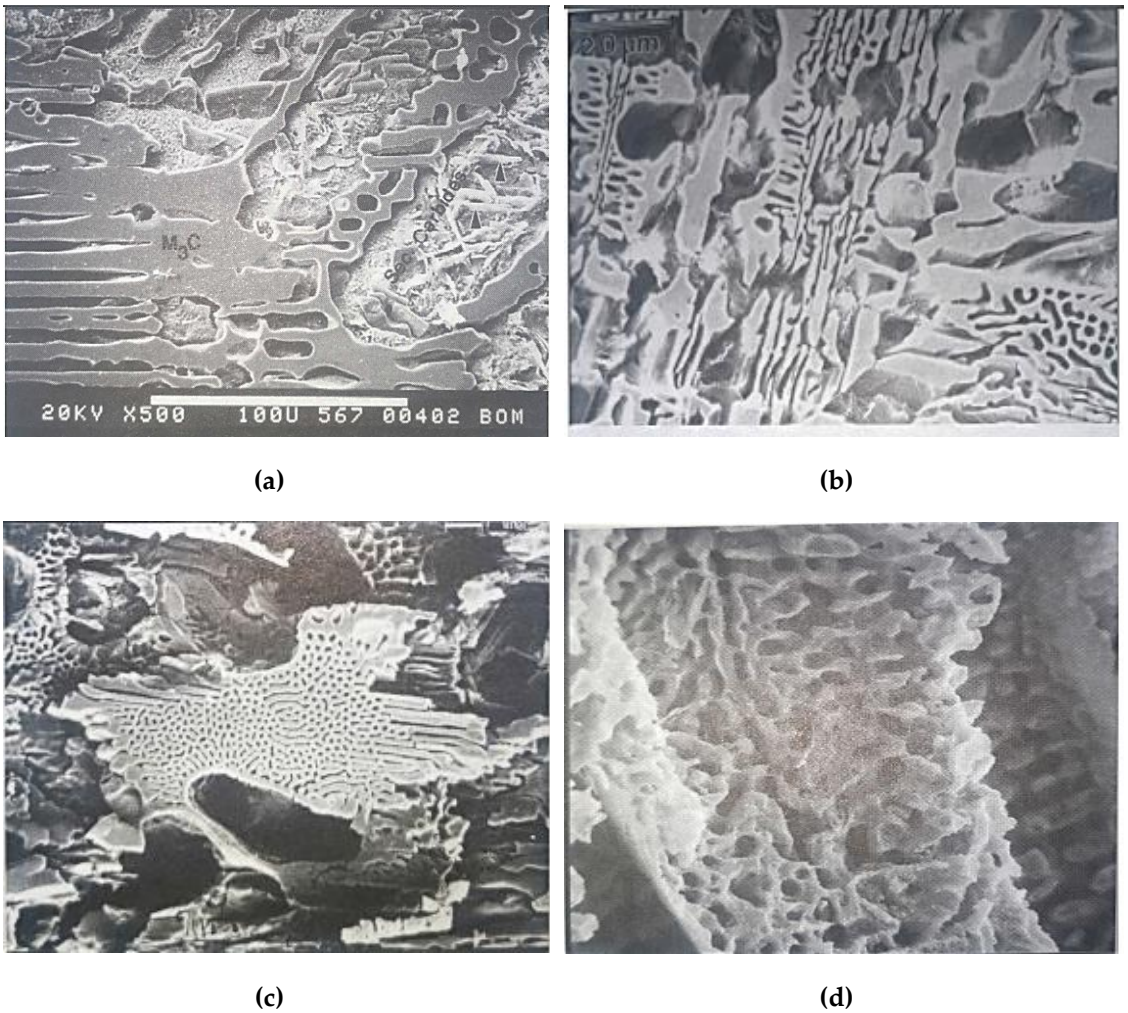

(a) **(b)**

(c) **(d)**

Figura 10.- Distintas morfologías del carburo M_3C en fundiciones altamente aleadas en Cr; (**a**) hipoeutéctica; (**b**)eutéctica; (**c**) hipereutéctica; (**d**) Agujeros característicos de este tipo de carburo.

Carburo M_7C_3: la morfología de este carburo mostrada en la Figura 11 [8,10] es totalmente diferente al carburo anterior. Esta diferencia tan abrupta es en gran medida, lo que separa a las fundiciones perlíticas y Nihard-1 y 2 de las fundiciones de alto Cr. Este carburo consta de estructuras en forma de varilla o cuchilla caracterizadas por una dirección de crecimiento dominante a lo largo del eje de estas. El crecimiento de estas estructuras en forma de varillas y cuchillas se limita a la "celda eutéctica" para las hipoeutécticas y eutécticas, mientras que en las hipereutécticas estos carburos pueden ser extremadamente finos y largos. Para las hipoeutécticas y eutécticas, la longitud de cualquier varilla o cuchilla está limitada por el tamaño de la colonia eutéctica. En las hipereutécticas, la longitud de una varilla solo está limitada por el crecimiento de éstas, dentro de la masa fundida. En consecuencia, las fundiciones de este tipo hipereutécticas pueden tener "fibras" de carburo individualmente, que son extremadamente largas (incluso en el orden de milímetros).

Si existe un fuerte gradiente térmico cerca de la superficie, los carburos crecen predominantemente perpendiculares a esta superficie. Este efecto es aparente solo a 5 mm de la superficie. Como cabe esperar, más lejos de la superficie, la morfología de crecimiento del carburo se vuelve más aleatoria.

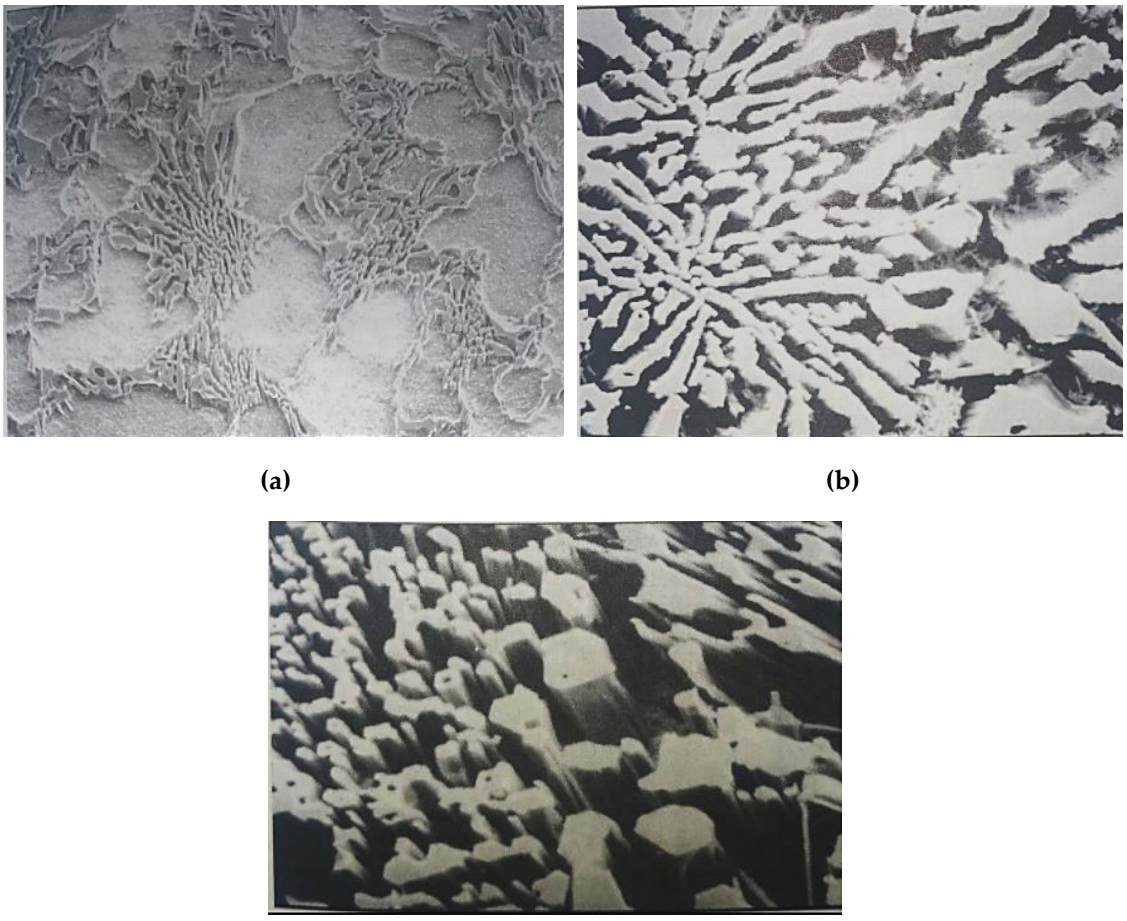

(a) **(b)**

(c)

Figura 11.- Morfologías del carburo M_7C_3 en fundiciones altamente aleadas en Cr; (**a**) hipoeutéctica; (**b**) eutéctica; (**c**) hipereutéctica.

Los carburos secundarios también tendrán la misma morfología característica de los M_7C_3. En este caso, dado que hay poca competencia por solidificar los dendritos, la morfología es mayoritariamente en forma de varilla, como muestra la Figura 12 (c) y (d) [11].

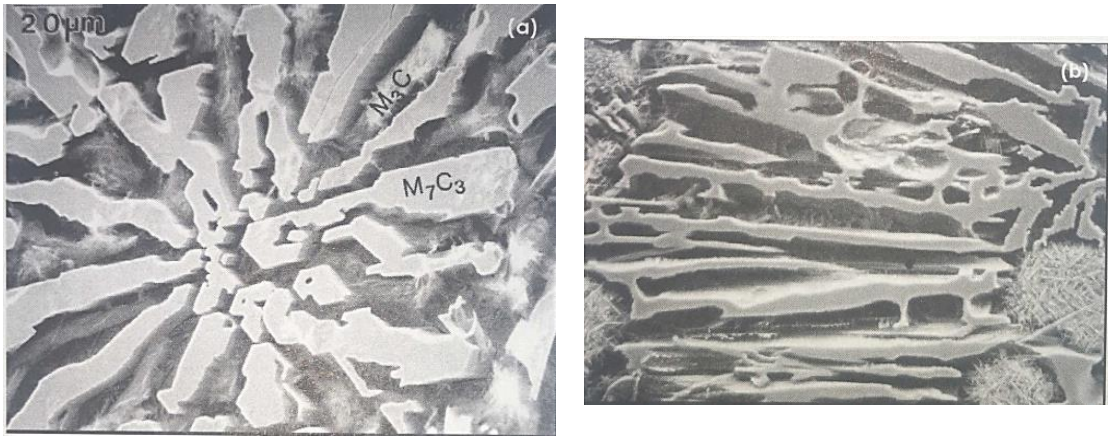

(a) **(b)**

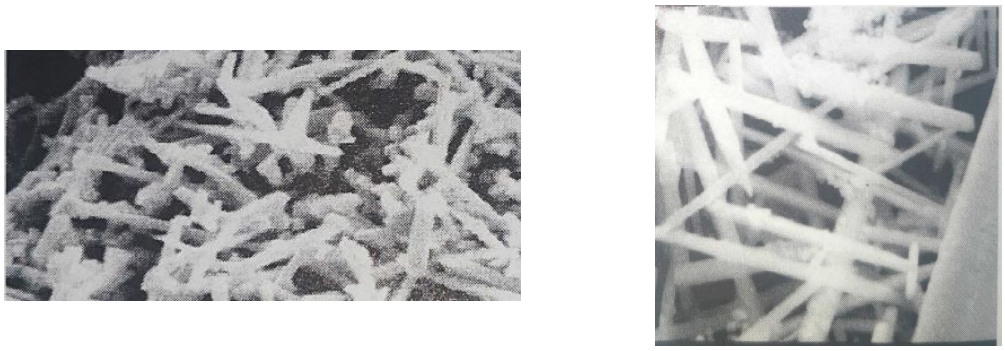

(c) **(d)**

Figura 12.- Morfología característica de los carburos M_7C_3: (**a**) en forma de cuchillas; (**b**) en forma de varillas; (**c**) y (**d**) morfología de carburos secundarios en forma de varillas.

Carburo $M_{23}C_6$: este carburo rara vez se ve en fundiciones comerciales y, según el conocimiento de diversos autores en este campo, no se fabrican fundiciones comerciales a partir de carburos primarios o eutécticos $M_{23}C_6$. Aparece como un carburo secundario en las fundiciones de muy alto contenido de Cr, también con morfología de varillas, como se muestra en la Figura 13 [12].

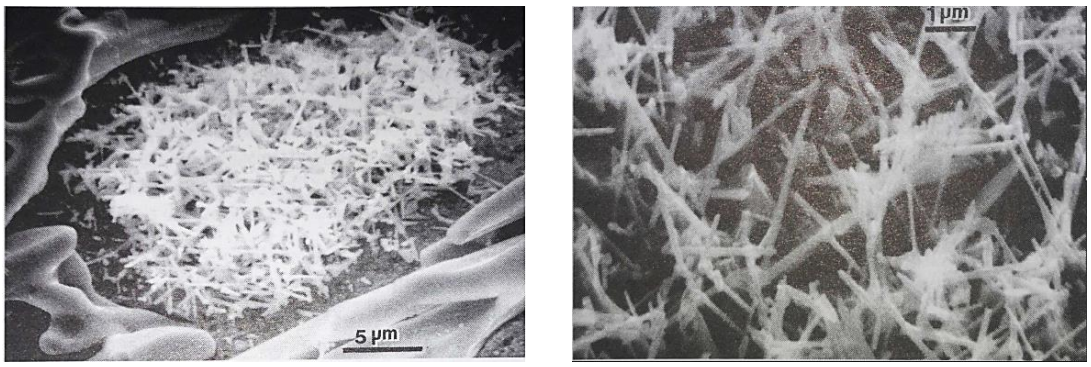

(a) **(b)**

Figura 13.- Morfología del carburo $M_{23}C_6$ en el dendrito de austenita.

Carburo M_2C (asociado al Mo): La morfología característica de este carburo mostrada en la Figura 14 [11] está caracterizada por segmentos parecidos a los huesos de las falanges de las manos humanas. Este carburo se forma al final de la solidificación en las fundiciones de alto Cr. En esta etapa de solidificación, la acumulación de líquido restante está fuertemente restringido por los dendritos adyacentes ya solidificados. La solidificación progresa ($L \rightarrow Mo_2C + Fe(\gamma)$) y la eutéctica solidifica como un mixto de carburo y austenita. Este carburo es fácil de encontrar en fundiciones resistentes al desgaste que estén aleadas con un contenido superior al 3% de Mo. Su morfología suele depender de las demás fases que solidificaron primero. Para contenidos bajos, como por ejemplo el 2%, este carburo puede aparecer a lo largo de las juntas de grano y disuelto en la matriz o en el carburo M_7C_3.

Figura 14.- Morfología de los carburos de molibdeno Mo_2C. Se puede observar su forma de falanges.

1.3.2- Propiedades mecánicas y físicas de los carburos antes mencionados.

Carburo M_3C: la dureza de este carburo no es nada extraordinaria, teniendo un rango que va desde los 800 hasta los 1000 HV. Lo que hace que el carburo M_3C sea extraordinario es su capacidad para formarse en cantidades masivas. Por ejemplo, es común encontrar distintos tipos de fundiciones resistentes al desgaste como las perlíticas y Ni-hard 1, que contienen hasta un 40% de fracción de volumen de carburo. Con una fracción en volumen tan alta, el carburo M_3C domina la resistencia a la abrasión de la fundición.

La reactividad o resistencia a la oxidación del carburo M_3C no se encontró en la literatura. Se puede razonar que su inestabilidad química o reactividad está ligada a su energía libre de formación de Gibbs mostrada en la Figura 15 [13]. Esta energía es la que se libera durante la formación del compuesto. Si el compuesto libera una gran cantidad de energía, entonces se requiere una cantidad similar de energía para descomponer el compuesto.

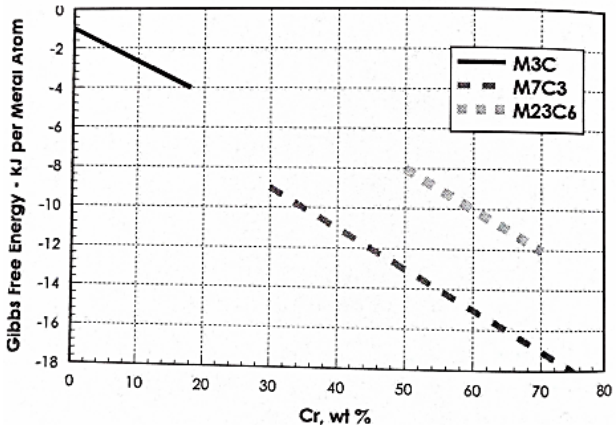

Figura 15.- Energía libre de Gibbs para la formación de carburos M_3C, M_7C_3 y $M_{23}C_6$, con el aumento del %Cr.

Centrándose solo en el carburo M_3C, la energía libre de formación de Gibbs se vuelve cada vez menos negativa a medida que disminuye el contenido en Cr. Al 0% de Cr, el carburo se vuelve inestable a medida que la energía libre de Gibbs se acerca a cero. Esto tiene una aplicación directa en fundiciones perlíticas donde el contenido en Cr puede ser extremadamente bajo (<0,5%).

Carburo M_7C_3: la dureza de este carburo puede variar entre los 1000 y los 1800 HV, aunque lo más aceptado generalmente es que varíe entre los 1200 y los 1500 HV. Hay varias razones por las

cuales la dureza de este carburo varía. Dependiendo del eje del carburo que sea indentado, el resultado de la dureza variará. Si el carburo es indentado en el extremo de la varilla, la dureza es de aproximadamente 1500 HV, pero si el carburo es indentado a lo largo de la varilla, la dureza es solamente de 1000 HV. Esta anisotropía en la dureza es una razón por la cual las fundiciones enfriadas rápidamente producen índices de dureza ligeramente más altos, ya que, cerca de la superficie de esta, el penetrador debe empujar contra el lado más duro del carburo.

Otros estudios sobre la dureza del carburo M_7C_3 han mostrado una variabilidad aún mayor. En la Figura 16 [14] se muestran unas mediciones en las que se constatan grandes rangos de dureza para los carburos M_3C y M_7C_3 dependiendo del contenido en Cr. Sus durezas fueron medidas en fundiciones coladas con enfriamientos rápidos, y sus indentaciones fueron hechas en dirección perpendicular al eje del carburo, y en la zona de mayor dureza.

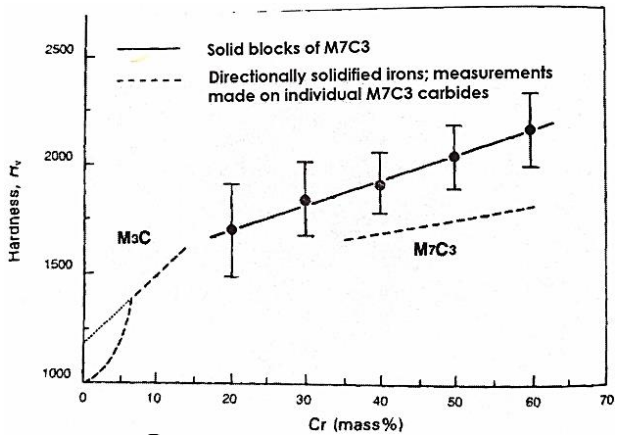

Figura 16.- Dureza de los carburos M_3C y M_7C_3 en función de su contenido en Cr. Las medidas fueron realizadas con 1kgf.

En la Figura 17 [15] se puede ver fácilmente el contenido en Cr para el carburo M_7C_3 en las fundiciones resistentes al desgaste más habituales. Con un contenido dado, la dureza del carburo M_7C_3 se puede determinar utilizando la Figura 16 [14]. Desde las fundiciones perlíticas hasta las Nihard 1 y 2 que contienen bajos contenidos en Cr, se puede esperar una pequeña variación en la dureza del carburo M_3C. En fundiciones de alto contenido en Cr, la relación entre el contenido en Cr y la dureza del carburo M_7C_3 proporciona información respecto al rendimiento frente al desgaste por abrasión de la Nihard 4, teniendo mejor rendimiento las primeras.

La estabilidad química del carburo M_7C_3 está parcialmente ligada a su contenido de Cr. Como se muestra en la Figura 15 [13], cuando aumenta el contenido en Cr, también lo hace la energía libre de Gibbs hacia valores cada vez más negativos, aumentando la estabilidad de dicho carburo. Esto es importante para los usuarios que optan por fundiciones resistentes al desgaste bajo condiciones de corrosión u oxidación extrema.

En la literatura, el Cr_7C_3 puro se dice que se oxidará en presencia de oxígeno a 800°C. Se puede interpretar como consecuencia, que, a concentraciones menos puras del Cr_7C_3, las temperaturas a las que ocurrirá la oxidación serán menores.

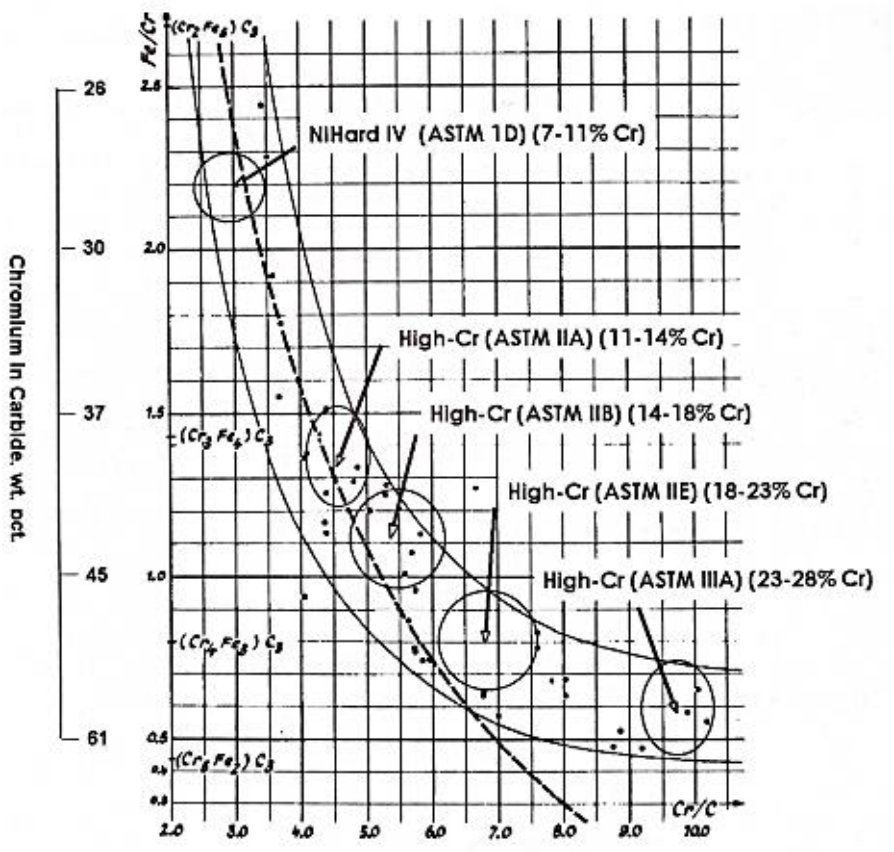

Figura 17.- Relación entre el ratio Cr:C y el esperado contenido en Cr del carburo M_7C_3.

En atmósferas oxidantes, el Cr_7C_3 permanecerá relativamente estable debido a la formación de una película de óxido de cromo. Como se puede predecir, el carburo M_3C no es tan estable, ya que su contenido de Cr es notablemente menor en comparación con el contenido de Cr del M_7C_3.

Para finalizar, en ambientes reductores el M_7C_3 será disuelto.

Carburo $M_{23}C_6$: la dureza de este carburo es más baja que la del M_7C_3 pero ligeramente superior al M_3C. No se encontró un rango de durezas para el $M_{23}C_6$, solamente para el carburo puro $Cr_{23}C_6$, cuya dureza es de aproximadamente 1000 HV. Como se ha visto en la Figura 15 [13], la estabilidad química de este carburo también es menor al M_7C_3. Sin embargo, al tener mayor porcentaje en Cr, es más resistente en atmósferas oxidantes que el M_7C_3.

Carburo Mo_2C: la dureza de este carburo varía desde los 1500 HV a los 1800 HV. Dado que se forman como carburos interdendríticos muy finos y, en la mayoría de las fundiciones, están presentes en pequeñas trazas (<1% de fracción de volumen de carburo), su efecto sobre la dureza y las propiedades resistentes al desgaste es insignificante.

Este carburo es rápidamente atacado y disuelto por HF concentrado, HNO_3 Y H_2SO_4. Como curiosidad, no se ve afectado por el HCl concentrado. Durante el tratamiento térmico, el carburo permanece estable y no se transforma. En parte, esta propiedad es debida a su alta energía libre de Gibbs.

En la Tabla 2 que se muestra a continuación se puede ver de manera resumida las propiedades más relevantes de los distintos tipos de carburos que se encuentran o se pueden encontrar en este tipo de fundiciones.

Tipos de Carburos presentes en estas fundiciones resistentes al desgaste

Se muestra a continuación un sumario de los posibles carburos presentes en estas fundiciones altamente aleadas en cromo. De manera habitual, hay dos tipos de carburos mayoritarios de interés, el M_3C y el M_7C_3.

Tabla 2. Clasificación de los carburos presentes en las fundiciones blancas con alto %Cr.

Carburo	Elementos químicos que lo forman en wt%.	%C	Densidad (g/cm^3)	Cristalografía	Morfología	Dureza (HV)	Energía libre de Gibbs (kJ/mol)
M_3C	Mayoritariamente formado por Fe. El Cr también se puede disolver en el carburo M_3C hasta en un 17%. Mo tiene una solubilidad muy limitada dentro del carburo M_3C.	6,7-6,9	7,4-7,6	Ortorómbico	Plaquetas	800-1100	+1 a -10
M_7C_3	Mayoritariamente Cr, sin embargo, el contenido en Cr puede variar del 24 al 50%. El carburo puede contener un porcentaje <7%Mo.	8,6-8,9	6,6-8,9	Trigonal	Varillas y cuchillas	1000-1800	-10 a -20
$M_{23}C_6$	Mayoritariamente Cr con un porcentaje mayor del 60%. La solubilidad de otros elementos en este es ligeramente mayor al M_7C_3 (Mo<10%).	5,3-5,7	7,2-7,7	FCC-compleja	Varillas	1000	-8 a -15
M_2C	Normalmente aparecen en junta de grano de la austenita. Suele ser puro, aunque pueden contener algo de Cr cuando solidifica en aleaciones con alto contenido en Cr.	5,9	9,1	Ortorómbico	Varillas, Falanges de dedos humanos.	1500-1800	-25 a -30

1.4- Microestructura y propiedades mecánicas de la fase matriz.

La matriz metálica de estas fundiciones está constituida por distintas fases del hierro. Las fases principales son la austenita, la perlita, la bainita y la martensita. En función de la fracción en volumen de estas fases, la dureza, la tenacidad y la resistencia al desgaste de la fundición puede variar de manera significativa.

Austenita: esta es la primera fase que se forma en todas estas fundiciones. Un ejemplo de su morfología dendrítica se puede observar en la Figura 18 [11]. Los dendritos crecen preferentemente de acuerdo con su gradiente térmico dentro del molde y hasta cierto punto, muestran cómo los elementos de aleación (C, Cr, Si, Mo, etc.), se segregan durante la solidificación.

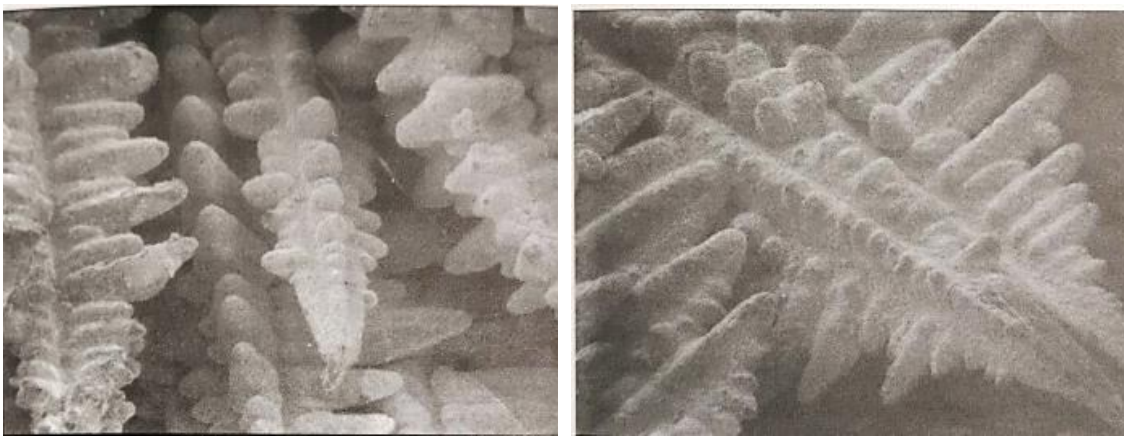

(a) **(b)**

Figura 18.- Dendritos de austenita durante la solidificación. Fe(γ).

Dependiendo del contenido en Cr de la matriz austenítica y del tratamiento térmico, el contenido en C puede variar desde un máximo de 2,11% hasta un mínimo de 0,3%. De todos los elementos, el C tiene la mayor influencia para estabilizar a la austenita a temperatura ambiente, es decir, el C tiene un efecto muy significativo para que la temperatura de inicio de transformación martensítica baje y dificulte su transformación en perlita, como se observa en la Figura 19 (a) [16]. El contenido en C también causa también un incremento del parámetro de red de la austenita y sus transformaciones como se observa en la Figura 19 (b) [16].

La dureza de la austenita retenida es muy variable. Normalmente está entre los 250 y los 500 HV, dependiendo de diversos factores. Por ejemplo, de estar la austenita poco aleada a estar muy aleada la dureza puede variar desde los 250-350 HV hasta los 300-600 HV.

Esta variación de dureza en función del contenido de elementos de aleación (principalmente el C) se debe en gran parte a la naturaleza inestable de la austenita retenida a temperatura ambiente. Cuando se realiza una medida de dureza, un indentador penetra en el cristal de austenita provocando una deformación plástica irreversible. La austenita de alrededor y la que está justo debajo del penetrador experimenta una deformación plástica del orden del 10%. Dependiendo de la estabilidad de la austenita retenida, esta deformación mecánica hará que una cierta fracción de volumen de la austenita retenida se transforme en martensita. La transformación mecánica de austenita en martensita da como resultado la formación de la denominada martensita inducida

por deformación, siendo este proceso muy interesante para la resistencia a la abrasión de estas fundiciones.

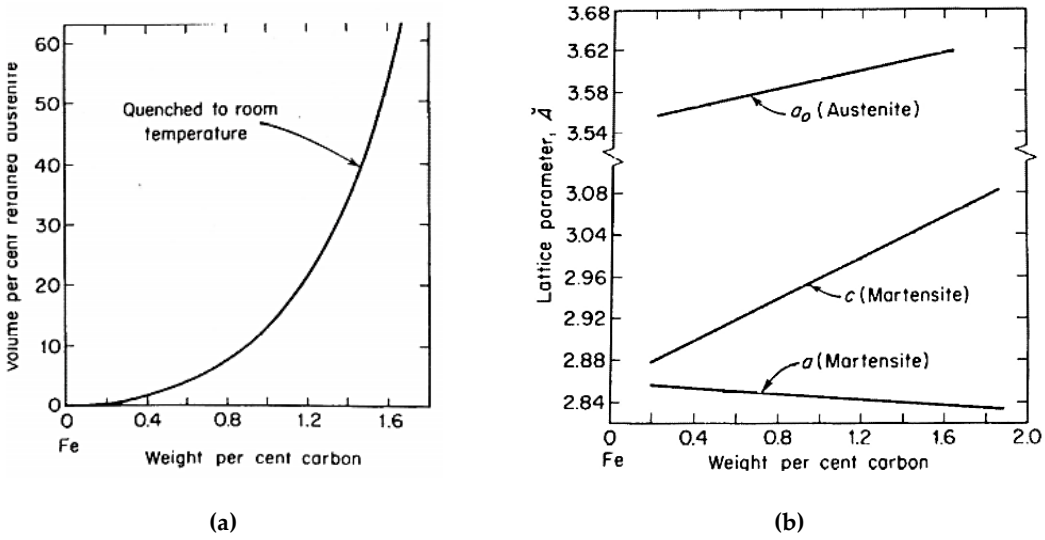

(a) **(b)**

Figura 19.- (**a**) Austenita retenida en un acero en función el %C; (**b**) Variación de los parámetros de red de la austenita y de la martensita en función del %C.

La estabilidad química de las austenitas pobres en Cr se comporta prácticamente igual que un acero normal y puede ser fácilmente corroído por distintos tipos de ácidos como el nítrico o el clorhídrico y por ambientes húmedos. Con un mayor contenido de Cr, la matriz de austenita es casi idéntica a la que se encuentra en los aceros inoxidables austeníticos. Con estas propiedades, una fundición altamente aleada en Cr tiene una resistencia a la corrosión idéntica a la de un acero inoxidable. Si el porcentaje en Cr de la matriz es superior al 11%, se produce una capa muy fina protectora de Cr_2O_3, proporcionando una barrera a la penetración de la oxidación. Sin embargo, si estos niveles de Cr no son constantes a lo largo de toda la matriz austenítica, pueden existir zonas atacadas por la corrosión. Estas zonas atacadas que son más pobres en Cr, pueden corroerse más de lo esperado.

Ferrita: Como se ha dicho, en las fundiciones hipoeutécticas la primera fase en formarse es la austenita, pero cuando el contenido en C es bajo y el de Cr es alto, la fase que se forma es ferrita, como se puede observar en la Figura 20 [11,17]. En cualquiera de los casos, la morfología es dendrítica.

La ferrita o Fe(δ) tiene una solubilidad máxima de 0,17% en C a 1492°C. La solubilidad en la ferrita desciende hasta una solubilidad máxima del 0,0005% a temperatura ambiente. La razón fundamental de que la ferrita admita muy poco C en solución sólida es el poco espacio que existe en la red cúbica BCC para que quepan esos átomos. Al igual que en la estructura austenítica (FCC), el C encaja en la estructura de la BCC como un intersticial. En la celda de la ferrita (BCC), los intersticiales encajan en los intersticios octaédricos como muestra la Figura 21 [18]. Estos sitios intersticiales son 1/3 más grandes que los del cristal de austenita FCC. Esta gran diferencia explica la muy limitada solubilidad del C en la ferrita.

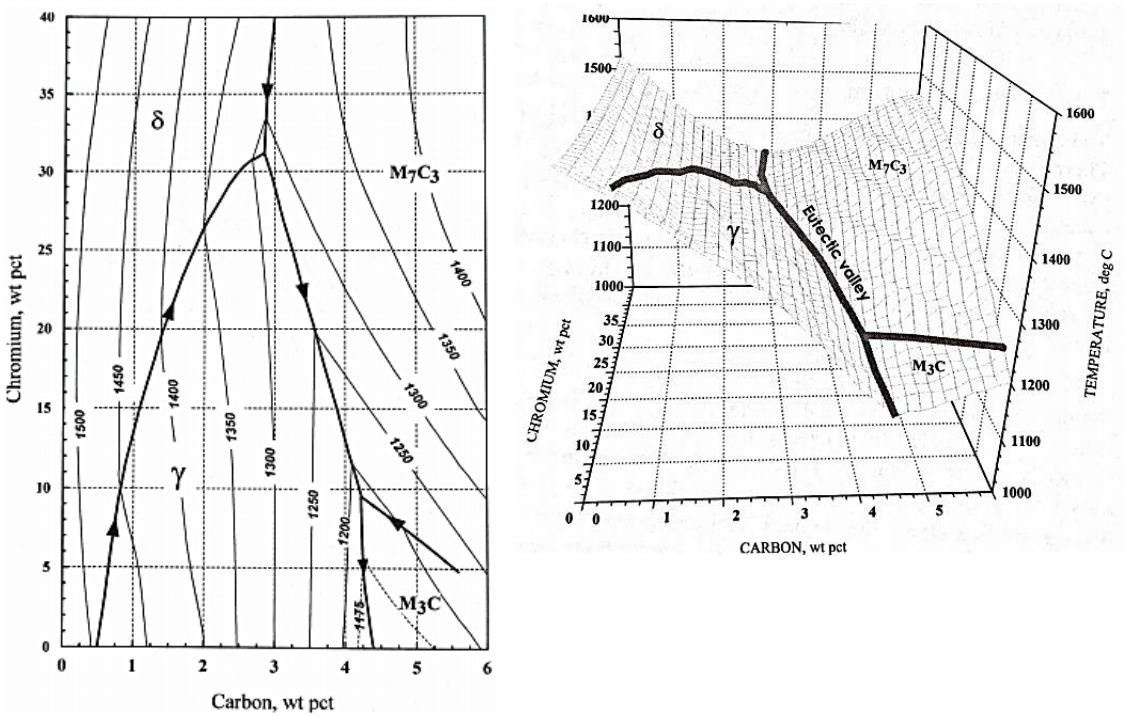

(a) **(b)**

Figura 20.- (**a**) Vista en 2D del diagrama Fe-C-Cr metaestable en su zona de líquidus, es decir, la temperatura a la cual el líquido comienza a solidificar; (**b**) Se corresponde al diagrama (a) pero en 3D.

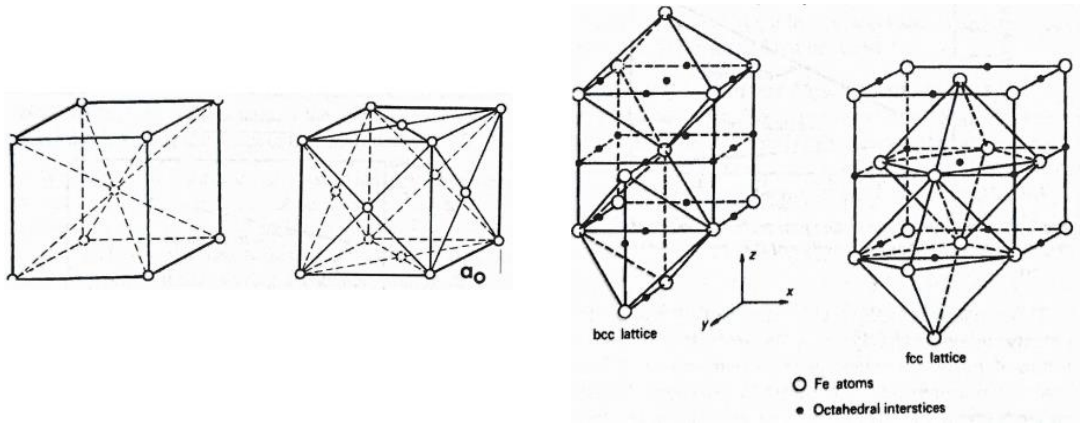

(a) **(b)**

Figura 21.- (**a**) Esquema de las estructuras cristalinas BCC y FCC; (**b**) Intersticios octaédricos en las estructuras de hierro BCC y FCC.

A temperaturas por encima de la temperatura ambiente, es posible tener una estructura constituida por ferrita y carburos M_7C_3 con un 2%C y un 30%Cr. En este caso, la ferrita a temperatura ambiente estaría en equilibrio. Sin embargo, está sobresaturada en C y si se calienta la aleación entre los 600 y los 750°C, se descompondría en perlita.

La ferrita también se puede formar en las fundiciones resistentes al desgaste, cuando se agregan grandes cantidades de Si al caldo. Este mecanismo es bastante complejo y no está bien documentado en la literatura. Durante la solidificación, el carburo rechaza completamente el Si

en su crecimiento. En consecuencia, una capa de alto Si rodeará los carburos primarios o eutécticos. Si el contenido de Cr es alto, la austenita que se está formando también será baja en C. Si se combina el efecto de tener austenita de bajo contenido en C, con que existen regiones localizadas con alto contenido de Si alrededor de los carburos, en esas zonas se reducirá aún más el contenido de C disuelto en la austenita.

No está claro si la ferrita se forma debido a un cambio en la solidificación o debido a la transformación del estado sólido al enfriarse a temperatura ambiente. No obstante, se han encontrado grandes cantidades de ferrita en una fundición experimental que tiene una composición química de 2,6%C, 2,6%Si y 20%Cr. Teóricamente, no se encontraría la transformación de estado sólido de austenita a ferrita.

En cuanto a sus propiedades mecánicas, le ferrita es blanda, variando la dureza desde los 215 a los 270 HV. Químicamente, el aspecto de mayor interés es que cuando el contenido en Cr es superior al 11%, la ferrita se vuelve resistente a la corrosión.

Martensita: Si la fundición tiene matriz austenítica, cabe la posibilidad de transformarla en martensita tras un enfriamiento a temperatura ambiente. La austenita sufrirá un cambio en su red cristalina repentino. Este cambio es instantáneo y sin difusión de átomos. El resultado es que la red FCC se transforma en una red cúbica centrada en el cuerpo tetragonal (BCT), como se observa en la Figura 22 (a) [19]. Al ser un proceso adifusional, el contenido en C previo que se encontraba en la austenita está ahora en la martensita.

Esta red es similar a la BCC, pero el alto contenido en C la distorsiona de tal forma que deja de ser una red cúbica simétrica. Cuanto más C esté en solución sólida, más se distorsiona la red, como se puede observar en la Figura 22 (b) [11].

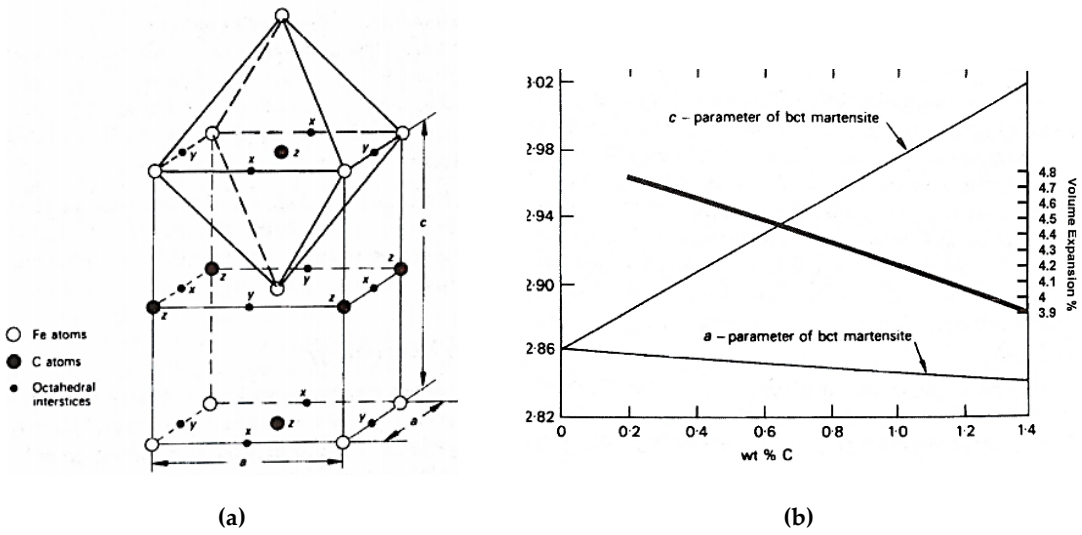

Figura 22. (**a**) Red tetragonal de martensita que muestra los sitios octaédricos donde pueden residir los átomos de C. Debe existir suficiente C para ocupar completamente el espacio en el eje z para crear una estructura cristalográfica estable; (**b**) Gráfico donde se observa que, a medida que aumenta el contenido en C en la austenita, el volumen de la red de la martensita formada a partir de esa austenita decrece.

Esta distorsión, por tanto, tiene el efecto de incrementar la dureza de la martensita. Además, cuando la austenita se transforma en martensita, existe una expansión de volumen de un 4,3%.

Es interesante destacar que como se indica en la Figura 22 (b) [11], a medida que aumenta el porcentaje de C de la austenita, la expansión de volumen sufrida por la celda en la transformación martensítica decrece. No obstante, la disminución es bastante menor en comparación con la magnitud general de la transformación. Con carácter general, se asume que la expansión de volumen en dicha transformación es del 4%. Cabe señalar que esta expansión se corresponde con la totalidad de la austenita transformada en martensita. De esta manera, si hubiese una fracción en volumen de carburos del 30% y se logra transformar el 90% de la austenita en martensita, se obtendría un porcentaje total de martensita en la estructura del (70·90=63) 63%, lo que significa que la expansión sufrida por la aleación es de (0,63·4,3=2,72) 2,72%.

Esta expansión de volumen sufrida durante la transformación es importante para entender los tratamientos térmicos y comportamientos frente al desgaste de este tipo de fundiciones. Por ejemplo, si la fundición sufre transformaciones que no estén controladas, pueden aparecer tensiones internas que deriven en micro roturas en el material que lo dañen severamente.

La morfología de la martensita se muestra en la Figura 23 [20]. Es descrita habitualmente con forma acicular o de lajas en forma de plaqueta, siendo esta más habitual en las fundiciones de alto contenido en Cr.

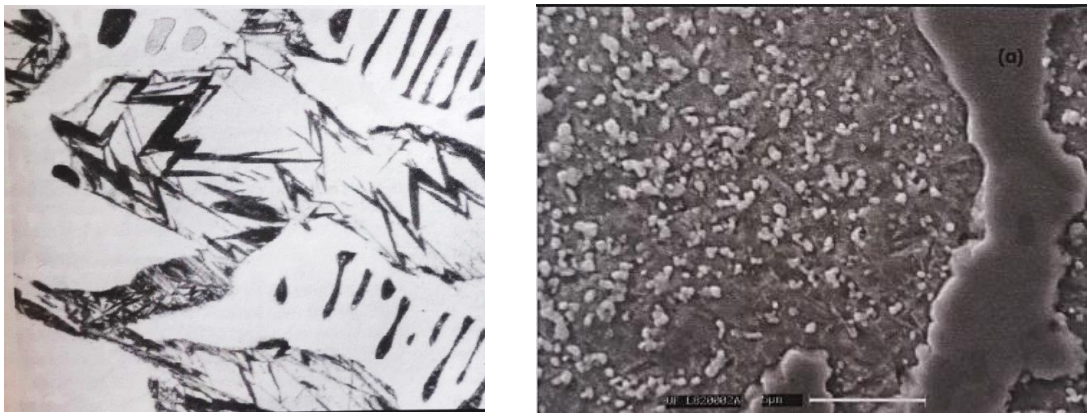

(a) **(b)**

Figura 23. (**a**) Morfología de la martensita en forma de acícula; (**b)** Morfología de la martensita en forma de lajas o plaquetas (a estos aumentos se ve en la zona más oscura un cierto relieve que delata la presencia de dicha fase).

Como es sabido, cuanto mayor sea el porcentaje en C de la austenita, mayor será la dureza de la martensita formada, pero mayor será también la fracción de austenita retenida a temperatura ambiente, pues disminuye la temperatura del inicio de transformación martensítica Ms.

En cuanto a sus propiedades mecánicas, la más importante es su elevada dureza, siendo esta consecuencia del grado de distorsión de la celda BCT. Cuando el contenido en C aumenta, incrementa el grado de distorsión o tensionamiento, ofreciendo una gran resistencia al movimiento de dislocaciones. A su vez, también se vuelve más complicada la transformación de la austenita en martensita. Como consecuencia, en ocasiones no se logra la dureza esperada de una martensita de alto C, debido precisamente a que no es la estructura 100% martensítica.

Dado que no es una fase estable dentro de las aleaciones férreas, tiene tendencia a descomponerse en sus constituyentes básicos, siendo estos ferrita y carburos. En el caso de que la martensita sea de alto C, tiende a disminuir el porcentaje de este, precipitando carburos con tratamientos

térmicos de baja temperatura. Lógicamente, a mayor temperatura se acelera el proceso. Este tratamiento térmico es el revenido. En redes BCT muy tensionadas el revenido persigue primero que la red expulse una pequeña cantidad de átomos de C, formando una martensita de bajo C y carburos épsilon (ε), de estructura hexagonal compacta y fórmula aproximada $Fe_{2,4}C$. Si se continúa se llega a la estructura mixta de equilibrio de ferrita y carburos.

Un efecto secundario de este proceso de revenido es que la red de martensita se contraerá. A medida que C va siendo expulsado de la red BCT se contrae, dando como resultado una contracción de su forma distorsionada anterior. Este proceso es comúnmente utilizado para eliminar la deformación en las piezas martensíticas. El revenido suele suavizar la martensita.

Sin embargo, dependiendo del contenido de C de la aleación y la temperatura de revenido, el Fe puede endurecerse como se puede observar en la Figura 24 [21].

Como era de esperar, la estabilidad química de la martensita es mucho menor que la de la austenita o la ferrita, debido a su estado de alta tensión. Cuando se expone a ácidos, la fase de martensita se disolverá fácilmente, al contrario de lo que ocurre en la austenita o la ferrita. El final del resultado de este proceso permite al metalógrafo confirmar claramente si la martensita está presente en la aleación.

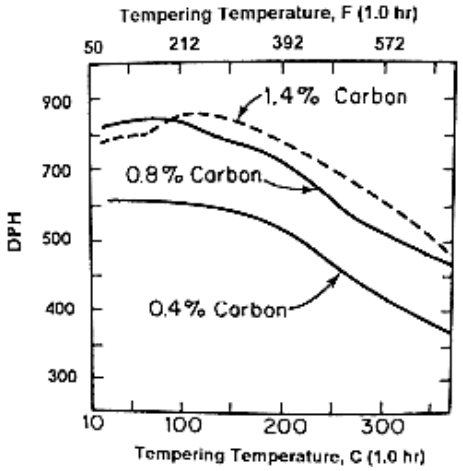

Figura 24. Evolución del revenido en función del %C. Si hay muy poca austenita retenida (0,4%C), el revenido reducirá la dureza de la martensita. A mayor C (0,8%C), el revenido también promoverá la transformación de la austenita retenida en martensita dura, produciendo un pequeño aumento en la dureza a temperaturas justo por encima de la temperatura ambiente. A temperaturas más altas y un mayor contenido de C (1,4%C), puede producirse un aumento de la dureza debido a la formación del anteriormente mencionado carburo ε.

Perlita: es una fase habitual que puede encontrarse en el estado bruto de moldeo. Esta fase crece por un proceso de nucleación y crecimiento desde las juntas de grano austeníticas. La clave de este proceso de crecimiento es la alta movilidad del C a esas temperaturas de formación de la perlita. El hecho de que la ferrita tolere una cantidad de C muy baja, implica la formación del carburo M_3C.

Su microestructura consiste en láminas de carburo y de ferrita, como se indica en la Figura 25 [11]. El espaciamiento entre estas láminas viene dado por la relación entre aleantes (el Cr, Ni, Mo y Mn afinan este espaciamiento), velocidades de enfriamiento y temperaturas de formación.

Cabe destacar que un tratamiento térmico para transformar la austenita retenida en perlita, y además globulizar el carburo M_3C (previamente laminar) da unas ventajas a la hora de mecanizar la fundición por varias razones. Entre otras están que la austenita es amagnética, complicando el rectificado de piezas. Además, durante el mecanizado, la austenita genera una viruta en la herramienta de corte que dificulta el trabajo. Con la globulización de la perlita existe una matriz ferrítica blanda y que desgasta poco la herramienta y como constituyente disperso glóbulos de M_3C duros y frágiles que facilitan el autolimpiado de la herramienta al facilitar el arranque de la viruta formada.

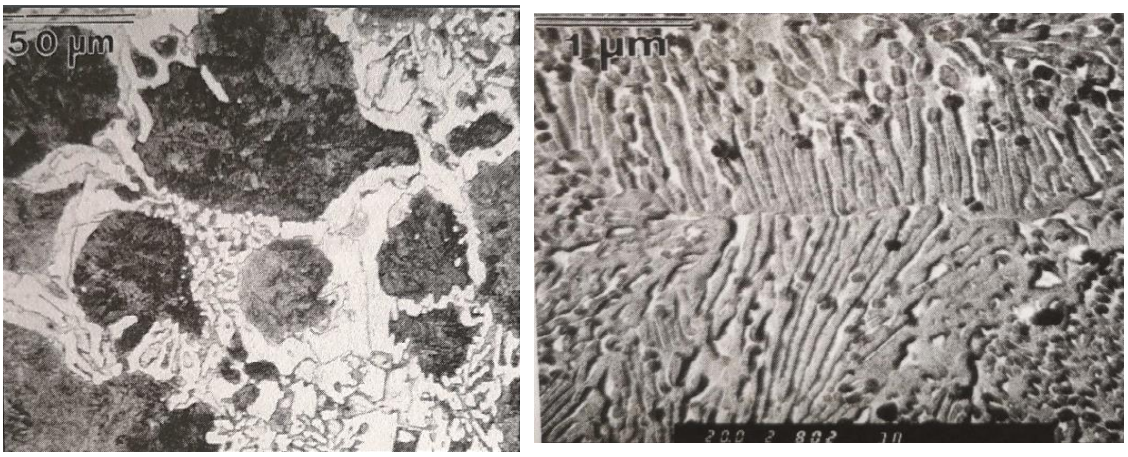

(a) **(b)**

Figura 25. (a) Microestructura tomada en microscopio óptico, donde se observa el constituyente matriz formado por austenita retenida (fase blanca) y perlita (fase oscura); **(b)** Microestructura tomada en el microscopio electrónico de barrido, donde a mayor número de aumentos, se observan las láminas intercaladas de ferrita y M_3C.

La dureza de la perlita oscila entre los 250 y los 450 HV. Esta dureza viene principalmente por el espaciado interlaminar siendo más dura cuando más delgado sea este espaciado.

Bainita: Se forma en el rango de temperaturas comprendidas entre 250 y 500°C. La bainita tiene características tanto de perlita como de martensita. El crecimiento de la fase de ferrita está parcialmente controlado por la difusión del C. Por tanto, la bainita crecerá aproximadamente un orden de magnitud más rápido de lo que se esperaría si se basara estrictamente en la difusión de C. Esta tasa de crecimiento más rápida se atribuye a la morfología de la ferrita. Como se puede apreciar en la Figura 26 [20] un pequeño germen de ferrita nuclea y crece a lo largo de un plano cristalográfico preferente. Durante su crecimiento, el C difunde parcialmente hasta la austenita circundante. Después de ese crecimiento, quedan lajas de ferrita sobresaturadas en C. Consecuentemente, para continuar con el crecimiento, las lajas de ferrita deben expulsar el C hacia la austenita adyacente en forma de pequeños carburos, que serán del tipo M_3C.

Cuando se habla de bainita, cabe especificar si es superior o inferior porque, aunque las dos estén compuestas por ferrita y carburo, tienen diferente morfología. La bainita superior formada a temperaturas mayores tiene una estructura más gruesa que la bainita inferior. Además, a altas temperaturas el C tiene más capacidad para difundir hasta la frontera de la laja de ferrita, precipitando en forma de carburo, mientras que en la inferior (formación a menor temperatura) el C se ve obligado a precipitar en el interior de la laja de ferrita.

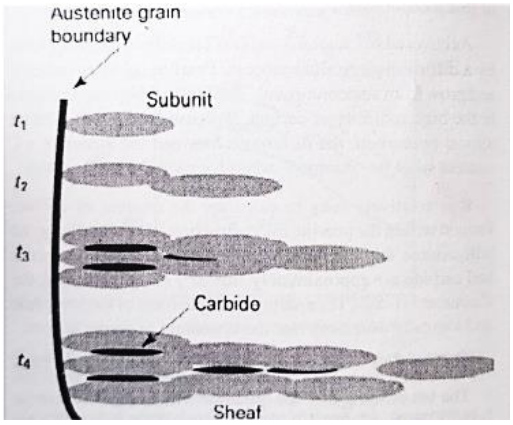

Figura 26. Esquema del crecimiento de la bainita desde la junta de grano austenítica. Inicialmente (t_1) solo aparece una pequeña laja de ferrita. A medida que progresa el carburo se va formando y se forma la bainita completa (t_4).

La transformación de austenita en bainita conlleva una expansión de volumen del 3% aproximadamente, siendo bastante agresiva y causando distorsiones dentro de la matriz austenítica. Se puede observar en la Figura 27 [20] la distorsión en esa transformación. En muchos aspectos, es idéntico a la transformación martensítica, exceptuando que ocurre a mayor temperatura, lo que origina que gran parte de esa tensión se atenúa debido al movimiento más libre de dislocaciones.

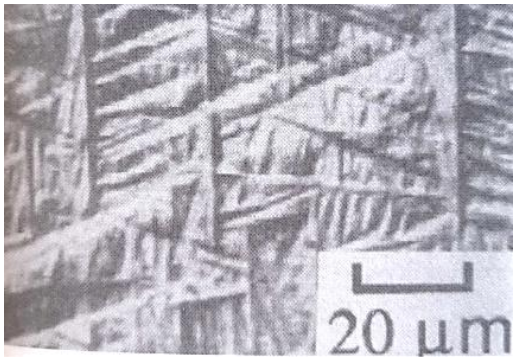

Figura 27. Distorsión que genera la transformación bainítica en la austenita.

La morfología de la bainita es similar a la de la martensita. En la Figura 28 [15] se ve un ejemplo de una fundición resistente al desgaste con matriz parcial de bainita, pero que a priori es difícil asegurar si se trata de bainita o de martensita.

En fundiciones altamente aleadas, la transformación completa de austenita en bainita es muy difícil debido a los elementos de aleación. La temperatura de inicio de transformación bainítica se deprime al añadir a la aleación elementos como el C, Mn, Ni, Cr o Mo, todos ellos muy utilizados en este tipo de fundiciones resistentes a desgaste. Por tanto, si se observa bainita en una fundición de este tipo, representará solo una proporción de la fase matriz, no superando nunca el 50%.

La dureza de la bainita depende de la temperatura de transformación y del porcentaje de C de la austenita previa a la transformación. Como norma general, tiene una dureza intermedia entre la perlita y la martensita. La bainita es resistente al revenido y no tiene ningún efecto un revenido bajo, por lo que resulta inadecuado realizarlo. A altas temperaturas los carburos embebidos entre las agujas de ferrita, coalescen y engrosan disminuyendo la dureza de dicha fase.

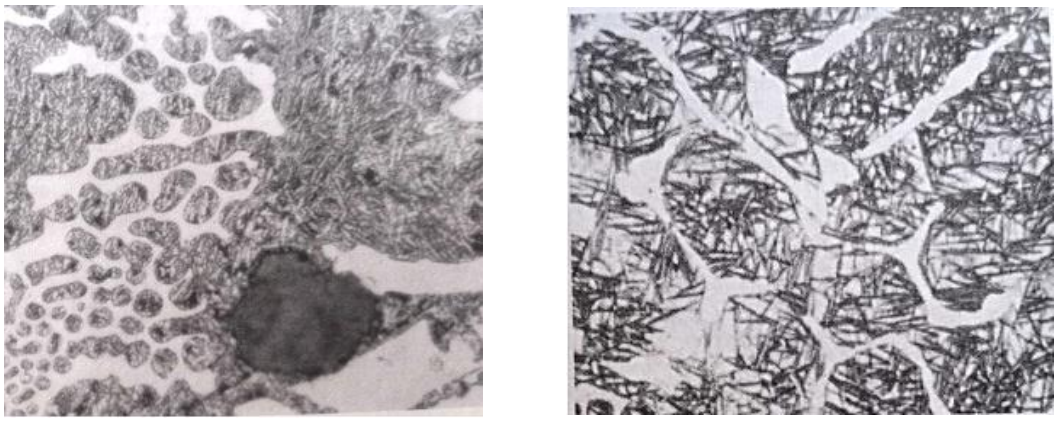

(a) **(b)**

Figura 28. Matriz formada por bainita y austenita. Las lajas oscuras son bainitas, las cuales se atacan fácilmente (ferrita), mientras que la austenita es más resistente y permanece inalterada.

1.5- Microestructura bruto de moldeo de estas fundiciones y desestabilización de la austenita.

Estas aleaciones presentan un porcentaje en Cr entre el 15 y el 30 % [4], aumentando la resistencia al desgaste conforme aumenta el porcentaje en este elemento [22]. Las fundiciones aleadas con un porcentaje de Cr superior al 15% en peso presentan dos peculiaridades microestructurales que condicionan sus propiedades. Hasta aproximadamente un 16% de contenido de Cr, el constituyente eutéctico es ledeburítico, donde la fase de matriz de este constituyente son carburos mezclados del tipo M_3C. Sin embargo, cuando el contenido en peso de Cr supera el 16%, el constituyente eutéctico deja de ser ledeburítico, siendo la austenita mayoritariamente -y, en menor proporción alguna de las fases o constituyentes derivados de su transformación- [3], la fase matriz de este eutéctico. Esto justifica que estas fundiciones muestren una mayor tenacidad que las fundiciones Ni-hard [23–25], mientras que los carburos dispersos que lo acompañan son carburos mixtos del tipo $(Fe,Cr)_7C_3$, también denominados carburos K_2 [26], presentando una morfología similar a laminas o plaquetas [27]. Que el constituyente continuo de la eutéctica sea austenita en lugar del carburo K_2, favorece tareas de mecanizado cuando se somete a un tratamiento isotérmico de perlitización [26].

El contenido de carburos eutécticos de tipo M_7C_3 se incrementa gradualmente con el aumento del contenido de Cr [28]. Estos carburos manifiestan una dureza entre 1500 y 1800 HV [2,24,29,30], por lo que supera la dureza de la mayoría de los materiales abrasivos, entre los que cabría destacar el corindón (1300 HV) y el cuarzo (800-1000 HV). Únicamente le superaría en dureza el SiC (2500 HV) [31]. De todo ello, se deduce que no se produciría el desgaste erosivo de estos carburos, si no su desprendimiento cuando la matriz que los sostiene se desgasta [32]. Las fundiciones férreas con un porcentaje muy elevado en Cr son las que presentan mayor resistencia a la oxidación y a la corrosión. En particular, las relaciones Cr/C mayores de 10 resultan favorables [33]. Este grupo de fundiciones férreas altamente aleadas en Cr resistentes al desgaste y a la corrosión incluiría aquellas con un contenido de Cr de alrededor del 25% y un contenido de C de alrededor de 2,5-2,8%. La resistencia a la abrasión de las fundiciones blancas depende en gran medida de las propiedades y microestructura del material, así como de las condiciones de desgaste [34].

La austenita sobresaturada en C y Cr presenta una elevada templabilidad, lo que dificulta su transformación en el enfriamiento en perlita o bainita, permitiendo su transformación parcial en martensita mediante un enfriamiento al aire [35]. Sin embargo, desciende bruscamente también la temperatura Ms, dificultando su transformación completa en martensita y quedando a temperatura ambiente un porcentaje muy elevado de austenita retenida.

La resistencia al desgaste mejora si se realiza un tratamiento de austenización [36,37] con el objetivo de desestabilizar la austenita, promoviendo la precipitación de carburos secundarios ricos en Cr [25,37], distribuidos uniformemente en una matriz predominantemente martensítica. Estos carburos secundarios precipitan como resultado de la desestabilización de la austenita a temperaturas de alrededor de 1000 °C o superiores [4,27,29,33,37–44].

El temple en aceite disminuiría el porcentaje de austenita retenida a temperatura ambiente en comparación con el enfriamiento al aire, ya que en el primero se producirá una mayor velocidad de enfriamiento entre Ms y Mf y, por tanto, una mayor conversión de austenita en martensita.

Como resultado de dicha desestabilización de la austenita a temperaturas alrededor de 1000 °C, precipitan principalmente carburos secundarios del tipo K_2 [25,29,33,37-39,41-49] como consecuencia del rechazo por parte de la austenita de los elementos de aleación por los que se encuentra sobresaturada, y que promueven una mayor resistencia a la abrasión y un aumento en la temperatura de Ms, lo que conduce a una reducción de la austenita retenida y a disminuir el riesgo de agrietamiento durante el enfriamiento [29,36,42,50,51]. Estudios previos confirman que cuanto mayor es el tiempo de permanencia a la temperatura antes mencionada, mayor es la precipitación de estos carburos [27]. La adición de Mo aumenta también la templabilidad [25, 29,33,36–38,41–44,47,49–54], aumentando la dureza [55] y mejorando la resistencia al desgaste [56–58]. Si la temperatura de desestabilización es baja, disminuye el límite de solubilidad del C en la austenita y, por tanto, aumenta la cantidad de carburos secundarios [59]. La desestabilización de la austenita requiere de tiempos de permanencia elevados a la temperatura de austenización. Esto se debe a la elevada concentración de elementos de aleación en la celda cristalina de la austenita, lo cual dificulta la difusión del carbono. A su vez, como consecuencia de una solidificación de no equilibrio, hay más eutéctica que la correspondiente al diagrama de equilibrio [45,60]. Según aumenta el tiempo de permanencia a la temperatura de desestabilización dos cinéticas compiten de manera simultánea: por una parte, la disolución de carburos eutécticos de inequilibrio que quedarán en solución sólida de la austenita, y, por otra parte, la cinética de precipitación de carburos secundarios a partir de esa austenita sobresaturada, que conlleva el aumento de la densidad de carburos secundarios [32]. Un tiempo excesivo de permanencia a la temperatura de desestabilización produce el engrosamiento de los carburos secundarios y la disminución de la dureza [42].

Los carburos secundarios precipitados durante la desestabilización de la austenita a 1000 °C son los carburos M_7C_3 en fundiciones con 20% en Cr [33]. Sin embargo, estarían presentes conjuntamente los carburos secundarios de estequiometrias M_7C_3 y $M_{23}C_6$, denominados también K_1, en fundiciones con 27% en Cr [4,33,61]. Algunos autores concluyen también que durante la desestabilización de la austenita el carburo M_7C_3 es el primero en precipitar durante el calentamiento y que, durante el mantenimiento a la temperatura de desestabilización, se transformaría en $M_{23}C_6$ [62]. A su vez, estos también afirman que se produce una precipitación adicional de $M_{23}C_6$ durante el enfriamiento, en el rango de temperatura 980–750 °C. Cuando predominan los carburos secundarios del tipo M_7C_3 frente a los $M_{23}C_6$ la dureza aumenta [33]. La fracción en volumen de carburos secundarios aumenta a temperaturas de desestabilización bajas

(900 °C) y tiempos de permanencia elevados (8 horas) [27]. Otros estudios concluyen que temperaturas de desestabilización altas favorecen la presencia de austenita retenida [63].

La presencia de Mo en la composición química favorece la precipitación de carburos M_2C eutécticos [56,58,61,64–66], que permiten aumentar la dureza y la resistencia a la abrasión [56,64,67]. El Mo también puede disolverse en los carburos mixtos del tipo M_7C_3 [68], sustituyendo a los átomos de Fe, produciendo una distorsión en su celda elemental y sin una influencia significativa sobre su dureza. La adición de Mo produce una caída tanto en la temperatura del líquido como en la temperatura eutéctica. La adición de Mo también aumenta la templabilidad del material [69], aumentando su dureza [55] y su resistencia al desgaste [56–58]. Además, la presencia de Mo conduce, durante el revenido a alta temperatura [33], a la formación de carburos M_2C, los cuales nuclean a partir de carburos M_7C_3 para extenderse a través de la matriz martensítica [29,70].

1.6- Tratamientos térmicos de revenido aplicables a estas fundiciones.

Los carburos, además de precipitar durante el tratamiento de desestabilización de la austenita, pueden precipitar durante el revenido [49].

Las temperaturas para el revenido de la martensita se sitúan en el rango de los 200–250 °C. Sin embargo, a temperaturas entre 400 y 600 °C, sería posible lograr una segunda desestabilización de la austenita retenida [29,32,71–74], aumentando la dureza y resistencia al desgaste [75], favoreciendo su transformación en bainita [66,76].

Otros estudios indican que se podría obtener una mayor fracción de carburos terciarios durante el revenido entre 400 y 600 °C [53], con porcentajes crecientes formados con medios de enfriamiento de mayor severidad, por ejemplo, durante tratamientos criogénicos [51–53]. Durante los procesos de alto revenido, los carburos mixtos $(Mo, X)_2C$ pueden nuclear en la frontera de los carburos eutécticos K_2 [33], creciendo hacia la matriz [29].

Sin embargo, una excesiva temperatura de revenido podría provocar una redisolución de átomos de C en la matriz de martensita revenida [56]. Este C procedería de los carburos precipitados a las temperaturas más bajas del revenido. La temperatura de revenido óptima para aumentar la dureza y resistencia al desgaste parece situarse en el entorno de los 500 °C [29,77] y a tiempos del entorno a las 6 horas, eliminando la presencia de austenita retenida. La temperatura de revenido resulta decisiva en la resistencia al desgaste y en la dureza del constituyente matriz de estas fundiciones. Bajas temperaturas de revenido no desestabilizan completamente la austenita [78].

1.7- Tratamientos superficiales adicionales.

Un tratamiento adicional de nitruración podría producir un endurecimiento superficial y favorecer un aumento de la resistencia al desgaste erosivo por la formación de carbonitruros en la matriz de martensita revenida.

En los aceros, un tratamiento termoquímico de nitruración produce un endurecimiento de la superficie mediante la formación de subnitruros de Cr, V, Mo y Al en la matriz de martensita revenida [79]. La importancia de que la martensita esté revenida radica en la facilidad de la difusión del N [80], ya que el N difunde intersticialmente a través de la red de la ferrita α-BCC.

Si se nitrura en martensita obtenida tras temple, debido a la sobresaturación de la red se dificultaría la difusión del N. La ferrita admite N en solución sólida, pero la presencia de precipitados de tipo carburo homogéneamente distribuidos en ésta, hace que el N se incorpore como parte de la red del carburo para formar carbonitruros, en lugar de quedar en solución sólida en el Fe(α), estando constituida por nitruros del tipo ε-$Fe_{2\text{-}3}N$, del tipo γ'-Fe_4N [81], que generan una elevada distorsión en la matriz ferrítica dando una elevada fragilidad. Sin embargo, no hay informes previos sobre la nitruración de fundiciones blancas con alto contenido de cromo. En el caso de aceros pertenecientes al sistema Fe-Cr-Mo, el tipo de nitruros $(CrMo)_xN_y$ dependerá de la relación Cr / Mo [82].

1.8- Qué se pretende en este trabajo.

En la presente Tesis Doctoral, mediante la aplicación de sucesivos diseños de experimentos, se pretende maximizar la dureza y la resistencia al desgaste de fundiciones blancas altamente aleadas con un 18% y un 25% en Cr cuyas composiciones químicas se muestran en las Tablas 3 y 4. Para ello, mediante la variación controlada de parámetros de proceso relacionados con los tratamientos térmicos se mide y analiza la respuesta del material. Se pretende correlacionar los resultados con las variaciones microestructurales sufridas por el material tras dichas modificaciones de proceso. En particular, se analizan parámetros relacionados con la desestabilización de la austenita, con el medio de enfriamiento en el temple, con las condiciones de revenido y en ocasiones, con un posible tratamiento superficial de nitruración. La metodología general de investigación seguida fue la aplicación de varios Diseños de Experimentos fraccionados [83] , donde se analizan una serie de factores, ejecutando 8 experimentos por diseño. Los resultados permitirán a los fabricantes de este material diseñar el tratamiento térmico más adecuado para que el material ofrezca una elevada resistencia al desgaste en las industrias anteriormente señaladas.

Tabla 3. Composición Química (% en peso).

C	Si	Mn	Cr	Mo
2.9	1.2	0.8	18.1	1.8

Tabla 4. Composición Química (% en peso).

C	Si	Mn	Cr	Mo
2.7	1.2	0.8	25.1	0.5

1.9- Publicaciones JCR derivadas de la Tesis Doctoral y resumen de los principales objetivos alcanzados en cada publicación.

(a) En este trabajo se analizan diferentes tiempos de desestabilización de la austenita a 1000ºC para analizar la influencia de dos cinéticas complementarias sobre la resistencia al desgaste erosivo. Estas cinéticas son: a) la desestabilización de la austenita para la precipitación de carburos secundarios y la reducción de austenita retenida; b) la disolución de carburos eutécticos precipitados en condiciones de no equilibrio. *Este ha sido el objetivo del primer artículo:* ***"Erosive Wear Resistance Regarding Different Destabilization Heat Treatments of Austenite in High Chromium White Cast Iron, Alloyed with Mo".***

(b) El objetivo del primer diseño de experimentos fue analizar la dureza y resistencia al desgaste erosivo de una fundición blanca hipoeutéctica que contiene 18% Cr y 2% Mo analizando seis

factores, realizando un total de ocho experimentos. Específicamente, se analizaron los parámetros relacionados con la desestabilización de la austenita, siendo estos la temperatura y la permanencia de tiempo a esta temperatura de desestabilización. Parámetros relacionados con el medio de enfriamiento y el revenido. Dentro de este último tratamiento térmico, se analizaron las condiciones de temperatura, tiempos de revenido y número de revenidos. Este ha sido el objetivo del segundo artículo: ***"Influence of Thermal Parameters Related to Destabilization Treatments on Erosive Wear Resistance and Microstructural Variation of White Cast Iron Containing 18% Cr. Application of Design of Experiments and Rietveld Structural Analysis".***

(c) El objetivo del segundo y último diseño de experimentos de 6 factores y 8 experimentos en la fundición blanca de 18%Cr fue el de analizar la influencia de las variables del proceso relacionadas con la austenización, el temple y revenido, y la opción de un posible tratamiento superficial de nitruración posterior en esta fundición para averiguar si influye de manera satisfactoria en la dureza y la resistencia al desgaste erosivo, siendo esto, un aspecto totalmente novedoso en este tipo de fundiciones. Este ha sido el objetivo del tercer artículo: ***"Optimization, by Means of a Design of Experiments, of Heat Processes to Increase the Erosive Wear Resistance of White Hypoeutectic Cast Irons Alloyed with Cr and Mo".***

(d) El primer estudio de la fundición blanca con 25%Cr consistió en optimizar la resistencia al desgaste erosivo mediante la aplicación de un Diseño de Experimentos similar al primero realizado en la fundición 18%Cr, solo que en este caso se eliminó como factor el número de revenidos y se añadió como factor un tratamiento isotérmico previo, de perlitización de la austenita para facilitar las labores de mecanizado. El objetivo fue correlacionar los resultados con las variaciones microestructurales que el material sufre después de estas modificaciones de proceso. En particular, los parámetros relacionados con la desestabilización de la austenita, el medio de enfriamiento de temple y las condiciones de revenido. Este ha sido el objetivo del cuarto artículo: ***"Optimization of Thermal Processes Applied to Hypoeutectic White Cast Iron containing 25% Cr Aimed at Increasing Erosive Wear Resistance".***

(e) El objetivo del segundo estudio de la fundición aleada con 25%Cr, fue el de analizar la influencia de factores relacionados con la desestabilización de la austenita, temple y revenido sobre el porcentaje de los diferentes carburos que se forman, el porcentaje de martensita y el porcentaje de austenita retenida. Un objetivo secundario es determinar cómo la variación de estos factores de procesamiento afectan a la dureza del material. Se analizaron cinco factores, realizando ocho experimentos. Este ha sido el objetivo del quinto artículo: ***"Influence of Thermal Processing Factors, Linked to the Destabilisation of Austenite, on the Microstructural Variation of a White Cast Iron Containing 25% Cr and 0.6% Mo".***

(f) El objetivo del tercer trabajo de la fundición aleada con 25%Cr, fue analizar el efecto de un tratamiento de nitruración iónica, junto con la variación deliberada de diferentes parámetros térmicos asociados a la desestabilización de la austenita sobre la resistencia al desgaste erosivo. La metodología de investigación seguida fue la de un diseño de experimentos con 6 factores y 8 experimentos. Este ha sido el objetivo del sexto artículo: ***"The Joint Effects of Nitriding and Parameters Related to the Destabilisation of Austenite on Wear Resistance in White Cast Iron with 25% Cr".***

(g) El objetivo del cuarto trabajo de la fundición aleada con 25%Cr, fue el de optimizar el tratamiento térmico adecuado centrándose en la desestabilización de la austenita a diferentes temperaturas a las utilizadas en estudios anteriores y en tratamientos de revenido para aumentar la resistencia al desgaste abrasivo con arena seca evitando la merma drástica de tenacidad al impacto de estas fundiciones. La metodología de investigación seguida fue la de un diseño de experimentos con 4 factores y 8 experimentos. Este ha sido el objetivo del séptimo artículo: ***"Improvement of Impact Toughness and Abrasion Resistance of a 3C-25Cr-0.5Mo Alloy Using a***

Design of Experiment Statistical Technique: Microstructural Correlations after Heat Treatments".

(h) El objetivo del quinto trabajo de la fundición aleada con 25%Cr, fue aplicar el mismo diseño de experimentos anterior, pero en este caso se buscó aumentar la resistencia al desgaste adhesivo para simular otras condiciones no contempladas en el desgaste abrasivo de arena, minimizando la pérdida de tenacidad absorbida por el material mediante el ensayo de flexión en tres puntos. *Este ha sido el objetivo del octavo artículo*: ***"Evaluation of Hardness, Sliding Wear and Strength of a Hypoeutectic White Iron with 25%Cr after Heat Treatments".***

2. PARTE EXPERIMENTAL

2.1- Diseño de experimentos y principales conceptos.

2.1.1- Introducción.

En la industria, las técnicas de diseño y análisis de experimentos se utilizan básicamente en dos áreas: el diseño o mejora de productos y el diseño o mejora de procesos. En la actualidad, tanto los productos como los procesos son tan complejos, que resulta casi imposible encontrar maneras de mejorarlos a base de consideraciones de tipo teórico.

Los modelos teóricos son útiles para describir las grandes líneas de comportamiento de los productos y procesos, pero no suelen servir para describir y mejorar el proceso concreto, por ser con mucha frecuencia excesivamente complejo. En estos casos puede ser muy útil una descripción limitada a la zona de interés, con un rango de variación de los factores restringido obtenida a partir de la experimentación.

Experimentar es variar deliberadamente las condiciones habituales de trabajo para encontrar mejores maneras de proceder y ganar al mismo tiempo un conocimiento más profundo sobre el comportamiento del producto o del proceso. El problema básico es decidir qué conjunto de pruebas pondrán de manifiesto de forma clara y con menor esfuerzo los aspectos más relevantes del problema.

El principal inconveniente al diseño de experimentos es que se ha de tener una buena formación previa en el área de conocimiento donde se va a aplicar y una importante inversión en tiempo, materias primas, etc. Esto provoca que en la investigación el número de experimentos tiene que ser limitado. Por tanto, el objetivo es obtener la máxima información con el mínimo de recursos.

Hay tres tipos de estrategias experimentales:

a) Experimentar sin planificar.

Se usa la intuición para realizar pruebas, sin excesivo orden por iniciativas personales aprovechando momentos de relajación de la carga de trabajo para llevarlos a cabo.

b) Decidir de primeras cómo se va a invertir todo el presupuesto.

Consiste en decidir de entrada en qué condiciones se van a realizar todos y cada uno de los experimentos que permite el presupuesto disponible. Esta decisión se realiza tras haber considerado los objetivos del experimento y estudiado todos los aspectos que por razones teóricas o de experiencia se conocen sobre el problema en cuestión.

c) Estrategia secuencial.

En este caso, tras considerar los objetivos y recursos disponibles, se decide en qué condiciones se van a realizar un reducido número de experimentos. De esta manera, los conocimientos adquiridos en esta fase se utilizan para decidir en qué condiciones realizar los siguientes. Lo recomendable es invertir un 40% del presupuesto en una primera decisión.

Esta última es, sin duda, la más recomendable, pues reserva una parte del presupuesto para aclarar las cuestiones confusas que hayan surgido (algo que sucede con mucha frecuencia) como consecuencia del análisis del primer experimento y además permite aproximarse paulatinamente

a la zona donde los resultados son óptimos invirtiendo en ella un mayor número de experimentos.

Los diseños que permiten experimentar todas las combinaciones de variables y niveles se denominan diseños factoriales, presentando una serie de ventajas como permitir ser utilizados secuencialmente, acercarse al óptimo y estimar interacciones y proporcionar estimaciones de los efectos de las variables estudiadas con una varianza reducida, además de ser relativamente sencillos de construir y analizar.

Su principal inconveniente es que requieren de un gran número de experimentos, cuya solución, es la utilización de un diseño factorial fraccionado, que es el utilizado en esta investigación.

2.1.2- Conceptos de interacción, efecto y resolución.

Interacción: Para explicar este concepto se va a hacer uso de un buen ejemplo propuesto en el curso de diseño de experimentos de la Asociación Española para la Calidad.

En él se expone el efecto conocido que tiene en el organismo una dosis moderada de alcohol (euforia) y el efecto que tiene un medicamento clásico para tratar los síntomas de la gripe (disminuir la fiebre, bienestar). Representando los efectos de estos factores (alcohol y medicamento) gráficamente en la figura 29, se obtiene lo siguiente:

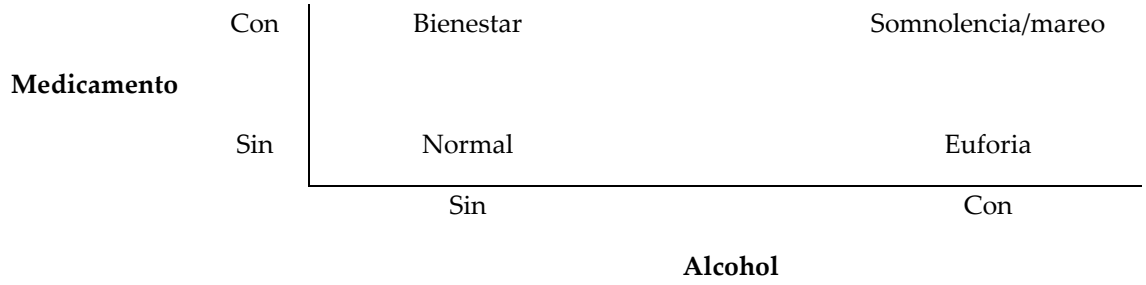

Figura 29. Representación de la interacción medicamento-alcohol [83].

Si se ingieren las dos cosas, la intuición parece indicar que se debería de sentir sensación de euforia y bienestar. Sin embargo, la experiencia y la medicina demuestran que la sensación producida será de somnolencia y mareo, un caso típico de interacción, donde los efectos producidos por los factores considerados no son aditivos.

Esto ocurre con frecuencia en los procesos industriales donde es común que, en procesos complejos, no siempre éstos funcionen igual y lo que un día parece funcionar mejor, a la semana siguiente es otra distinta. Esta situación es, casi con seguridad, el reflejo de las interacciones.

Para las variables cuantitativas, los efectos principales e interacciones se pueden asociar con los términos de un desarrollo de Taylor de la función respuesta, por lo que al despreciar interacciones de tercer orden se estarían despreciando los términos de tercer orden del desarrollo de Taylor. Esto posibilita la realización de diseños de experimentos fraccionados, reduciendo el número de experimentos, pero asumiendo un posible error que se deriva de despreciar interacciones entre factores. El objetivo de utilizar un enfoque fraccionario no es hacer un buen ajuste, sino tratar de averiguar qué factores tienen una influencia significativa sobre la variable respuesta. El grado de

ajuste de esta función dependerá de la "curvatura" de la función respuesta en la zona de trabajo y del grado de fraccionamiento. La zona de trabajo queda definida por los niveles de los factores estudiados.

Efecto: Se define efecto de un factor a la variación de la función respuesta como consecuencia de la variación de dicho factor. Se definen los efectos principales como aquellos efectos sobre la función respuesta derivados de cada factor por separado, es decir, el cambio de la función respuesta al variar un determinado factor de su nivel más bajo, -1, a su nivel más alto, +1.

Resolución: Cabe señalar que cuando a dos efectos les corresponden la misma columna de signos se dice que están confundidos, y que el contraste lineal definido por esa columna estima la suma de sus efectos. La resolución de un diseño indica el nivel de confusiones que se presentan en la estimación de los efectos, es decir, representa la pérdida de información de posibles interacciones entre factores. En general, un diseño de experimentos de resolución N es aquel en el que ningún efecto de k factores está confundido con otro que contenga menos de N-k factores. Un ejemplo de Diseño de Experimentos planteado en el que su resolución sea IV, los efectos principales están confundidos con interacciones de 3 factores. Compruébese que 4 (resolución) = 1(efectos principales) + 3 (interacciones de 3 factores) o bien se confunden interacciones de 2 entre sí. O si por ejemplo la resolución es 3, se confunden efectos principales con interacciones de 2.

2.1.3-Variabilidad de la respuesta.

En la práctica, ningún sistema es totalmente determinista. Es decir, si se repiten exactamente las mismas acciones varias veces, no siempre se obtiene exactamente el mismo resultado. Ello es debido a que, en el complejo mundo de la industria, cada característica depende de un gran número de variables incontrolables, como las condiciones ambientales, diferencias en materias primas, operarios, etc. Este tipo de variables son las que provocan esa fluctuación en principio no explicada y que se suele denominar parte aleatoria o fluctuación, y que provoca variaciones en la respuesta sin ser consideradas en el modelo.

Centrándose en una de las grandes contribuciones de G. Taguchi, se puede centrar el objetivo de la investigación en conseguir, con rigor estadístico, reducir la variabilidad de la respuesta provocada por algunas de las variables no consideradas inicialmente en el modelo que se sabe que pueden afectar a la respuesta, pero que son imposibles de controlar.

2.1.4-Diseños factoriales con las variables a dos niveles.

Los conceptos fundamentales que intervienen en el planteamiento de este tipo de diseños experimentales.

a) Respuesta: es el nombre genérico que se da a la/s característica/s estudiada/s.
b) Factores: son las variables que se consideran que pueden afectar a la/s respuesta/s y por tanto se incluyen en el diseño experimental.
c) Niveles: son los niveles que toma un factor en un determinado experimento.

La notación utilizada para referirse a los diseños factoriales es una potencia de n, del tipo n^k. La n significa que cada factor tomará n niveles y que k es el número total de factores que intervienen en la experimentación. El resultado de elevar n^k proporciona el número de experimentos que se deben realizar. En el caso, por ejemplo, de estudiar el proceso de fabricación de un muelle donde

se estudien 3 factores (longitud, grosor y tipo de acero) con dos niveles para cada factor, el diseño factorial adecuado constaría de $2^3 = 8$ experimentos.

En la industria son los diseños más utilizados debido principalmente a tres motivos:

a) Proporcionan una excelente relación entre el esfuerzo experimental y la información obtenida.
b) Son sencillos de construir, realizar, analizar e interpretar.
c) Son fáciles de combinar entre ellos para obtener otros diseños más complejos.

A la hora de realizar los experimentos, conviene aleatorizarlos, ya que ello protege contra posibles efectos de factores no considerados en el experimento e ignorados por el operario. El orden estándar sin embargo es muy conveniente para escribir la matriz de experimentos pues será de forma más ordenada.

Una vez realizado el experimento, se procede a calcular de qué manera los factores con los que se ha experimentado afectan a la respuesta.

En primer lugar, se calculan los efectos de cada factor por separado, los cuales se denominan factores principales. El efecto principal de un factor indica cuanto cambia la respuesta (en promedio) al pasar dicho factor del nivel bajo (-1) al nivel alto (+1). A continuación, se analizan las posibles interacciones entre factores.

2.1.5-Interpretación de resultados.

Que la estimación de un efecto hallada a través de la experimentación sea distinta de cero, no implica que afecte en forma detectable a la respuesta. El origen de esto reside en que cuando se determina una respuesta, está afectada por una determinada variabilidad que se transmite inevitablemente a los efectos, de forma que, si un efecto es nulo, el valor que de él se obtiene como consecuencia de la experimentación no será exactamente nulo, sino un valor en torno a cero, que puede estar tanto más alejado cuanto mayor sea la variabilidad del sistema [83].

Por tanto, una vez calculados los efectos, la primera tarea será distinguir mediante la técnica estadística más adecuada cuales son significativamente distintos de cero, es decir, cuales tienen efecto significativo.

Hay dos situaciones de partida distintas al abordar este problema. Cuando se ha replicado el experimento, y cuando el experimento se ha llevado a cabo una sola vez. Por razones obvias de economía experimental, la segunda situación es la más habitual.

La respuesta experimental está sometida a una variación aleatoria. Esta variación seguirá una ley normal, donde su desviación típica refleja el error experimental. Los efectos, son combinaciones lineales de las respuestas, por lo que, por aplicación del Teorema Central del Límite, siguen una ley normal [83].

Cada efecto principal puede considerarse una variable aleatoria donde el valor obtenido es una estimación de su media, por lo que este valor va acompañado de la estimación de su desviación típica.

Si todos los efectos fueran no significativos, éstos seguirán una ley $N(0,\sigma)$ por lo que aparecerían alineados en una representación de los efectos sobre papel probabilístico normal. Si algún efecto

resultara significativo, éste seguirá una ley $N(\mu,\sigma)$ no apareciendo alineado con los no significativos [83].

El efecto estandarizado es el cociente entre la diferencia del valor de la variable y su media con la desviación típica. Esto representa no sólo si el valor de la variable está por encima o por debajo de la media, si no también cuánto se aleja de ella. Para decidir si un efecto resulta significativo podemos comparar dicho efecto estandarizado en un papel probabilístico normal [83].

Aquellos efectos que se alejen de la recta hacia los extremos resultan significativos. Aquellos factores significativos que se alejen de la recta a su izquierda señalan que su nivel -1 hace aumentar la función respuesta respecto a su nivel +1. Aquellos factores significativos que se alejen de la recta a su derecha señalan que su nivel +1 hace aumentar la función respuesta respecto a su nivel -1.

La recta que se representa en papel probabilístico normal pasa aproximadamente por el punto (50,0), indicando que la media de la distribución es cero [83]. Asimismo, la pendiente de la recta es una representación de la variabilidad de los resultados.

Una vez calculados los efectos y hallado cuáles son significativos, lo último que queda es interpretar los resultados de los efectos principales y de las interacciones por medio de gráficos. Cabe decir que es imprescindible hacer estas interpretaciones con unos conocimientos previos consolidados sobre el problema estudiado.

2.1.6-Diseños factoriales fraccionales.

Después de explicar el diseño factorial completo, ventajas y desventajas (el elevado número de experimentos), se procede a hacer lo propio con el fraccionado, que es el utilizado en la investigación de esta Tesis Doctoral.

Dada la notación utilizada 2^k, el número de experimentos crece de manera exponencial al aumentar el número de factores analizados. En la industria e investigaciones industriales y de proceso se estudian en muchas ocasiones el efecto de 5, 6, 7 o más factores sobre una respuesta. En el caso de considerar 6 factores, habría que realizar $2^6 = 64$ experimentos, siendo tal volumen de experimentación poco productiva desde el punto de vista económico y del tiempo necesario para llevarla a cabo. Por ello, los diseños factoriales fraccionados permiten estudiar un elevado número de factores en un número de experimentos mucho menor de lo que requeriría uno factorial completo.

En la práctica resulta raro que aparezcan interacciones de tres o más factores. De hecho, se obtiene información relevante y suficiente de los comportamientos considerando solo los efectos principales y las interacciones de dos factores, dado que éstas tienen más peso que las interacciones de tres factores, y estas a su vez más que las de cuatro, y así sucesivamente [83].

Se podría, por tanto, prescindir de parte de la información que proporciona un diseño 2^6 completo, permitiendo reducir el número de experimentos. Los principales efectos y las interacciones pueden estar asociados con los términos de una serie de Taylor de la función de respuesta. Por lo tanto, al excluir las interacciones de tercer orden, los términos de tercer orden de la serie de Taylor también serían excluidos. Esto permite realizar DoE (Diseño de Experimentos) fraccionados, reduciendo el número de experimentos, pero asumiendo un posible error resultante de excluir interacciones entre factores. El patrón de confusión debería incluir

todos los efectos confundidos entre sí. Sin embargo, en muchos diseños para realizar este estudio se muestra un factor de confusión restringido en el que sólo se representan los efectos principales y las interacciones de dos factores. El uso de un enfoque fraccional no es para lograr un buen ajuste, sino para tratar de determinar qué factores tienen un efecto significativo sobre la variable respuesta.

Para estudiar los efectos de interés, será necesario con estudiar una parte (una fracción) del diseño completo, que es el caso que se está tratando en este apartado. Para los diseños fraccionados se utiliza la notación $2^{k-p,}$ donde 2 sigue siendo el número de niveles, k el número de factores y p indica el grado de fraccionamiento.

Otra justificación para la realización de este tipo de diseño fraccionado es que se cumple, en la significación de los efectos, el Principio de Pareto, donde, sobre todo, en las fases iniciales de una experimentación, se incluye, un elevado número de factores, donde sólo unos pocos son responsables de la mayor parte de las variaciones significativas en las respuestas, mientras que la mayoría de los factores producen cambios en las respuestas indistinguibles del ruido experimental.

Resumiendo todo lo anterior

La aplicación de la técnica estadística del diseño de experimentos pretende modificar deliberadamente las condiciones normales de trabajo para producir cambios en algunas de las respuestas estudiadas. Estos cambios, que son intencionados sobre las condiciones normales de trabajo se realizan sobre determinados factores productivos, previamente seleccionados. El problema básico para la aplicación de un diseño de experimentos reside en decidir qué conjunto de pruebas permiten, con la menor cantidad de recursos, alcanzar el nivel de conocimiento deseado. En los procesos industriales es habitual que unos pocos factores sean responsables de la mayor parte de las variaciones de la respuesta, resultando el resto de los factores responsables de variaciones de menor cuantía, indistinguibles del ruido experimental. Los diseños de experimentos factoriales completos requieren de un elevado número de experimentos, que crece de manera exponencial en función del número de factores estudiados. Cuando existen k factores a estudiar en un diseño de experimentos factorial completo el número de ensayos es 2^k, donde 2 es el número de niveles que aplicamos a cada uno de los factores. Los diseños factoriales fraccionales permiten estudiar un elevado número de factores con un número de experimentos mucho menor, asumiendo la pérdida de información de posibles interacciones entre factores, que en la práctica no suelen resultar muy significativas. Debe señalarse que los diseños fraccionales se simbolizan como $2_N{}^{k-p}$, donde 2 es el número de niveles, k el número de factores, p el grado de fraccionamiento, y N su resolución.

2.2- Diseños de experimentos empleados.

El primer trabajo ***"Erosive Wear Resistance Regarding Different Destabilization Heat Treatments of Austenite in High Chromium White Cast Iron, Alloyed with Mo"***, se realizó sin utilizar la técnica de diseño de experimentos empleada en el resto de los trabajos, tomándolo como un preámbulo para estudiar y tener una base sólida de lo que implicaban los procesos de desestabilización de estas aleaciones, antes de pasar a estudiar más aspectos, conllevando un grado de complejidad de la investigación más alta.

Previo a la preparación de las muestras para su estudio, el material recién fundido se sometió a un tratamiento isotérmico a 700°C durante 24 h con enfriamiento al aire para facilitar el corte de

las muestras. En total, se trataron 8 muestras a 1000°C durante 4, 8, 12 y 24 h en pares, es decir dos probetas por cada tiempo. Cada una de ellas fue sometida al temple en aceite o a un enfriamiento al aire.

En el segundo trabajo con título "***Influence of Thermal Parameters Related to Destabilization Treatments on Erosive Wear Resistance and Microstructural Variation of White Cast Iron Containing 18% Cr. Application of Design of Experiments and Rietveld Structural Analysis***", el propósito del Diseño de Experimentos (DoE) fue modificar deliberadamente ciertos parámetros de diseño de trabajo relacionados con los tratamientos térmicos, con el objetivo de generar cambios en respuestas del material. En concreto, el objetivo era analizar las variaciones de dureza y la resistencia al desgaste erosivo, así como los cambios microestructurales resultantes, correlacionando posteriormente los resultados.

El análisis de estos cambios permitió determinar cuál de los parámetros de trabajo tiene un efecto significativo sobre estas respuestas. La Tabla 4 muestra los parámetros analizados y los niveles elegidos para modificar estas condiciones de trabajo de forma ordenada.

Tabla 4. Factores y Niveles

	Factores	**Niveles**	
Código	**Parámetro metalúrgico**	**Nivel –1**	**Nivel +1**
A	Temperatura de desestabilización de la austenita (°C)	1000	1100
B	Tiempo de permanencia a la temperatura de desestabilización (h)	4	8
C	Número de revenidos	1	2
D	Medio de enfriamiento en el temple	aire	aceite
E	Temperatura de revenido (°C)	200	500
F	Tiempo de permanencia en el revenido (h)	3	6

En el tercer trabajo titulado ***"Optimization, by Means of a Design of Experiments, of Heat Processes to Increase the Erosive Wear Resistance of White Hypoeutectic Cast Irons Alloyed with Cr and Mo"***, el diseño de experimentos empleado es nuevamente un $2^{6-3} = 8$. La tabla 5 muestra los factores y niveles analizados. Los factores analizados corresponden a las variables de proceso relacionadas con el temple, revenido y posible nitruración posterior, nuevo parámetro sometido a estudio para ver qué consecuencias tiene en este tipo de aleaciones, puesto que no existen estudios previos al respecto.

Tabla 5. Factores y Niveles

	Factores	**Niveles**	
Código	**Parámetro metalúrgico**	**Nivel –1**	**Nivel +1**
A	Temperatura de desestabilización de la austenita (°C)	1000	1100
B	Tiempo de permanencia a la temperatura de desestabilización (h)	4	8
C	Nitruración	No	Si
D	Medio de enfriamiento en el temple	aire	aceite
E	Temperatura de revenido (°C)	200	500
F	Tiempo de permanencia en el revenido (h)	3	6

En el cuarto estudio denominado ***"Optimization of Thermal Processes Applied to Hypoeutectic White Cast Iron containing 25% Cr Aimed at Increasing Erosive Wear Resistance"***, el objetivo es analizar las variaciones en la resistencia al desgaste erosivo y la microestructura del material para correlacionar posteriormente el rendimiento durante su puesta en servicio con estos cambios microestructurales.

De entre los factores enumerados en la Tabla 6, es necesario aclarar el significado del factor C. Se trata de un tratamiento térmico de desestabilización de la austenita para transformarla posteriormente en perlita con el objetivo de facilitar el mecanizado de este material antes del tratamiento de endurecimiento [84]. Este tratamiento térmico consistió en 2 horas a 1000°C y posteriormente un tratamiento isotérmico a 700°C durante 24 horas.

Tabla 6. Factores y Niveles

	Factores	**Niveles**	
Código	**Parámetro metalúrgico**	**Nivel –1**	**Nivel +1**
A	Temperatura de desestabilización de la austenita (°C)	1000	1100
B	Tiempo de permanencia a la temperatura de desestabilización (h)	4	8
C	Tratamiento de ablandamiento previo al endurecimiento	Si	No
D	Medio de enfriamiento en el temple	aire	aceite
E	Temperatura de revenido (°C)	200	500
F	Tiempo de permanencia en el revenido (h)	3	6

En el quinto estudio, cuyo título es ***"Influence of Thermal Processing Factors, Linked to the Destabilisation of Austenite, on the Microstructural Variation of a White Cast Iron Containing 25% Cr and 0.6% Mo"***, se ha analizado el efecto de 5 factores con 8 experimentos. Si quisiéramos analizar todas las interacciones posibles con estos 5 factores necesitaríamos realizar 32 experimentos ($2^5 = 32$). Sin embargo, en este caso únicamente se han estimado 8 efectos (2^{5-2}). Se trataría, por tanto, de un Diseño de Experimentos fraccionado a la cuarta parte (32/4 = 8). La Tabla 7 muestra los factores analizados y los niveles de análisis. En este estudio todas las probetas son enfriadas al aire.

Tabla 7. Factores y Niveles

	Factores	**Niveles**	
Código	**Parámetro metalúrgico**	**Nivel –1**	**Nivel +1**
A	Temperatura de desestabilización de la austenita (°C)	900	1000
B	Tiempo de permanencia a la temperatura de desestabilización (h)	4	8
C	Temperatura de revenido (°C)	500	600
D	Número de revenidos	1	2
E	Tiempo de permanencia en el revenido (h)	2	4

En el sexto estudio denominado ***"The Joint Effects of Nitriding and Parameters Related to the Destabilisation of Austenite on Wear Resistance in White Cast Iron with 25% Cr"***, la metodología de investigación seguida fue la aplicación de un diseño experimental fraccionado, donde se analizaron seis factores mediante la realización de ocho experimentos (2^{6-3}), lo que significa una alta pérdida de información que, sin embargo, no es significativa en la práctica

industrial. La Tabla 8 muestra los principales parámetros del proceso con los que se realizó la nitruración en experimentos 5 a 8.

Tabla 8. Factores y Niveles

Factores		Niveles	
Código	**Parámetro metalúrgico**	**Nivel –1**	**Nivel +1**
A	Temperatura de desestabilización de la austenita (°C)	1000	1100
B	Tiempo de permanencia a la temperatura de desestabilización (h)	4	8
C	Nitruración	No	Si
D	Medio de enfriamiento en el temple	aire	aceite
E	Temperatura de revenido (°C)	200	500
F	Tiempo de permanencia en el revenido (h)	3	6

En el séptimo y octavo estudio denominados ***"Improvement of Impact Toughness and Abrasion Resistance of a 3C-25Cr-0.5Mo Alloy Using a Design of Experiment Statistical Technique: Microstructural Correlations after Heat Treatments"*** y ***"Evaluation of Hardness, Sliding Wear and Strength of a Hypoeutectic White Iron with 25%Cr after Heat Treatments"***, la metodología de investigación seguida fue la aplicación de un diseño experimental fraccionado, donde se analizaron cuatro factores mediante la realización de ocho experimentos (2^{4-1}), lo que significa una baja pérdida de información, la cuál es aún más insignificante que en el caso anterior en la práctica industrial. La Tabla 9 muestra los principales parámetros del proceso. La desestabilización fue siempre durante periodos de 5 horas.

Tabla 9. Factores y Niveles

Factores		Niveles	
Código	**Parámetro metalúrgico**	**Nivel –1**	**Nivel +1**
A	Temperatura de desestabilización de la austenita (°C) 5h	950	1050
B	Medio de enfriamiento en el temple	Horno con corriente de aire a 150ºC	Aceite
C	Temperatura de revenido (°C)	400	550
D	Tiempo de permanencia en el revenido (h)	2	6

2.3- Respuestas analizadas en estos estudios.

2.3.1- Preparación metalográfica. Microestructura óptica y electrónica.

Para la preparación de las muestras, primero se corta un cubo por experimento con la tronzadora, dentro de cada estudio anteriormente mencionado. Estos cubos son de $1cm^3$ aproximadamente. A continuación, una vez que se dispone de los cubos necesarios, se realiza el tratamiento térmico correspondiente.

Una vez finalizado el tratamiento térmico, estos cubos se cortan por la mitad con la tronzadora, y si por algún casual alguno era ligeramente más pequeño complicando esta tarea debido a la dificultad de amarre con las mordazas, se recurre a la cortadora de precisión. Posteriormente se embuten en baquelita las dos mitades, quedando vistas las caras que sufrieron este último corte.

Esta tarea se lleva a cabo debido a la descarburación que sufre la austenita al estar sometida a altas temperaturas durante varias horas en las superficies de cubo y que afectarían sin duda a los resultados de dureza, mediante los ensayos que se explicarán a continuación, falseándolos y dando resultados inferiores al valor real. Como esta descarburación puede penetrar un máximo de 2mm, al cortarlo por la mitad se asegura la no influencia de este proceso químico.

La siguiente fase es la de desbaste. En esta fase se desbaste con lijas de SiC utilizando la siguiente secuencia de granos: P-60, P-180, P-320, P-600 y P-800.

A continuación, las muestras se pulen en dos fases. La primera se realiza con disco de tela y pasta de diamante de 6μm, mientras que en la segunda y última fase se realiza con disco de pelo corto y pasta de diamante de 1μm.

Es en este punto en el que se realizan las durezas del material, de forma previa al ataque químico para visualizar la microestructura, con el objeto de facilitar con perfecta nitidez la huella que deja el penetrador Vickers en el material.

Una vez calculadas las durezas y comprobar que los resultados tienen rigor estadístico, se procede al ataque químico de las muestras. Primero se probó con Nital-2% tanto con la de 18%Cr como con la de 25%Cr. Apenas atacaba las muestras de 18%Cr dejando intacta la de 25%Cr. Este ataque no era factible, pues a la única que revelaba su microestructura, había que estar largos períodos de tiempo de ataque. Se cambió al Nital-4% además de calentar ligeramente las muestras previo al ataque en un secamanos de aire caliente del que se dispone en el laboratorio. La fundición de 18%Cr se atacó y se pudo revelar correctamente la microestructura, resistiéndose aún la de 25%Cr. Consultada la literatura técnica en revelado de estructuras, se probó para esta aleación el reactivo Fry (30ml-H_2O + 25ml-Etanol + 40ml-HCl + 5g-$CuCl_2$), dando un buen resultado y durante períodos de tiempo cortos (del orden de 2/3 segundos) se conseguió ver perfectamente la microestructura de esta aleación.

Una vez finalizada la preparación metalográfica, se utilizó el microscopio óptico modelo NIKON Epiphot 200 (Nikon, Tokio, Japón), y las imágenes fueron obtenidas mediante el analizador de imagen Omnimet Enterprise.

Algunas muestras de interés fueron analizadas también en el microscopio electrónico de barrido (SEM) JEOL JSM-5600 (Laboratorio de Óptica Electrónica de Japón, Tokio, Japón), equipado con el sistema de microanálisis por dispersión de rayos X característicos (EDX).

Cabe decir que con la experiencia adquirida a lo largo de estos trabajos se ha demostrado que, para realizar un buen análisis en el SEM, así como microanálisis por EDX, el ataque químico sufrido por las muestras es recomendable que sea ligeramente menor que para analizarlas en el microscopio óptico de reflexión.

2.3.2- Análisis cuantitativo de fases presentes en las muestras. DRX.

Las muestras para DRX se cortaron en el laboratorio partiendo de los testigos de colada, y luego se llevaron a mecanizar mediante la técnica de fresado y rectificado, puesto que, en primer lugar, las dimensiones son muy estrictas, y, en segundo lugar, el acabado superficial para que el ensayo se haga de manera adecuada tiene que ser prácticamente liso, de tal manera que se obtuviesen unas tabletas de las siguientes medidas: 50mm de largo x 30mm de ancho x 5-7mm de espesor.

Los porcentajes y tipos de fases precipitadas se determinaron por medio de difracción de rayos X. El difractómetro utilizado fue el SEIFERT XRD 3000 T / T (Baker Hughes, Celle, Alemania) empleando un confocal Bragg-Brentano con rotación inversa acoplada al detector. La radiación fue emitida a través de un tubo de Mo de enfoque fino a una potencia de trabajo de 40 kV y 40

mA, y fue monocromatizada al doblete Kα: λ1 = 0,709316 Å y λ2 = 0,713607 Å. La intensidad difractada salvo en la excepción que se hizo uso de este análisis para determinar fases que tuviesen N, fue determinada en un rango 2θ de 7 a 57º y tiempo de conteo de aproximadamente 0.03 y 22 s, respectivamente. Para el caso concreto del análisis para comprobar la existencia del CrN, la intensidad difractada se determinó en un rango de 2θ de 7 a 38° con el mismo tiempo de conteo. Para calibrar el equipo, la posición de las reflexiones y los perfiles de los picos de Bragg asociados se calibraron con el Instituto Nacional de Estándares y Tecnología (NIST) estándar Si (640C) y estándar LaB6 (660a) respectivamente.

La determinación del porcentaje de fases cristalinas se ha establecido mediante el ajuste de los difractogramas utilizando el método de afinamiento estructural Rietveld [36]. Para ello, a partir del registro de las figuras de difracción, se realizó un afinamiento estructural empleando los ficheros de información cristalográfica presentes en la base de datos de estructuras inorgánicas ICSD (versión 2016, FIZ Karlsruhe, Eggenstein-Leopoldshafen, Alemania) pertenecientes a las fases que, según la literatura técnica puede precipitarse después de los distintos tratamientos térmicos. El programa empleado fue FullProf.2k, en su versión 6.20 (2018). El incremento de la anchura observado en los picos de las fases mayoritarias se ha modelado utilizando la formulación de Stephens [85], que está implementada en este programa de análisis.

Con ello se analizaron las siguientes variables microestructurales:

- Porcentaje en peso de martensita (α').
- Porcentaje en peso de austenita (γ).
- Carburos mixtos Cr / Fe (en particular con estequiometrías 3:2, 7:3 y 23:6) y carburos mixtos de Mo_2C y Fe_3C [24, 76, 86].
- Tetragonalidad de la martensita.

2.3.3- Ensayos de Dureza del material

La metodología que se empleó para determinar la dureza de las muestras fue la siguiente:

Para la determinación de la dureza global de la muestra, como se mencionó anteriormente, se preparaba la muestra deteniéndose justo antes del ataque químico. Una vez en este punto, se midió la dureza Vickers con el durómetro Albert Gnemm, aplicando una carga en la mayoría de los trabajos de 30kgf (294,2N). Normalmente se alcanzaba un buen rigor estadístico haciendo un total de 10/12 mediciones.

Una vez realizadas las 12 indentaciones (6 en cada cara del cubo; recuérdese que el cubo se cortaba a la mitad después del tratamiento térmico para evitar influencias de descarburación), las diagonales se midieron en la lupa (Nikon SMZ 745T).

La dureza es un parámetro importante y que lógicamente no se puede despreciar, pues ofrece la dureza que tiene el material en su conjunto. Esto significa que ese dato está influenciado por la matriz austenítica transformada en la fase correspondiente junto con los carburos de desestabilización y revenido homogéneamente distribuidos en esta, y por los carburos eutécticos de solidificación. Obviamente, estos últimos no van a sufrir ninguna modificación en cuanto a dureza durante los tratamientos térmicos, al no superar nunca en la investigación la temperatura eutéctica de la aleación y, por tanto, inducir al "perlaje" de la misma.

Sin embargo, la matriz sí sufre cambios según los tratamientos térmicos sufridos, siendo el corazón de la investigación. Estos cambios se reflejan en la cantidad de austenita retenida y, por tanto, porcentaje de martensita, bainita, etc., transformada, y los carburos de desestabilización y revenido.

Por todo ello, es indispensable realizar microdurezas en el constituyente matriz sin la influencia de los carburos eutécticos, dado que pueden enmascarar o empeorar la nitidez en el resultado de posibles factores con efecto significativo que hacen que aumente la dureza del material.

Para la realización de este ensayo, las probetas se atacan ligeramente con el objetivo de diferenciar la austenita parcial o totalmente transformada de los carburos eutécticos. Y es un ataque ligero, porque si se ataca de la misma manera que para observarlas al microscopio óptico, es decir, con más severidad, se oscurece la austenita de tal manera que resulta muy complicada la medición de las diagonales de las huellas.

Una vez tenido esto en cuenta, se procede a realizar el ensayo en un microdurómetro Akashi con penetrador Vickers con carga de 50gf (0,49N), haciendo un total de 20/24 indentaciones para un buen rigor estadístico. Estas huellas se midieron en el microscopio óptico a 600 o 1000 aumentos en función del tamaño de la huella mediante el analizador de imagen Omnimet Enterprise.

Para los casos donde hubo que calcular la dureza de la capa nitrurada, se hizo un ataque muy ligero. Esto quiere decir que se ataca lo necesario para que la capa tenga un tono ligeramente más oscuro, quedando prácticamente inalterado el metal base. Esto es así porque se ha notado que la capa nitrurada se ataca extremadamente rápido, por lo que este proceso de ataque es de 1 segundo aproximadamente.

Una vez atacada la muestra se lleva al microdurómetro Akashi con penetrador Knoop y una carga de 50gf (0,49N). Las huellas se realizaron de forma escalonada o al tresbolillo, hasta el metal base.

2.3.4- Ensayos de Desgaste del material

• Para el ensayo de desgaste erosivo con la máquina Microtest MTDA/G76 se utilizaron las probetas que previamente se analizaron por DRX, por lo que las dimensiones fueron de, aproximadamente, 50x30x7mm.

Para evaluar la resistencia del material al desgaste erosivo, se midió mediante chorro de aire comprimido con partículas de corindón de tamaño de grano 50μm, según la norma ASTM G76, aplicando presiones que variaron de 2 a 4 bares, y caudales de arena de 100 g/min con un ángulo de incidencia para todos los ensayos de 30° sobre la superficie de la muestra y durante un tiempo determinado (entre 1 y 6 minutos). Se realizaron cinco repeticiones para cada experimento.

Como se señala en la mencionada norma, los resultados se muestran en mm^3 de pérdida de material por gramo de abrasivo (mm^3/g).

• Para el ensayo de resistencia al desgaste abrasivo, mediante el ensayo de vaivén según la norma ASTM G133-05, se utilizaron probetas con las mismas dimensiones (50x30x7mm) en el equipo de Microtest (Madrid) Modelo MT/60/MC_v2. Las condiciones de ensayo fueron: 30 N de peso, velocidad de giro de 150rpm, un radio de 40mm, y una distancia de 10km recorrida. La bola utilizada fue de carburo de wolframio de 4mm de diámetro.

• El ensayo de desgaste de rueda seca con arena se realizó según la norma ASTM G40-92. Las probetas son de dimensiones similares a las que se utilizaron para el resto de los ensayos

de desgate. Los parámetros de ensayo vienen recogidos en la Tabla 10. Los tiempos de ensayo fueron 10 y 30 minutos.

Tabla 10. Parámetros de ensayo de desgaste abrasivo

Diámetro de rueda	228.6 mm
Dureza de goma	60±2 Shore A
Abrasivo	Arena AF50/70
Flujo de Arena	300-400 g/min
Carga aplicada	130 N
Velocidad de giro	200 rpm

2.3.5- Ensayos de resiliencia y tenacidad del material

• La resiliencia se ha llevado a cabo mediante el péndulo Hounsfield. Este ensayo es perfectamente válido y comparable a los ensayos más conocidos, como lo son el ensayo Charpy o el Izod. La decisión de apostar por este ensayo ha sido el hecho de que se puede realizar con probetas cilíndricas, siendo éstas de las que se disponía en el material que quedaba para la investigación. En este ensayo, a diferencia de los otros dos mencionados, es la propia probeta la que va en movimiento y golpea contra dos apoyos fijos por cada uno de sus extremos, provocando una fractura en la parte central de la probeta. Este ensayo se realizó sin entalla debido a la fragilidad inherente a estas fundiciones en comparación con ciertos aceros de bajo contenido en carbono que suelen tener una gran absorción de energía, evitando un concentrador de tensiones como es cualquier tipo de entalla en la sección donde se produce la fractura al impacto.

• La tenacidad a rotura se determinó mediante el ensayo de flexión en 3 puntos con las siguientes condiciones: distancia entre rodillos, L = 30 mm; ancho (w) y espesor (t) de las probetas ensayadas, 14 mm y 3,5 mm, respectivamente; diámetro del rodillo central para la aplicación de la carga y diámetros de los rodillos de soporte: 10 mm; Velocidad de ensayo: 5 $mm \cdot min^{-1}$.

2.3.6- Representación de los resultados del diseño de experimentos

El análisis estadístico para la comparación de los efectos estandarizados en gráficos de probabilidad se realizó con la ayuda del programa Statgraphics Centurion XVI, versión 16.1.18 (Statgraphics Technologies, Inc., The Plains, VA, EE. UU.).

2.3.7- Tratamientos de nitruración

Los tratamientos de nitruración fueron llevados a cabo por la empresa de tratamientos térmicos VACUTREM, S.A ubicada en Martorelles (Barcelona). Se trató de una nitruración iónica con los siguientes parámetros de nitruración que se muestran en la Tabla 11.

Tabla 11. Parámetros utilizados en el proceso de nitruración por plasma

Gas mixto	70%N_2 + 30%H_2
Flujo de gas (cm^3/min)	500
Temperatura (°C)	540
Presión (Pa)	400
Tiempo (min)	120
Tensión de salida (V)	500

metals

MDPI

Article

Erosive Wear Resistance Regarding Different Destabilization Heat Treatments of Austenite in High Chromium White Cast Iron, Alloyed with Mo

Alejandro Gonzalez-Pociño, Florentino Alvarez-Antolin * and Juan Asensio-Lozano

Materials Pro Group, Departamento de Ciencia de los Materiales e Ingeniería Metalúrgica, Universidad de Oviedo; Independencia 13, 33004 Oviedo, Spain; UO204622@uniovi.es (A.G.-P.); jasensio@uniovi.es (J.A.-L.)

* Correspondence: alvarezflorentino@uniovi.es; Tel.: +34-985-181-949

Received: 14 April 2019; Accepted: 5 May 2019; Published: 7 May 2019

Abstract: With the aim of improving erosive wear resistance in hypoeutectic white cast irons with 18% Cr and 2% Mo, several samples of this grade were subjected to different heat treatments at 1000 ◦C to destabilize the austenite. The dwell times at this temperature varied from 4 to 24 h and the samples were cooled in air or oil. The existing phases were identified and quantified by applying the Rietveld structural refinement method. The results were correlated with the hardness of the material and with the microhardness of the matrix constituent. The greatest resistance to erosive wear was achieved in those samples that had a higher percentage of secondary carbides. The longer the dwell time at the destabilization temperature of austenite, the greater the amount of precipitated secondary carbides. However, the percentage of dissolved eutectic carbides is also higher. These eutectic carbides were formed as a result of non-equilibrium solidification. Low cooling rates (in still air) can offset this solution of eutectic carbides via the additional precipitation of secondary carbides in the 600–400 ◦C temperature range. A sharp decrease is observed in the percentage of retained austenite in those treatments with dwell times at 1000 ◦C equal to or greater than 12 h, reaching minimum values of around 2% volume. The percentage of retained austenite was always lower after oil quenching and the hardness of oil quenched samples was observed to be greater than those quenched in air. In these samples, the maximum hardness value obtained was 993 HV after a 12 h dwell, which result from the optimum balance between the percentages of retained austenite and of precipitated carbides.

Keywords: high chromium white cast iron; Rietveld refinement; secondary carbides; X-ray diffraction; retained austenite

1. Introduction

White cast irons highly alloyed with Cr are used in environments where resistance to abrasive wear is a priority requirement. Up to approximately a 16% Cr content, the eutectic constituent is ledeburitic, where the matrix phase of this constituent is mixed carbides with a 3:1 stoichiometry. However, when the weight content of Cr exceeds 16%, the eutectic constituent is no longer ledeburitic but austenite, being the matrix phase of this eutectic, while the dispersed carbides that accompany it are mixed carbides with a 7:3 stoichiometry [1], presenting a similar morphology to bars or plates [2]. Due to the high concentration of dissolved elements in solid solution, the austenite displays high hardenability, so the precipitation of martensite is obtained by cooling in air [1]. As a result of the destabilization of austenite at temperatures around 1000 °C, Cr-rich secondary carbides precipitate [3–17] which promotes enhanced abrasion resistance and an increase in the Ms temperature [18], thereby leading to a reduction in retained austenite [19]. Previous studies confirm that the longer the dwell time at the aforementioned temperature, the greater the precipitation of these carbides [2]. Other studies indicate that a higher fraction of secondary carbides could be obtained during tempering between 400 and 600 °C [20], with increasing percentages formed with higher severity quench media, for example, during cryogenic treatments [14,20,21]. The addition of Mo increases hardenability [6,22], increasing hardness [23], and enhancing wear resistance [24–26]. During high tempering processes, mixed $(Mo,X)_2C$ carbides, can nucleate heterogeneously at eutectic Cr rich carbide boundaries [10], progressing in the matrix [13]. The objectives of this paper were, on the one hand, to optimize the destabilization heat treatment of austenite and the type of quenching to increase wear resistance, and on the other, to correlate the results of hardness and wear with the microstructural variations resulting from these treatments. To this end, several samples were taken from a hypoeutectic white cast iron with 18% Cr and 2% Mo which was subjected to several destabilization heat treatments at 1000 °C, employing different dwell times ranging from 4 to 24 h and subsequent cooling in air or oil. The aim of testing several dwell times at 1000 °C was to assess the possible impoverishment in chromium and carbon of the austenite, which would lead to an increase in the Ms temperature. This increase would reduce the theoretical risk of cracking on quenching, allowing this cooling to take place in oil and producing a decrease in the retained austenite.

2. Materials and Methods

Table 1 shows the chemical composition of the white cast iron under analysis. Prior to preparing the samples, the as-cast material was subjected to an isothermal treatment at 700 °C for 24 h with air cooling to facilitate the cutting of the samples. This treatment was reported to increase hardness after subsequent quench [27]. In all, 8 samples were treated at 1000 °C for 4, 8, 12, and 24 h in pairs and then quenched in air or oil. The evolution of the material's microstructure following these heat treatments was analyzed by means of optical microscopy (Nikon, Tokyo, Japan) and scanning electron microscopy (JEOL, Nieuw-Vennep, The Netherlands). Grinding was carried out with 60, 120, 240, 400, and 600 grit size SiC paper. Subsequently, the samples were polished in two consecutive stages with 6 µm and 1 µm diamond paste, respectively. Nital 5 was used as the chemical reagent to reveal the microstructure of the material. The percentages and types of precipitated phases were determined by X-ray diffraction, employing molybdenum as the emitting metal. The diffractograms were measured on the Seifert XRD 3000 T/T diffractometer (Baker Hughes, Celle, Germany) employing a Bragg-Brentano parfocal optical configuration with reverse rotation coupled to the detector. The radiation emitted by the fine focus Mo tube, at 40 kV and 40 mA, was monochromatized to the Kα doublet: $\lambda 1$ = 0.709316 Å and $\lambda 2$ = 0.713607 Å. The patterns were recorded by means of a NaI (Tl) scintillation detector measuring the 2θ angular range. This was found to be between 12° and 56°, with a 0.025° step and a counting time per step

of 30 s. Determination of the percentage of crystalline phases was established by fitting the aforementioned diffractograms using the Rietveld structural refinement method. To do so, starting with the recording of the diffraction figures obtained in both grades, a structural refinement was carried out using the crystallographic information files present in the ICSD inorganic structures database (version 2016, FIZ Karlsruhe, Eggenstein-Leopoldshafen, Germany) belonging to the phases that, according to the technical literature, may be precipitated after the various thermal treatments. These mainly include: Martensite (α'), Austenite (γ), mixed Cr/Fe carbides (in particular with 3:2, 7:3 and 23:6 stoichiometries) and mixed Mo2C and Fe3C carbides [1,28,29]. Applying the Rietveld structural refinement method, a fitting of the diffraction experimental figures was consequently made based on the diffraction patterns of these phases.

To measure the overall hardness of each sample, the Vickers hardness was measured applying a 10 N load. Furthermore, the hardness of the eutectic constituent, without including primary carbides, was obtained applying a 0.5 N load. In all cases, 10 indentations were made in each of the samples. The diagonals of the indentations were measured under an optical microscope at 1000 magnifications.

The erosive wear resistance was measured by means of compressed air blasting with corundum particles according to the ASTM G76 standard, applying a pressure of 4 bar, a flow rate of 160 g/min and a 30◦ angle of incidence on the sample surface. Five repetitions were performed for each experimental condition. The duration of each test was set to 1 min. The dimensions of the experimental specimens corresponded to prisms of 50 by 30 by 10 mm3.

Table 1. Chemical composition of the analyzed samples (wt. %).

C	Si	Mn	Cr	Mo	S	P
3.0	1.2	0.8	18.2	2.0	0.009	0.024

3. Results

Figure 1 shows the microstructure obtained in the as-cast state. The presence of eutectic carbides and pearlite can be observed in a matrix with abundant retained austenite. A high percentage of the eutectic constituent and a relatively fine structure of this constituent are observed. This suggests the possibility of non-equilibrium solidification. By means of an isothermal treatment at 700 ◦C, the retained austenite may be transformed into pearlite, thereby favoring subsequent machining for the preparation of the samples (Figure 2).

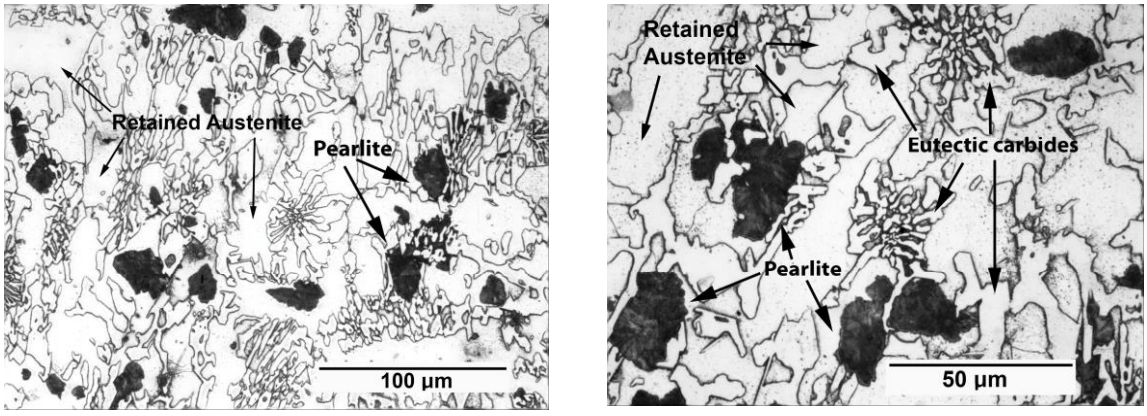

(**a**) (**b**)

Figure 1. Microstructure obtained in the as-cast state. Optical microscope: (**a**) 500 magnifications; (**b**) 1000 magnifications.

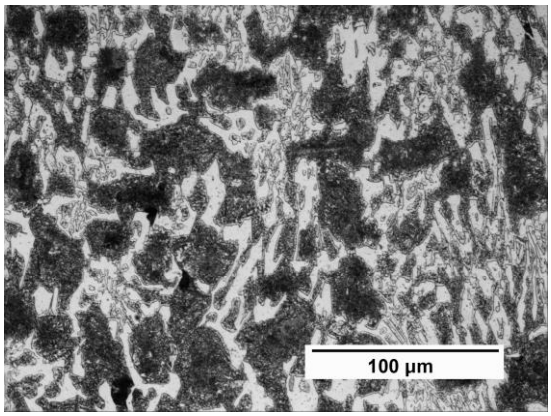

Figure 2. Microstructure after an isothermal treatment at 700 °C for 24 h. Optical microscope: 500 magnifications.

Figure 3 shows the microstructure obtained after the different heat treatments at 1000 °C used to destabilize the austenite. The microstructure is made up of proeutectic austenite and a eutectic constituent in which austenite forms the matrix phase, while the dispersed phase is formed by eutectic M_7C_3 carbides. This austenite would have been mainly transformed into martensite. The presence of secondary carbides largely precipitated in the proeutectic austenite and showing a darker coloring than the austenite of the eutectic constituent, is worth noting. The greater density of secondary carbides in the proeutectic austenite compared to the austenite of the eutectic constituent may be due to the segregation of Mo towards the eutectic liquid, favoring the enrichment of the eutectic austenite in this element, which has an inhibiting effect on the precipitation of secondary carbides [30]. The observed microstructure is a consequence of three simultaneously competing kinetics:

1. A greater density of secondary carbides with increasing dwell time at 1000 °C, which leads to an increase in the Ms temperature, thus favoring a decrease in the retained austenite.
2. Also, as the dwell time at 1000 °C is increased, the dissolution of those eutectic carbides that have precipitated as a consequence of the non-equilibrium solidification takes place.
3. Furthermore, additional precipitation of secondary carbides takes place in the 600–400 °C temperature range when the cooling rate is low (cooling in still air).

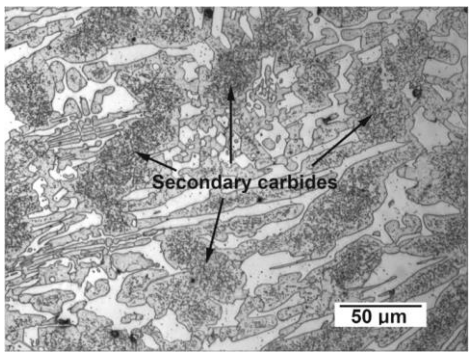

(**a**) After 4 h dwell time at 1000 °C and air quenching

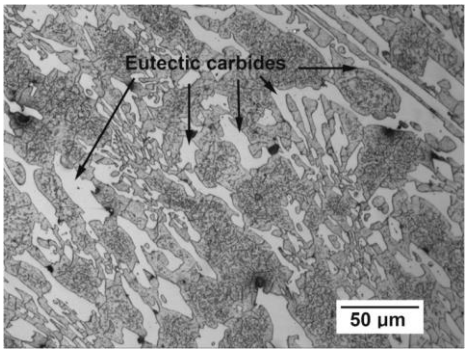

(**b**) After 8 h dwell time at 1000 °C and air quenching

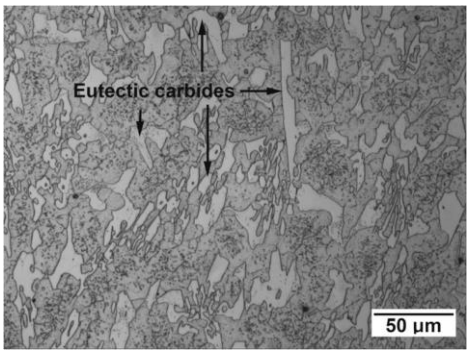

(**c**) After 12 h dwell time at 1000 °C and air quenching

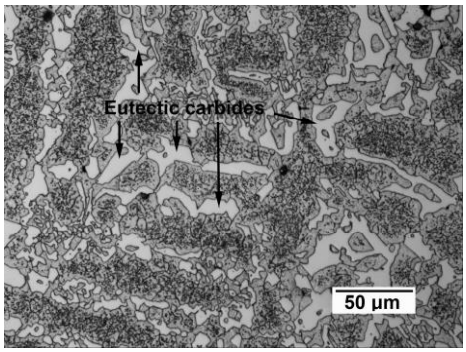

(**d**) After 24 h dwell time at 1000 °C and air quenching

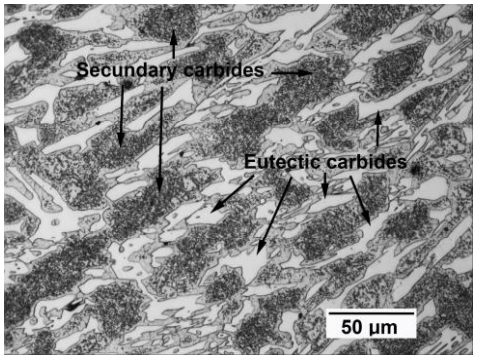

(**e**) After 4 h dwell time at 1000 °C and oil quenching

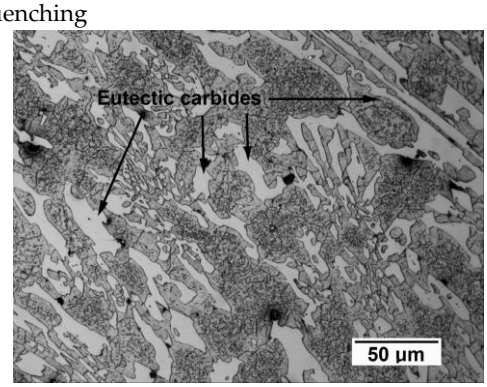

(**f**) After 8 h dwell time at 1000 °C and oil quenching

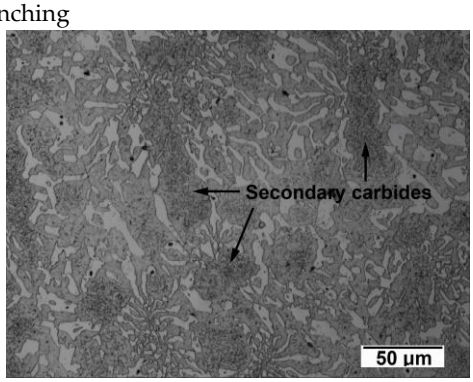

(**g**) After 12 h dwell time at 1000 °C and oil quenching

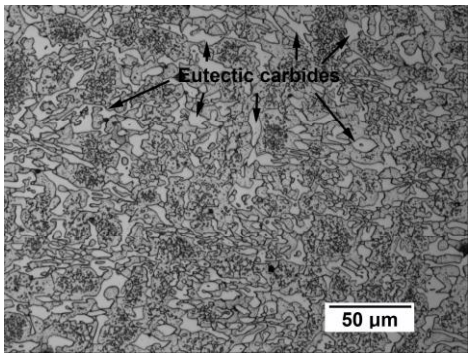

(**h**) After 24 h dwell time at 1000 °C and oil quenching

Figure3. Microstructureafterthedifferenttreatmentsfordestabilizingtheaustenite. Opticalmicroscope: 500 magnifications.

Figure 4 shows the diffractograms obtained after the different heat treatments used to destabilize the austenite. Figure 4a represents the air-quenched samples and Figure 4b, the oil-quenched samples. The Rietveld structural refinement method was used to identify the existing phases and determine their weight percentages.

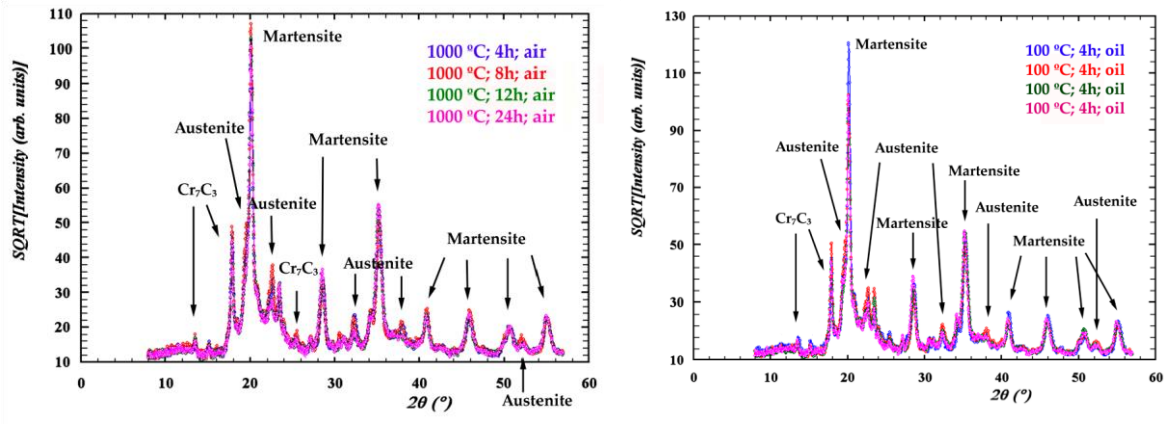

(**a**) (**b**)

Figure 4. (**a**) Diffractograms for the air-quenched samples; (**b**) diffractograms for the oil-quenched samples.

Table 2 shows the volume percentages of the identified phases in each diffractogram. The percentage of retained austenite is always seen to be lower in the oil-quenched samples. In general, an abrupt decrease in the percentage of retained austenite is observed in the destabilization treatments with a dwell time of 12 and 24 h compared to those lasting 4 and 8 h. On the other hand, it can be seen that the precipitated carbides are all of the M_7C_3 type. The specimens cooled in air showed a smaller difference between the percentages by volume of total carbides, ranging between 52% and 55%. However, these variations were found to be greater in the samples quenched in oil, whose values were comprised between 43% to 56%. In both cases, the overall percentage of carbides is a consequence of the following:

- The longer the dwell time at 1000 °C, the greater the percentage of precipitated secondary carbides.
- The longer the dwell time at 1000 °C, the greater the percentage of eutectic carbides that dissolve. These eutectic carbides will be those formed as a result of non-equilibrium solidification. It should be noted that the solubility limit of the C in the austenite will increase until 1000 °C is reached.
- Moreover, additional precipitation of secondary carbides in the 600–400 °C temperature range is produced in air-cooled samples. This precipitation tends to offset the dissolution of eutectic carbides.
- In the oil-quenched samples, the lowest percentage of total carbides is obtained in the samples with the shortest and longest dwell times at the destabilization temperature, i.e., 4 and 24 h, respectively. Four hours at 1000 °C is not enough time for a significant number of secondary carbides to precipitate. After 24 h at 1000 °C, the dissolution of eutectic carbides has offset the precipitation of secondary carbides. The highest percentage of carbides is obtained after 8 h dwell time at 1000 °C, subsequently decreasing slightly after a dwell time of 12 h and once again reaching the minimum percentage of carbides after a dwell time of 24 h. The comparison between the samples with a 4 h dwell time at 1000 °C and respective cooling in air and oil is worth highlighting. The samples that were cooled in air reach 55.17% by volume of carbides; however, those cooled in oil only reach 43.33%. The slower cooling equivalent to a staircase where horizontal sections are longer than if the cooling was faster. This would favor the precipitation of new secondary carbides in the temperature range between 600 and 400 °C.

Table 2. Microstructural parameters and weight distributions of the precipitated phases. Esd represents the statistical error.

Quenching (Destabilization Heat Treatment at 1000 °C)		Rietveld Fitting	Phases	Bragg R-Factor	Volume %	Esd.
Air	4 h	Rwp = 9.66 Chi² = 2.37	α′ γ M_7C_3	1.5 4.76 2.72	36.59 8.24 55.17	±094 ±0.41 ±1.51
	8 h	R_{wp} = 11 Chi² = 2.77	α′ γ M_7C_3	1.04 7.86 4.5	35.48 9.94 54.58	±0.91 ±0.44 ±1.47
	12 h	Rwp = 10.2 Chi² = 2.62	α′ γ M_7C_3	4.39 5.54 3.71	45.63 2.61 51.76	±1.07 ±0.29 ±1.50
	24 h	Rwp = 10.7 Chi² = 2.74	α′ γ M_7C_3	5.34 6.15 4.58	44.30 2.83 52.87	±1.1 ±0.3 ±1.54
Oil	4 h	Rwp = 11.3 Chi² = 2.77	α′ γ M_7C_3	3.96 8.28 8.82	50.09 6.59 43.33	±1.49 ±0.42 ±1.63
	8 h	Rwp = 10.9 Chi² = 1.99	α′ γ M_7C_3	3.43 3.85 4.69	36.53 6.94 56.52	±1.17 ±0.57 ±1.80
	12 h	Rwp = 11.7 Chi² = 2.67	α′ γ M_7C_3	8.16 8.9 8.12	44.84 2.26 52.90	±1.39 ±0.45 ±1.84
	24 h	Rwp = 11.6 Chi² = 2.45	α′ γ M_7C_3	6.44 9.1 8.47	51.35 2.22 46.43	±1.57 ±0.48 ±1.81

Figure 5 shows a representative image of both cases, where it can be seen that the density and size of secondary carbides is significantly lower when the cooling takes place in oil.

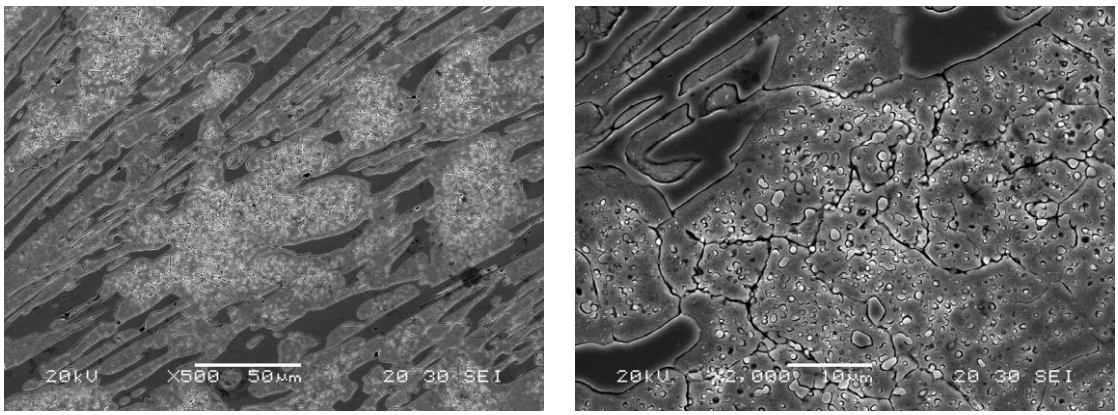

(**a**) (**b**)

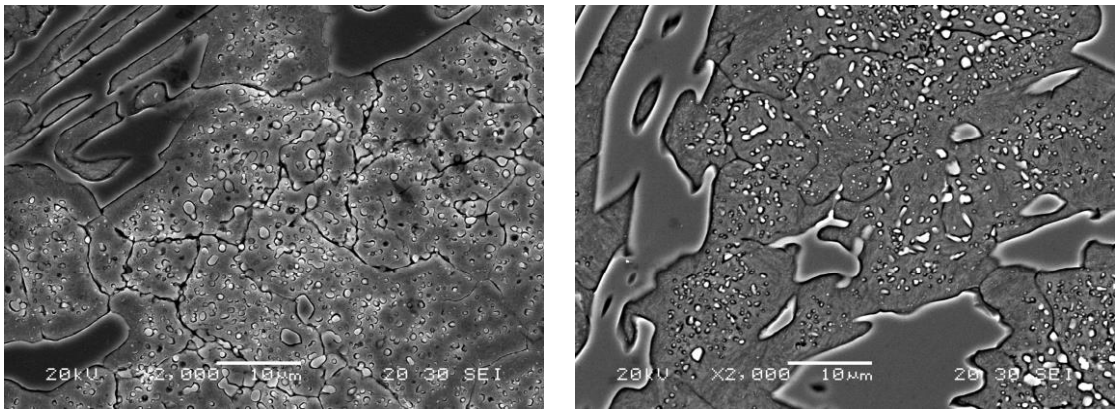

(**c**) (**d**)

Figure 5. Comparison of the density of secondary carbides in samples subjected to destabilization heat treatments of 4 h and quenching in air or oil. Scanning electron microscope; (**a**) quenching in air. 500×; (**b**) quenching in air. 2000×; (**c**) quenching in oil. 500×; (**d**) quenching in oil. 2000×.

Figure 6 shows the hardness values obtained. Figure 6a shows the hardness of the material applying a 10 N load. Note that the hardness is always higher after oil quenching. In air quenching, the hardness is also found to increase with increasing dwell time at the destabilization temperature,

while the retained austenite decreases. However, among the samples quenched in oil, the highest hardness was obtained when the destabilization heat treatment lasted 12 h, in which a very low amount of retained austenite (2.26%) and a high amount of carbides (52.90%) were obtained. Figure 6b shows the microhardness values obtained in the matrix constituent applying a 0.5 N load. In this case, the highest hardness among the samples quenched in oil is once again obtained after 12 h dwell time at 1000 °C, which is when the optimum balance between retained austenite and secondary carbides is reached. When the dwell time is 24 h, there is a decrease in the total percentage of carbides (to 46.43%). In the case of the air-quenched samples, in which the percentage of carbides under goes a much lower variation than in those quenched in oil, the highest hardness of the matrix constituent is obtained in the sample subjected to the destabilization heat treatment at 1000 °C for 24 h, resulting in a lower percentage of retained austenite.

Figure 7 shows the results obtained after the wear test. The error bar shows the difference between the average value and the maximum and minimum values reached.

In the case of the specimens that were cooled in the air, the highest wear resistance is obtained after 4 and 24 h of dwell at the destabilizing temperature, which correspond to the samples with a higher percentage by weight of carbides. And yet the treatment of 4 h at 1000 °C provided the lowest hardness value. This is thought to be related to the high presence of retained austenite leading to a somewhat lower hardness, and the higher fraction of secondary carbides conducting to a better performance in the erosive wear testing in turn. In contrast to this, the sample that remained 24 h at 1000 °C displayed the highest hardness, and the lowest austenite retained.

In the case of the specimens that were oil quenched, a maximum in the wear resistance were obtained after 8 and 12 h of austenite destabilization, which corresponds to the samples for which the highest percentage of secondary carbides were measured. Out of these, the sample which was subjected to a 12 h destabilization treatment and checked to have a higher hardness had a lower percentage of retained austenite in its microstructure. It then follows that an optimal resistance to erosive wear could be achieved with the highest percentage of secondary carbides formed during the destabilization of austenite. And it seems less relevant for improved wear resistance the resulting hardness achieved by martensite, carbides, and retained austenite

[11,13,17]. In turn, the percentage of secondary carbides formed over destabilization period seems to be influenced, not only by the dwell time at the destabilization temperature, but also by the cooling rate.

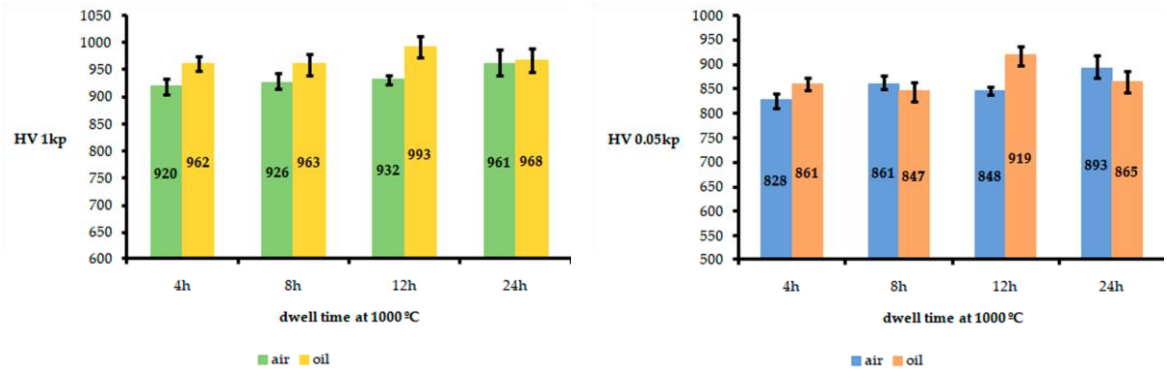

(**a**) (**b**)

Figure 6. Hardness values. The error bars show the distance between the mean value and the maximum and minimum values. Ten (10) indentations were made in each sample; (**a**) hardness values obtained in the overall microstructure applying a 10 N load; (**b**) hardness values obtained in the constituent matrix applying a 0.5 N load.

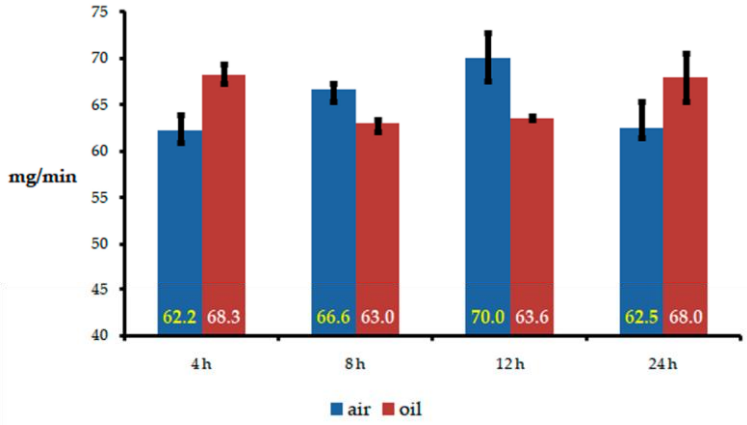

Figure 7. Resistance to erosive wear. Weight loss per unit of time.

4. Conclusions

After performing different heat treatments at 1000 °C to destabilize the austenite in white cast irons with 18% Cr and 2% Mo, with quenching in air and oil, the following conclusions may be drawn:

- The longer the dwell time at the destabilization temperature of austenite (1000 °C), the greater the amount of precipitated secondary carbides. However, the percentage of dissolved eutectic carbides is also higher. These dissolved eutectic carbides will have been formed as a result of non-equilibrium solidification. Low cooling rates (in still air) can offset this solution of carbides via the additional precipitation of secondary carbides in the 600–400 °C temperature range.
- The erosive wear resistance depends mainly on the volume fraction of secondary carbides precipitated during the destabilization of austenite. The maximum wear resistance in air cooled samples corresponded to a destabilizing treatment at 1000

°C for 4h and 24 h. However, in those samples quenched in oil, the maximum wear resistances were obtained on those samples destabilized at 1000 °C for 8 h and 12 h.

- There is a sharp decrease exists in the percentage of retained austenite in those treatments with dwell times at 1000 °C equal to or greater than 12 h, reaching minimum values of around 3 wt. %.
- In the oil-quenched samples, the lowest percentage of carbides obtained is 43–46% after dwell times of 4 h and 24 h, reaching a maximum value of 56% when employing a dwell time of 8 h.
- In the air-quenched samples, an increase in hardness is observed with increasing dwell time at the destabilization temperature and as the retained austenite decreases, obtaining a maximum hardness of 961 HV after a dwell time of 24 h. In the oil-quenched samples, however, the maximum hardness was 993 HV after a dwell time of 12 h, which is when an optimum balance is obtained between the percentages of retained austenite and the percentages of precipitated carbides.

Author Contributions: J.A.-L. conceived and designed the investigation; A.G.-P. performed all laboratory work; F.A.-A. led the investigation, analyzed the data and wrote the paper.

Funding: This research received no external funding

Conflicts of Interest: The authors declare no conflict of interest.

References

1. Pero-Sanz, J.A. *Fundiciones Férreas*; Dossat: Madrid, Spain, 1994; p. 154.
2. Bedolla-Jacuinde, A.; Arias, L.; Hernandez, B. Kinetics of secondary carbides precipitation in a high-chromium white iron. *J. Mater. Eng. Perform.* **2003**, *12*, 371–382. [CrossRef]
3. Powell, G.L.F.; Bee, J.V. Secondary carbide precipitation in an 18 wt.% Cr-1 wt.% Mo white iron. *J. Mater. Sci.* **1996**, *31*, 707–711. [CrossRef]
4. Zhi, X.H.; Xing, J.D.; Gao, Y.M.; Fu, H.G.; Peng, J.Y.; Xiao, B. Effect of heat treatment on microstructure and mechanical properties of a Ti-bearing hypereutectic high chromium white cast iron. *Mater. Sci. Eng. A* **2008**, *487*, 171–179. [CrossRef]
5. Carpenter, S.D.; Carpenter, D.; Pearce, J.T.H. XRD and electron microscope study of a heat treated 26.6% chromium white iron microstructure. *Mater. Chem. Phys.* **2007**, *101*, 49–55. [CrossRef]
6. Karantzalis, A.E.; Lekatou, A.; Diavati, E. Effect of Destabilization Heat Treatments on the Microstructure of High-Chromium Cast Iron: A Microscopy Examination Approach. *J. Mater. Eng. Perform.* **2009**, *18*, 1078–1085. [CrossRef]
7. Kootsookos, A.; Gates, J.D. The role of secondary carbide precipitation on the fracture toughness of a reduced carbon white iron. *Mater. Sci. Eng. A* **2008**, *490*, 313–318. [CrossRef]
8. Efremenko, V.; Shimizu, K.; Chabak, Y. Effect of Destabilizing Heat Treatment on Solid-State Phase Transformation in High-Chromium Cast Irons. *Metall. Mater. Trans. A* **2013**, *44*, 5434–5446. [CrossRef]
9. Liu, Q.; Shibata, H.; Hedstrom, P.; Joonsson, P.G.; Nakajima, K. Dynamic Precipitation Behavior of Secondary M7C3 Carbides in Ti-alloyed High Chromium Cast Iron. *Isij Int.* **2013**, *53*, 1237–1244. [CrossRef]
10. Wiengmoon, A.; Pearce, J.T.H.; Chairuangsri, T. Relationship between microstructure, hardness and corrosion resistance in 20 wt. % Cr, 27 wt. % Cr and 36 wt. % Cr high chromium cast irons. *Mater. Chem. Phys.* **2011**, *125*, 739–748. [CrossRef]

11. Bedolla-Jacuinde, A.; Guerra, F.V.; Mejia, I.; Zuno-Silva, J.; Rainforth, M. Abrasive wear of V-Nb-Ti alloyed high-chromium white irons. *Wear* **2015**, *332*, 1006–1011. [CrossRef]
12. Lai, J.P.; Pan, Q.L.; Sun, Y.W.; Xiao, C.A. Effect of Si Content on the Microstructure and Wear Resistance of High Chromium Cast Iron. *ISIJ Int.* **2018**, *58*, 1532–1537. [CrossRef]
13. Antolin, J.F.A.; Garrote, L.F.; Lozano, J.A. Application of Rietveld Refinement to the correlation of the microstructure evolution of white cast irons with 18 and 25%-wt. Cr after oil quench and successive temper treatments, with abrasive wear and bending testing. *Rev. Metal.* **2018**, *54*, 11. [CrossRef]
14. Wang, J.; Xiong, J.; Fan, H.Y.; Yang, H.S.; Liu, H.H.; Shen, B.L. Effects of high temperature and cryogenic treatment on the microstructure and abrasion resistance of a high chromium cast iron. *J. Mater. Process. Technol.* **2009**, *209*, 3236–3240. [CrossRef]
15. Liu, H.H.; Wang, J.; Yang, H.S.; Shen, B.L. Effects of cryogenic treatment on microstructure and abrasion resistance of CrMnB high-chromium cast iron subjected to sub-critical treatment. *Mater. Sci. Eng. A* **2008**, *478*, 324–328. [CrossRef]
16. Filipovic, M.M. Iron-chromium-carbon-vanadium white cast irons—The microstructure and properties. *Hemijska Industrija* **2014**, *68*, 413–427. [CrossRef]
17. Guitar, M.A.; Suarez, S.; Prat, O.; Guigou, M.D.; Gari, V.; Pereira, G.; Mucklich, F. High Chromium Cast Irons:
    Destabilized-Subcritical Secondary Carbide Precipitation and Its Effect on Hardness and Wear Properties.
    J. Mater. Eng. Perform. **2018**, *27*, 3877–3885. [CrossRef]
18. Jia, X.S.; Hao, Q.G.; Zuo, X.W.; Chen, N.L.; Rong, Y.H. High hardness and toughness of white cast iron: The proposal of a novel process. *Mater. Sci. Eng. A* **2014**, *618*, 96–103. [CrossRef]
19. Gasan, H.; Erturk, F. Effects of a Destabilization Heat Treatment on the Microstructure and Abrasive Wear
    Behavior of High-Chromium White Cast Iron Investigated Using Different Characterization Techniques. *Metall. Mater. Trans. A* **2013**, *44*, 4993–5005. [CrossRef]
20. Liu, H.H.; Wang, J.; Shen, B.L.; Yang, H.S.; Gao, S.J.; Huang, S.J. Effects of deep cryogenic treatment on property of 3Cr13Mo1V1.5 high chromium cast iron. *Mater. Des.* **2007**, *28*, 1059–1064. [CrossRef]
21. Yang, H.S.; Wang, J.; Shen, B.L.; Liu, H.H.; Gao, S.J.; Huang, S.J. Effect of cryogenic treatment on the matrix structure and abrasion resistance of white cast iron subjected to destabilization treatment. *Wear* **2006**, *261*, 1150–1154. [CrossRef]
22. Inthidech, S.; Sricharoenchai, P.; Matsubara, Y. Effect of molybdenum content on subcritical heat treatment behaviour of hypoeutectic 16 and 26 wt-% chromium cast irons. *Int. J. Cast Met. Res.* **2012**, *25*, 257–263. [CrossRef]
23. Cetinkaya, C. An investigation of the wear behaviours of white cast irons under different compositions. *Mater. Des.* **2006**, *27*, 437–445. [CrossRef]
24. Li, Y.C.; Li, P.; Wang, K.; Li, H.Z.; Gong, M.Y.; Tong, W.P. Microstructure and mechanical properties of a Mo alloyed high chromium cast iron after different heat treatments. *Vacuum* **2018**, *156*, 59–67. [CrossRef]
25. Oh, H.; Lee, S.; Jung, J.Y.; Ahn, S. Correlation of microstructure with the wear resistance and fracture toughness of duocast materials composed of high-chromium white cast iron and low-chromium steel. *Metall. Mater. Trans. A* **2001**, *32*, 515–524. [CrossRef]
26. Scandian, C.; Boher, C.; de Mello, J.D.B.; Rezai-Aria, F. Effect of molybdenum and chromium contents in sliding wear of high-chromium white cast iron: The relationship between microstructure and wear. *Wear* **2009**, *267*, 401–408. [CrossRef]

27. Wiengmoon, A.; Khantee, J.; Pearce, J.T.H.; Chairuangsri, T. Effect of pre-annealing heat treatment on destabilization behavior of 28 wt. % Cr-2.6 wt. % C high-chromium cast iron. In Proceedings of the 7th Global Conference on Materials Science and Engineering (CMSE2018), Xi'an, China, 1–4 November 2018.
28. Fairhust, W.; Rohrig, K. Abrasion resistant high chromium cast irons. *Foundry Trade J.* **1974**, *136*, 685–698.
29. Wang, J.; Li, C.; Liu, H.H.; Yang, H.S.; Shen, B.L.; Gao, S.J.; Huang, S.J. The precipitation and transformation of secondary carbides in a high chromium cast iron. *Mater. Charact.* **2006**, *56*, 73–78. [CrossRef]
30. Efremenko, V.G.; Chabak, Y.G.; Brykov, M.N. Kinetic Parameters of Secondary Carbide Precipitation in
High-Cr White Iron Alloyed by Mn-Ni-Mo-V Complex. *J. Mater. Eng. Perform.* **2013**, *22*, 1378–1385. [CrossRef]

materials

MDPI

Article

Influence of Thermal Parameters Related to Destabilization Treatments on Erosive Wear Resistance and Microstructural Variation of White Cast Iron Containing 18% Cr. Application of Design of Experiments and Rietveld Structural Analysis

Alejandro Gonzalez-Pociño[1], Florentino Alvarez-Antolin [1]* and Juan Asensio-Lozano[1]

[1]Materials Pro Group, Departamento de Ciencia de los Materiales e Ingeniería Metalúrgica, Universidad de Oviedo, Independencia 13, 33004 Oviedo, Spain; UO204622@uniovi.es (A.G.-P.); jasensio@uniovi.es (J.A.-L.)

* Correspondence: alvarezflorentino@uniovi.es; Tel.: +34-985-181-949

Received: 6 September 2019; Accepted: 4 October 2019; Published: 5 October 2019

Abstract: High-Cr hypo-eutectic white cast irons are used in very demanding environments that require high resistance to erosive wear. The influence on the microstructural variation and erosive wear resistance of several fundamental factors related to the thermal treatments of these cast irons was analysed by means of a fractional Design of Experiments (DoE). These factors included the ones related to the destabilization of austenite. The precipitated phases were identified by X-ray diffraction (XRD), while the Rietveld structural refinement method was used to determine their percentages by weight. Erosion wear resistance was calculated using the test defined by ASTM G76. It was concluded that the quench cooling medium does not significantly influence either erosive wear resistance or the proportion of martensite or retained austenite. The destabilization temperature is a key factor with respect to the percentage of retained austenite. In order to increase the amount of martensite and decrease the amount of retained austenite, temperatures not exceeding 1000 °C are required. An increase of 100 °C in the destabilization temperature can lead to a 25% increase in retained austenite. Moreover, tempering temperatures of around 500 °C favour an additional increase in the percentage of martensite. Erosive wear commences on the matrix constituent without initially affecting the eutectic carbides. Once the deterioration of the matrix constituent surrounding these carbides occurs, they are released. High tempering times provide an increase in resistance to erosive wear due to a second destabilization of austenite during the said tempering.

Keywords: high chromium white cast iron; erosive wear; secondary carbides; retained austenite; destabilization of austenite

1. Introduction

High-Cr hypoeutectic white cast irons are used in harsh environments that require high resistance to erosive wear [1]. Examples include the mining, cement and thermal power industries [2,3]. These cast irons show two microstructural peculiarities that condition their properties. The first is that the matrix phase of their eutectic constituent is made up of austenite, while the second is that the carbides which form part of the said eutectic are of the $(Fe,Cr)_7C_3$ type, also known as K_2 carbides. These carbides show hardness values ranging between 1500 and 1800 HV [1,4,5]. Austenite has high hardenability, allowing its partial transformation into martensite via air cooling [5]. Furthermore, the austenite is found in the supersaturated state as a result of non-equilibrium solidification [6,7]. To enhance the wear resistance of these cast irons, it is advisable to carry out a treatment to destabilize this austenite, which entails an austenization treatment [8,9]. During this treatment, the precipitation of carbides is produced from the alloy elements rejected by the austenite, mainly chromium carbides of the K_2 type [6,10,11]. As a result of this treatment, the increase in wear resistance and the reduction in retained austenite are favoured by the increase in the Ms (martensitic transformation temperature) [12,13]. If the destabilization temperature is low, e.g., 900 °C, the solubility limit of the C in the austenite decreases and hence the amount of secondary carbides increases [14]. The destabilization of austenite requires long dwell times at the austenization temperature. This is because of the high concentration of alloy elements in the austenite crystalline cell, which hinders the diffusion of carbon. As the dwell time at the destabilization temperature increases, two kinetics simultaneously compete with one another: on the one hand, increase in the density of secondary carbides; and on the other, dissolution of those eutectic carbides formed as a result of non-equilibrium solidification [15]. An excessive dwell time can lead to "thickening" of the secondary carbides [12]. Besides the austenite destabilization treatment, subsequent quenching and tempering treatment are required for the proper use of these cast irons. The tempering temperatures for martensite usually fall within the 200–250 °C range. However, it would be possible to achieve a second destabilization of the retained austenite at temperatures between 400 and 600 °C [4,16,17]. This would favour its transformation into martensite during cooling after this tempering [18]. Thus, the hardness and erosive wear resistance of these cast irons can be substantially enhanced by means of a suitable heat treatment [19]. The aim of this study was to analyse the hardness and erosive wear resistance of a hypo-eutectic white cast iron containing 18% Cr and 2% Mo by varying the process variables related to the thermal treatments of the said cast iron. A further aim was to correlate the results with the microstructural variation that the material undergoes. Specifically, parameters related to the destabilization of austenite were analysed, namely the temperature and dwell time at this destabilization temperature. Parameters related to the quench medium and tempering conditions were also analysed, such as temperature, tempering times and number of tempers. Table 1 shows the chemical composition of the white cast iron. The applied research method was a fractional Design of Experiments (DoE), analysing six factors and conducting eight experiments [20]. The results will allow manufacturers of this grade of cast iron to design the most suitable industrial heat treatment for this material to offer high hardness and high wear resistance.

Table 1. Composition (wt %).

C	Si	Mn	Cr	Mo
2.9	1.2	0.8	18.1	1.8

2. Materials and Methods

The purpose of applying a Design of Experiments (DoE) was to deliberately modify certain working design parameters related to heat treatments, the aim being to generate changes in certain responses of the material. Specifically, the goal was to analyse the variations in hardness and erosive wear resistance as well as the resulting microstructural changes, subsequently correlating the results. The analysis of these changes allowed us to determine which of the working parameters have a significant effect on these responses. Table 2 shows the analysed parameters and the levels chosen to modify these working conditions in an orderly way. The DoE allows the effect of the variation of a factor on a given response to be determined. An example would be the effect on hardness of varying the destabilization of austenite temperature from 1000 to 1100 °C. The effect of the variation of a single factor is called a principal effect. Although the calculation of the effects is complex and laborious, it can be simplified using the Yates algorithm [20]. This algorithm can be straightforwardly implemented on a spreadsheet. The effect of one factor may often depend on the value that another takes; when this occurs, these factors are said to interact. The "weight" of the main effects on the variations is greater than that of the interactions of 2 factors, while the importance of the latter is in turn greater than that of the interactions of 3 factors, and so on. In industrial practice, it is sufficient to consider only the main effects and the 2-factor interactions, which enables the number of experiments to be reduced [20]. Based on this premise, 8 experiments were accordingly carried out in the present study, which supposes a 1/8 (64/8 = 8) fractional factorial design. If we wished to analyse all the possible interactions, we would need to perform 64 experiments ($2^6 = 64$). In the case in hand, we estimated only 8 effects (2^{6-3}). Table 3 shows the array of experiments thus generated to carry out a DoE with 6 factors, 2 levels and 8 experiments. Columns D, E and F have been respectively constructed from the product of columns A × B, A × C and B × C. The "Restricted Confounding Pattern" column indicates only the main effects and those 2-factor interactions whose effects are confounded with the main effects. The effects are linear combinations of the analysed responses. Hence, applying the central limit theorem (CLT), they will follow a normal law. If all the effects were non-significant, they would follow an N (0,σ) law and would thus appear aligned when represented on a normal probability plot. The normal probability plot scale makes it possible to convert the distribution function of the N (0,σ) law into a straight line. The coordinate point (0.50) is thus situated on this line. If any effect is significant, however, it will follow an N (μ,σ) law, not appearing aligned with the non-significant effects. Those effects that deviate from the straight line towards the ends on the normal probability plot are considered significant. For example, if an effect deviates to the left, this would indicate that the factor associated with this effect at its –1 level would increase the value of the response. Similarly, if an effect deviates to the right of the straight line, this would indicate that the factor associated with this effect at its +1 level would increase the value of the response [20]. The statistical analysis was carried out with the help of the Statgraphics Centurion XVI program, version 16.1.18.

Table 2. Factors and Levels. The factors analysed in the Design of Experiments (DoE) are shown. These factors are denominated using the letters A to F.

Factors			Levels	
Code	**Description of the Factors**	**Units**	**−1 Level**	**+1 Level**
A	Destabilization temperature of austenite	°C	1000	1100
B	Dwell time at the destabilization temperature	h	4	8
C	Number of tempers	–	1	2
D	Quench cooling medium	–	air	oil
E	Tempering temperature	°C	200	500
F	Tempering time (h)	h	3	6

Table 3. Array of Experiments. The samples corresponding to each experiment were prepared by placing the analysis factors at the levels indicated in this array.

No.	A	B	C	D	E	F	Restricted Confounding Pattern
1	−1	−1	−1	+1	+1	+1	A + BD + CE B + AD + CF C + AE + BF D + AB + EF E + AC + DF F + BC + DE AF + BE + CD
2	+1	−1	−1	−1	−1	+1	
3	−1	+1	−1	−1	+1	-1	
4	+1	+1	−1	+1	−1	-1	
5	−1	−1	+1	+1	−1	-1	
6	+1	−1	+1	−1	+1	-1	
7	−1	+1	+1	−1	−1	+1	
8	+1	+1	+1	+1	+1	+1	

The analysed responses were:

- The Vickers hardness. The applied load was of 981 N, while the hardness value was the average value obtained from 10 indentations.
- Erosive wear resistance. This test was carried out as per ASTM G76 [21] by means of compressed air blasting with corundum particles, applying a pressure of 4 bar, a flow rate of 120 g/min and a 30° angle of incidence on the sample surface. Three repetitions were performed per test.

  The duration of each test was 1 min. The abrasive particles were 50 microns in size and had an angular surface.
- The following microstructural variables:
  - Percentage by weight of austenite
  - Percentage by weight of martensite
  - Percentage by weight of carbides
  - Volume of the austenite crystal cell

3. Results and Discussion

Figure 1 shows the microstructure of these cast irons in the as-cast state. This microstructure is mainly made up of eutectic carbides of the K_2 type, retained austenite and pearlite.

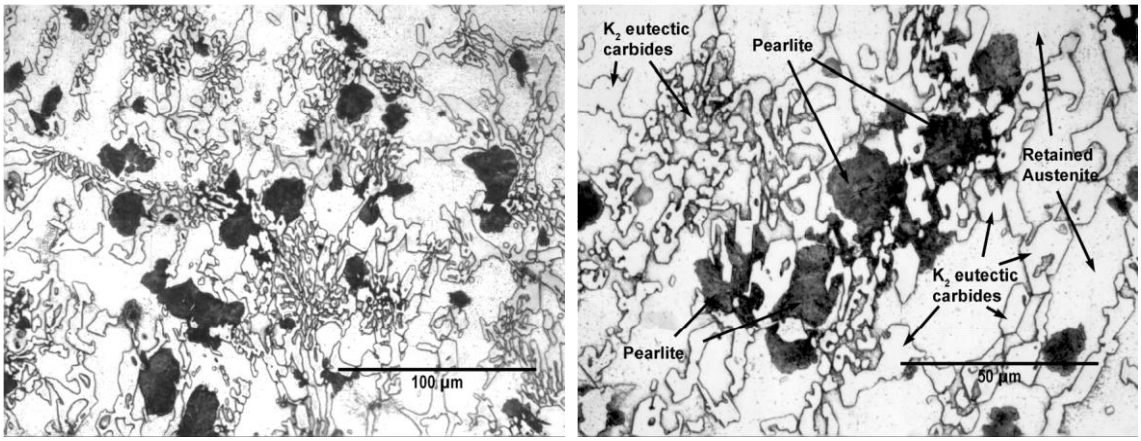

(**a**) (**b**)

Figure 1. As-cast Microstructure: (**a**) ×500 magnification; (**b**) ×1000 magnification.

Figure 2 shows the diffractograms obtained in the 8 experiments. The analysis was carried out after having performed all the heat treatments indicated in Table 3 (array of experiments). The Bragg peaks corresponding to martensite were indexed to their reflections with Miller indices (110), (200) and (211). The Bragg peaks corresponding to austenite were indexed to their reflections with Miller indices (111), (200) and (222). Furthermore, other Bragg peaks can be appreciated on the irregular background produced by the fluorescence of the compositions that were identified with the structure of mixed carbides of type K_2 (M_7C_3). The individual profile of each Bragg peak was fitted using pseudo-Voigt functions. Table 4 provides the 2θ and intensity (I) values of the Bragg peaks that stood out the most.

Figure 3 shows the overall fittings using the Rietveld method. Red crosses mark the observed intensities; the blue line, the intensity calculated according to the Rietveld structural model; the green line, the difference between the two; and the asterisks, the positions of the reflections.

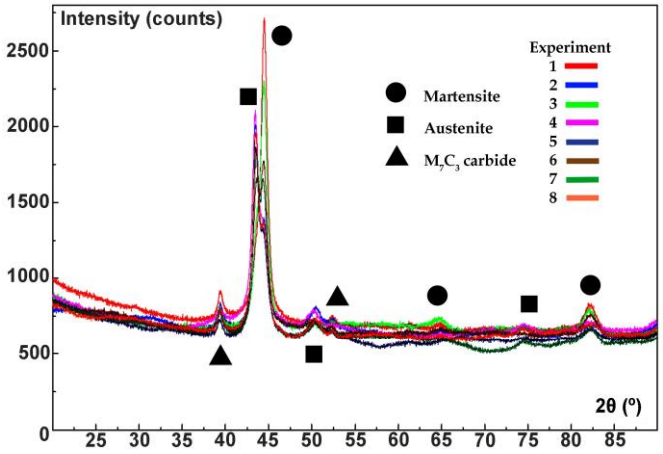

Figure 2. The diffractograms of the 8 experiments are shown in conjunction. The differences in intensities of the Bragg peaks associated with each of the experiments can be appreciated.

Table 4. The 2θ (°) and I (counts) values obtained from the fitting of the Bragg peaks.

(**a**) Austenite

No.	(111)		(200)		(222)	
	2θ (°)	I	2θ (°)	I	2θ (°)	I
1	43.657	2115	49.893	83	74.581	133
2	43.472	8041	50.395	737	74.438	367
3	44.110	4967	50.117	148	74.565	114
4	43.430	8417	50.183	575	74.562	121
5	43.529	5346	50.176	268	74.275	119
6	43.462	6454	50.276	532	74.171	95
7	43.466	6238	50.103	128	74.263	92
8	43.483	8096	49.469	116	74.368	217

(**b**) Martensite

No.	(110)		(200)		(211)	
	2θ (°)	I	2θ (°)	I	2θ (°)	I
1	44.501	12203	64.743	270	82.118	1158
2	44.447	3817	65.095	183	82.632	319
3	44.498	6010	64.631	434	82.044	956
4	44.353	3029	64.733	180	82.142	224
5	44.431	6427	64.874	171	82.120	778
6	44.418	3521	67.232	108	82.167	383
7	44.438	5827	64.898	106	82.165	381
8	44.479	3675	64.926	104	82.374	321

(**c**) M7C3 type Carbide

No.	2θ (°)	I	2θ (°)	I
1	39.417	1032	52.358	317
2	39.413	1035	52.391	399
3	39.354	814	52.356	148
4	39.351	378	52.292	186
5	39.354	731	52.219	175
6	39.337	591	52.358	317
7	39.405	798	52.319	163
8	39.413	803	52.405	221

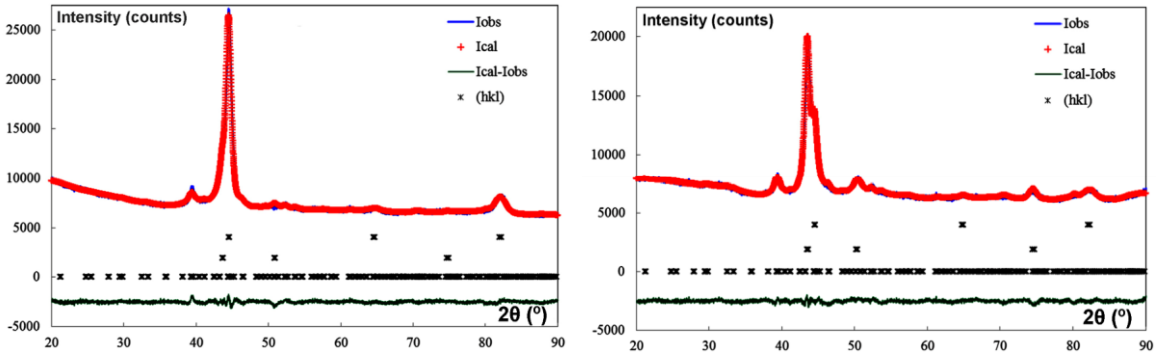

(**a**) (**b**)

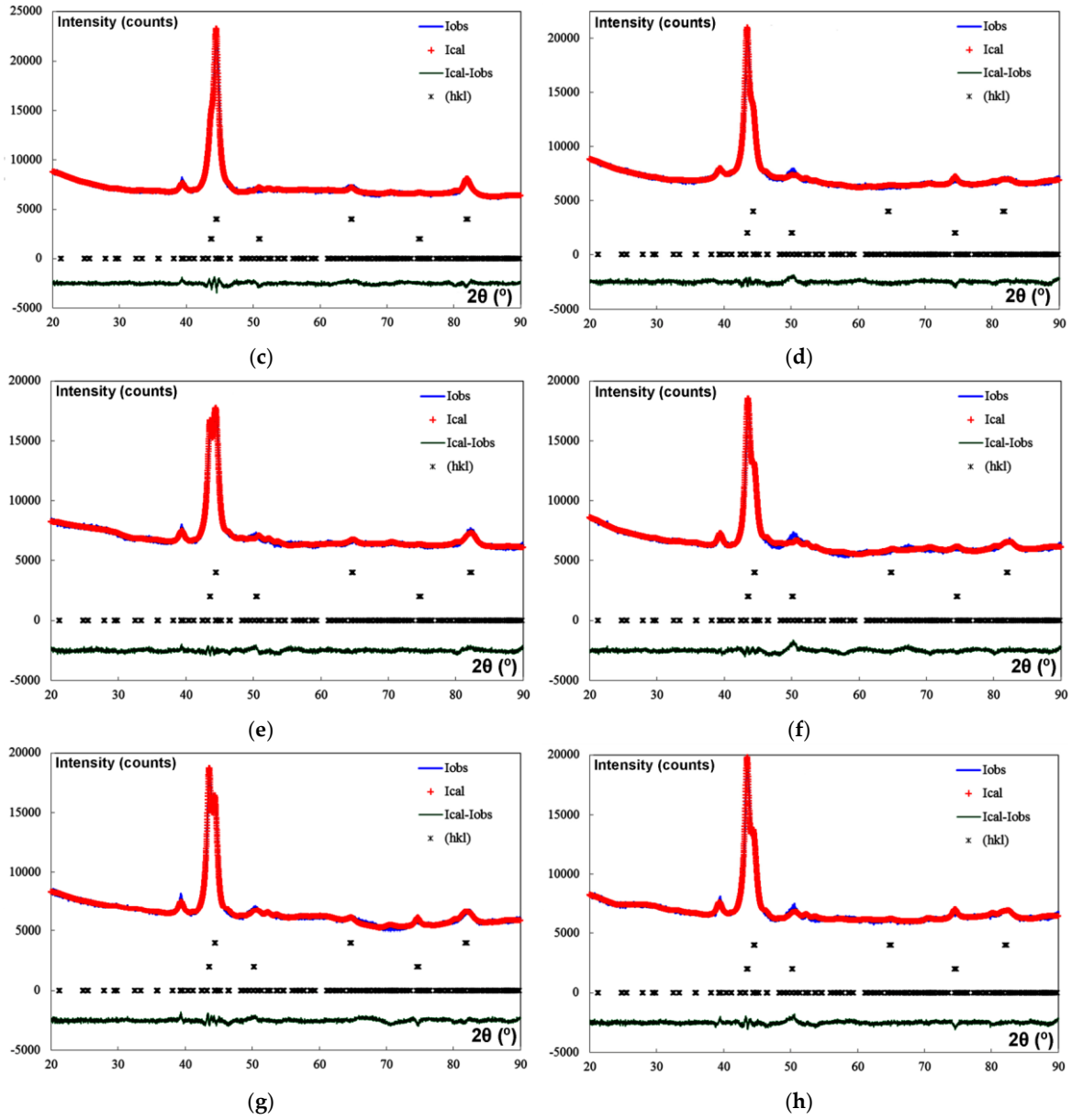

Figure 3. Overall fittings obtained by means of Rietveld structural refinement. The blue plots show the observed intensities and the red line, the intensities obtained using the Rietveld structural model. The dark green line indicates the difference between these intensities: (**a**) Experiment 1 (No.1); (**b**) Experiment 2 (No.2); (**c**) Experiment 3 (No.3); (**d**) Experiment 4 (No.4); (**e**) Experiment 5 (No.5); (**f**) Experiment 6 (No.6); (**g**) Experiment 7 (No.7); (**h**) Experiment 8 (No.8).

Table 5 shows the percentages by weight and the network parameters of the main crystalline phases detected by XRD in each of the 8 experiments. The degree of accuracy of the fittings can be assessed by comparing the R_{wp} agreement factor and the R_{exp} index. The relationship between their squares, $Chi^2 = (R_{wp}/R_{exp})^2$, is known as the goodness of fit. In our case, a large part of the obtained fittings reaches values around 2, which corroborates a high degree of certainty in the analysis.

Table 5. Microstructural parameters, weight distributions of the precipitated phases and volume of austenite.

No.	Rietveld Fitting	Phases	a (Å)	b (Å)	c (Å)	wt. %	Vol. (Å³)
1	Rwp = 9.54	Martensite	2.87643	-	-	50.48 ± 1.59	-
	Rexp = 6.67	Austenite	3.59057	-	-	12.76 ± 1.17	46.290 ± 0.019
	Chi^2 = 2.05	K_2 carbide	4.46111	6.99491	12.10891	36.76 ± 2.15	-
2	Rwp = 10.1	Martensite	2.87511	-	-	10.05 ± 0.86	-
	Rexp = 7.25	Austenite	3.59862	-	-	42.2 ± 1.38	46.602 ± 0.004
	Chi^2 = 1.95	K_2 carbide	4.46111	6.99491	12.10891	47.74 ± 2.25	-
3	Rwp = 10.0	Martensite	2.87890	-	-	48.47 ± 1.61	-
	Rexp = 6.72	Austenite	3.58676	-	-	19.69 ± 1.39	46.143 ± 0.013
	Chi^2 = 2.22	K_2 carbide	4.46111	6.99491	12.10891	31.83 ± 1.95	-
4	Rwp = 11.4	Martensite	2.88817	-	-	9.34 ± 1.14	-
	Rexp = 7.71	Austenite	3.60308	-	-	61.09 ± 2.12	46.776 ± 0.005
	Chi^2 = 2.18	K_2 carbide	4.46111	6.99491	12.10891	29.57 ± 2.03	-
5	Rwp = 10.5	Martensite	2.88171	-	-	29.15 ± 1.32	-
	Rexp = 7.37	Austenite	3.59555	-	-	34.22 ± 1.53	46.483 ± 0.007
	Chi^2 = 2.04	K_2 carbide	4.46111	6.99491	12.10891	36.63 ± 2.15	-
6	Rwp = 13.4	Martensite	2.87831	-	-	10.52 ± 0.99	-
	R_{exp} = 7.5	Austenite	3.59951	-	-	49.58 ± 1.73	46.637 ± 0.005
	Chi^2 = 3.2	K_2 carbide	4.46111	6.99491	12.10891	39.91 ± 2.16	-
7	Rwp=11.6	Martensite	2.88122	-	-	19.01 ± 0.96	-
	Rexp = 7.05	Austenite	3.58456	-	-	41.51 ± 1.36	46.445 ± 0.005
	Chi^2 = 2.69	K_2 carbide	4.46111	6.99491	12.10891	39.48 ± 2.05	-
8	Rwp = 11.0	Martensite	2.87366	-	-	1.09 ± 0.62	-
	Rexp = 7.18	Austenite	3.59837	-	-	56.95 ± 1.68	46.593 ± 0.004
	Chi^2 = 2.35	K_2 carbide	4.46111	6.99491	12.10891	41.97 ± 2.22	-

Table 6 shows the average values obtained in each experiment, together with the effects corresponding to the restricted confounding pattern specified in the array of experiments. The row corresponding to the average shows the average value obtained for each of the responses. Figure 4 shows the representation of these effects on a normal probability plot, highlighting those that have a significant effect on these responses.

Figure 4a shows that the main factors that have a significant effect on the percentage of martensite are Factors A (destabilization of austenite temperature) and E (tempering temperature). Thus, if the aim is to increase this percentage, both factors should be placed at their respective −1 and +1 levels; i.e., a destabilization temperature of 1000 °C and a tempering temperature of 500 °C. It appears to be confirmed that the austenite will be partially converted to martensite during cooling after tempering at 500 °C [4]. Figure 4a also shows the significant effect of the interaction of both factors, an increase in the percentage in martensite being produced when both factors are simultaneously placed at their respective −1 and +1 levels. Furthermore, Figure 4b shows that the destabilization temperature also has a significant effect on the percentage of retained austenite: placing this factor at 1100 °C leads to an increase in the percentage of austenite. Note that an increase of 100 °C in the destabilization temperature can lead to an increase of more

than 25% in retained austenite. This value is similar to the increase in martensite (29%) that reducing these 100 °C induces.

Table 6. Average values and effects obtained for the analysed responses.

(a) Percentage by weight of the phases present

No.	Martensite		Austenite		M_7C_3		Calculated Effects
	(wt %)	Effect	(wt %)	Effect	(wt %)	Effect	
1	50.48	22.313	12.76	39.750	36.76	37.986	Average
2	10.05	-29.127	42.2	25.41	47.74	3.622	A+BD+CE
3	48.87	-5.472	19.69	10.12	31.83	-4.547	B+AD+CF
4	9.34	-14.742	61.09	11.63	29.57	3.022	C+AE+BF
5	29.15	0.402	34.22	3.01	36.63	-3.507	D+AB+EF
6	10.52	10.852	49.58	-10.01	39.91	-0.737	E+AC+DF
7	19.01	-4.312	41.51	-2.79	39.48	7.002	F+BC+DE
8	1.09	-0.047	56.95	2.97	41.97	3.112	AF+BE+CD

(b) Volume of the austenite crystal cell

No.	Å^3	Effect	Calculated Effects
1	46.29	46.496	Average
2	46.602	0.311	A+BD+CE
3	46.143	-0.013	B+AD+CF
4	46.776	0.086	C+AE+BF
5	46.483	0.078	D+AB+EF
6	46.637	-0.160	E+AC+DF
7	46.445	-0.027	F+BC+DE
8	46.593	-0.081	AF+BE+CD

(c) Hardness and weight loss in the erosive wear test

No.	Hardness		Weight Loss		Calculated Effects
	HV100	Effect	mg	Effect	
1	833	781.75	79.23	83.095	Average
2	679	-142.5	80.95	-0.99	A+BD+CE
3	877	-1.5	86.13	0.52	B+AD+CF
4	693	22.5	83.25	1.41	C+AE+BF
5	859	-15.5	86.73	-0.7	D+AB+EF
6	759	26.5	84.43	-0.41	E+AC+DF
7	843	-30.5	82.27	-4.08	F+BC+DE
8	711	-0.5	81.77	1.6	AF+BE+CD

Figure 4c shows that none of the analysed factors has a significant effect on the percentage of precipitated K_2 carbides. However, if a Pareto chart is used to represent the obtained effects, it can be seen that, although it does not show a significant effect, Factor F (tempering time) is the one that produces a greater effect on the percentage of these carbides (see Figure 5). Thus, placing this factor at its +1 level leads to a 7% by weight increase in carbide density. In this respect, the question may arise as to whether a high background of the diffractograms, due to the high fluorescence of the very Fe-rich compounds, might make it difficult to identify low intensity Bragg peaks belonging to carbides precipitated in a second destabilization of the austenite.

Should this be the case, it might conceal the significant effect of Factor F on the percentage by weight of the precipitated carbides.

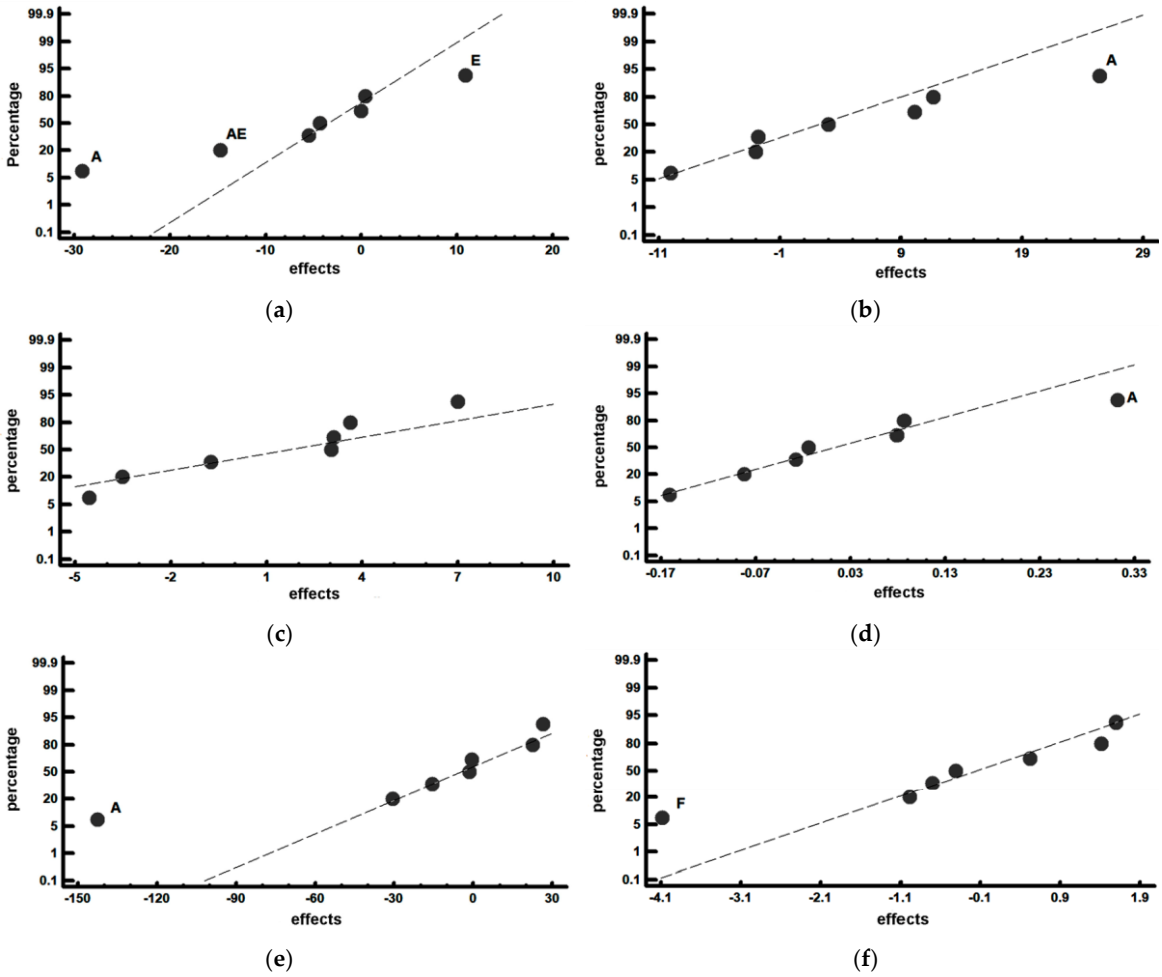

Figure 4. Representation of the effects on a normal probability plot. Those factors with a significant effect on the analysed responses are highlighted. (**a**) Percentage by weight of martensite; (**b**) Percentage by weight of austenite; (**c**) Percentage by weight of type K2 carbides; (**d**) Volume of the austenite crystal cell (Å^3); (**e**) Vickers hardness; and (**f**) Weight loss in the erosive wear test (mg).

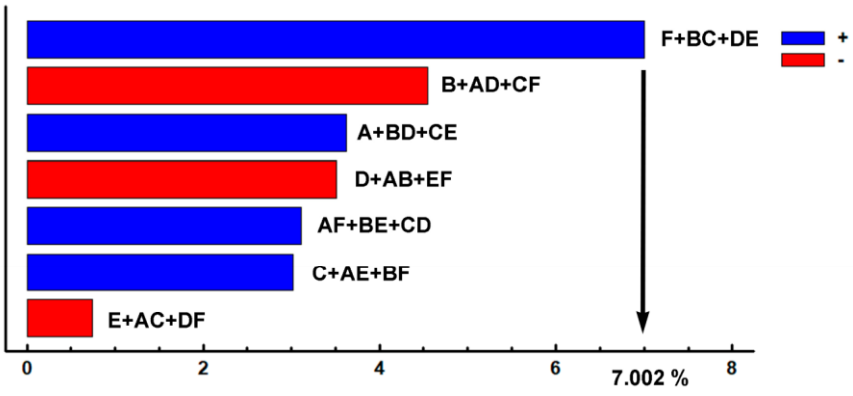

Figure 5. Pareto chart of the effects of each factor on the percentage by weight of K_2 carbides. Placing Factor F at its +1 level (6-h tempering time) could produce a 7% increase in the weight percentage of carbides.

Figure 4d shows the significant effect of Factor A (destabilization temperature) on the volume of retained austenite: an increase in this temperature to 1100 °C leads to an increase in the said volume. This could be due to the increase in the solubility limit of C in the austenite.

Figure 4e shows, once again, that the destabilization temperature (Factor A) has a significant effect on the hardness of the material. Thus, there is an increase in the said hardness when this temperature is placed at its −1 level (1000 °C). This could be due to the increase in martensite (and the decrease in the amount of retained austenite) resulting from placing the destabilization temperature at 1000 °C.

Figure 4f shows that Factor F (tempering time) has a significant effect on abrasive wear resistance: placing this factor at its −1 level (3 h) leads to an increase in the percentage wear. To increase the material's resistance to erosive wear, the tempering time should be increased to 6 h (+1 level). This increase in wear resistance could be due to the second destabilization of austenite during tempering, resulting in the precipitation of secondary carbides, which would confirm the comments related to Figure 4c. This second destabilization requires a long time due to the difficulty of diffusion of the carbon atoms at the tempering temperatures.

Figure 6 shows the microstructure of some specimens obtained after the different heat treatments; in particular, those corresponding to Experiments 1, 2, 6 and 8. Figure 6a, which corresponds to Experiment 1, shows the majority presence of martensite. Figure 6b–d corresponding respectively to Experiments 2, 6 and 8, show a greater amount of retained austenite. Figure 6c,d, with a slightly longer exposure to the etching reagent than in Figure 6b, reveal the characteristic martensite needles embedded in the retained austenite. Secondary carbides which precipitated during the destabilization of austenite can be observed in Figure 6a,b.

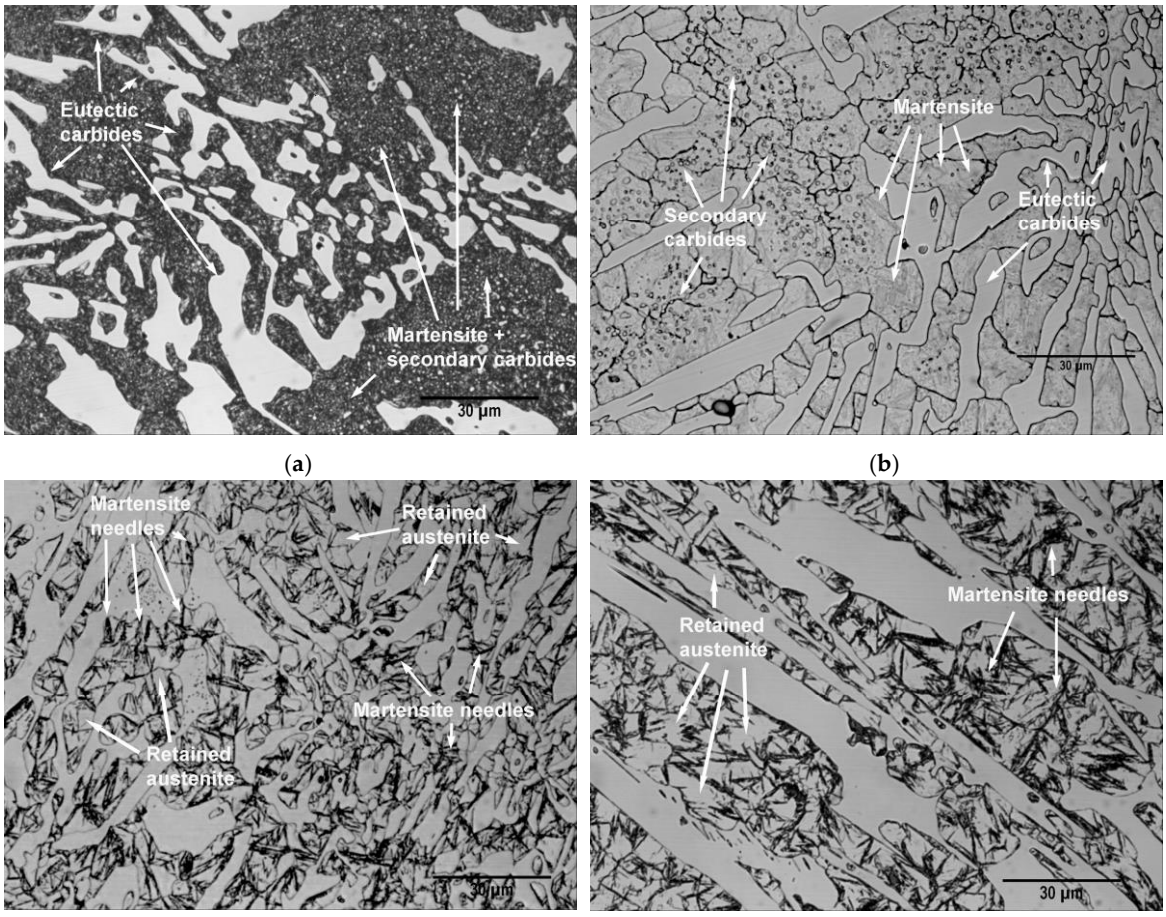

Figure 6. Representative micrographs of the microstructure obtained after the different heat treatments (all at ×1000 magnification): (**a**) Experiment 1; (**b**) Experiment 2; (**c**) Experiment 6; (**d**) Experiment 8.

Figure 7 provides representative images of the morphology of one of the wear tracks corresponding to one of the specimens in Experiment 5. The white arrows in Figure 7a indicate impact marks of corundum particles, located in the vicinity of the main wear track. Figure 7b shows the microstructure in one of the regions adjacent to the wear track, where these impact marks appear. It can be seen that the impact of corundum particles initially produces deterioration of the matrix constituent (austenite and martensite) without affecting the eutectic carbides. Once the deterioration of the matrix constituent surrounding these carbides occurs, they are released. Figure 7c shows the profile of one of the wear tracks.

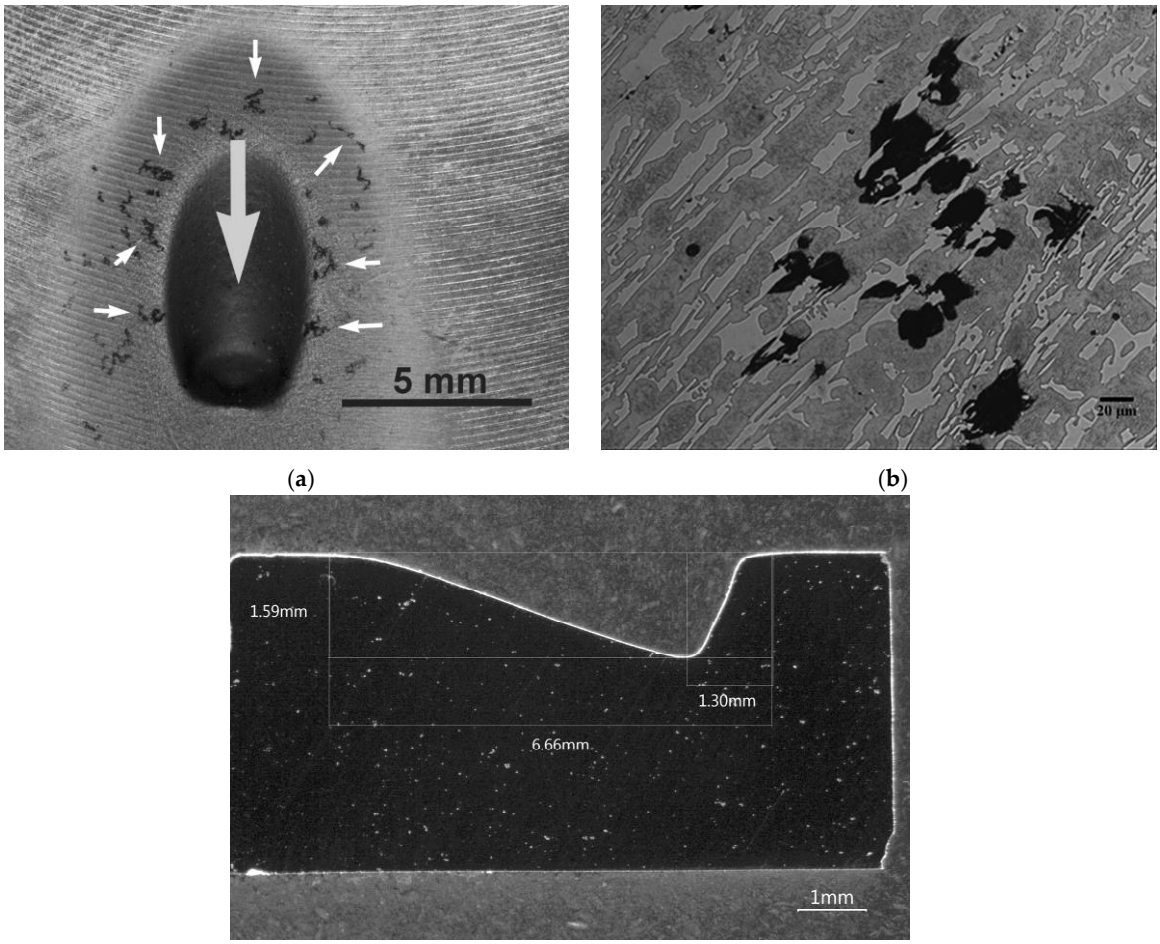

(**a**) (**b**)

(**c**)

Figure 7. Morphology of the wear track. A track obtained from one of the specimens corresponding to Experiment 5: (**a**) The light grey arrow indicates the direction of impact of the corundum jet. The white arrows point to different impact marks of corundum particles around the wear track; (**b**) The impact of corundum particles produces deterioration of the matrix constituent without initially affecting the eutectic carbides. Once the deterioration of the matrix constituent surrounding these carbides occurs, they are released. (**c**) Profile of the wear track.

Bearing in mind this wear mechanism, it seems reasonable to conclude that the improvement in the erosive wear resistance of this white cast iron would be the result of an increase in the wear resistance of its matrix constituent. This improvement could be based on the development of new chemical compositions, together with changes in heat treatments, which allow the density of secondary carbides in the matrix constituent to be increased.

4. Conclusions

Based on the deliberate variation of parameters related to the heat treatment of a hypo-eutectic white cast iron containing 18% Cr and, in particular, taking into account those parameters related to the destabilization of austenite, it is concluded that:

1. The severity of the quench cooling medium does not significantly influence hardness, erosive wear resistance or the proportion of martensite or retained austenite.

2. The destabilization temperature is a key factor with respect to the percentage of retained austenite. In order to increase the amount of martensite and decrease the amount of retained austenite, low destabilization temperatures not exceeding 1000 °C are required. An increase of 100 °C in the destabilization temperature can lead to a 25% increase in retained austenite.
3. Moreover, tempering temperatures of around 500 °C favour an additional increase in the percentage of martensite.
4. Erosive wear commences on the matrix constituent without initially affecting the eutectic carbides. Once the deterioration of the matrix constituent surrounding these carbides occurs, they are released.
5. Long tempering times, of around 6 h, provide an increase in resistance to erosive wear due to a second destabilization of austenite during the said tempering. This destabilization delays the deterioration of the matrix constituent.

Author Contributions: Methodology, F.A.-A. and J.A.-L.; Investigation, A.G.-P.; Writing-Review & Editing, F.A.-A.; Supervision, J.A.-L.

Funding: This research received no external funding.

Conflicts of Interest: The authors declare no conflict of interest.

References

1. Maja, M. Effect of niobium on the solidification structure and properties of hypoeutectic high-chromium white cast irons. *J. South. Afr. Inst. Min. Met.* **2016**, *116*, 981–986. [CrossRef]
2. Hadji, A.; Bouhamla, K.; Maouche, H. Improving Wear Properties of High-Chromium Cast Iron by Manganese Alloying. *Int. J. Met.* **2016**, *10*, 43–55. [CrossRef]
3. Pearce, J.T.H. Structural characterisation of high chromium cast irons. In Proceedings of the International Conference on Solidification Science and Processing: Outlook for the 21st Century, Bangalore, India, 18–21 February 2001.
4. Antolin, J.F.A.; Garrote, L.F.; Lozano, J.A. Application of Rietveld Refinement to the correlation of the microstructure evolution of white cast irons with 18 and 25%-wt. Cr after oil quench and successive temper treatments, with abrasive wear and bending testing. *Rev. De Metal.* **2018**, *54*, 11. [CrossRef]
5. Pero-Sanz Elorz, J.A. *Ciencia e Ingeniería de Materiales*, 5th ed.; Cie Inversiones Editoriales-Dossat: Madrid, Spain, 2000; p. 673.
6. Powell, G.L.F.; Bee, J.V. Secondary carbide precipitation in an 18 wt%Cr-1 wt% Mo white iron. *J. Mater. Sci.* **1996**, *31*, 707–711. [CrossRef]
7. Sun, Z.; Zuo, R.; Li, C.; Shen, B.; Yan, J.; Huang, S. TEM study on precipitation and transformation of secondary carbides in 16Cr–1Mo–1Cu white iron subjected to subcritical treatment. *Mater. Charact.* **2004**, *53*, 403–409. [CrossRef]
8. Gasan, H.; Erturk, F. Effects of a Destabilization Heat Treatment on the Microstructure and Abrasive Wear
   Behavior of High-Chromium White Cast Iron Investigated Using Different Characterization Techniques. *Met. Mater. Trans. A* **2013**, *44*, 4993–5005. [CrossRef]
9. Guitar, M.A.; Suárez, S.; Prat, O.; Guigou, M.D.; Gari, V.; Pereira, G.; Mücklich, F. High Chromium Cast Irons:
   Destabilized-Subcritical Secondary Carbide Precipitation and Its Effect on Hardness and Wear Properties. *J. Mater. Eng. Perform.* **2018**, *27*, 3877–3885. [CrossRef]

10. Wiengmoon, A.; Pearce, J.; Chairuangsri, T. Relationship between microstructure, hardness and corrosion resistance in 20wt.%Cr, 27wt.%Cr and 36wt.%Cr high chromium cast irons. *Mater. Chem. Phys.* **2011**, *125*, 739–748. [CrossRef]
11. Bedolla-Jacuide, A.; Arias, L.; Hernandez, B.; Jacuinde, A.B. Kinetics of Secondary Carbides Precipitation in a High-Chromium White Iron. *J. Mater. Eng. Perform.* **2003**, *12*, 371–382. [CrossRef]
12. Efremenko, V.; Shimizu, K.; Chabak, Y. Effect of Destabilizing Heat Treatment on Solid-State Phase Transformation in High-Chromium Cast Irons. *Met. Mater. Trans. A* **2013**, *44*, 5434–5446. [CrossRef]
13. Yang, H.-S.; Jun, W.; Bao-Luo, S.; Hao-Huai, L.; Sheng-Ji, G.; Si-Jiu, H. Effect of cryogenic treatment on the matrix structure and abrasion resistance of white cast iron subjected to destabilization treatment. *Wear* **2006**, *261*, 1150–1154. [CrossRef]
14. Bedolla-Jacuinde, A.; Guerra, F.V.; Mejia, I.; Zuno-Silva, J.; Maldonado, C. Boron effect on the precipitation of secondary carbides during destabilisation of high chromium white iron. *Int. J. Cast Met. Res.* **2016**, *29*, 55–61. [CrossRef]
15. Gonzalez-Pociño, A.; Alvarez-Antolin, F.; Asensio-Lozano, J. Erosive Wear Resistance Regarding Different Destabilization Heat Treatments of Austenite in High Chromium White Cast Iron, Alloyed with Mo. *Metals* **2019**, *9*, 522. [CrossRef]
16. Opapaiboon, J.; Sricharoenchai, P.; Inthidech, S.; Matsubara, Y. Effect of Carbon Content on Heat Treatment
Behavior of Multi-Alloyed White Cast Iron for Abrasive Wear Resistance. *Mater. Trans.* **2015**, *56*, 720–725. [CrossRef]
17. Liu, Z.L.; Li, Y.X.; Chen, X. Effect of tempering temperature on microstructure and mechanical properties of high boron white cast iron. *China Foundry* **2012**, *9*, 313–317.
18. Opapaiboon, J.; Na Ayudhaya, M.S.; Sricharoenchai, P.; Inthidech, S.; Matsubara, Y. Effect of Chromium
Content on Heat Treatment Behavior of Multi-Alloyed White Cast Iron for Abrasive Wear Resistance. *Mater. Trans.* **2019**, *60*, 346–354. [CrossRef]
19. Li, D.; Liu, L.; Zhang, Y.; Ye, C.; Ren, X.; Yang, Y.; Yang, Q. Phase diagram calculation of high chromium cast irons and influence of its chemical composition. *Mater. Des.* **2009**, *30*, 340–345. [CrossRef]
20. Prat-Bartés, A.; Tort-Martorell, X.; Grima-Cintas, P.; Pozueta-Fernández, L.; Solé-Vidal, I. *Métodos Estadísticos*, 2nd ed.; UPC: Barcelona, Spain, 2004; pp. 127–200.
21. ASTM G76-18. *Standard Test Method for Conducting Erosion Tests by Solid Particle Impingement Using Gas Jets*; ASTM International: West Conshohocken, PA, USA, 2018.

metals

MDPI

Article

Optimization, by Means of a Design of Experiments, of Heat Processes to Increase the Erosive Wear Resistance of White Hypoeutectic Cast Irons Alloyed with Cr and Mo

Alejandro Gonzalez-Pociño[1], Florentino Alvarez-Antolin [1]* and Juan Asensio-Lozano[1]

[1]Materials Pro Group, Departamento de Ciencia de los Materiales e IngenieríaMetalúrgica, Universidad de Oviedo, Independencia 13, 33004 Oviedo, Spain; UO204622@uniovi.es (A.G.-P.); jasensio@uniovi.es (J.A.-L.)

* Correspondence: alvarezflorentino@uniovi.es; Tel.: +34-985-181-949

Received: 28 February 2019; Accepted: 29 March 2019; Published: 2 April 2019

Abstract: To identify the design parameters in heat treatments that have a significant effect on the erosive wear resistance of hypoeutectic high chromium white cast irons, a design of experiment was applied to a white cast iron with 18wt.% Cr and 2wt.% Mo. The analyzed factors were the destabilization heat treatment of austenite (1000 or 1100 °C, for 4 or 8 h), different quench cooling media (in air or oil), different tempering treatments (200 or 500 °C, for 3 or 6 h), and the application of an ionic nitriding treatment. Despite what was expected, the nitriding treatment was not found to have a significant effect on said wear resistance. However, it is concluded that the highest wear resistance is obtained with the shortest dwell time at the destabilization temperature (4 h), quenching in oil, and with the shortest tempering times (3 h). Among the nitrided samples, the highest nitrided layer thicknesses were obtained when the destabilization temperature of the austenite was 1000 °C and the tempering temperature was 200 °C.

Keywords: high chromium white cast iron; destabilization of the austenite; erosive wear; plasma nitriding

1. Introduction

White cast irons with a percentage of Cr greater than 15wt.% show two microstructural peculiarities that condition their properties. One of these is that the matrix phase of the eutectic constituent is, in fact, unstable austenite at room temperature (retained austenite), which affords a greater toughness compared to other white cast irons and also allows them to be machined when subjected to an isothermal treatment that transforms the austenite into pearlite [1]. The other peculiarity is that the carbides that form part of their eutectic are mixed M_7C_3 carbides, typically $(Fe,Cr)_7C_3$, which have a hardness value between 1200 and 1600 HV [2]. The content of M_7C_3 type eutectic carbides increases gradually with the increase in chromium content [3]. These carbides have a similar morphology to bars or plates [4]. These cast irons are widely used in applications that require a high resistance to wear, as would be the case of processes linked to the treatment of raw materials in the cement industry and thermal power stations, as well as in crushing and grinding processes in the mining industry. Abrasion resistance of white cast irons depends greatly on the properties and microstructure of the material, as well as on the wear conditions [5]. Martensite may form at relatively low cooling rates due to the high hardenability conferred by a high alloy content in solid solution of austenite prior to quenching. One such alloying element is chromium, which allows martensite to form by air cooling [1]. However, wear resistance is improved if the precipitation of chromium-rich secondary carbides [6,7], uniformly distributed in a predominantly martensitic matrix, is promoted and if the percentage of retained austenite is reduced [8].These secondary carbides are precipitated as a result of the destabilization of austenite at temperatures around 1000 °C or higher [4,7,9–19]. This precipitation favors an increase in the M_s temperature, reducing the risk of cracking in cooling media with harsher cooling conditions than air [1]. Quenching in oil would decrease the percentage of retained austenite at room temperature as compared to air quench, as in the former a higher cooling rate between M_s and M_f will take place. Hence, a higher conversion of austenite into martensite. Tempering temperatures according to industrial practices usually fall within the 200–250 °C range [1]. At higher temperatures of between 400 and 600 °C, however, it should be possible to achieve a second destabilization of the retained austenite, leading to its transformation into new martensite [20]. Higher hardness values would be obtained with double tempering around 500 °C [21]. The addition of Mo produces a drop in both the liquidus temperature and the eutectic temperature. This in turn leads to an increase in the size of the eutectic cell and greater spacing between the carbide particles [22]. The addition of Mo likewise increases the hardenability of the material [23], increasing its hardness [24] and wear resistance [25–27]. Furthermore, the presence of Mo leads to the formation of M_2C carbides, and it has been found that these nucleate from M_7C_3 carbides to spread through the martensitic matrix [10,28]. This precipitation may occur during high temperature tempering [14]. In steels, a thermochemical nitriding treatment produces surface hardening via the formation of subnitrides of Cr, V, Mo, and Al in the tempered martensite matrix [29,30]. However, there are no previous reports of the nitriding of high chromium white cast irons. In the case of steels belonging to the Fe–Cr–Mo system, the type of $(CrMo)_xN_y$ nitrides will depend on the Cr/Mo ratio [30].

The aim of this paper is to analyze the influence of the process variables related to the quenching, tempering and possible subsequent nitriding of a white cast iron with 18 wt.% Cr and 2 wt.% Mo on its hardness and resistance to erosive wear. The temperatures chosen in this study to determine the possible effect of temperature on the destabilization of austenite were 1000 and 1100 °C, the goal being to determine whether an increase of this temperature up to 1100 °C might lead to an improvement in wear resistance due to an increase in the precipitation of these secondary carbides.

2. Materials and Methods

The experimental method applied was a design of experiments (DOE) with 6 factors, 2 levels for each factor, and 8 experiments in all [31]. The purpose of applying the DOE statistical technique is to modify normal working conditions deliberately so as to produce changes in some of the responses under study. These deliberate changes in normal working conditions are carried out on specific, previously-selected factors of the manufacturing process. Full factorial designs of experiments require a large number of experiments, which grow exponentially depending on the number of factors studied. When there are k factors to study in a full factorial DOE, the number of tests is 2^k, where 2 is the number of levels applied to each of the factors. Fractional DOEs allow a large number of factors to be studied by means of a much smaller number of experiments, assuming the loss of information of possible interactions between factors, which are not usually very significant in practice. It should be noted that fractional factorial DOEs are symbolized as 2^{k-p}, where 2 is the number of levels, k the number of factors and p the degree of fractionation. In our case, the design of experiments employed would be $2^{6-3} = 8$. Table 1 shows the chemical composition of the white cast iron under analysis. Table 2 shows the analyzed factors and levels, while Table 3 displays the array of experiments, together with the confounding pattern. The analyzed factors correspond to the process variables related to quenching, tempering and possible subsequent nitriding. The set of generators associated with this array of experiments is D=AB, E=AC and F= BC, of which the resulting relation definition is I=ABD=ACD=BCF, where I is a column formed only by some (+1) [31]. This means that the interactions ABD, ACD, and BCF are confounded with the mean. The resolution of this design is III; i.e., the main effects are confounded with the interactions of two factors [31]. In general, a DOE with resolution N is one in which no effect of q factors is confounded with another containing less than N-q factors. In our case, the proposed DOE is of type 2^{k-p}, which means that it has a resolution of III because the main effects are confounded with the interactions of 2 factors. Note that 3 (resolution) = 1 (main effects) + 2 (interactions of 2 factors). The "Confounding Pattern" column in Table 3 indicates those interactions of two factors which are confounded with the main effects.

Table 1. Chemical composition (% in weight).

C	Si	Mn	Cr	Mo	Fe
3.02	1.17	0.80	18.21	2.05	≤74.75.

Table 2. Factors and levels analyzed in the design of experiments (DOE) (cooling medium after tempering: Air).

	Factors	Levels	
Code	Metallurgical Parameter	Level –1	Level +1
A	Destabilization temperature of austenite (°C)	1000	1100
B	Dwell time at the destabilization temperature (h)	4	8
C	Nitriding	No	Yes
D	Quench cooling medium	air	oil
E	Temperingtemperature (°C)	200	500
F	Dwell timeat temperature during tempering(h)	3	6

Table 3. Array of Experiments.

No	A	B	C	D	E	F	Confounding Pattern
1	–1	–1	–1	+1	+1	+1	A+BD+CE
2	+1	–1	–1	–1	–1	+1	B+AD+CF
3	–1	+1	–1	–1	+1	–1	C+AE+BF
4	+1	+1	–1	+1	–1	–1	D+AB+EF
5	–1	–1	+1	+1	–1	–1	E+AC+DF
6	+1	–1	+1	–1	+1	–1	F+BC+DE
7	–1	+1	+1	–1	–1	+1	AF+BE+CD
8	+1	+1	+1	+1	+1	+1	

The analyzed responses were:

- The Vickers hardness, representative of each of the 8 experiments. The applied load was 125 kgf (1225.83 N). In all cases, 10 indentations were made in each of the samples. The hardness values were obtained on a cross-section in areas at a distance from the edge of the specimen, avoiding indentations in areas near the edge. Moreover, face milling was used to remove 1 mm of the surface material so as to avoid the influence of any possible surface decarburization.
- The microhardness of the matrix phase, that is to say austenite mainly transformed into martensite, and pre-existing secondary carbides dispersed in the former. These secondary carbides were obtained during destabilization of austenite at 1000 or 1100 °C, which is a former stage prior to cooling in air or oil. This practice of austenite destabilization allows for austenite depletion in carbon and alloying elements in solid solution, which allows M_s to increase enabling to increase the section size to quench without cracking as well as to obtain less retained austenite after quenching. In the present experimental procedure, the applied load was 0.05 kgf (0.49 N), performing 10 indentations in each of the samples. Similar to the previous case, microhardness measurements
  were made on the cross-section after removing 1 mm of the material by milling.
- The erosive wear resistance, which was measured by means of compressed air blasting with corundum particles according to the ASTM G76 standard, applying a pressure of 4 bar, a flow rate of 1 g/s and a 30° angle of incidence on the sample surface. Five repetitions were performed in each test. The duration of each trial was 1 minute. The dimensions of the tested specimens were those of a prism measuring 60 mm × 40 mm × 15 mm.

The effect of a factor on the variation in the response function is defined as a consequence of the variation of said factor. The main effect of a factor indicates how much the response changes when this factor changes from its –1 level to its +1 level. The effect of one factor may often depend on the value that another takes. When this occurs, these factors are said to interact. Interactions between 2 factors are defined as the variation between the average effect of one factor with the other factor at its low level, –1, and the average effect of the same factor with the other at its high level, +1. The interactions between several factors are similarly defined. The importance of the main effects tends to be greater than the importance of the interactions of 2 factors, while the latter are in turn greater than the interactions of 3 factors, and so on.

The experimental response was subject to random variation. This variation followed a normal law, where its standard deviation reflects experimental error. The effects are linear combinations of the responses. Hence, applying the central limit theorem (CLT), they followed a normal law. Each main effect may be considered a random variable where the obtained value is an estimate of its mean; hence, this value is accompanied by the estimation of its standard deviation. If all the effects were non-significant, they would follow an $N(0,\sigma)$ law and would thus appear aligned in a representation of the effects on a normal probability plot. If any effect was significant, it will follow an $N(\mu,\sigma)$ law, not appearing aligned with the non-significant effects. The standardized effect is the ratio between the difference in the value of the response and its mean and standard deviation. This represents not only whether the value of the variable is above or below the mean, but also how far it deviates from it. Those standardized effects that deviate from the straight line towards the ends on the normal probability plot are significant. Those that deviate to the left indicate that the value of the response increases at their −1 level, while, analogously, those that deviate to the right indicate that the value of the response increases at their +1 level [31]. The standardized effects were compared on a normal probability plot using the Statgraphics Plus (version 5.1) program.

The microstructural changes in the eight experiments were analyzed by means of optical microscopy and scanning electron microscopy. Table 4 shows the parameters used in the nitriding process. The optical microscope employed was a NIKON Epiphot 200 (Nikon, Tokyo, Japan) and the scanning electron microscopy employed was a JEOL JSM-5600 (JEOL, Nieuw-Vennep, The Netherlands). The method followed consisted of washing the plasma treatment chamber with mixing gas for a period of 10 min, after which the treatment commenced.

Table 4. Parameters used in the plasma nitriding process.

Gas Mixture	**70vol.%N_2 + 30vol.%H_2**
Gas flow(cm^3/s)	0.14
Temperature (°C)	540
Pressure (Pa)	400
Time (min)	120
Output voltage (V)	500

3. Results

Table 5 shows the mean values obtained for the studied responses and the standardized effects corresponding to the Factors and Interactions indicated in the column denominated "Confounding Pattern". The row corresponding to the mean shows the average value obtained for each of the responses.

Table 5. Mean values and standardized effects for the analyzed parameters.

Experiment	Mean Hardness HV125		Microhardness of Matrix Phase HV0.05		Wear (mg/min)		Confounding Pattern
	Values	Effect	Values	Effect	Values	Effect	
1	833	948.6	764	879.2	59.64	60.73	Mean
2	679	−169.2	603	−186.5	61.9	−0.23	A+BC+CE
3	877	0.2	792	16	61.92	0.70	B+AD+CF
4	693	356.2	643	375.5	59.2	0.13	C+AE+BF
5	1178	−55.2	1129	−36	58.8	−2.55	D+AB+EF
6	1104	−0.2	989	−31.5	61.18	0.00	E+AC+DF
7	1245	−28.7	1205	18	63.04	0.91	F+BC+DE
8	980	−40.2	909	42	60.18	−0.06	AF+BE+CD

Figures 1–3 show the representation of these standardized effects on a normal probabilistic plot, highlighting those that have a significant effect on these responses (these Factors do not appear aligned in a representation of the effects on a normal probability plot).

1. Figure 1 shows that Factors A (austenitization temperature) and C (nitriding) have a significant effect on the representative hardness of the material: If Factor A is placed at its −1 level (1000 °C) and Factor C at its +1 level (nitriding treatment), there is a significant increase in hardness.
2. Figure 2 shows the analysis of the hardness on the matrix constituent, mainly made up of martensite, retained austenite and secondary carbides formed during the destabilization of austenite. It is confirmed that if the aforementioned Factors (destabilization heat temperature of the austenite and nitriding treatment) are placed at their respective −1 and +1 levels, there is an increase in said hardness.
3. Figure 3 shows that the Factors found to have a significant effect on erosive wear are B (dwell time at the destabilization heat temperature of austenite), D (cooling medium used in the quench) and F (tempering time).To increase the wear resistance of the material, these Factors should be placed at their respective −1 (dwell time at the destabilization temperature of austenite: 4 h), +1 (quenching in oil) and −1 (dwell time at the tempering temperature: 3 h) levels. It is worth noting that, in this case, neither the nitriding treatment nor the tempering temperature was found to have a significant effect on said erosive wear resistance.

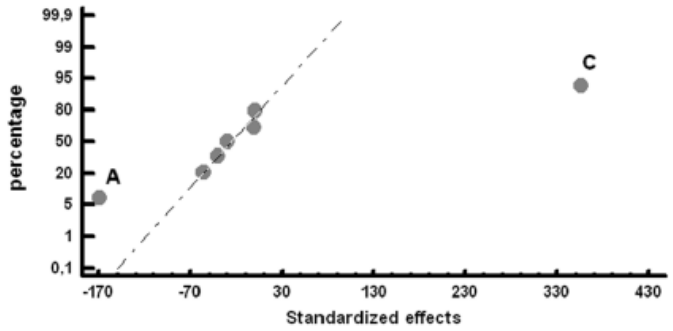

Figure 1. Standardized effects on the overall hardness, on a normal probability plot.

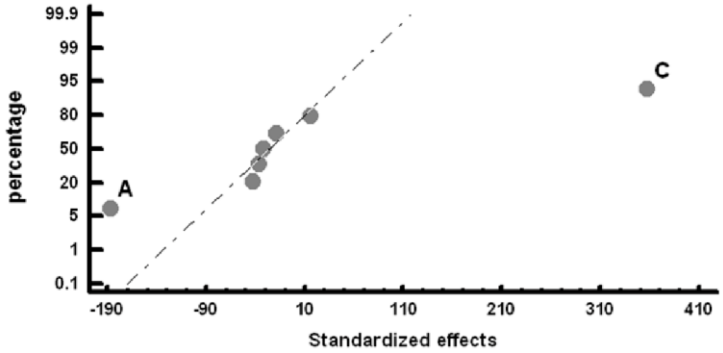

Figure 2. Standardized effects on the hardness of the matrix, on a normal probability plot.

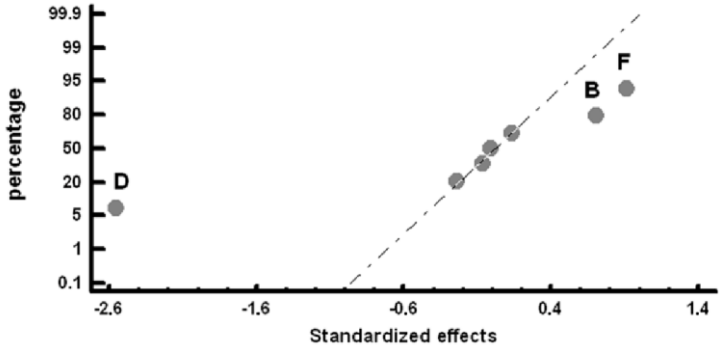

Figure 3. Standardized effects on the erosive wear, on a normal probability plot.

Figure 4 provides a representative image of the thickness of the nitrided layer in Experiments 5 to 8. It can be seen that the thickness of the nitrided layer varies between 50 and 75 µm. The greatest layer thicknesses are obtained in Experiments 5 and 7, where the mean thicknesses are 70 and 62 µm, respectively. These two experiments coincide in terms of the temperature applied to destabilize the austenite (1000 °C) and the lowest tempering temperature (200 °C). Figure 5 shows the phases and constituents that were analyzed semi-quantitatively by energy-dispersive X-ray (EDX) microanalysis in the nitrided layers of Experiments 5 to 8. Table 6 shows the results thus obtained. It should be noted that pre-existing eutectic carbides of the M_7C_3 type, transform into carbonitrides [32] after nitriding treatment (Spectra 1 and 3). The values show weight percentages exceeding 14 wt.%N. However, the matrix constituent of the nitrided layer reaches mean values of 4–8 wt.% N (Spectra 2,4,7,8,10 and 11) denoting lower N enrichment. Due to the low solubility of N in Fe and its higher affinity of this element for Cr and Mo (Ellingham diagram of nitride formation), it is reasonable to expect the presence of nitrides of Cr

and Mo in tempered martensite, in addition to Fe–N system nitrides. This outmost layer is hard and yet very fragile. During the process of erosive wear peeling of this layer could occur, thus failing to provide further wear resistance. Spectra 5,6,9,12,13 and14 show the approximate weight percentages of the elements that constitute the eutectic carbides M_7C_3 and the eutectic constituent, formed by martensite, retained austenite and secondary carbides, which are located outside the nitride layer.

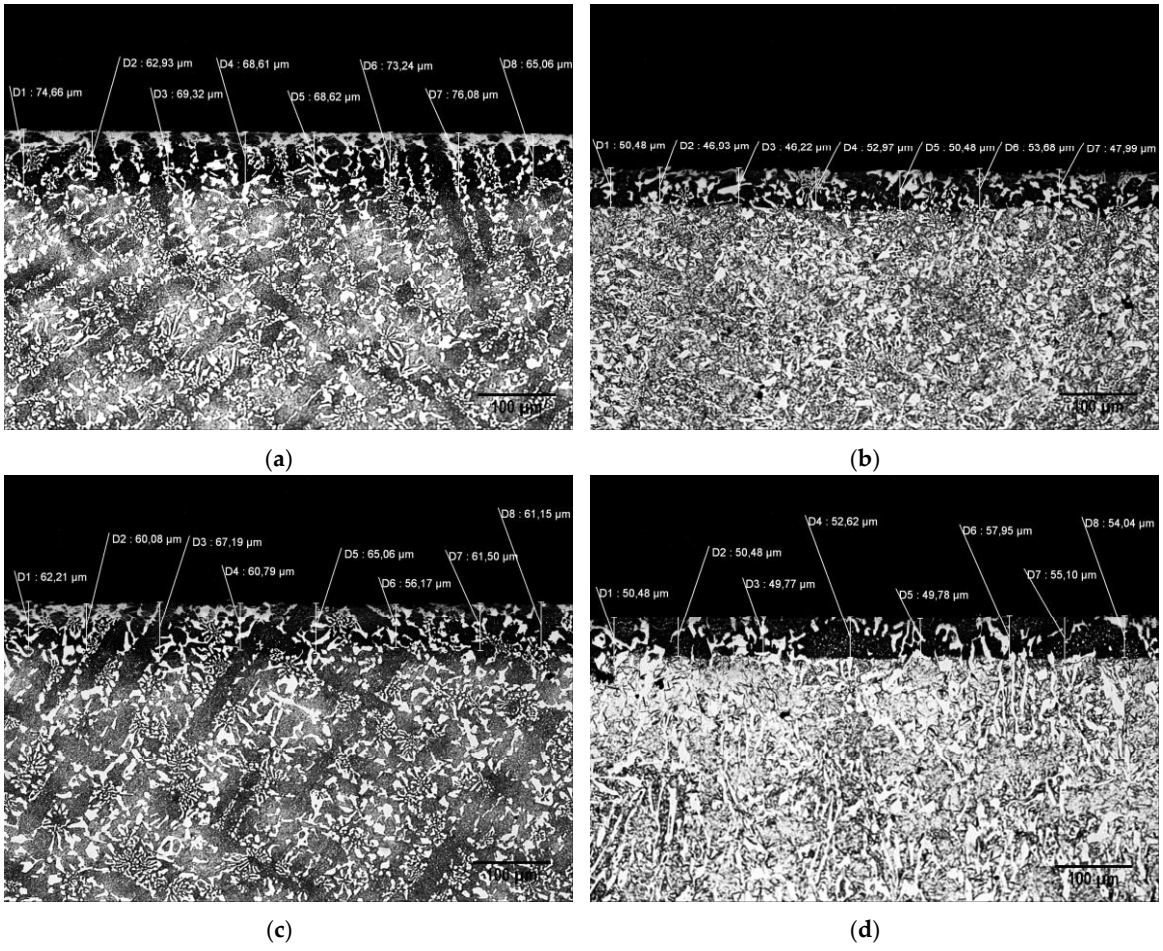

Figure 4. Representative image of the thickness of the nitrided layer. (**a**): Experiment 5; (**b**): Experiment 6; (**c**): Experiment 7; (**d**): Experiment 8.

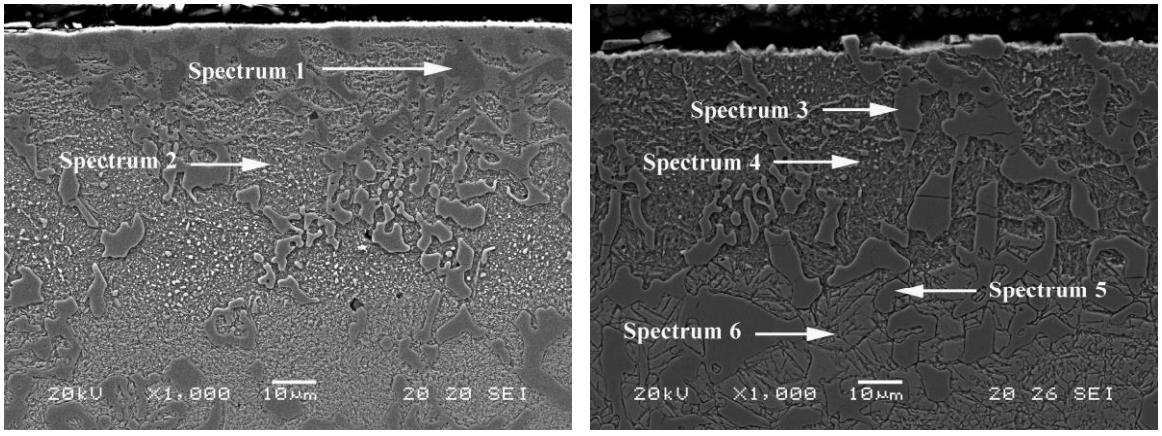

Figure 5. *Cont.*

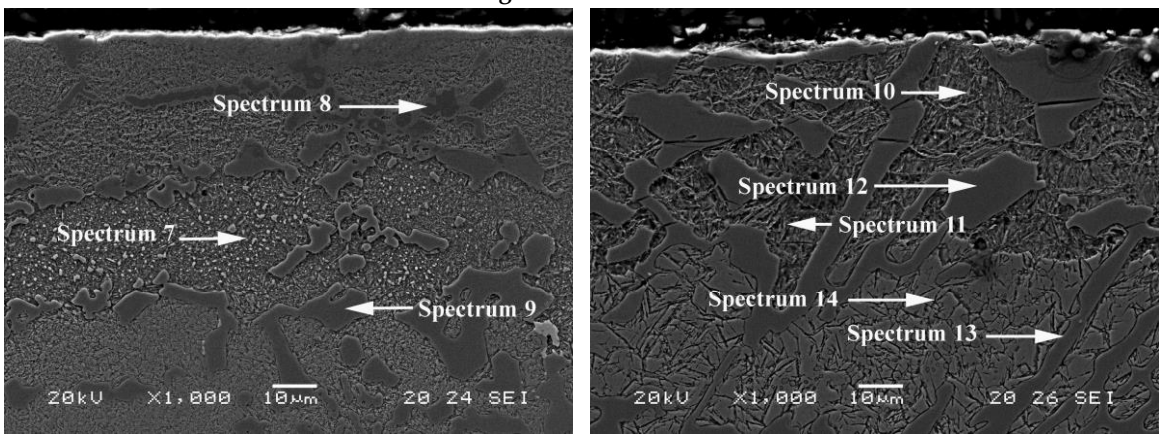

(**c**) (**d**)

Figure 5. Phases and constituents in the nitrided layer analyzed by energy dispersive X-ray (EDX) microanalysis. (**a**) Experiment 5; (**b**) Experiment 6; (**c**) Experiment 7; (**d**) Experiment 8.

Table 6. Semi-quantitative analysis of the phases listed in Figure 5, determined by characteristic energy dispersive X-ray (EDX) microanalysis. (% in weight).

Figure	Exp.	Spectrum	N	Si	Cr	Fe	Mo	Quenching			Tempering	
(a)	5	1	16.1	-	44.5	37.2	2.2	1000 ^{0}C	4 h	Oil	200 ^{0}C	3 h
		2	4.1	1.7	7.5	86.6	-					
(b)	6	3	14.9	-	36.0	46.5	2.5	1100 ^{0}C	4 h	Air	500 ^{0}C	3 h
		4	8.4	1.7	10	77.3	2.6					
		5	-	-	51.8	45.9	2.2					
		6	-	1.8	7.9	89.3	1.1					
(c)	7	7	15.1	-	48.3	34.7	1.8	1000 ^{0}C	8 h	Air	200 ^{0}C	6 h
		8	6.3	1.6	8.3	82.7	1.3					
		9	-	-	56.8	43.2	-					
(d)	8	10	6.7	2.3	8.9	80.7	1.4	1100 ^{0}C	8 h	Oil	500 ^{0}C	6 h
		11	8.6	2.2	8.9	78.6	1.7					
		12	15.2	-	42.4	39.3	3.1					
		13	-	-	51.8	45.5	2.6					
		14	-	1.8	8.1	89.5	0.7					

4. Conclusions

With regard to hypoeutectic white cast irons with 18 wt.% Cr and 2 wt.% Mo, subjected to different heat treatments to destabilize austenite, different quench conditions, different tempering conditions, with or without ionic nitriding treatment, it is concluded that:

1. There is a difference between the Factors that condition the hardness of the material and those that condition its erosive wear resistance. The highest increase in hardness is obtained when the temperature employed to destabilize the austenite is 1000 °C and when the material is subjected to a nitriding treatment. However, the highest erosive wear resistance is obtained with the shortest dwell time at the destabilization temperature (4 h), quenching in oil, and employing the shortest tempering times (3 h).
2. Among the nitrided samples, it was found that the eutectic carbides located in the nitrided layer are transformed into carbonitrides and that the greater thicknesses of nitrided layers

are obtained when the temperature employed to destabilize the austenite was 1000 °C and the tempering temperature was 200 °C. However, despite what was expected, the nitriding treatment does not have a significant effect on erosive wear resistance.

Author Contributions: J.A.-L. conceived and designed the experiments; A.G.-P. performed the experiments; and F.A.-A. analyzed the data and wrote the paper.

Acknowledgments: To carry out this study, we are grateful to the Spanish company Acutrim, and in particular we thank the Director of the company, Joaquim Morell, for the help provided in the nitriding of the samples.

Conflicts of Interest: The authors declare no conflict of interest.

References

1. Pero-Sanz, J.A. *Fundiciones Férreas*; Dossat: Madrid, Spain, 1994; p. 154.
2. Fairhust, W.; Rohrig, K. Abrasion resistant high chromium cast irons. *Foundry Trade J.* **1974**, *136*, 685–698.
3. Ju, J.; Fu, H.G.; Fu, D.M.; Wei, S.Z.; Sang, P.; Wu, Z.W.; Tang, K.Z.; Lei, Y.P. Effects of Cr and V additions on the microstructure and properties of high-vanadium wear-resistant alloy steel. *Ironmak. Steelmak.* **2018**, *45*, 176–186. [CrossRef]
4. Bedolla-Jacuinde, A.; Arias, L.; Hernandez, B. Kinetics of secondary carbides precipitation in a high-chromium white iron. *J. Mater. Eng. Perform.* **2003**, *12*, 371–382. [CrossRef]
5. Heino, V.; Kallio, M.; Valtonen, K.; Kuokkala, V.T. The role of microstructure in high stress abrasion of white cast irons. *Wear* **2017**, *388*, 119–125. [CrossRef]
6. Filipovic, M.M. Iron-chromium-carbon-vanadium white cast irons—The microstructure and properties. *Hem. Ind.* **2014**, *68*, 413–427. [CrossRef]
7. Guitar, M.A.; Suarez, S.; Prat, O.; Guigou, M.D.; Gari, V.; Pereira, G.; Mucklich, F. High Chromium Cast Irons:
   Destabilized-Subcritical Secondary Carbide Precipitation and Its Effect on Hardness and Wear Properties.
   J. Mater. Eng. Perform. **2018**, *27*, 3877–3885. [CrossRef]
8. Gasan, H.; Erturk, F. Effects of a Destabilization Heat Treatment on the Microstructure and Abrasive Wear
   Behavior of High-Chromium White Cast Iron Investigated Using Different Characterization Techniques.
   Metall. Mater. Trans. A Phys. Metall. Mater. Sci. **2013**, *44*, 4993–5005. [CrossRef]
9. Lai, J.P.; Pan, Q.L.; Sun, Y.W.; Xiao, C.A. Effect of Si Content on the Microstructure and Wear Resistance of High Chromium Cast Iron. *ISIJ Int.* **2018**, *58*, 1532–1537. [CrossRef]
10. Antolin, J.F.A.; Garrote, L.F.; Lozano, J.A. Application of Rietveld Refinement to the correlation of the microstructure evolution of white cast irons with 18 and 25 %-wt. Cr after oil quench and successive temper treatments, with abrasive wear and bending testing. *Rev. Metal.* **2018**, *54*, 11. [CrossRef]
11. Bedolla-Jacuinde, A.; Guerra, F.V.; Mejia, I.; Zuno-Silva, J.; Rainforth, M. Abrasive wear of V-Nb-Ti alloyed high-chromium white irons. *Wear* **2015**, *332*, 1006–1011. [CrossRef]
12. Efremenko, V.; Shimizu, K.; Chabak, Y. Effect of Destabilizing Heat Treatment on Solid-State Phase Transformation in High-Chromium Cast Irons. *Metall. Mater. Trans. A Phys. Metall. Mater. Sci.* **2013**, *44*, 5434–5446. [CrossRef]

13. Liu, Q.; Shibata, H.; Hedstrom, P.; Joonsson, P.G.; Nakajima, K. Dynamic Precipitation Behavior of Secondary M7C3 Carbides in Ti-alloyed High Chromium Cast Iron. *ISIJ Int.* **2013**, *53*, 1237–1244. [CrossRef]
14. Wiengmoon, A.; Pearce, J.T.H.; Chairuangsri, T. Relationship between microstructure, hardness and corrosion resistance in 20 wt.%Cr, 27 wt.%Cr and 36 wt.%Cr high chromium cast irons. *Mater. Chem. Phys.* **2011**, *125*, 739–748. [CrossRef]
15. Karantzalis, A.E.; Lekatou, A.; Diavati, E. Effect of Destabilization Heat Treatments on the Microstructure of High-Chromium Cast Iron: A Microscopy Examination Approach. *J. Mater. Eng. Perform.* **2009**, *18*, 1078–1085. [CrossRef]
16. Kootsookos, A.; Gates, J.D. The role of secondary carbide precipitation on the fracture toughness of a reduced carbon white iron. *Mater. Sci. Eng. A Struct. Mater. Prop. Microstruct. Process.* **2008**, *490*, 313–318. [CrossRef]
17. Carpenter, S.D.; Carpenter, D.; Pearce, J.T.H. XRD and electron microscope study of a heat treated 26.6% chromium white iron microstructure. *Mater. Chem. Phys.* **2007**, *101*, 49–55. [CrossRef]
18. Wang, J.; Sun, Z.P.; Zuo, R.L.; Li, C.; Shen, B.L.; Gao, S.J.; Huang, S.J. Effects of secondary carbide precipitation and transformation on abrasion resistance of the 16Cr-1Mo-1Cu white iron. *J. Mater. Eng. Perform.* **2006**, *15*, 316–319. [CrossRef]
19. Pearce, J.T.H. Structural characterisation of high chromium cast irons. In Proceedings of the International Conference on Solidification Science and Processing: Outlook for the 21st Century, Bangalore, India, 18–21 February 2001; pp. 241–247.
20. Wang, J.; Li, C.; Liu, H.H.; Yang, H.S.; Shen, B.L.; Gao, S.J.; Huang, S.J. The precipitation and transformation of secondary carbides in a high chromium cast iron. *Mater. Charact.* **2006**, *56*, 73–78. [CrossRef]
21. Fernandez-Pariente, I.; Belzunce-Varela, F.J. Influence of different heat treatments on the microstructure of a high chromium white cast iron. *Rev. Metal.* **2006**, *42*, 279–286. [CrossRef]
22. Tenorio, J.A.S.; Albertin, E.; Espinosa, D.C.R. Effects of Mo additions on the solidification of high chromium cast iron. *Int. J. Cast Met. Res.* **2000**, *13*, 99–105. [CrossRef]
23. Karantzalis, E.; Lekatou, A.; Mavros, H. Microstructure and properties of high chromium cast irons: Effect of heat treatments and alloying additions. *Int. J. Cast Met. Res.* **2009**, *22*, 448–456. [CrossRef]
24. Cetinkaya, C. An investigation of the wear behaviours of white cast irons under different compositions. *Mater. Des.* **2006**, *27*, 437–445. [CrossRef]
25. Li, Y.C.; Li, P.; Wang, K.; Li, H.Z.; Gong, M.Y.; Tong, W.P. Microstructure and mechanical properties of a Mo alloyed high chromium cast iron after different heat treatments. *Vacuum* **2018**, *156*, 59–67. [CrossRef]
26. Scandian, C.; Boher, C.; de Mello, J.D.B.; Rezai-Aria, F. Effect of molybdenum and chromium contents in sliding wear of high-chromium white cast iron: The relationship between microstructure and wear. *Wear* **2009**, *267*, 401–408. [CrossRef]
27. Oh, H.; Lee, S.; Jung, J.Y.; Ahn, S. Correlation of microstructure with the wear resistance and fracture toughness of duocast materials composed of high-chromium white cast iron and low-chromium steel. *Metall. Mater. Trans. A Phys. Metall. Mater. Sci.* **2001**, *32*, 515–524. [CrossRef]
28. Nurjaman, F.; Sumardi, S.; Shofi, A.; Aryati, M.; Suharno, B. Effect of Molybdenum, Vanadium, Boron on Mechanical Properties of High Chromium White Cast Iron in As-Cast Condition. In Proceedings of the International Symposium on Frontier of Applied Physics (ISFAP), Bandung, Indonesia, 5–7 October 2016.
29. Pero-Sanz, J.A. *Aceros*; Dossat: Madrid, Spain, 2004; p. 558.

30. Steiner, T.; Meka, S.R.; Bischoff, E.; Waldenmaier, T.; Mittemeijer, E.J. Nitriding of ternary Fe-Cr-Mo alloys; role of the Cr/Mo-ratio. *Surf. Coat. Technol.* **2016**, *291*, 21–33. [CrossRef]
31. Prat-Bartés, A.; Tort-Martorell, X.; Grima-Cintas, P.; Pozueta-Fernández, L.; Solé-Vidal, I. *Métodos Estadísticos*, 2nd ed.; Cataluña, U.P.d., Ed.; Trillas: Jardines del Bosque, Mexico, 2004; p. 376.
32. Tancret, F.; Laigo, J.; Christien, F.; Le Gall, R.; Furtado, J. Phase transformations in Fe-Ni-Cr heat-resistant alloys for reformer tube applications. *Mater. Sci. Technol.* **2018**, *34*, 1333–1343. [CrossRef]

metals

MDPI

Article

Optimization of Thermal Processes Applied to Hypoeutectic White Cast Iron containing 25% Cr Aimed at Increasing Erosive Wear Resistance.

Alejandro Gonzalez-Pociño[1], Florentino Alvarez-Antolin [1]* and Juan Asensio-Lozano[1]

[1]Materials Pro Group, Departamento de Ciencia de los Materiales e Ingeniería Metalúrgica, Universidad de Oviedo, Independencia 13, 33004 Oviedo, Spain; gonzalezpalejandro@uniovi.es (A.G.); jasensio@uniovi.es (J.A.)

* Correspondence: alvarezflorentino@uniovi.es; Tel.: +34-985-181-949

Received: 9 February 2020; Accepted: 6 March 2020; Published: 9 March 2020

Abstract: Hypoeutectic white cast irons containing 25% Cr are used in very demanding environments that require high resistance to erosive wear, for instance, the crushing and processing of minerals or the manufacture of cement. This high percentage in Cr, in turn, favors corrosion resistance. The application of a Design of Experiments (DoE) allows the analysis of the effects of modifying certain factors related to the heat treatments applied to these alloys. Among these factors, the influence of prior softening treatment to facilitate the machining of these cast irons and the influence of the factors related to the destabilization of austenite, during both quenching and tempering, were analyzed. The precipitated phases were identified by X-ray diffraction (XRD), while the Rietveld structural refinement method was used to determine their percentages by weight. Erosive wear resistance was calculated using the ASTM G76 standard test method. It is concluded that the thermal softening treatment, consisting of 2 h at 1000 °C and 24 h at 700 °C, does not result in additional softening of the material compared to its as-cast state. Furthermore, it is observed that not only eutectic carbides influence wear resistance, but that the influence of the matrix constituent is also significant. It is also verified that the tempering treatment plays a decisive role in wear resistance. Temperatures of 500 °C and tempering times of 6 h increase the wear resistance and hardness of the aforementioned matrix constituent. Tempering temperatures of 200 °C lead to an increase in retained austenite content and the presence of M3C carbides versus mixed M7C3 and M23C6 carbides. The quench cooling medium is not found to have a significant influence on the hardness or wear resistance.

Keywords: high-Cr white cast irons; Rietveld structural refinement; erosive wear resistance; destabilization of austenite; secondary carbides; tempering

1. Introduction

High-Cr white cast irons are widely used to withstand abrasive and erosive wear in applications such as the crushing and processing of minerals, cement manufacturing, and the pumping of sludge generated in these industries [1,2]. These alloys usually contain between 15 and 30% Cr [1]. Wear resistance increases as the percentage of chromium increases [3]. The type and distribution of eutectic or secondary carbides depend on the composition of the alloy and the heat treatments it is subjected to [1]. To enhance the wear resistance of these cast irons, it is advisable to carry out a treatment to destabilize the austenite [4]. The destabilization of austenite requires long dwell times at the austenitization temperature, due to the high concentration of alloy elements in the austenite crystalline cell, which hinders the diffusion of carbon. With increasing dwell time at the destabilization temperature, two kinetics simultaneously compete with one another: On the one hand, the dissolution of eutectic carbides that have formed as a result of non-equilibrium solidification and, on the other, an increase in the amount of precipitated secondary carbides [5]. Excessive dwell times can lead to the thickening of these secondary carbides [6]. Eutectic carbides are always of the M7C3 type, also called K2 carbides. However, depending on the chromium content, the secondary carbides can be of the M7C3 type and the M23C6 type also called K1 carbides [1,7–10]. Besides precipitating during the austenite destabilization treatment, secondary carbides can precipitate during tempering [11]. Carpenter et al. conclude that the majority of secondary carbides precipitated in cast irons with 26% Cr are of type K1, which would have a cubic structure with a mesh parameter of 1.04 nm [12].

The matrix phase of these cast irons is austenite, which explains why they show greater toughness than Ni-hard cast irons [7,13,14]. This austenite has a high hardenability that allows its transformation into martensite by means of simple air cooling [15]. Erosive wear resistance fundamentally depends on the behavior of the matrix constituent, made up of austenite and secondary carbides [2]. The hardness of K2 carbides falls within the 1500–1800 HV range, so the hardness of the matrix constituent exceeds that of most abrasive materials, particularly corundum (1300 HV) and quartz (800–1000 HV). Only SiC (2500 HV) would exceed it in terms of hardness [16]. From all the above, it follows that erosive wear of these carbides would not occur, but rather their detachment when the surrounding phase becomes worn [17]. Cast irons with a very high percentage in Cr are those that show greater resistance to oxidation and corrosion. In particular, Cr/C ratios close to or greater than 10 are found to be favorable [18]. This group of wear- and corrosion-resistant Crrich alloy cast irons would include those with a Cr content of around 25% and a C content of around 2.5–2.8%.

The aim of this study is to optimize the erosive wear resistance of a white cast iron containing 25% Cr by the application of a Design of Experiments (DoE). For this purpose, the difference in results obtained via the controlled variation of the process parameters related to the applied heat treatments is measured and analyzed. The aim is to correlate the results with the microstructural variations the material undergoes following these process modifications. In particular, parameters related to the destabilization of austenite, the quench cooling medium, and the tempering conditions are analyzed. Table 1 shows the chemical composition of this white cast iron. The research methodology followed was the application of a fractional DoE, in which six factors were analyzed, performing eight experiments in all [19]. The results will allow manufacturers of this material to design the most suitable heat treatment so that the material offers high wear resistance in the aforementioned industries.

Table 1. Chemical Composition (% by weight).

C	Si	Mn	Cr	Mo
2.7	1.2	0.8	25.1	0.5

2. Materials and Methods

Via the application of a DoE, the aim is to modify certain manufacturing parameters in a deliberate and controlled manner so as to analyze the variations produced in the properties of the material. In this case, the aim is to analyze the variations in the erosive wear resistance and microstructure of the material so as to subsequently correlate in-service performance with these microstructural changes. Statistical analysis of the variations in the responses of the material enables us to determine which of the analyzed factors has a significant effect on its wear resistance. Table 2 shows the analyzed factors and the levels of analysis in each of these factors. Among the factors listed in Table 2, the meaning of factor C needs clarifying. This is a softening treatment aimed at facilitating the machining of this material before the hardening treatment [20]. This heat treatment consisted of 2 h at 1000 °C and 24 h at 700 °C. The goals of this treatment would be to destabilize the retained austenite and to seek a majority presence of perlite, thus facilitating hypothetical machining should it be necessary for the manufacture of industrial components using this material. The proposed dwell times at the destabilization temperature of austenite in the quenching process, Factor B, are higher than usual. The redissolution of any possible cementite carbides precipitated during the softening treatment is, thus sought, thereby favoring the precipitation of Cr-rich secondary carbides and an increase in the Ms temperature so as to avoid the presence of retained austenite as far as possible after quenching [20].

Table 2. Factors and Levels.

	Factors	**Levels**	
Code	**Metallurgical parameter**	**Level −1**	**Level +1**
A	Destabilization temperature of austenite (°C)	1000	1100
B	Dwell time at the destabilization temperature of austenite (h)	4	8
C	Softening treatment prior to hardening	yes	no
D	Quench cooling medium	air	oil
E	Tempering temperature (°C)	200	500
F	Tempering dwell time (h)	3	6

The effect of a factor is defined as the variation in certain property of the material as a result of the variation of said factor. The property of the material may be the wearing resistance, hardness, the volume fraction of retained austenite, et cetera. This type of effect is called the main effect. Sometimes, the effect of one factor depends on the value that another takes. When this occurs, these factors are said to interact. The influence of the main effects on the variations in the response of the material is greater than that of the two-factor interactions. In turn, the influence of the two-factor interactions is greater than that of the three-factor interactions, and so on successively. In industrial practice, it is sufficient to take into account the main effects and two-factors interactions. This simplification allows for reducing the number of experiments. In this study, the effect of six factors with eight experiments has been analyzed. If the aim were to analyze all the possible interactions, it would be necessary to perform 64 experiments ($2^6 = 64$). In the case in hand, however, only eight effects (2^{6-3}) have been estimated, which means a 1/8 (64/8 = 8) fractional factorial design. Table 3 shows the array of experiments thus generated to carry out a DoE with six factors, two levels for each factor, and eight experiments. Columns D, E, and F have been, respectively, constructed from the product of columns A × B, A × C, and B × C. The "Restricted Confounding Pattern" column indicates only the main effects and those 2-factor interactions whose effects are confounded with the main effects. The main effects and interactions

may be associated with the terms of a Taylor series of the response function. Hence, by excluding third-order interactions, the third-order terms of the Taylor series would likewise be excluded. This allows performing fractional DOEs, reducing the number of experiments, but assuming a possible error resulting from excluding interactions between factors. The confounding pattern should include all the effects confounded with each other. However, Table 3 shows a restricted confounding pattern in which only the main effects and the two-factor interactions are represented. The aim of using a fractional approach is not to achieve a good fit, but to try to determine which factors have a significant effect on the response variable.

Table 3. The array of Experiments.

Experiment	A	B	C	D = A × B	E = A × C	F = B × C	Restricted Confounding Pattern
1	-1	-1	-1	+1	+1	+1	A + BD + CE
2	+1	−1	−1	−1	−1	+1	B + AD + CF
3	−1	+1	−1	−1	+1	−1	C + AE + BF
4	+1	+1	−1	+1	−1	−1	D + AB + EF
5	−1	−1	+1	+1	−1	−1	E + AC + DF
6	+1	−1	+1	−1	+1	−1	F + BC + DE
7	−1	+1	+1	−1	−1	+1	AF + BE + CD
8	+1	+1	+1	+1	+1	+1	

The effects are linear combinations of the analyzed responses. Hence, applying the central limit theorem (CLT), they will follow a normal law. If we represent the distribution function of the N (0,σ) law on the normal probability plot scale, it will take the form of a straight line. This line must necessarily pass through the coordinate point (0.50). If any calculated effect followed a different normal law, e.g., N (μ,σ'), it would not appear aligned along this line. Those effects that deviate from the straight line towards the ends on the normal probability plot are considered significant. For example, if an effect deviates to the left, this would indicate that the factor associated with this effect at its −1 level would increase the value of the response. Similarly, if an effect deviates to the right of the straight line, this would indicate that the factor associated with this effect at its +1 level would increase the value of the response. The statistical analysis was carried out with the help of the Statagraphics Centurion XVI program, version 16.1.18.

The wear resistance, hardness, and hardness of the matrix constituent were analyzed via the eight experiments listed in Table 3. The aim of the last analysis was to test whether the wear resistance of the material might have some kind of relationship with the hardness of the matrix constituent. Moreover, the possible relationship between the microstructure obtained in these experiments and the wear resistance of the material was likewise analyzed. The analyzed responses were:

- Vickers hardness of the material. The applied load was 300 N, while the hardness value was the average value obtained from 10 indentations.
- The Vickers hardness of the constituent matrix. In this case, the applied load was 0.5 N, while the hardness value was calculated as the average value obtained from 10 indentations.
- Erosive wear resistance. This test was carried out as per ASTM G76 [21] by means of compressed air blasting with corundum particles, applying a pressure of 2 bar, a flow rate of 250 g/min and a 30° angle of incidence on the sample surface. The times employed in each experiment were 2, 4, and 6 min. Three repetitions were performed per test. The weight loss per unit time (mg/min) was determined from the average values obtained at each test time. As noted in the aforementioned standard, the results are shown in mm^3 of material loss per gram of abrasive (mm^3/g).
- The following microstructural variables:

- percentage by weight of austenite
- percentage by weight of martensite
- percentage by weight of carbides
- volume of the austenite crystal cell

The microstructural variables were determined by X-ray diffraction on a SEIFERT XRD 3000 T/T diffractometer (Baker Hughes, Celle, Germany). The radiation was emitted via a fine-focus Mo tube at a working power of 40 kV × 40 mA and monochromatized to the Kα doublet: λ_1 = 0.7093616 Å and λ_2 = 0.713607 Å. The diffracted intensity was determined in a 2θ range from 7 to 57° with an angular step and counting time of approximately 0.03° and 22 s, respectively. To calibrate the equipment, the position of the reflections and the profiles of the associated Bragg peaks were calibrated with the National Institute of Standards and Technology (NIST) Si (640C) standard and LaB6 (660a) standard, respectively. The Rietveld structural refinement method was used to determine the percentage of the crystalline phases via fitting of the diffractograms. To this end, following the recording of the diffraction figures, a structural refinement was carried out using the crystallographic information files present in the Inorganic Crystal Structure Database (ICSD), FIZ Karlsruhe, Germany. The program employed for this purpose was FullProf.2k, version 6.20 (2018). The increase in width observed in the peaks of the majority phases were modeled using Stephens' formulation [22], which is implemented in the aforementioned analysis program.

3. Results

Figure 1 shows the microstructure of these cast irons in the as-cast state following solidification in a sand mold. This microstructure is mainly made up of eutectic carbides of the K_2 type, retained austenite and pearlite. The proeutectic austenite presents a dendritic growth model. The presence of the eutectic constituent can be observed between these dendrites. The hardness of the cast iron in this state was 305 HV.

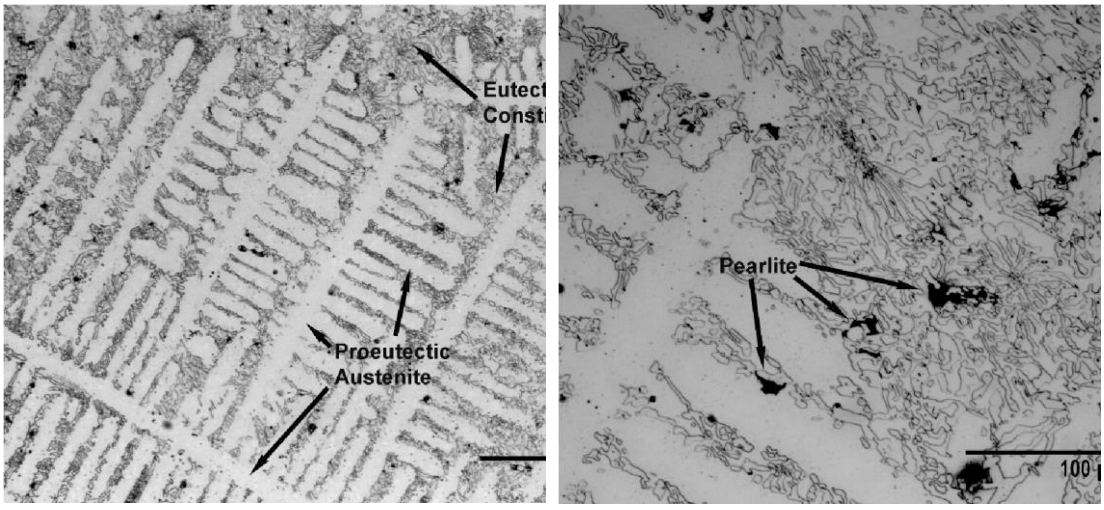

(**a**) (**b**)

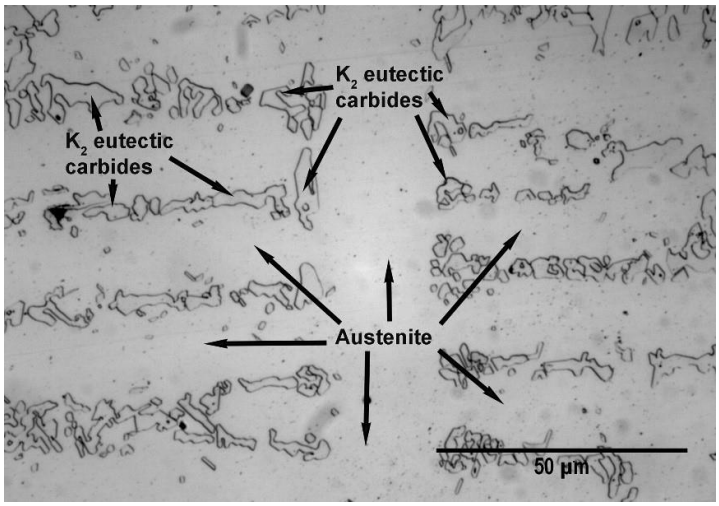

(**c**)

Figure 1. As-cast microstructure: (**a**) ×200 magnification; (**b**) ×500 magnification; (**c**) ×1000 magnification.

One of the analyzed factors was the effect of a possible softening treatment designed to facilitate machining of this material with chip removal [20]. Figure 2 shows the microstructure obtained following this treatment. Coalescence and thickening of the secondary carbides precipitated during the destabilization of austenite, prior to the isothermal dwell time at 700 °C, can be observed [20,23]. However, the measured hardness in this state reached an average value of 360 HV, which was greater than of the as-cast state. This reason for this could be the high volume fraction of retained austenite that these cast irons present in said as-cast state [24]. From all the above, it follows that if the aim were to machine this material before its hardening by heat treatment, it would not be necessary to perform a prior softening treatment, contrary to what was concluded in a previous study on white cast irons containing 18% Cr.

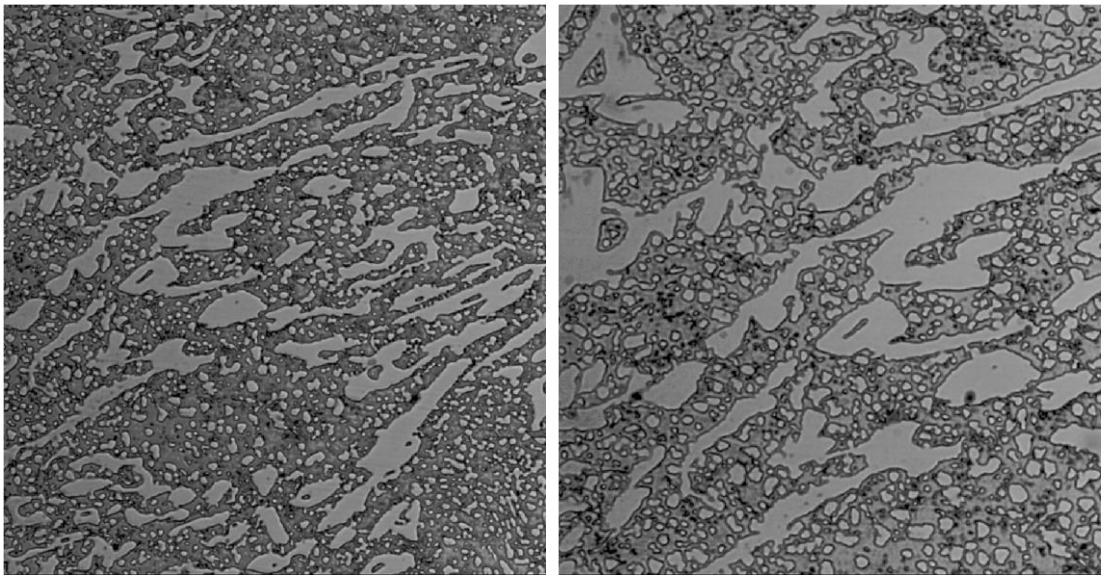

(a) **(b)**

Figure 2. Microstructure following the softening treatment: (**a**) 400× magnification; (**b**) 600× magnification.

Table 4 shows the results obtained from the analysis of:

- the overall hardness of the material
- the hardness of the constituent matrix, whose microstructure is a consequence of the destabilization of austenite and its transformation
- the weight loss in the erosive wear test.

Figure 3 shows the representation of these effects on a normal probabilistic plot, highlighting those that have a significant influence on the analyzed responses.

Figure 3a shows that factors A and E (destabilization temperature of austenite and tempering temperature) have a significant effect on the hardness of the material. Placing these two factors at their +1 level (1100 °C and 500 °C, respectively) would result in an increase in hardness. It can further be seen that some of the AE and BF interactions would have a significant effect on hardness. Table 5 shows the results of the analysis of these interactions. It can be seen that the interaction that produces a greater increase in hardness is AE when both factors are placed at their +1 level.

Figure 3b shows that E (tempering temperature) and F (tempering time) are the factors that have a significant effect on the hardness of the matrix constituent. An increase in this hardness would be achieved by placing these two factors at their +1 level (500 °C and 6 h, respectively). From these results, it may be deduced that a high tempering temperature and long tempering times favor a second destabilization of the retained austenite. The significant effect of interactions AF and BE can also be appreciated. Table 6 shows the results of the analysis of these two interactions. It follows that the effect of factor F is favored when factor A (destabilization temperature of austenite) is placed at its +1 level (1100 °C). Similarly, it follows that the effect of factor E is favored when factor B (dwell time at the destabilization temperature) is placed at its +1 level (8 h).

Figure 3c shows that factors E (tempering temperature) and F (tempering time) have a significant effect on erosive wear resistance. Placing both factors at their +1 level (500 °C and 6 h, respectively) would result in an increase in wear resistance. It should be noted that these same factors are those that have a significant influence on the hardness of the matrix constituent, thus corroborating the importance of this constituent with respect to the wear resistance.

It should also be noted that the quench cooling medium is not found to have a significant influence either on the hardness or wear resistance of the material.

Table 4. Hardness and weight loss in the erosive wear test.

No.	Hardness		Microhardness		Weight loss		Calculated
	HV (300 N)	Effect	HV (0.5 N)	Effect	$mm^3/g \times 10^6$	Effect	Effects
1	613	664.62	570	550.75	14.5	21.73	Average
2	655	64.25	570	-0.5	19.5	1.57	A+BD+CE
3	642	15.75	597	2.5	25.1	3.57	B+AD+CF
4	670	39.25	459	3.5	25	1.27	C+AE+BF
5	639	2.75	498	-31.5	25.1	-0.87	D+AB+EF
6	720	29.25	560	68.5	20.7	-4.47	E+AC+DF
7	636	-6.25	539	44.5	19.1	1.42	F+BC+DE
8	742	9.75	613	37.5	24.1	3.82	AF+BE+CD

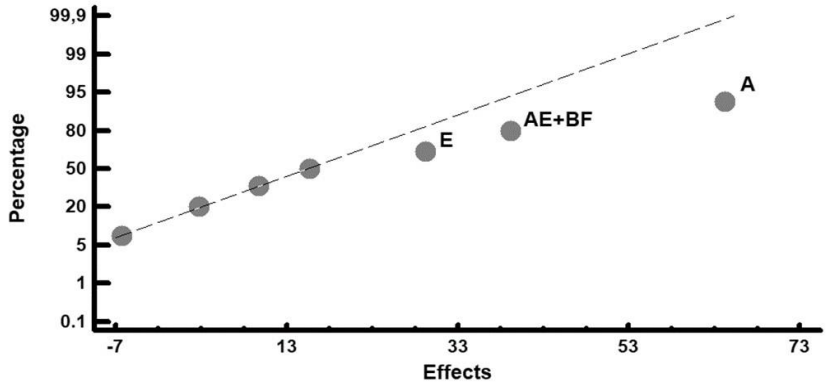

(**a**)

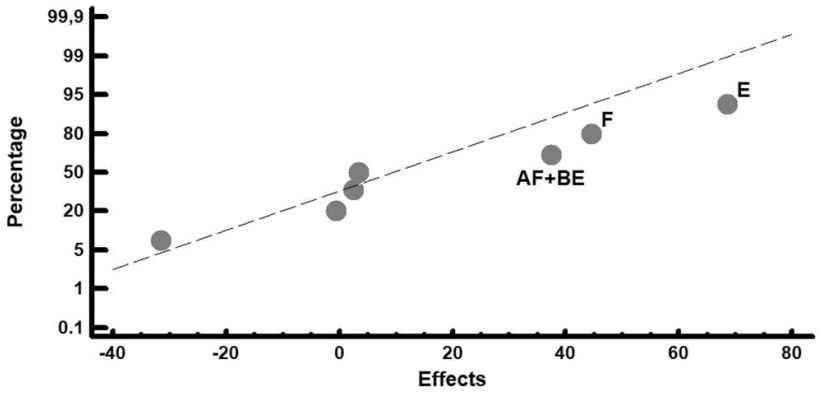

(**b**)

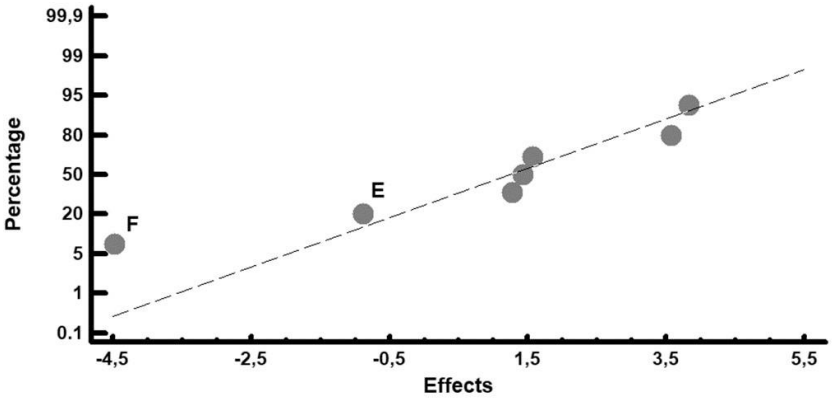

(**c**)

Figure 3. Representation of the effects on a normal probability plot. Those factors with a significant effect on the analyzed responses are highlighted. (**a**) overall hardness; (**b**) hardness of the matrix phase; (**c**) weight loss in the erosive wear test ($mm^3/g \times 10^6$).

Table 5. Analysis of the effects of interactions AE and BF on the hardness of the material.

AE	**−1**	**+1**	**BF**	**−1**	**+1**
−1	638	613	**−1**	680	634
+1	663	**731**	**+1**	656	689

Table 6. Analysis of the effects of interactions AF and BE on the hardness of the matrix constituent.

AE	−1	+1	BF	−1	+1
−1	547	555	**−1**	534	565
+1	509	**592**	**+1**	499	**605**

Figure 4 shows the diffractograms obtained in the eight experiments, highlighting the main identified phases.

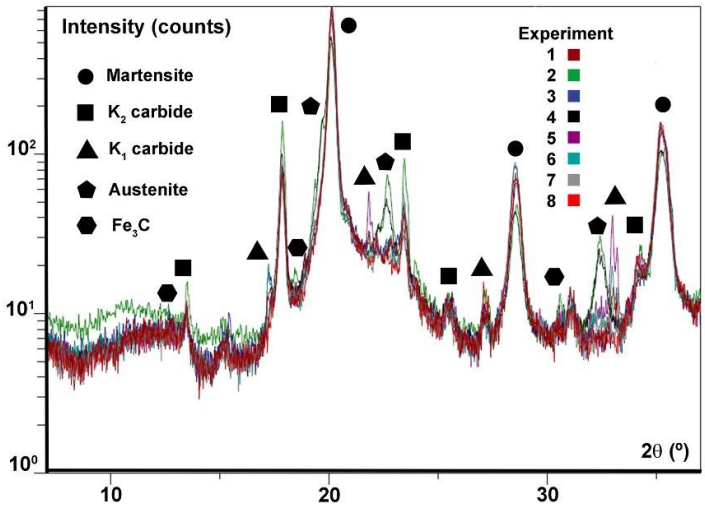

Figure 4. Superimposed diffractograms obtained in the eight experiments.

Figure 5 shows the overall fittings using the Rietveld method. The red marks indicate the observed intensities; the black line, the intensity calculated according to the Rietveld structural model; the blue line, the difference between the two, while the vertical segments indicate the angular positions of the different identified phases.

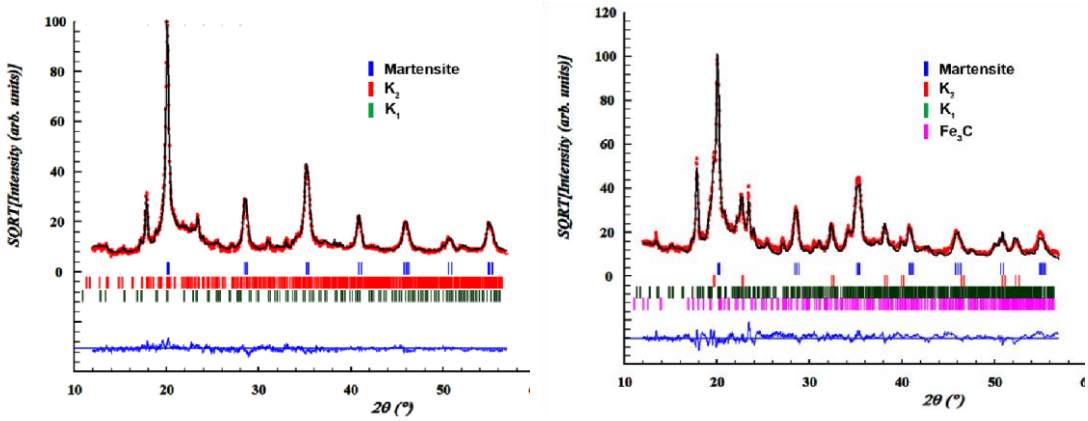

Experiment 1 Experiment 2

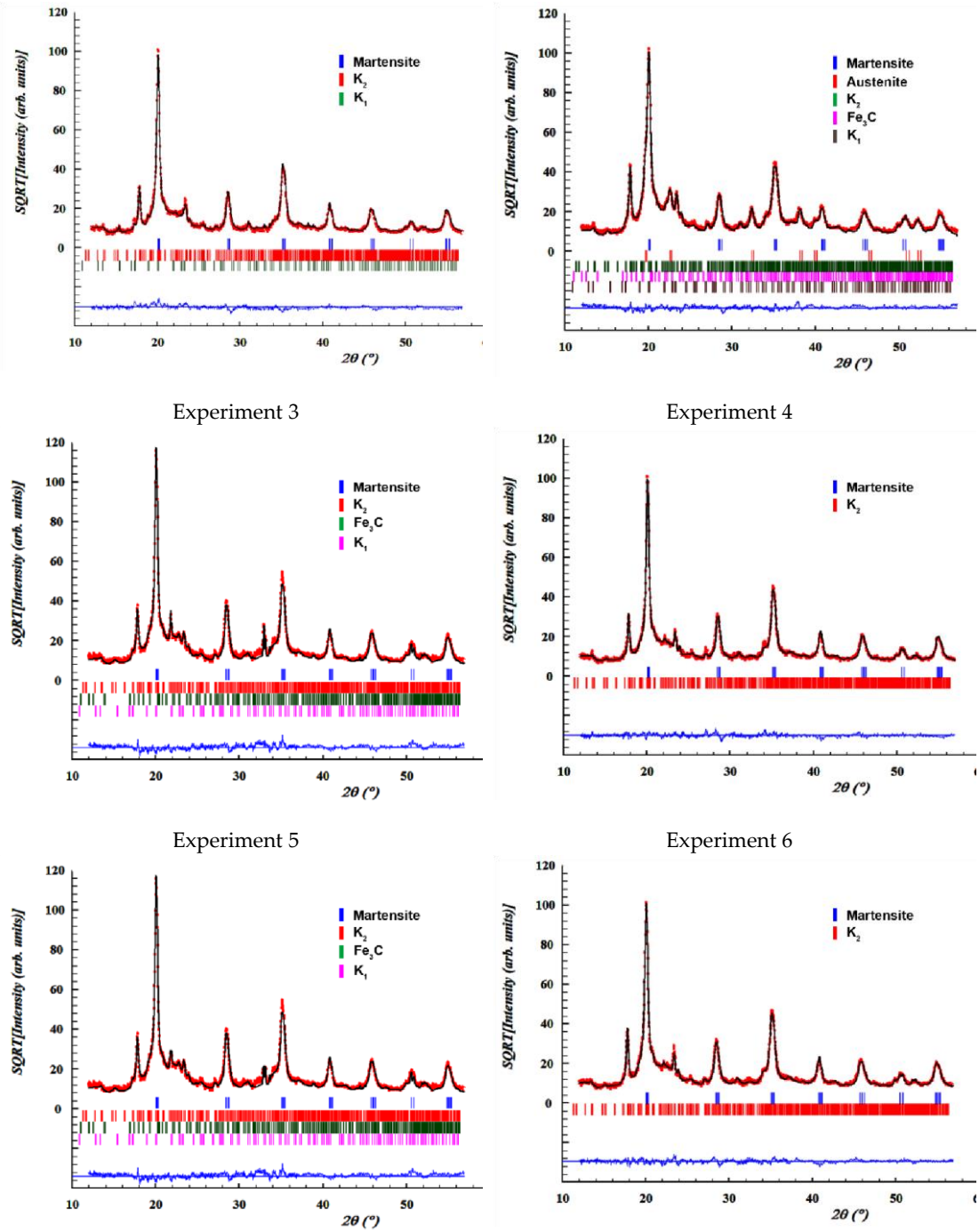

Figure 5. Overall fittings using the Rietveld method. The red marks define the observed intensities

Table 7 shows the percentages by weight and the mesh parameters of the main crystalline phases detected by XRD. The goodness-of-fit is defined by factor Rwp, index Rexp, and the ratio of their squares, $Chi^2 = (Rwp/Rexp)^2$.

Table 7. Microstructural parameters, weight distributions of the precipitated phases, and volume of austenite. The statistical error is given between parentheses.

Experiment	Rietveld fitting	Phases	a (Å)	b (Å)	c (Å)	wt. %
1	Rwp = 13.6 Rexp = 7.94 Chi² = 2.95	Martensite K_2 carbides K_1 carbides	2.87106 (0.0005) 4.49539 (0.0157) 10.60637 (0.0008)	7.00445 (0.0079)	2.88359 (0.0010) 12.09299 (0.0081)	44.5 (4.5) 53.5 (6.8) 0.7 (0.5)
2	Rwp = 14.9 Rexp = 6.8 Chi² = 4.80	Martensite Austenite K_2 carbides Fe_3C	2.86693 (0.0009) 3.60039 (0.0006) 4.50051 (0.0036) 4.84209 (0.0029)	 6.99363 (0.0035) 6.79065 (0.0041)	2.88730 (0.0011) 12.09151 (0.0037) 4.41551 (0.0023)	13.1 (1.1) 9.0 (0.7) 75.9 (4.6) 2.0 (0.5)
3	Rwp = 15.2 Rexp = 7.85 Chi² = 3.76	Martensite K_2 carbides K_1 carbides	2.87043 (0.0005) 4.49884 (0.0166) 10.60637 (0.0008)	7.00169 (0.0081)	2.88247 (0.0011) 12.09704 (0.0083)	42.5 (3.3) 56.6 (7.1) 0.9 (0.4)
4	Rwp =11.2 Rexp = 5.85 Chi² =3.65	Martensite Austenite K_2 carbides K_1 carbides Fe_3C	2.87520 (0.011) 3.59992 (0.0009) 4.49662 (0.0098) 10.60637 (0.0008) 4.84209 (0.0029)	 7.00633 (0.0062) 6.79065 (0.0041)	2.89022 (0.0015) 12.11956 (0.0067) 4.41551 (0.0023)	26.0 (1.5) 7.3 (0.9) 65.3 (5.4) 0.1 (0.1) 1.3 (0.5)
5	Rwp =14.0 Rexp = 7.02 Chi² =3.98	Martensite K_2 carbides K_1 carbides Fe_3C	2.87064 (0.0004) 4.49496 (0.0057) 10.60637 (0.0008) 4.84209 (0.0029)	7.00124 (0.0073) 6.79065 (0.0041)	2.88780 (0.0006) 12.11749 (0.0092) 4.41551 (0.0023)	31.0 (2.0) 48.9 (3.5) 18.8 (1.7) 1.3 (0.6)
6	Rwp = 11.9 Rexp = 7.54 Chi² = 2.49	Martensite K_2 carbides	2.87125 (0.0005) 4.49711 (0.0098)	 7.00760 (0.0064)	2.88696 (0.0009) 12.10338 (0.0069)	47.5 (4.2) 52.5 (5.6)
7	Rwp = 12.7 Rexp = 7.88 Chi² =2.61	Martensite K_2 carbides K_1 carbides Fe_3C	2.87138 (0.0004) 4.49164 (0.0064) 10.60637 (0.0008) 4.84209 (0.0031)	 7.01520 (0.0064) 6.79065 (0.0043)	2.88712 (0.0007) 12.10307 (0.0079) 4.41551 (0.0028)	40 (3.8) 53.3 (5.0) 5.5 (1.5) 0.8 (0.4)
8	Rwp = 11.2 Rexp = 7.01 Chi² =2.56	Martensite K_2 carbides	2.87225 (0.0006) 4.50240 (0.0089)	 7.00719 (0.0057)	2.89017 (0.0011) 12.10593 (0.0065)	45.4 (3.2) 54.6 (5.4)

Table 6 shows the average values obtained in each experiment, together with the effects corresponding to the restricted confounding pattern specified in the array of experiments. The row corresponding to the average shows the average value obtained for each of the analyzed responses. Figure 6 shows the representation of these effects on a normal probability plot, highlighting those that have a significant effect on these responses.

Table 6. Average values and effects obtained for the phases present in the material.

(a) Percentage by weight of martensite and austenite

Experiment	martensite		austenite		Calculated effects
	(wt.%)	Effect	(wt.%)	Effect	
1	44.77	36.3463	-	2.0337	Average
2	13.09	-6.682	9.01	4.067	A + BD + CE
3	42.54	4.507	-	-0.437	B + AD + CF
4	26	9.492	7.26	-4.067	C + AE + BF
5	31.02	0.922	-	-0.437	D + AB + EF
6	47.49	17.427	-	-4.067	E + AC + DF
7	40.42	-0.832	-	0.437	F + BC + DE
8	45.44	-6.647	-	0.437	AF + BE + CD

(b) Percentage by weight of carbides

Experiment	K_1 carbides		K_2 carbides		Fe_3C		Calculated effects
	(wt. %)	Effect	(wt. %)	Effect	(wt. %)	Effect	
1	0.75	3.251	53.47	57.56	-	0.6787	Average
2	--	-6.45	75.87	9.01	2.03	0.302	A + BD + CE
3	0.87	-3.27	56.59	-0.24	-	-0.307	B + AD + CF
4	0.10	5.64	65.35	-10.51	1.29	-0.302	C + AE + BF
5	18.8	3.32	48.89	-3.99	1.30	-0.062	D + AB + EF
6	--	-5.69	52.51	-6.56	-	-1.357	E +AC + DF
7	5.49	-3.38	53.28	3.46	0.81	0.062	F + BC + DE
8	--	3.33	54.56	2.82	-	0.307	AF + BE + CD

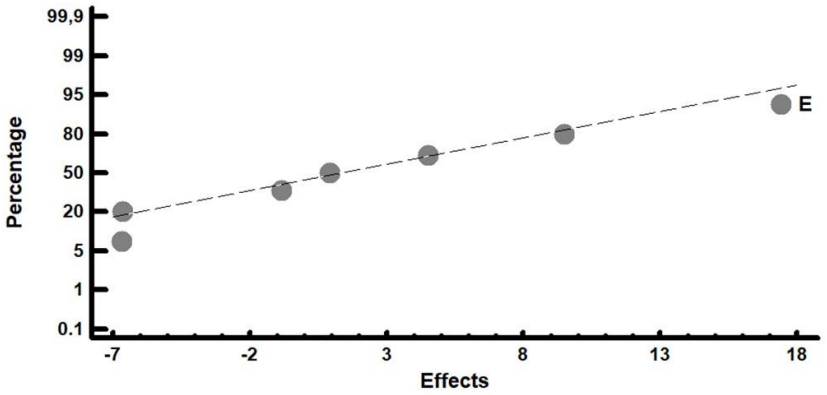

(**a**)

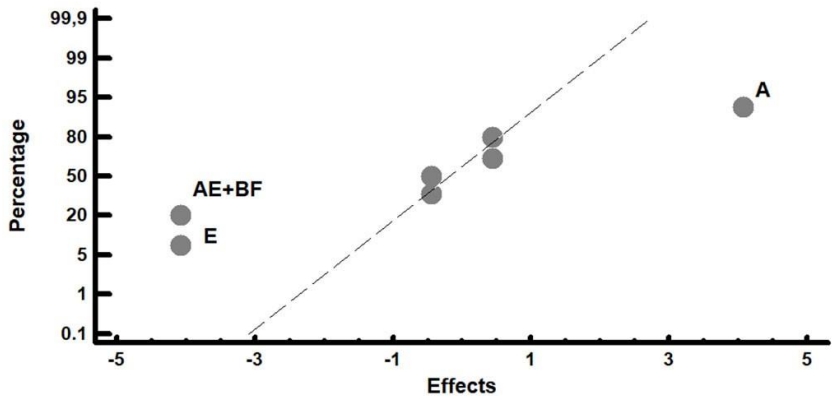

(**b**)

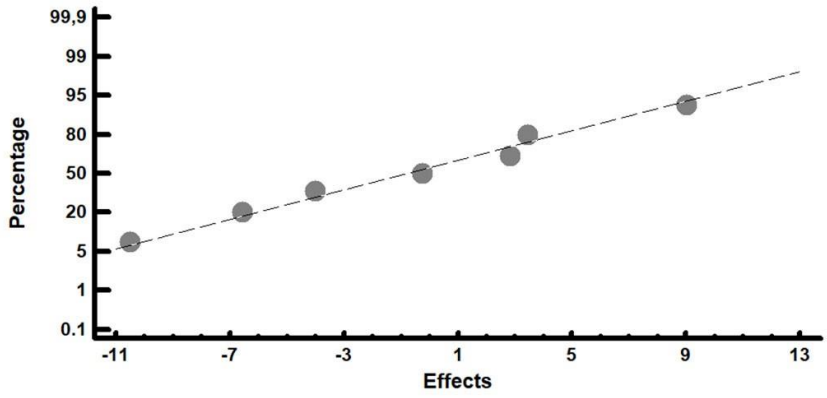

(**c**)

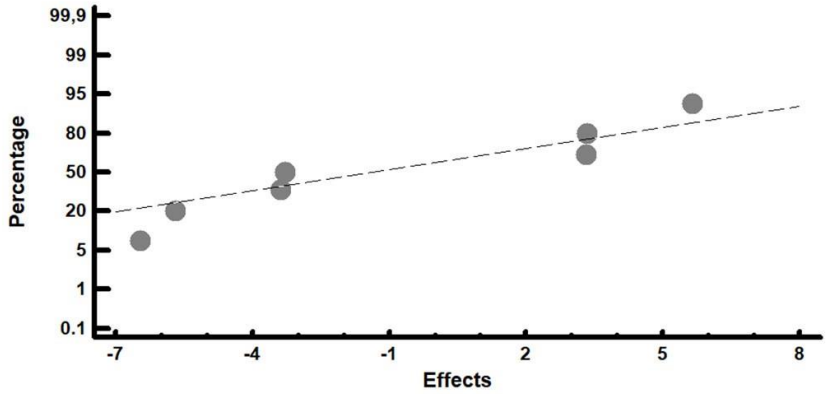

(**d**)

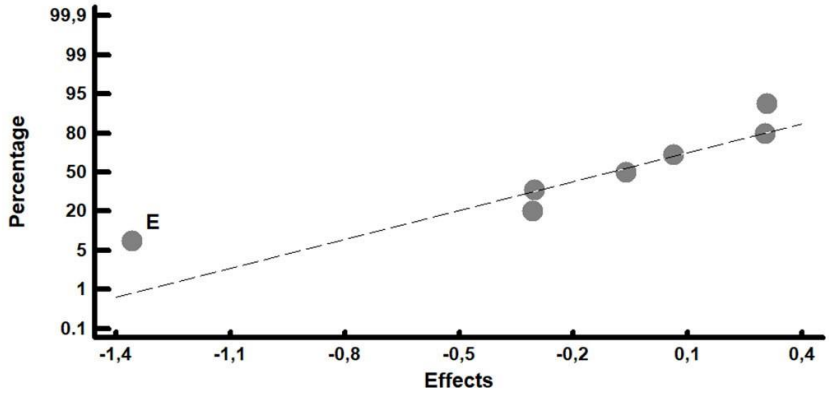

(**e**)

Figure 6. Representation of the effects on the percentages by weight of the precipitated phases on a normal probability plot. Those factors with a significant effect are highlighted. (**a**) tempered martensite; (**b**) austenite; (**c**) K_2 carbides; (**d**) K_1 carbides; (**e**) Fe_3C.

Figure 6a shows that factor E (tempering temperature) has a significant influence on the percentage of tempered martensite. If the aim were to increase this content, this factor should be placed at its +1 level (500 °C). Figure 6b shows that factors A (destabilization of austenite temperature) and E (tempering temperature) have a significant effect on the percentage of retained austenite. An increase in this phase would be obtained by placing factor A at its +1 level (1100 °C) and factor E at its −1 level (200 °C). Interactions AE+BF are also found to have a significant influence. Table 8 shows the results of their analysis. It can be seen that the effect of

factors A and E increase when these factors are respectively placed at their +1 and −1 level. From the XRD analysis, it is concluded that retained austenite is only observed in Experiments 2 and 4. These are the experiments in which a low tempering temperature (200 °C) was employed. This finding is consistent with the results shown in Figure 6b and Table 8. However, a softening treatment was also employed in these experiments. Hence, it follows that the austenitization temperature at 1100 °C is high enough to dissolve precipitated carbides during this softening treatment, thereby favoring an increase in retained austenite after cooling [25]. This austenite would be destabilized when tempering at 500 °C, but not when tempering at 200 °C. Figure 7 shows the microstructure obtained after the reported softening treatment, followed by austenitization at 1100 °C for 8 h and oil cooling. It can be seen that the precipitated carbides were considerably reduced during the softening treatment compared to Figure 2. Subsequent tempering at 500 °C would remove this retained austenite.

Table 8. Analysis of the effects of interactions AE and BF on the retained austenite.

AE	**−1**	**+1**	**BF**	**−1**	**+1**
−1	0.00	0.00	**−1**	0.00	4.50
+1	**8.13**	0.00	**+1**	3.63	0.00

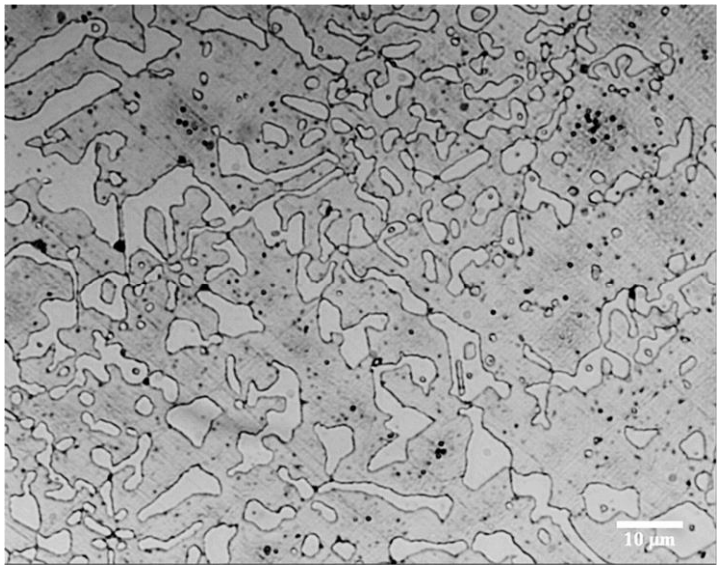

Figure 7. Microstructure obtained after the softening treatment, followed by austenitization at 1100 °C for 8 h and oil cooling. The redissolution of the carbides precipitated during the softening treatment can be observed.

Figure 6 c,d shows that none of the factors studied in this paper (within the range of levels indicated in Table 2) have a significant effect on the percentage of K_2 or K_1 carbides. However, Figure 6e shows that factor E (tempering temperature) does have a significant effect on the percentage of Fe_3C. An increase in this phase would be achieved by placing this factor at its −1 level (200 °C). Lower temperatures are required for Fe_3C to precipitate during the tempering of the martensite, as it is only the C atoms, dissolved in a solid insert solution, which have to diffuse until reaching the crystalline defects of the cubic martensite (tempered martensite). However, the precipitation of K_1 and K_2 carbides requires a) the diffusion of Cr atoms, dissolved in a solid replacement solution, and b) the prior redissolution of Fe_3C to provide C atoms in the precipitation of these carbides. Higher temperatures are necessary for these processes to take place. In the case of the precipitation of K_1 and K_2 carbides, it is necessary to reach a temperature of 500 °C. In turn, the transformation of retained austenite into martensite is also achieved by high tempering temperatures, as evidenced by the results shown in Figure 6b. This figure also

shows that high austenitization temperatures seem to favor the presence of retained austenite, as it is found alloyed with C and Cr. This could explain why the combination of a high austenitization and low tempering temperatures favored the presence of retained austenite.

Figure 8 shows a representative micrograph of each experiment that allows us to appreciate the general microstructure of these cast irons, consisting mainly of eutectic carbides of type K1, secondary carbides of type K_1, K_2, and Fe_3C (this last carbide when tempering at low temperatures, 200 °C), tempered martensite and the possible existence of retained austenite if the tempering takes place at low temperatures (200 °C).

Figure 9 shows, as a representative example, one of the tracks resulting from the wear test. In this case, the micrograph corresponds to one of the samples from Experiment 1 after 6 min of testing.

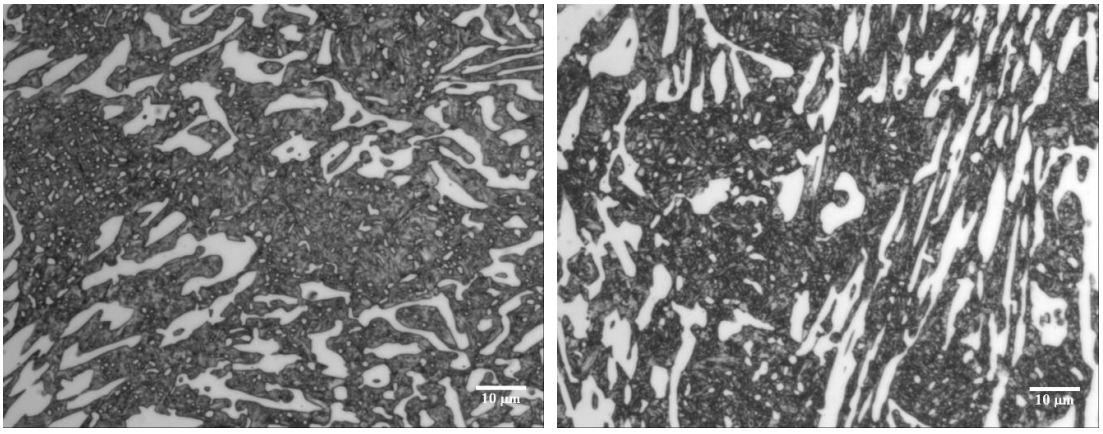

Experiment 1 Experiment 2

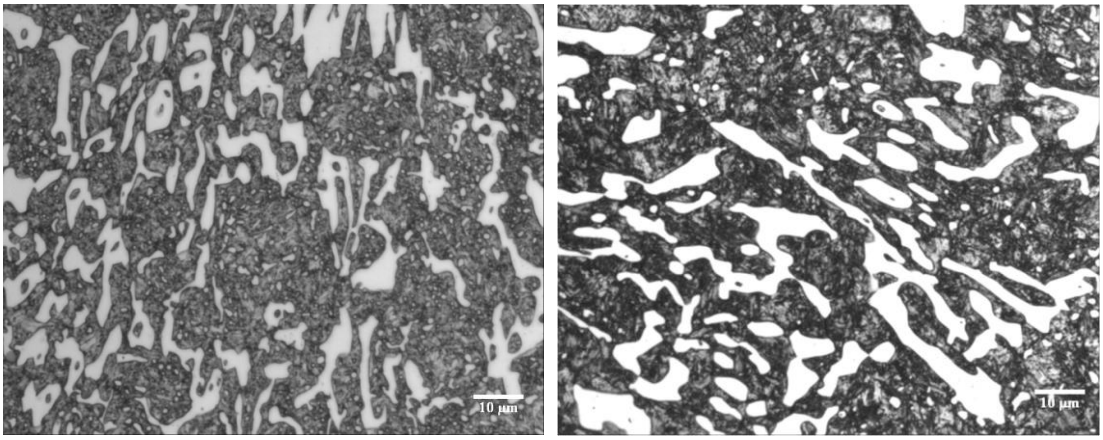

Experiment 3 Experiment 4

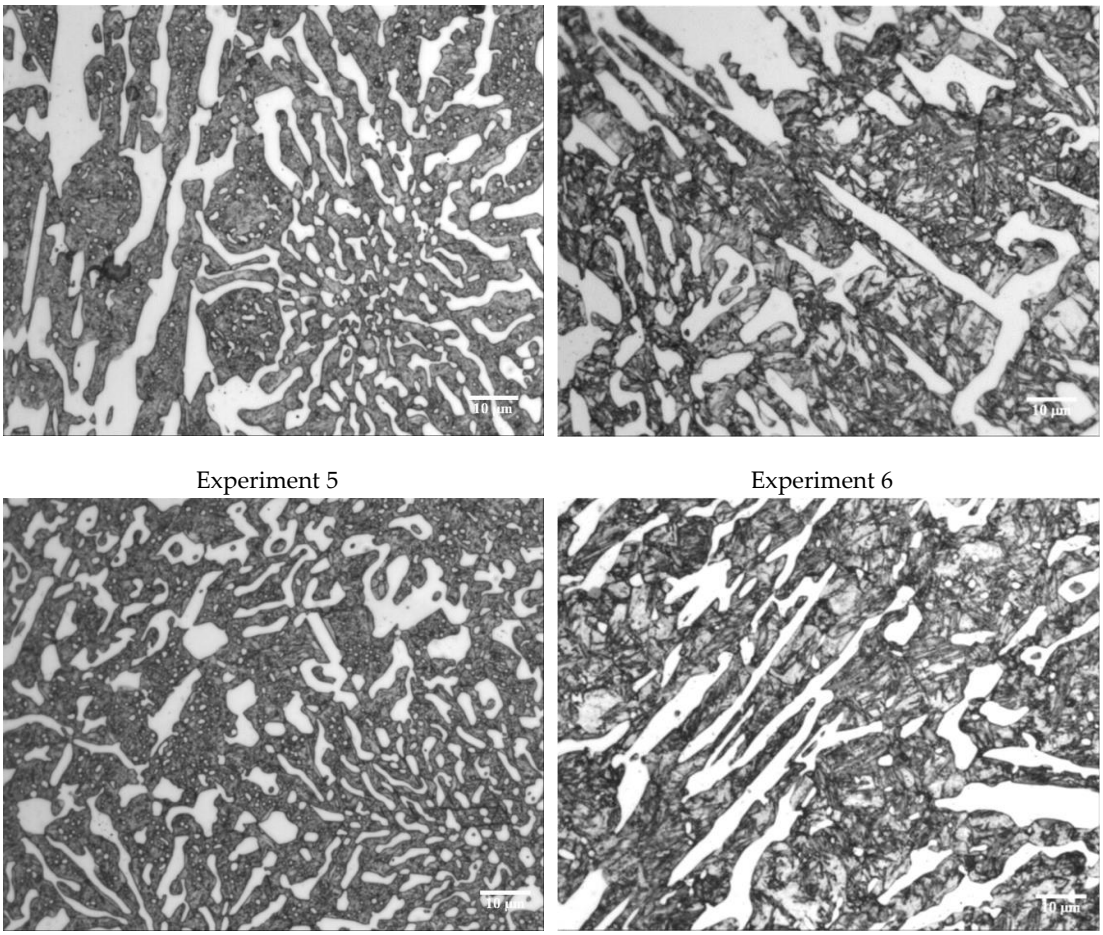

Figure 8. Representative micrographs of each of the eight experiments. All were obtained at 600× magnification.

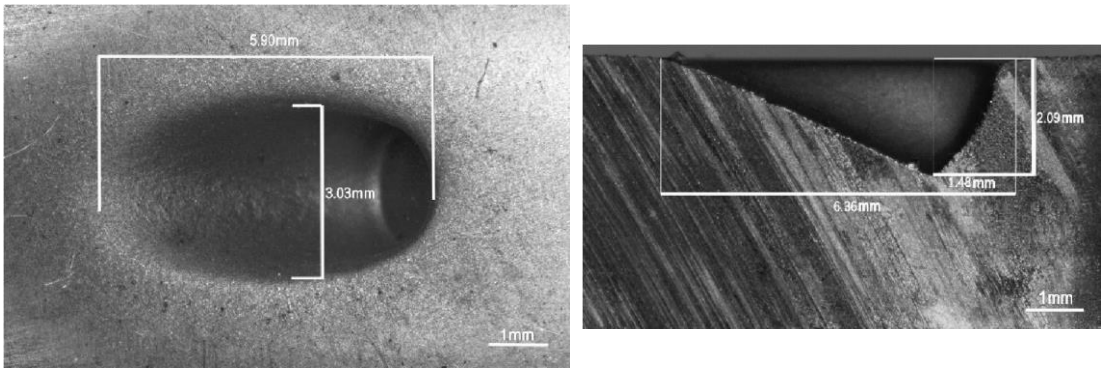

(**a**) (**b**)

Figure 9. Geometry of the wear track. This track corresponds to one of the samples from Experiment 1 after 6 min of testing. (**a**) plan view; (**b**) side view.

4. Conclusions

The application of a Design of Experiments (DoE) allowed the analysis of the effects of modifying a variety of factors related to the heat treatments applied to hypoeutectic white cast iron containing 25% Cr on the erosive wear resistance of this material. The influence of a prior

softening treatment aimed at facilitating machining of this cast iron, consisting of 2 h at 1000 °C and 24 h at 700 °C, was analyzed, as was the influence of those factors related to the destabilization of austenite. The main conclusions drawn from the study are as follows:

1. The softening heat treatment, following destabilization of the austenite, does not lead to lower hardness values with respect to the as-cast state. Isothermal softening annealing at 700 °C for 24 h following destabilization produces the coalescence and thickening of carbides that reduce the structural hardening achieved in the destabilization process.
2. An austenitization temperature of 1100 °C is high enough to redissolve the carbides precipitated during the softening treatment. After cooling, however, this favors the presence of retained austenite, which is removed if tempering is carried out at 500 °C.
3. The tempering temperature is found to be the key factor in the final percentage of martensite
   (α'). Tempering temperatures of 500 °C should be used to increase this percentage.
4. Following the quenching process, the tempering parameters have a significant influence on erosive wear resistance. Tempering temperatures of 500 °C and long tempering times, of around 6 h, favor an increase in wear resistance.
5. These same tempering conditions favor an increase in the hardness of the constituent matrix. This shows that it is not only the eutectic carbides that are responsible for wear resistance but that this is complemented by the resistance provided by the constituent matrix, mainly made up of tempered martensite and secondary carbides.
6. A low tempering temperature (200 °C) is not conducive to the complete transformation of the retained austenite, leading to M3C carbides being preferentially formed versus M7C3 and M23C6 carbides.

Author Contributions: J.A.-L. conceived and designed the investigation; A.G.-P. performed all laboratory work; F.A.-A. led the investigation, analyzed the data and wrote the paper. All authors have read, and agreed to the published version of the manuscript. All authors have read and agreed to the published version of the manuscript.

Funding: This research received no external funding

Conflicts of Interest: The authors declare no conflict of interest.

References

1. Pearce, J.T.H. Structural characterisation of high chromium cast irons. In Proceedings of the International Conference on Solidification Science and Processing: Outlook for the 21st Century, Bangalore, India, 18–21 February 2001; pp. 241–247.
2. Zhou, S.P.; Shen, Y.H.; Zhang, H.; Chen, D.Q. Heat Treatment Effect on Microstructure, Hardness and Wear Resistance of Cr26 White Cast Iron. *Chin. J. Mech. Eng.* **2015**, *28*, 140–147, doi:10.3901/cjme.2014.0620.116.
3. Shimizu, K.; Purba, R.H.; Kusumoto, K.; Yaer, X.B.; Ito, J.; Kasuga, H.; Gaqi, Y.L. Microstructural evaluation and high-temperature erosion characteristics of high chromium cast irons. *Wear* **2019**, *426*, 420–427, doi:10.1016/j.wear.2019.01.043.
4. Guitar, M.A.; Suarez, S.; Prat, O.; Guigou, M.D.; Gari, V.; Pereira, G.; Mucklich, F. High Chromium Cast
   Irons: Destabilized-Subcritical Secondary Carbide Precipitation and Its Effect on Hardness and Wear Properties. *J. Mater. Eng. Perform.* **2018**, *27*, 3877–3885, doi:10.1007/s11665-018-3347-1.
5. Gonzalez-Pocino, A.; Alvarez-Antolin, F.; Asensio-Lozano, J. Erosive Wear Resistance Regarding Different Destabilization Heat Treatments of Austenite in High Chromium White Cast Iron, Alloyed with Mo. *Metals* **2019**, *9*, 10, doi:10.3390/met9050522.

6. Efremenko, V.; Shimizu, K.; Chabak, Y. Effect of Destabilizing Heat Treatment on Solid-State Phase Transformation in High-Chromium Cast Irons. *Metall. Mater. Trans. A-Phys. Metall. Mater. Sci.* **2013**, *44A*, 5434–5446, doi:10.1007/s11661-013-1890-9.
7. Liu, Z.L.; Li, Y.X.; Chen, X.; Hu, K.H. Microstructure and mechanical properties of high boron white cast iron. *Mater. Sci. Eng. A-Struct. Mater. Prop. Microstruct. Process.* **2008**, *486*, 112–116, doi:10.1016/j.msea.2007.10.017.
8. Antolin, J.F.A.; Garrote, L.F.; Lozano, J.A. Application of Rietveld Refinement to the correlation of the microstructure evolution of white cast irons with 18 and 25 %-wt. Cr after oil quench and successive temper treatments, with abrasive wear and bending testing. *Rev. De Metal.* **2018**, *54*, 11, doi:10.3989/revmetalm.113.
9. Wang, J.; Sun, Z.P.; Zuo, R.L.; Li, C.; Shen, B.L.; Gao, S.J.; Huang, S.J. Effects of secondary carbide precipitation and transformation on abrasion resistance of the 16Cr-1Mo-1Cu white iron. *J. Mater. Eng. Perform.* **2006**, *15*, 316–319, doi:10.1361/105994906 × 108602.
10. Zhang, Z.G.; Yang, C.K.; Zhang, P.; Li, W. Microstructure and wear resistance of high chromium cast iron containing niobium. *China Foundry* **2014**, *11*, 179–184.
11. Liu, H.H.; Wang, J.; Yang, H.S.; Shen, B.L. Effects of cryogenic treatment on microstructure and abrasion resistance of CrMnB high-chromium cast iron subjected to sub-critical treatment. *Mater. Sci. Eng. A-Struct. Mater. Prop. Microstruct. Process.* **2008**, *478*, 324–328, doi:10.1016/j.msea.2007.06.012.
12. Carpenter, S.D.; Carpenter, D.; Pearce, J.T.H. XRD and electron microscope study of a heat treated 26.6% chromium white iron microstructure. *Mater. Chem. Phys.* **2007**, *101*, 49–55, doi:10.1016/j.matchemphys.2006.02.013.
13. Fairhust, W.; Rohrig, K. Abrasion resistant high chromium cast irons. *Foundry Trade J.* **1974**, *136*, 685–698.
14. Filipovic, M.M. Iron-chromium-carbon-vanadium white cast irons—The microstructure and properties. *Hem. Ind.* **2014**, *68*, 413–427, doi:10.2298/hemind130615064f.
15. Pero-Sanz Elorz, J.A. *Ciencia e Ingeniería de Materiales*, 5th ed.; Cie-Dossat: Madrid, Spain, 2006; p. 673.
16. Pero-Sanz, J.A. *Fundiciones Férreas*; Dossat: Madrid, Spain, 1994; p. 154.
17. Gonzalez-Pocino, A.; Alvarez-Antolin, F.; Asensio-Lozano, J. Influence of Thermal Parameters Related to Destabilization Treatments on Erosive Wear Resistance and Microstructural Variation of White Cast Iron Containing 18% Cr. Application of Design of Experiments and Rietveld Structural Analysis. *Materials* **2019**, *12*, 3252, doi:10.3390/ma12193252.
18. Wiengmoon, A.; Pearce, J.T.H.; Chairuangsri, T. Relationship between microstructure, hardness and corrosion resistance in 20 wt.%Cr, 27 wt.%Cr and 36 wt.%Cr high chromium cast irons. *Mater. Chem. Phys.* **2011**, *125*, 739–748, doi:10.1016/j.matchemphys.2010.09.064.
19. Prat-Bartés, A.; Tort-Martorell, X.; Grima-Cintas, P.; Pozueta-Fernández, L.; Solé-Vidal, I. *Métodos Estadísticos*, 2nd ed.; UPC: Barcelona, Spain, 2004; p. 376.
20. Efremenko, V.G.; Wu, K.M.; Chabak, Y.G.; Shimizu, K.; Isayev, O.B.; Kudin, V.V. Alternative Heat Treatments for Complex-Alloyed High-Cr Cast Iron Before Machining. *Metall. Mater. Trans. A-Phys. Metall. Mater. Sci.* **2018**, *49A*, 3430–3440, doi:10.1007/s11661-018-4722-0.
21. ASTM G76-18. *Standard Test Method for Conducting Erosion Tests by Solid Particle Impingement Using Gas Jets*; ASTM International: West Conshohocken, PA, USA, 2018.
22. Stephens, P.W. Phenomenological model of anisotropic peak broadening in powder diffraction. *J. Appl. Crystallogr.* **1999**, *32*, 281–289, doi:10.1107/s0021889898006001.
23. Karantzalis, E.; Lekatou, A.; Mavros, H. Microstructure and properties of high chromium cast irons: Effect of heat treatments and alloying additions. *Int. J. Cast Met. Res.* **2009**, *22*, 448–456, doi:10.1179/174313309 × 436637.
24. Yu, S.K.; Sasaguri, N.; Matsubara, Y. Effects of retained austenite on abrasion wear resistance and hardness of hypoeutectic high Cr white cast iron. *Int. J. Cast Met. Res.* **1999**, *11*, 561–566, doi:10.1080/13640461.1999.11819334.
25. Farah, A.F.; Crnkovic, O.R.; Canale, L.C.F. Heat treatment in high Cr white cast iron Nb alloy. *J. Mater. Eng. Perform.* **2001**, *10*, 42–45, doi:10.1361/105994901770345321.

metals

MDPI

Article

Influence of Thermal Processing Factors, Linked to the Destabilisation of Austenite, on the Microstructural Variation of a White Cast Iron Containing 25% Cr and 0.6% Mo

Alejandro González-Pociño[1], Florentino Alvarez-Antolin [1]*, Juan Asensio-Lozano[1] and Hugo Alvarez-Perez[1]

[1]Materials Pro Group, Department of Materials Science and Metallurgical Engineering, University of Oviedo; Independencia 13, 33004 Oviedo, Spain; gonzalezpalejandro@uniovi.es (A.G.-P.); jasensio@uniovi.es (J.A.-L.); cahualpe@hotmail.com (H.A.-P.)
* Correspondence: alvarezflorentino@uniovi.es; Tel.: +34-985-181-949

Received: 8 June 2020; Accepted: 21 June 2020; Published: 23 June 2020

Abstract: Hypoeutectic white cast irons containing 25% Cr are used in ore-processing industries due to their high resistance to erosive wear. Applying a Design of Experiments (DoE), the aim of this study is to analyse the influence of thermal processing factors on the microstructural variation of a white cast iron containing 25% Cr and 0.6% Mo. The carbides present in the as-cast state are of the M_7C_3, M_2C, and M_3C types. M_2C carbides precipitate on the eutectic M_7C_3 carbides favoured by heterogeneous nucleation conditions. Two kinetics compete during the destabilisation of austenite. One dissolves those eutectic carbides precipitated as a result of non-equilibrium solidification (M_7C_3 and M_2C), while the other enables the precipitation of secondary M_7C_3 and $M_{23}C_6$ carbides. The M_7C_3 carbides begin to precipitate first. Low destabilisation temperatures and short dwell times are insufficient to dissolve the precipitated eutectic carbides from non-equilibrium conditions, thus favouring the presence of M_2C carbides, which are associated with Mo. The factor that has the greatest influence on hardness is the tempering temperature. The optimal tempering temperature is found to be 500 °C. Short tempering times maintain the distortion of the ferrite unit cell. The precipitation of Cr carbides during tempering requires a temperature of 500 °C and the prior dissolution of the carbon precipitated during the initial stages of said tempering. With short tempering times, the Cr atoms still remain dissolved in the ferrite, distorting its unit cell and increasing the hardness of the matrix constituent of the alloy.

Keywords: white cast irons containing 25% Cr; hardness; destabilisation of austenite; distortion of the ferrite cell; secondary carbides; M_2C carbide

1. Introduction

The microstructure of hypoeutectic white cast irons containing between 15% and 30% Cr is mainly composed of eutectic carbides in an austenite matrix, or of any of the phases or constituents resulting from their transformation [1,2]. The austenite will be supersaturated mainly in Cr and C. This austenite can be destabilised by means of a high-temperature heat treatment, causing the precipitation of Cr-rich carbides. This precipitation results in an increase in the Ms temperature, thus reducing the risk of cracking during cooling [3,4]. Wiengmoon et al. [5] conclude that the secondary carbides which precipitated during the destabilisation of austenite at 1000 °C are M_7C_3-type carbides in cast irons containing 20% Cr. However, secondary carbides with M_7C_3 and $M_{23}C_6$ stoichiometries would be jointly present in cast irons containing 27% Cr. Guitar et al. [6] conclude that M_7C_3 carbides are the first to precipitate during the destabilisation of the austenite heating process. During the dwell time at the destabilisation temperature, they would transform into $M_{23}C_6$ carbides. Furthermore, Guitar et al. [6] state that additional precipitation of secondary carbides takes place during cooling in the 980–750 °C range. Hardness increases when M_7C_3 secondary carbides predominate over $M_{23}C_6$ carbides [5]. Bedolla et al. conclude that the volume fraction of secondary carbides increases at low destabilisation temperatures (900 °C) and high dwell times (8 h) [7]. Excessive dwell times at the destabilisation temperature lead to thickening of the secondary carbides and a reduction in hardness [3]. Khanitnantharak et al. conclude that high destabilisation temperatures favour the presence of retained austenite [8]. The presence of Mo in the chemical composition favours the precipitation of eutectic M_2C carbides [9–13], leading to an increase in both hardness and wear resistance [9,12,14]. Mo can also dissolve in mixed carbides of the M_7C_3 type [15], replacing the Fe atoms and producing a distortion of their unit cell without having a significant influence on hardness. A suitable tempering temperature favours the reduction in retained austenite via a second destabilisation of this austenite [16–18]. However, an excessive tempering temperature could result in the redissolution of the C atoms in the tempered martensite matrix [12]. This carbon would come from carbides precipitated at the lowest tempering temperatures. The optimal tempering temperature to increase the hardness and wear resistance appears to be around 500 °C [4]. The presence of hard carbides gives these cast irons a high resistance to wear, which is why they are widely used in ore-processing industries [1,19]. Alloys in the 25–30% Cr range have a very high hardness [20]. The tempering temperature is decisive in both the wear resistance and hardness of the constituent matrix of these cast irons. Low tempering temperatures do not completely destabilise the austenite [21]. Solidification and thermal processing parameters can alter the microstructure of the material and its properties and hence influence its inservice performance [22]. The aim of this study is to analyse the influence of thermal processing factors on the microstructural variation of a white cast iron containing 25% Cr and 0.6% Mo via the application of a Design of Experiments (DoE), analysing how the modifications of those factors that affect the destabilisation of austenite influence the percentage of the different carbides that are formed, the percentage of martensite, and the percentage of retained austenite. A secondary goal is to determine how the variation of these processing factors would affect the hardness of the material. Five factors were analysed, performing eight experiments [23]. The results will allow the manufacturers of these alloys containing 25% Cr to correlate the parameters of thermal processing with the microstructure and hardness of the material.

2. Materials and Methods

Applying a DoE, the aim is to modify certain thermal processing parameters in a deliberate and controlled manner so as to analyse the microstructural variations produced in the material. In other words, it is a matter of determining which factors have a significant influence on this microstructure and in what way the variation of these factors exerts an influence. Table 1

shows the analysed factors and the levels of analysis. The proposed dwell times for the destabilisation of austenite, Factor B, are higher than those usually employed. These longer dwell times are intended to promote the precipitation of secondary carbides and an increase in the Ms Temperature so as to avoid the presence of retained austenite after quenching as far as possible.

Table 1. Factors and Levels.

	Factors	**Levels**	
Code	**Metallurgical parameter**	**Level−1**	**Level +1**
A	Destabilisation temperature of austenite (°C)	900	1000
B	Dwell time at the destabilisation temperature (h)	4	8
C	Tempering temperature (°C)	500	600
D	Number of tempers	1	2
E	Tempering time (h)	2	4

The effect of a factor is measured as the consequence of its variation on a certain microstructural feature of the material. This type of effect is called a main effect. The effect of one factor may possibly depend on the value that another takes. When this occurs, these factors are said to interact. The influence of the main effects is greater than that of the 2-factor interactions. In turn, the influence of the 2-factor interactions is greater than that of the 3-factor interactions, and so on successively. In practical terms, it is sufficient to consider only the main effects and the 2-factor interactions, which allows the number of experiments to be reduced [23]. In this study, the effect of 5 factors performing 8 experiments has been analysed. If the aim were to analyse all the possible interactions with these 5 factors, it would be necessary to perform 32 experiments ($2^5 = 32$). However, in this case, only 8 effects (2^{5-2}) have been estimated, which therefore means a 1/4 (32/4 = 8) fractional factorial design. Table 2 shows the array of experiments. Columns D and E have been respectively constructed from the product of columns A × B and A × C [23]. The "Confounding Pattern" column indicates only the main effects and those 2-factor interactions whose effects are confounded with the main effects.

Table 2. Array of Experiments.

Experiment	**A**	**B**	**C**	**D**	**E**	**Confounding Pattern**
1	-1	-1	-1	+1	+1	A + BD + CE
2	+1	−1	−1	−1	−1	B + AD
3	−1	+1	−1	−1	+1	C + AE
4	+1	+1	−1	+1	−1	D + AB
5	−1	−1	+1	+1	−1	E + AC
6	+1	−1	+1	−1	+1	BC + DE
7	−1	+1	+1	−1	−1	BE + CD
8	+1	+1	+1	+1	+1	

The effects are linear combinations of the analysed responses or features. Therefore, according to the Central Limit Theorem, they will follow a normal law. The representation of the distribution function of the $N(0,\sigma)$ law on a normal probabilistic plot scale will be a straight line that passes through the coordinate point (0,50). If any of the effects followed a different normal law, it would not appear aligned along this straight line. Those factors associated with effects that do not follow the distribution function of the $N(0,\sigma)$ law are considered significant and will hence be found at a certain distance from the straight line on the normal probabilistic plot. If any effect deviates to the right of this straight line, that would mean that this factor would produce an increase in the analysed feature when placed at its +1 level. Likewise, if any effect deviates to the

left of this straight line, that would indicate that the factors associated with this effect produces an increase in the measured feature when placed at their −1 level. The features studied in this paper are:

- The Vickers hardness of the material. The applied load was 300 N, while the hardness value was calculated as the average value obtained from 10 indentations.
- The Vickers hardness of the constituent matrix, formed by tempered martensite and secondary carbides. In this case, the applied load was 0.5 N, while the hardness value was calculated as the average value obtained from 20 indentations. ◎ The following microstructural features:
    - Percentage by weight of austenite
    - Percentage by weight of tempered martensite (ferrite)
    - Volume of the unit cell of the tempered martensite (ferrite)
    - Percentage by weight of the M_7C_3, $M_{23}C_6$ and M_2C carbides

The microstructural features were determined by X-ray diffraction on a SEIFERT XRD 3000 T/T diffractometer (Baker Hughes, Celle, Germany). The radiation was emitted via a fine-focus Mo tube at a working power of 40 kV × 40 mA and monochromatised to the K α doublet: $\lambda 1 = 0.709316$ Å and $\lambda 2 = 0.713607$ Å. The diffracted intensity was determined in a 2θ range from 7° to 57°. The Rietveld structural refinement method was used to determine the percentage of the crystalline phases via fitting of the diffractograms [24]. To this end, following the recording of the diffraction figures, a structural refinement was carried out using the crystallographic information files present in the Inorganic Crystal Structure Database (ICSD), FIZ Karlsruhe, Germany. The program employed for this purpose was FullProf.2k, version 6.20 (2018). The increase in width observed in the peaks of the majority phases were modelled using Stephens' formulation [25], which is implemented in the aforementioned analysis program.

The optical microscope used was a NIKON Epiphot 200 (Nikon, Tokyo, Japan), and the images were obtained using Beuhler Omnimet Enterprise image analyser software (OmniMet Enterprise, Beuhler). The scanning electron microscope employed was a JEOL JSM-5600 (JEOL, Nieuw-Vennep, The Netherlands), equipped with the characteristic energy-dispersive X-ray (EDX) microanalysis system.

3. Results

Table 3 shows the chemical composition of the alloy under study. Figure 1 shows the microstructure in the as-cast state following solidification in a sand mould. Figure 1a,b shows that the microstructure is mainly composed of proeutectic austenite and a eutectic constituent. The proeutectic austenite presents a dendritic growth model, the presence of the eutectic constituent being observed between the dendritic "arms". M_7C_3 eutectic carbides can be seen in the latter constituent. Figure 1c,d show the presence of carbides, both in the proeutectic austenite and in the austenite of the eutectic constituent. These carbides have been identified as belonging to two different types. Mixed carbides with a grey colouring and diameter greater than 1 micron are of the M_7C_3 type. However, carbides of the M_3C type are also observed, which have a brighter colouring and a smaller size: less than 1 micron. Table 4 shows the results of the microanalysis performed on these two types of carbides (spectra 1 to 4). The hardness of the material in this state was 310 HV.

Table 3. Chemical Composition (% by weight).

C	Si	Mn	Cr	Mo
2.7	1.1	0.8	25.0	0.6

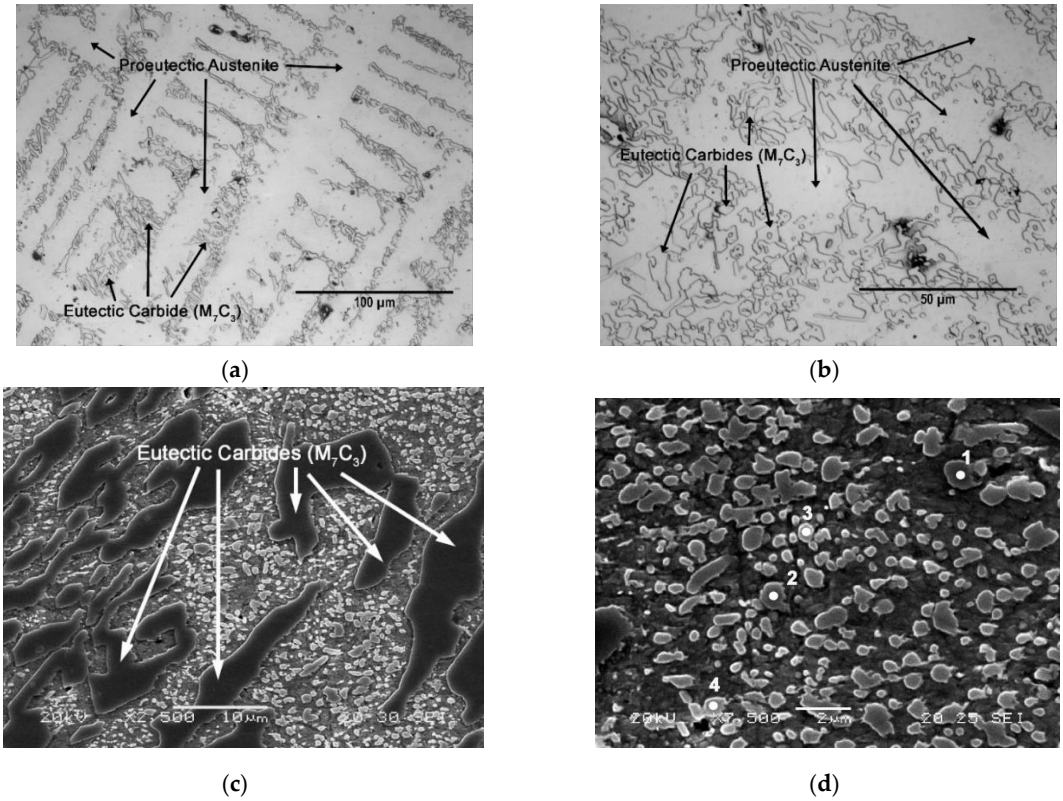

Figure 1. As-Cast Microstructure. (**a**) Optical microscope (500×); (**b**) Optical microscope (1000×); (**c**) Scanning electron microscope (2500×); (**d**) Scanning electron microscope (7500×).

Table 4. Results of the microanalysis performed by SEM-EDX (energy-dispersive X-ray), corresponding to Figure 1d. (at. %).

Spectrum	%C	%Cr	%Fe	%Mo
1	42.91	31.13	25.03	0.94
2	41.15	32.46	25.69	0.69
3	22.42	6.58	71.00	-
4	29.47	8.76	61.77	-

Figure 2 shows the presence of eutectic carbides of the M_2C type, associated with Mo. Figure 2a was taken with secondary electrons and Figure 2b was taken with backscattered electrons. The difference in contrast in the latter image reveals the presence of M_2C carbides associated with Mo. Their precipitation seems to be favoured by heterogeneous nucleation conditions from the eutectic M_7C_3-type carbides [4]. Table 5 shows the results of the microanalysis performed on this type of carbide (spectra 1)

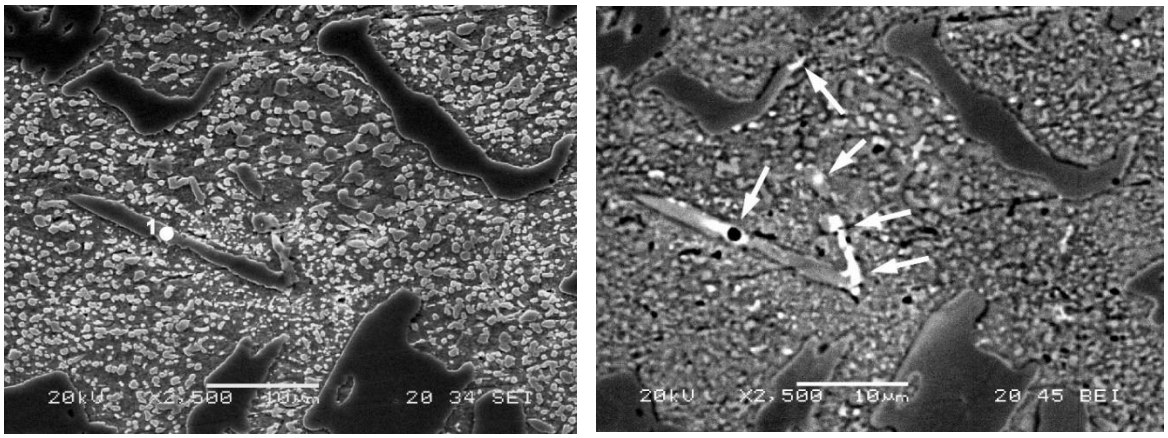

(**a**) (**b**)

Figure 2. As-Cast Microstructure. Presence of M_2C-type eutectic carbides. Images taken under a scanning electron microscope at 2500× magnification; (**a**) Image taken with secondary electrons; (**b**) Image taken with backscattered electrons.

Table 5. Results of the microanalysis performed by SEM-EDX, corresponding to Figure 2a (at %).

Spectrum	%C	%Cr	%Fe	%Mo
1	24.23	7.54	40.31	27.92

Figure 3 shows the overall fittings obtained by means of Rietveld structural refinement. The red marks indicate the observed intensities; the black line indicates the intensity calculated according to the Rietveld structural model; the blue line indicates the difference between the two; while the vertical segments indicate the angular positions of the different identified phases.

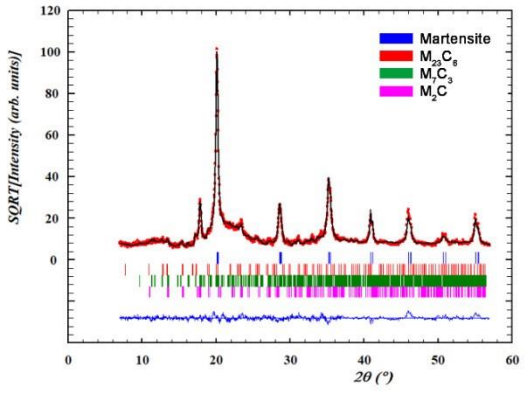

Experiment 1

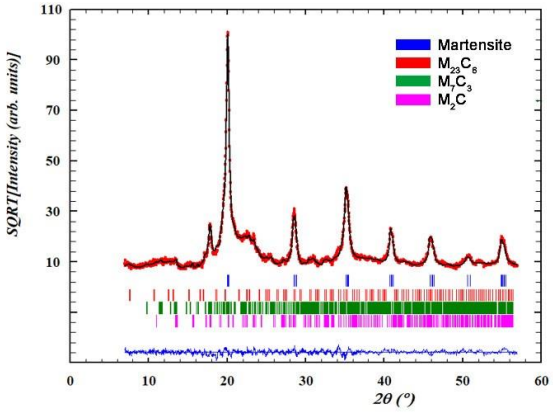

Experiment 2

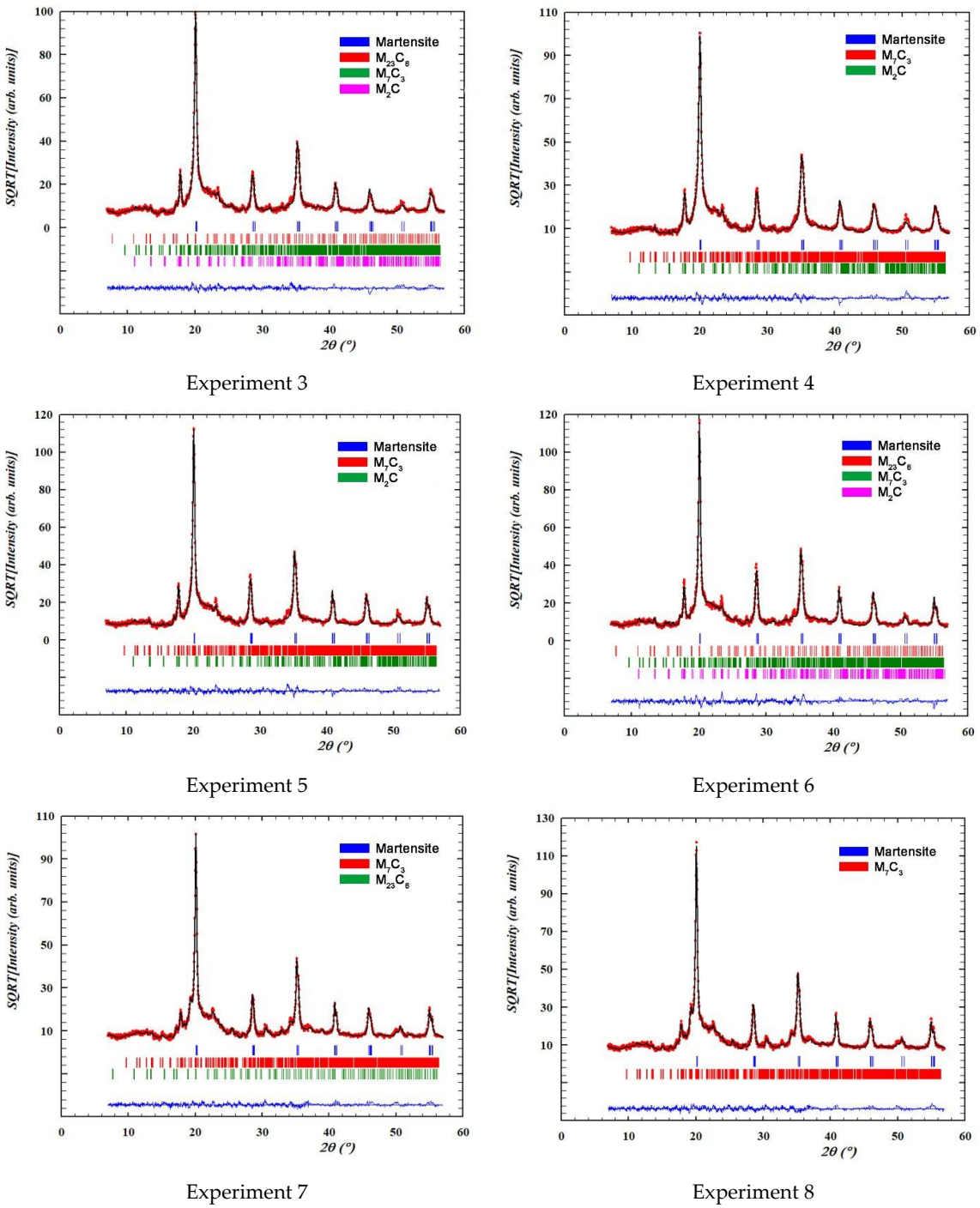

Figure 3. Overall fittings obtained by means of Rietveld structural refinement. The red marks define the observed intensities; the black line defines the intensity calculated according to the Rietveld structural model; the blue line defines the difference between the two intensities; while the vertical segments indicate the angular positions of the different identified phases.

Table 6 shows the percentages by weight and the network parameters of the main crystalline phases detected by XRD in each of the experiments. The goodness of fit is defined by the agreement factor, Rwp, the index, Rexp, and the relationship between their squares: $Chi^2 = (Rwp/ Rexp)^2$

Table 6. Percentage by weight of the precipitated phases and the volume of the unit cell of the tempered martensite.

Experiment	Rietveld Fitting	Phases	wt %	vol. (Å³)
1	*R*wp = 15.7 Rexp = 28.16 Chi² = 0.31	Martensite (α′) Cr_7C_3 carbide $Cr_{23}C_6$ carbide Mo_2C carbide	74 18 2 5	23.638
2	*R*wp = 13.3 *R*exp = 28.11 Chi² = 0.22	Martensite (α′) Cr_7C_3 carbide $Cr_{23}C_6$ carbide Mo_2C carbide	77 19 1 2	23.781
3	*R*wp = 13.5 *R*exp = 27.71 Chi² = 0.24	Martensite (α′) Cr_7C_3 carbide $Cr_{23}C_6$ carbide Mo_2C carbide	84 13 1 2	23.626
4	*R*wp = 13.1 *R*exp = 28.82 Chi² = 0.21	Martensite (α′) Cr_7C_3 carbide $Cr_{23}C_6$ carbide Mo_2C carbide	88 9 - 3	23.801
5	*R*wp = 13.9 *R*exp = 28.74 Chi² = 0.23	Martensite (α′) Cr_7C_3 carbide $Cr_{23}C_6$ carbide Mo_2C carbide	80 16 - 4	23.718
6	*R*wp = 16.9 *R*exp = 27.63 Chi² = 0.37	Martensite (α′) Cr_7C_3 carbide $Cr_{23}C_6$ carbide Mo_2C carbide	72 25 1 1	23.722
7	*R*wp = 12.8 *R*exp = 27.99 Chi² = 0.21	Martensite (α′) Cr_7C_3 carbide $Cr_{23}C_6$ carbide Mo_2C carbide	87 12 1 -	23.682
8	*R*wp = 14.3 *R*exp = 28.23 Chi² = 0.26	Martensite (α′) Cr_7C_3 carbide $Cr_{23}C_6$ carbide Mo_2C carbide	87 13 - -	23.737

Table 7 shows the results of the effects, corresponding to the confounding pattern given in the array of experiments outlined in Table 2. The row corresponding to the average shows the average value obtained considering all 8 experiments.

Table 7. Calculation of Effects.

(a) Percentage by Weight of Martensite and Volume of Its Unit Cell					
Experiment	**Martensite (α')**				**Calculated Effects**
	(wt. %)	**Effect**	**(vol. Å^3)**	**Effect**	
1	74	81.12	23.638	23.713	Average
2	77	−0.2	23.781	0.0942	A + BD + CE
3	84	10.7	23.626	−0.0032	B + AD
4	88	0.7	23.801	0.0032	C + AE
5	80	2.2	23.718	0.0207	D + AB
6	72	−3.7	23.722	−0.0647	E + AC
7	87	0.2	23.682	−0.0072	BC + DE
8	87	1.7	23.737	0.0047	BE + CD

(b) Percentage by Weight of Carbides							
Experiment	**Cr_7Cr_3 Carbide**		**$Cr_{23}Cr_6$ Carbide**		**Mo_2C Carbide**		**Calculated Effects**
	(wt. %)	**Effect**	**(wt. %)**	**Effect**	**(wt. %)**	**Effect**	
1	18	15.62	2	0.75	5	2.12	Average
2	19	1.7	1	-0.5	2	-1.25	A + BD + CE
3	13	-7.7	1	-0.5	2	-1.75	B + AD
4	9	1.7	0	-0.5	3	-1.75	C + AE
5	16	-3.2	0	-0.5	4	1.75	D + AB
6	25	3.2	1	0.5	1	-0.25	E + AC
7	12	-0.2	1	0.5	0	-0.75	BC + DE
8	13	-0.7	0	-0.5	0	-0.25	BE + CD

(c) Overall Hardness and Microhardness of the Microstructural Matrix					
Experiment	**Overall Hardness (HV)**		**Hardness of the Matrix (HV)**		**Calculated Effects**
	Kgf/mm^2	**Effect**	**Kgf/mm^2**	**Effect**	
1	484	517.62	371	398.00	Average
2	650	74.2	488	63.0	A + BD + CE
3	589	24.7	412	2.5	B + AD
4	623	-137.7	472	-75.5	C + AE
5	408	-44.2	333	-26.5	D + AB
6	479	-25.7	395	-25.5	E + AC
7	441	-14.2	350	-10.0	BC + DE
8	467	21.7	363	2.0	BE + CD

Figure 4 shows the representation of these effects on a normal probability plot, highlighting those that have a significant effect on these responses.

Figure 4a shows that the factors that have a significant effect on the percentage by weight of tempered martensite are B (dwell time at the austenisation temperature) and E (tempering time). Thus, if the aim is to increase this percentage, factor B should be placed at its +1 level (8 h) and Factor E should be placed at its −1 (2 h) level. Figure 4b shows that Factor A (austenisation temperature) and Factor E (tempering time) have a significant effect on the volume of the unit cell of the tempered martensite. An increase in the distortion of this phase would be obtained by placing Factor A at its +1 level (1000 °C) and Factor E at its −1 level (2 h). The significant effect of interaction AB is also observed, which means that the effect of the austenitisation temperature is reinforced if factor B (austenitisation time) is placed at its +1 level (8 h). It can de deduced from both these results that 2 complementary kinetics compete during the destabilisation treatment of austenite. One of them is related to the destabilisation of austenite itself, and the other is related

to the dissolution of those eutectic carbides that would have precipitated as a result of a possible non-equilibrium solidification [22]. High austenitisation temperatures and long dwell times at this temperature favour the dissolution of these eutectic carbides, precipitated in non-equilibrium conditions. This involves the dissolution not only of C atoms, but also of Cr atoms. The former precipitate in the early stages of tempering, forming ε (cementitic) carbides. However, the latter continue to occupy substitution positions in the unit cell of the tempered martensite (ferrite). Carbon atoms need to be available for the precipitation of the Cr carbides during tempering. This requires the prior dissolution of the cementitic carbides precipitated during the tempering process following the decomposition of their constituent atoms [26]. The precipitation of the Cr carbides during tempering requires longer dwell times that allow the prior dissolution of the carbon precipitated during the initial stages of the tempering process and their subsequent precipitation as M_7C_3 carbides. All this takes time, which justifies the finding that the tempered martensite presents network distortions due to Cr atoms which have not precipitated during this tempering when short tempering times are employed.

Figure 4c shows that Factor B (dwell time at the destabilisation temperature of austenite) has a significant effect on the percentage by weight of the M_7C_3 carbides: placing this factor at its −1 level (4 h) leads to an increase in the content in these carbides. Dwell times at the austenitisation temperature of 4 h may be too short for dissolution of the eutectic carbides, solidified under nonequilibrium conditions, to be observed. Therefore, it turns out that the dwell time of 4 h would be sufficient for the destabilisation of the austenite, but it is too short for the dissolution of the precipitated carbides in non-equilibrium conditions. This evidences that the first carbides formed by the destabilisation of austenite are of the M_7C_3 type. This effect is reinforced by interaction AB: placing Factor A (austenitisation temperature) at its +1 level (1000 °C) would lead to an increase in the rate of precipitation of M_7C_3 carbides. These results are in line with the recent conclusions reached by Guitar et al [6].

Figure 4d shows that no effect is found to significantly influence the percentage by weight of $M_{23}C_6$-type carbides. This does not contradict the previous results reported by Guitar et al. [6] or by Wiengmoon et al. Rather, it is possible that the redissolution of eutectic carbides precipitated due to a possible non-equilibrium solidification, observed with long dwell times at the austenitisation temperature, does not enable us to verify the partial transformation of M_7C_3 carbides into $M_{23}C_6$ carbides, or their precipitation.

Figure 4e shows the significant influence of interaction AB on the precipitation of M_2C eutectic carbides. Table 8 shows the analysis of this interaction. It is concluded that their presence is favoured when Factor A (austenitisation temperature) and Factor B (dwell time at said temperature) are simultaneously placed at their –1 levels. It is probable that the M_2C eutectic carbides were formed as a result of non-equilibrium solidification and that higher dwell times or higher temperatures enable the dissolution of these carbides.

Figure 4f shows the significant effect of Factor C (tempering temperature) on the overall hardness of the material: placing this factor at its −1 level (500 °C) produces an increase in hardness. This figure also shows the significant effect of Factor A (austenisation temperature) and of interaction CE. Table 9 simultaneously analyses both possibilities; placing Factor E (tempering time) at its −1 level (2 h) is found to reinforce the effect of Factor C at its −1 level (500 °C). That is, short tempering times reinforce the effect of the tempering temperature of 500 °C. It is precisely at this temperature that the precipitation of M_7C_3 carbides occurs during tempering [26]. With shorter tempering times, the tempered martensite (ferrite) maintains a greater distortion of its network.

Figure 4g shows the significant effect of Factor C (tempering temperature) on the overall hardness of the constituent matrix, which is formed by tempered martensite and secondary carbides. Placing this factor at its −1 level (500 °C) leads to an increase in this hardness. The significant effect of Factor A and of interaction CE can also be seen in this figure. Similar to the previous analysis, Table 10 simultaneously analyses both possibilities; placing Factor E

(tempering time) at its −1 level (2 h) is found to reinforce the effect of factor C at its −1 level (500 °C). On the other hand, high temperatures, or excessively long tempering times, can lead to the coalescence of secondary carbides precipitated during tempering, thereby negatively affecting hardness [26].

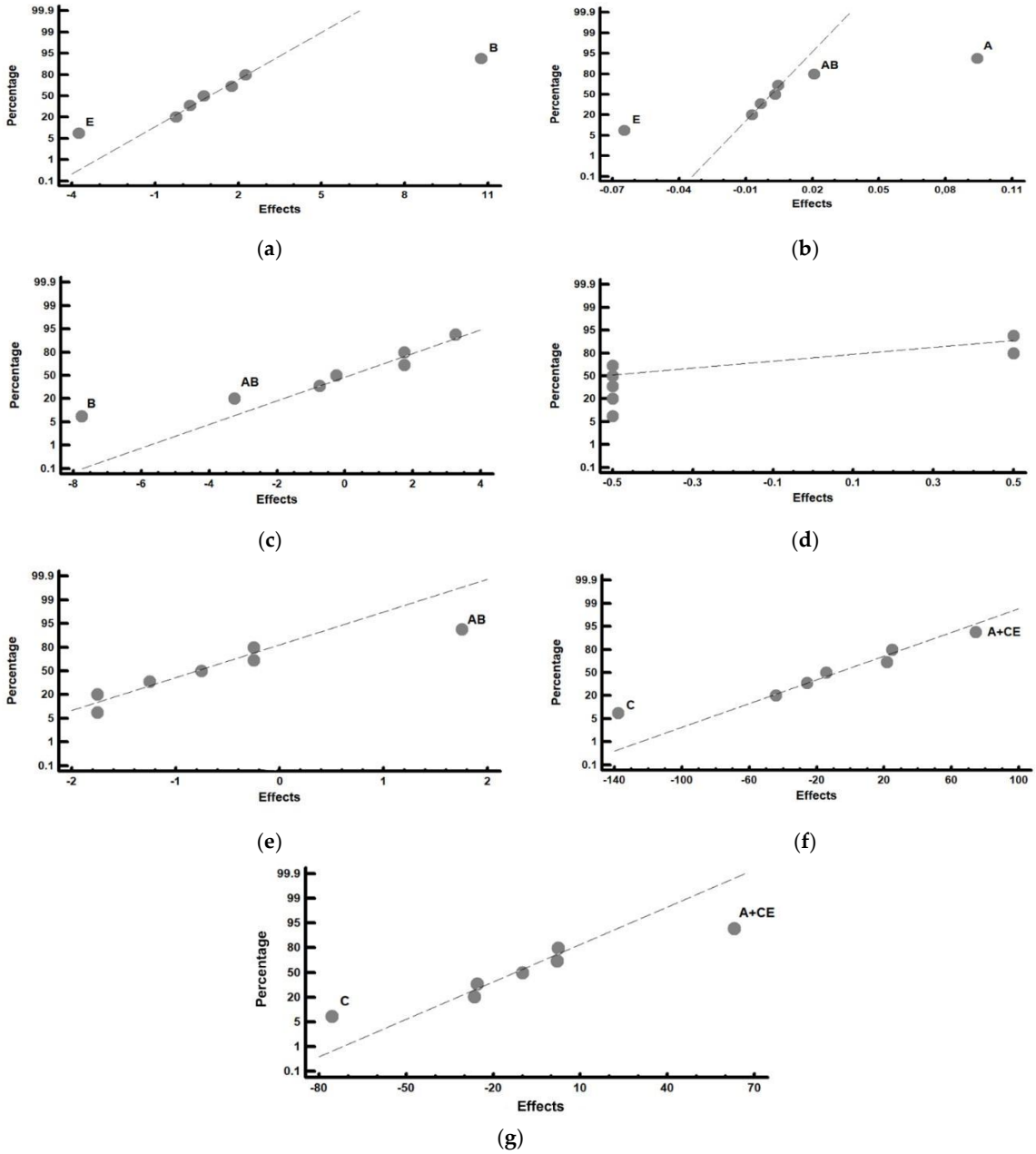

Figure 4. Representation of the effects on a normal probability plot. Those factors with a significant effect on the analysed responses are highlighted. (**a**) Percentage by weight of tempered martensite; (**b**) volume of the unit cell of the tempered martensite; (**c**) percentage by weight of the M_7C_3 carbides; (**d**) percentage by weight of the $M_{23}C_6$ carbides; (**e**) percentage by weight of the M_2C carbides; (**f**) overall hardness of the material; (**g**) hardness of the constituent matrix.

Table 8. Analysis of the effects of interaction AB on the percentage by weight of the M_2C carbides.

AB (wt % Mo2C)	−1	+1
−1	4.5	1
+1	1.5	1.5

Table 9. Analysis of the effects of Factor A and the interaction CE on the hardness of the material.

A	HV	CE (HV)	−1	+1
−1	481	−1	637	537
+1	555	+1	425	473

Table 10. Analysis of the effects of Factor A and the interaction CE on the hardness of the matrix constituent.

A	HV	CE (HV)	−1	+1
−1	367	−1	480	391
+1	429	+1	342	379

Figure 5 shows a representative micrograph of each experiment that allows us to appreciate the general microstructure of these cast irons.

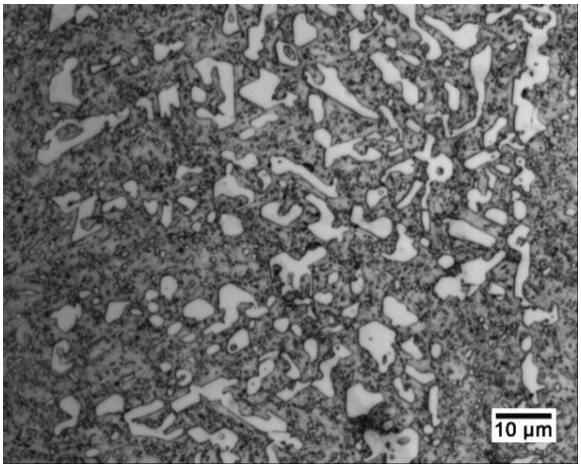

Experiment 1

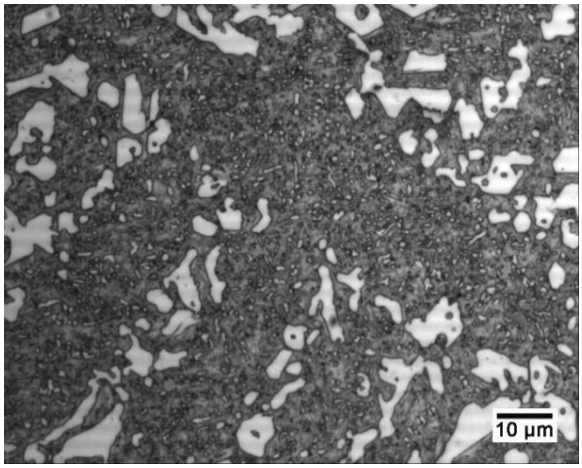

Experiment 2

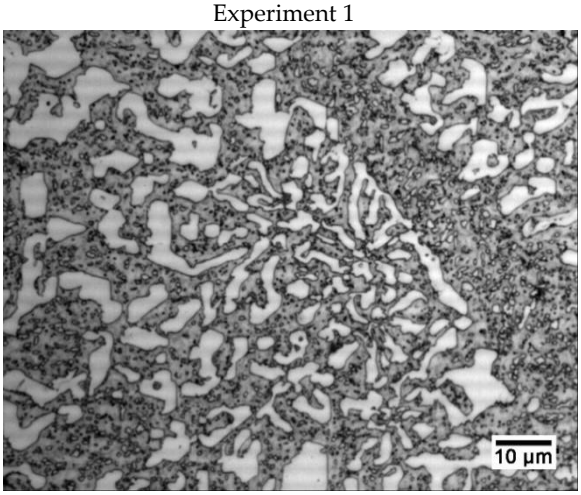

Experiment 3

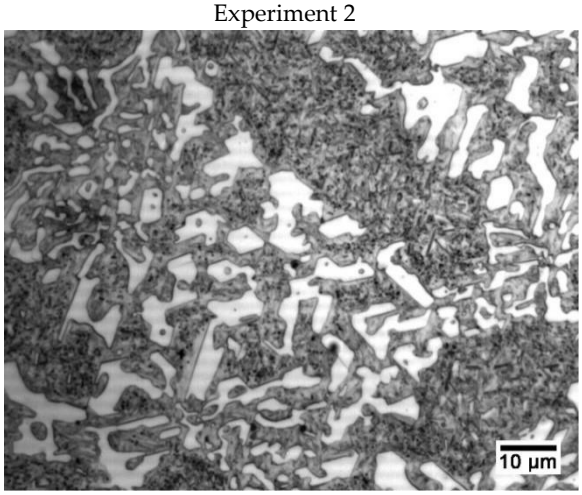

Experiment 4

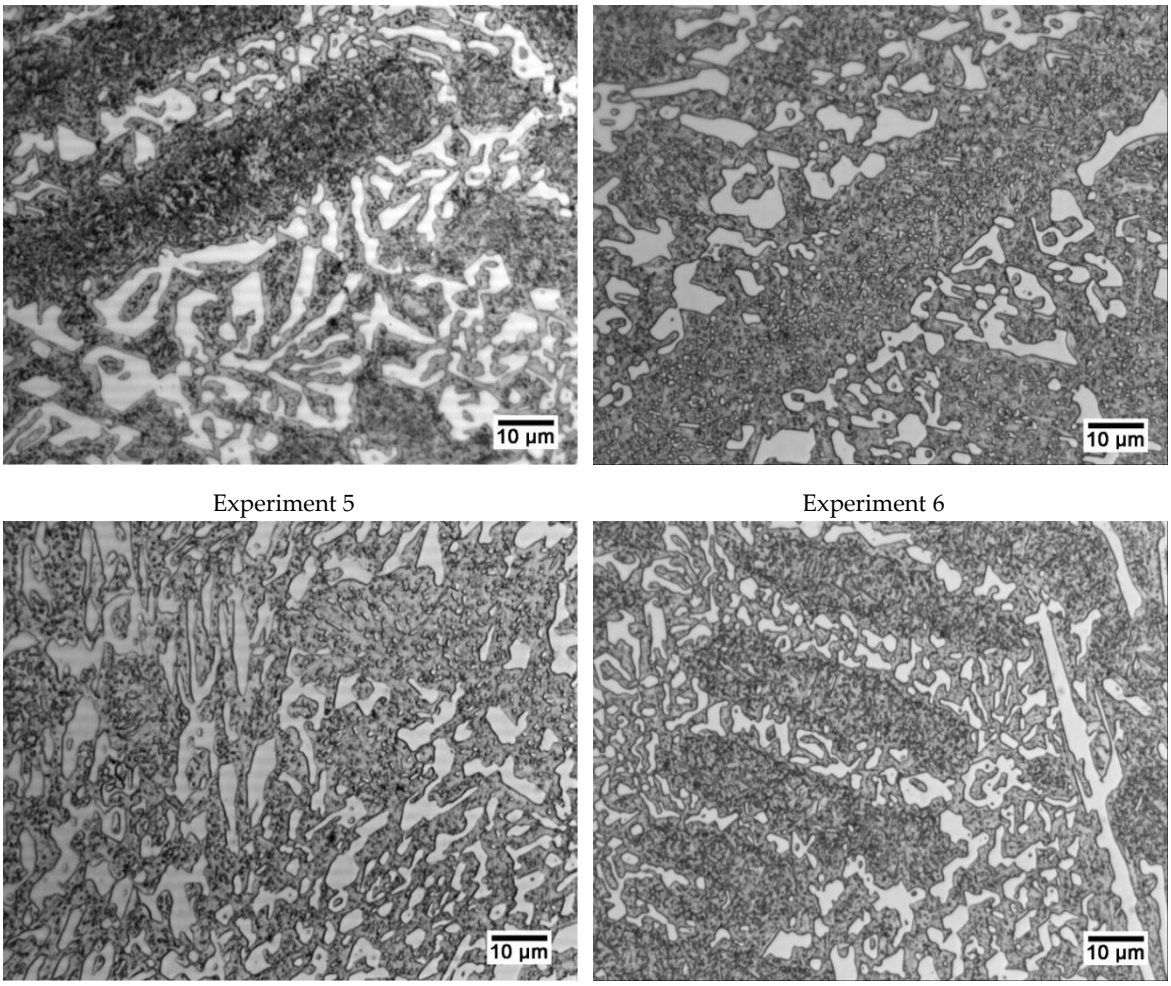

Figure 5. Representative micrographs of each of the 8 experiments. All were obtained at 600x magnification.

4. Conclusions

This paper has analysed the influence of different thermal processing factors on the microstructural variation of a white cast iron containing 25% Cr and 0.6% Mo via the application of a Design of Experiments (DoE). The main conclusions may be summarised as follows:

1. The carbides present in the microstructure are of the M_7C_3, $M_{23}C_6$ (both associated with Cr), and M_2C (associated with Mo) types. The M_7C_3 and M_2C carbides form part of the eutectic constituent. Part of this eutectic constituent was formed as a result of non-equilibrium solidification.
2. Two complementary kinetics compete during the high-temperature destabilisation treatment of the austenite. One of them is related to the destabilisation of austenite itself, via the precipitation of secondary carbides, and the other is related to the dissolution of those eutectic carbides that would have precipitated as a result of possible non-equilibrium solidification. The latter kinetics is favoured if the treatment is carried out at 1000 °C, compared to lower temperatures.
3. The carbides that form during the destabilisation of austenite at high temperatures are M_7C_3 and $M_{23}C_6$ carbides. The M_7C_3 carbides begin to precipitate first.
4. Mo tends to segregate into the eutectic fluid and to precipitate via heterogeneous nucleation on the M_7C_3 carbides. Low destabilisation temperatures and short dwell times

are insufficient for the dissolution to take place, which means that these conditions favour the presence of M_2C carbides.

5. The factor that most influences hardness is the tempering temperature. A temperature of 600 °C is found to be excessive. The optimal tempering temperature is 500 °C. The highest hardness would be achieved with short tempering times (2 h).
6. Short tempering times maintain the distortion of the tempered martensite unit cell. Precipitation of the Cr carbides during tempering requires longer dwell times that allow the prior dissolution of the carbon precipitated during the initial stages of the tempering process and their subsequent precipitation as M_7C_3 carbides.

Author Contributions: J.A.-L. and H.A.-P. conceived and designed the investigation; A.G.-P. performed all laboratory work; F.A.-A. led the investigation, analysed the data and wrote the paper. All authors have read and agreed to the published version of the manuscript.

Funding: This research received no external funding

Conflicts of Interest: The authors declare no conflict of interest.

References

1. Tabrett, C.P.; Sare, I.R.; Ghomashchi, M.R. Microstructure-property relationships in high chromium white iron alloys. *Int. Mater. Rev.* **1996**, *41*, 59–82, doi:10.1179/imr.1996.41.2.59.
2. Powell, G.L.F.; Bee, J.V. Secondary carbide precipitation in an 18 wt% Cr-1 wt% Mo white iron. *J. Mater. Sci.* **1996**, *31*, 707–711, doi:10.1007/bf00367889.
3. Efremenko, V.; Shimizu, K.; Chabak, Y. Effect of Destabilizing Heat Treatment on Solid-State Phase Transformation in High-Chromium Cast Irons. *Metall. Mater. Trans. A-Phys. Metall. Mater. Sci.* **2013**, *44*, 5434–5446, doi:10.1007/s11661-013-1890-9.
4. Antolin, J.F.A.; Garrote, L.F.; Lozano, J.A. Application of Rietveld Refinement to the correlation of the microstructure evolution of white cast irons with 18 and 25 %-wt. Cr after oil quench and successive temper treatments, with abrasive wear and bending testing. *Rev. De Metal.* **2018**, *54*, 11, doi:10.3989/revmetalm.113.
5. Wiengmoon, A.; Pearce, J.T.H.; Chairuangsri, T. Relationship between microstructure, hardness and corrosion resistance in 20 wt.%Cr, 27 wt.%Cr and 36 wt.%Cr high chromium cast irons. *Mater. Chem. Phys.* **2011**, *125*, 739–748, doi:10.1016/j.matchemphys.2010.09.064.
6. Guitar, M.A.; Nayak, U.P.; Britz, D.; Mucklich, F. The Effect of Thermal Processing and Chemical Composition on Secondary Carbide Precipitation and Hardness in High-Chromium Cast Irons. *Int. J. Met.* **2020**, *11*, 1–11, doi:10.1007/s40962-020-00407-4.
7. Bedolla-Jacuinde, A.; Arias, L.; Hernandez, B. Kinetics of secondary carbides precipitation in a highchromium white iron. *J. Mater. Eng. Perform.* **2003**, *12*, 371–382, doi:10.1361/105994903770342881.
8. Khanitnantharak, W.; Hashimoto, M.; Shimizu, K.; Yamamoto, K.; Sasaguri, N.; Matsubara, Y.; American Foundry, S. Effects of Carbon and Heat Treatment on the Hardness and Austenite Content of a MultiComponent White Cast Iron. *Trans. Am. Foundry Soc.* **2009**, *117*, 435.
9. Matsubara, Y.; Sasaguri, N.; Shimizu, K.; Yu, S.; Yu, K. Solidification and abrasion wear of white cast irons alloyed with 20% carbide forming elements. *Wear* **2001**, *250*, 502–510, doi:10.1016/s0043-1648(01)00599-3.
10. Hashimoto, M.; Kubo, O.; Matsubara, Y. Analysis of carbides in multi-component white cast iron for hot rolling mill rolls. *ISIJ Int.* **2004**, *44*, 372–380, doi:10.2355/isijinternational.44.372.
11. Scandian, C.; Boher, C.; de Mello, J.D.B.; Rezai-Aria, F. Effect of molybdenum and chromium contents in sliding wear of high-chromium white cast iron: The relationship between microstructure and wear. *Wear* **2009**, *267*, 401–408, doi:10.1016/j.wear.2008.12.095.
12. Li, Y.C.; Li, P.; Wang, K.; Li, H.Z.; Gong, M.Y.; Tong, W.P. Microstructure and mechanical properties of a Mo alloyed high chromium cast iron after different heat treatments. *Vacuum* **2018**, *156*, 59–67, doi:10.1016/j.vacuum.2018.07.013.

13. Opapaiboon, J.; Ayudhaya, M.S.N.; Sricharoenchai, P.; Inthidech, S.; Matsubara, Y. Effect of Chromium Content on Heat Treatment Behavior of Multi-Alloyed White Cast Iron for Abrasive Wear Resistance. *Mater. Trans.* **2019**, *60*, 346–354, doi:10.2320/matertrans.M2018318.
14. Meebupha, T.; Inthidec, S.; Sricharoenchai, P.; Matsubara, Y. Effect of Molybdenum Content on Heat Treatment Behavior of Multi-Alloyed White Cast Iron. *Mater. Trans.* **2017**, *58*, 655–662, doi:10.2320/matertrans.M2016396.
15. Yamamoto, K.; Inthidech, S.; Sasaguri, N.; Matsubara, Y. Influence of Mo and W on High Temperature Hardness of M_7C_3 Carbide in High Chromium White Cast Iron. *Mater. Trans.* **2014**, *55*, 684–689, doi:10.2320/matertrans.F-M2014801.
16. Sare, I.R.; Arnold, B.K. The influence of heat-treatment on the high-stress abrasion resistance and fracturetoughness of alloy white cast irons. *Metall. Mater. Trans. A-Phys. Metall. Mater. Sci.* **1995**, *26*, 1785–1793, doi:10.1007/bf02670766.
17. Chen, X.A.; Li, Y.X. Effect of heat treatment on microstructure and mechanical properties of high boron white cast iron. *Mater. Sci. Eng. A-Struct. Mater. Prop. Microstruct. Process.* **2010**, *528*, 770–775, doi:10.1016/j.msea.2010.09.092.
18. Gonzalez-Pociño, A.; Alvarez-Antolin, F.; Asensio-Lozano, J. Influence of Thermal Parameters Related to Destabilization Treatments on Erosive Wear Resistance and Microstructural Variation of White Cast Iron Containing 18% Cr. Application of Design of Experiments and Rietveld Structural Analysis. *Materials* **2019**, *12*, doi:10.3390/ma12193252.
19. Pearce, J.T.H. Structural characterisation of high chromium cast irons. In Proceedings of the International Conference on Solidification Science and Processing: Outlook for the 21st Century, Bangalore, India, 18−21 February, 2001; pp. 241–247.
20. Aso, S.; Tagami, M.; Goto, S. Mechanical-properties of Fe-Cr-C-B cast alloys. *J. Jpn. Inst. Met.* **1992**, *56*, 707– 714, doi:10.2320/jinstmet1952.56.6_707.
21. Gonzalez-Pociño, A.; Alvarez-Antolin, F.; Asensio-Lozano, J. Optimization of Thermal Processes Applied to Hypoeutectic White Cast Iron containing 25% Cr Aimed at Increasing Erosive Wear Resistance. *Metals* **2020**, *10*, 17, doi:10.3390/met10030359.
22. Gonzalez-Pociño, A.; Alvarez-Antolin, F.; Asensio-Lozano, J. Erosive Wear Resistance Regarding Diferent Destabilization Heat Treatments of Austenite in High Chromium White Cast Iron, Alloyed with Mo. *Metals* **2019**, *9*, 522, doi:10.3390/met9050522.
23. Prat-Bartés, A.; Tort-Martorell, X.; Grima-Cintas, P.; Pozueta-Fernández, L.; Solé-Vidal, I. *Métodos Estadísticos*, 2nd ed.; UPC: Barcelona, Spain, 2004; p. 376.
24. Gasan, H.; Erturk, F. Effects of a Destabilization Heat Treatment on the Microstructure and Abrasive Wear Behavior of High-Chromium White Cast Iron Investigated Using Different Characterization Techniques. *Metall. Mater. Trans. A-Phys. Metall. Mater. Sci.* **2013**, *44*, 4993–5005, doi:10.1007/s11661-013-1851-3.
25. Stephens, P.W. Phenomenological model of anisotropic peak broadening in powder diffraction. *J. Appl. Crystallogr.* **1999**, *32*, 281–289, doi:10.1107/s0021889898006001.
26. Pero-Sanz, J.A. *Aceros*; Ed.; Dossat: Madrid, Spain, 2004; p. 558.

metals

MDPI

Article

The Joint Effects of Nitriding and Parameters Related to the Destabilisation of Austenite on Wear Resistance in White Cast Iron with 25% Cr

Alejandro González-Pociño, Florentino Alvarez-Antolin * and Juan Asensio-Lozano

Materials Pro Group, Departamento de Ciencia de los Materiales e Ingeniería Metalúrgica, Universidad de Oviedo, Independencia 13, 33004 Oviedo, Spain; gonzalezpalejandro@uniovi.es (A.G.-P.); jasensio@uniovi.es (J.A.-L.)

* Correspondence: alvarezflorentino@uniovi.es; Tel.: +34-985-181-949

Citation: González-Pociño, A.;Alvarez-Antolin, F.; Asensio-Lozano,J. The Joint Effects of Nitriding and Parameters Related to the Destabilisation of Austenite on Wear Resistance in White Cast Iron with 25% Cr. *Metals* **2021**, *11*, 85. https:// doi.org/10.3390/met11010085

Received: 22 December 2020

Accepted: 30 December 2020

Published: 4 January 2021

Abstract: In this article, the effects of an ionic nitriding treatment are analysed, together with deliberate variation of different thermal parameters associated with the destabilisation of austenite, on erosive wear resistance of white cast irons with 25% Cr. The methodology followed in this research was an experimental design, where six factors were analyzed by performing eight experiments. The thickness of the nitrided layer is much smaller than in white cast iron with lower percentages in Cr, never reaching 20 microns. The nitriding treatment entails considerable softening of the material underneath the nitriding layer. This softening behaviour becomes partially inhibited when the destabilisation temperature of austenite is 1100 °C and dwell times at such temperature are prolonged. This temperature seems to play a significant role in the solubilization of non-equilibrium eutectic carbides, formed during industrial solidification. The nitriding treatment leads to additional hardening, which, in these cases, favours a second destabilisation of austenite, with additional precipitation of secondary carbides and the transformation of retained austenite into martensite. Despite softening of the material, the nitriding treatment, together with air-cooling after destabilisation of the austenite, allows a noticeable increase in resistance to erosive wear.

Keywords: erosive wear resistance; white cast irons containing 25% Cr; nitriding; destabilization of austenite; secondary carbides

1. Introduction

White cast irons highly alloyed with chromium have been widely used in very aggressive settings where a high level of resistance to erosive and abrasive wear is required.This high resistance is attributed to the presence of eutectic carbides of the type M_7C_3 [1,2].The hardness of these carbides can be found in the range of 1200 HV [1]. At the same time,these carbides are found embedded in a matrix of hard martensite and retained austenite,which lends the material a greater tenacity than traditional Nihard cast irons [1]. The Cr dissolved in the matrix constituent also favours resistance to erosive wear and resistance to oxidation [2]. To improve resistance to wear, it is recommendable to carry out a destabili-sation treatment of the austenite [3–5]. Austenite is found in a very alloyed state, which creates difficulties in the spread of C and, so, the times required for this destabilisation are long. During destabilisation of austenite the precipitation of secondary carbides is produced, which has a positive effect on resistance to wear [5–11]. At the same time, the Ms temperature rises, thus reducing the percentage of retained austenite [12]. If the time of permanence at the destabilisation temperature is high, dissolution of those eutectic car- bides precipitated may be produced simultaneously as a consequence of non-equilibrium solidification [6,13]. All of these factors could have a very significant influence on the in-service behaviour of these alloys. White cast irons with 25% chromium show a high resistance to wear. In these white cast irons, the microstructure of the matrix constituent isvery significant with regard to resistance to wear. This microstructure basically depends on the temperature of tempering. Tempering at 500 °C and tempering times of around 6 hours favour an increase in wear resistance, since, under these tempering conditions, the presence of retained austenite is eliminated and the percentage of secondary carbidesof the type M_7C_3 is increased [13,14]. An additional nitriding treatment could produce superficial hardening and favour an increase in resistance to erosive wear by the formation of sub-nitrides in the tempered martensite matrix. The presence of Cr, as the main alloying element in these alloys, could favour an additional hardening through a nitriding treatment [15]. This hardening could favour greater resistance to wear. However, this treatment is carried out at temperatures of around 500 °C [15], which could mean a softening of the surface areas of the material, which are not affected by the nitriding.The presence of tempered martensite would favour the diffusion of N [16], since N diffuses through of octahedral interstitial sites of the Fe-BCC [17]. The nitride layer could be made up of ni- trides of the type ε-$Fe_{2-3}N$ and of the type γ′-Fe_4N [17], which generate elevated distortionin the ferritic matrix. The thickness of this nitrided layer in white cast irons with 18% Cr is around 60–70 microns [10]. At the same time, nitriding favours the transformation of carbides M_7C_3 into carbonitrides [18,19]. In this study, by means of the application of an experimental design, an analysis is made of the joint effect of the variation of different thermal parameters associated with the destabilisation of austenite and the application of a plasma nitriding treatment on the resistance and wear of white cast irons with 25% Cr. Erosive wear is a phenomenon of surface damage that is caused by the impact of solid particles [2]. This type of wear, in the processing of this alloy, combines mechanisms of wear by impact and mechanisms of abrasive wear [20,21]. Erosion due to impact of hard particles is a common problem during crushing/grinding operations [22]. This study comes aboutas a complement and continuation of a previous study carried out by the authors on this same question [7]. This analysis includes the effect of the nitriding treatment (temperatures of 500 °C) on the part of the material not affected by nitriding.

2. Materials and Methods

Table 1 shows the chemical composition of the white cast iron analysed. The material used in this research was supplied by the Spanish company, Fundiciones del Estanda, S.A. (Beasain, Spain), and the chemical composition is that which is indicated by this company. The research methodology followed was the application of a fractional experimental design, where six factors were analysed by carrying out eight experiments [23].

Table 1. Chemical composition (% weight).

C	Si	Mn	Cr	Mo
2.7	1.2	0.8	25.1	0.5

Table 2 shows the analysed factors and the levels of analysis in each of these factors. It should be highlighted, with reference to factor B, that the experimental permanence times at the destabilisation temperature of austenite, were higher than usual. In view of this, the intention was to analyse the influence of a possible re-dissolution of carbides, precipitated as a consequence of non-equilibrium solidification, whose kinetics are complementary to that of secondary carbide precipitation of the type M_7C_3 during destabilisation of austenite.

In this study, the effect of six factors in eight experiments has been analysed. This entails a loss of information, corresponding to the majority of interactions. In order to be able to analyse all possible interactions 64 ($2^6 = 64$) experiments would need to be carried out. However, in this case, only eight effects (2^{6-3}) have been considered, which means a high loss of information which, however, is not significant in industrial practice. Table 3 shows the matrix of experiments. Columns D, E and F have been constructed from the product of columns A × B, A × C, and B × C. The column 'confounding patterns' shows the main effects and interactions of 2 factors whose effects remain confounded with the main effects.

Table 2. Factors and levels

Factors		Levels	
Code	**Thermal Parameter**	**Level -1**	**Level +1**
A	Temperature of destabilisation of the austenite (°C)	1000	1100
B	Time of permanence at the destabilisation temperature (h)	4	8
C	Nitriding	no	yes
D	Means of cooling in tempering	air	oil
E	Temperature of tempering (°C)	200	500
F	Time of permanence in tempering (h)	3	6

Table 3. Matrix of experimets

Experiment	A	B	C	D	E	F	Confounding Patterns
1	-1	-1	-1	+1	+1	+1	A + BD + CE
2	+1	-1	-1	-1	-1	+1	B + AD + CF
3	-1	+1	-1	-1	+1	-1	C + AE + BF
4	+1	+1	-1	+1	-1	-1	D + AB + EF
5	-1	-1	+1	+1	-1	-1	E + AC + DF
6	+1	-1	+1	-1	+1	-1	F + BC + DE
7	-1	+1	+1	-1	-1	+1	AF + BE + CD
8	+1	+1	+1	+1	+1	+1	

Table 4 shows the main process parameters with which nitriding was carried out in experiments 5 to 8.

Table 4. Parameters used in the plasma nitriding process.

Gas Mixture	70% N_2 + 30% H_2
Gas flux (cm^3/min)	500
Temperature (^{0}C)	540
Pressure (Pa)	400
Time (min)	120
Output voltage (V)	500

The results analysed were the resistance to erosive wear and the hardness of the material in the area adjacent to the nitrided layer. The test of resistance to erosive wear was carried out according to norm ASTM G76, by means of compressed air blasting with corundum particles. These corundum particles had a size of 50 μm. The pressure applied was 2 bar, and the flow of corundum was 100 g/min. The angle of incidence on the surfaces of the samples was 30°. The time used in each experiment was 4 minutes. Three repetitions per test were carried out.

Given that, the nitriding treatment entails maintaining the material at 540 °C for 2 h, the area not affected by the diffusion of N could be exposed to a kind of second tempering. This could affect the resistance of the material to wear, once the signs of wear pass through the nitrided layer. To analyse the influence of the nitriding treatment on the interior area, adjacent to the nitrided layer, tests were carried out on hardness and micro-hardness at an approximate distance of 2 mm from the end of the nitrided layer. Tests of micro-hardness were carried out with localised indentations in the constituent matrix. The load applied in hardness tests was of 300 N and in tests of micro-hardness, it was of 0.5 N.

The statistical analysis was carried out with the help of the programme Statgraphics Centurion XVI, version 16.1.18 (Statgraphics Technologies, Inc., The Plains, VA, USA).

For metallographic inspection, the samples were cut further and bakelite was mounted, followed by mechanical grinding with SiC sandpaper of 240, 320, 400, and 600 grit. Textile cloths with 6 and 1 micron diamond paste were used during the mechanical polishing. For final observation, the samples were further etched with nital 4 (4 mL nitric acid and 96 mL ethanol). The microstructures of the samples were analyzed under a NIKON Epiphot 200 optical microscope. The scanning electron microscope employed was a JEOL JSM-5600 (Japan Electron Optics Laboratory, Tokyo, Japan), equipped with the characteristic energy dispersive X-ray (EDX) microanalysis system.

The phases present on the nitrided surface were determined by X-ray diffraction on a

XRD 3000 T/T diffractometer (SEIFERT, Baker Hughes, Celle, Germany). The radiation was emitted via a fine-focus Mo tube at a working power of 40 kV × 40 mA and monochromatized to the Kα doublet: λ_1 = 0.7093616 Å and λ_2 = 0.713607 Å. The diffracted intensity was determined in a 2θ range from 7 to 38°, with an angular step and counting time of approximately 0.03° and 22 s, respectively.

3. Results

Figure 1 shows the initial microstructure, corresponding to the as-cast state. This microstructure is made up of proeutectic austenite, with mainly dendritic growth, see Figure 1a. At the same time, an eutectic constituent can be seen, formed mainly by austenite and mixed carbides of Fe and Cr with stoichiometry M_7C_3, see Figure 1b,c. In Figure 1d the presence of a high density of secondary mixed carbides can be observed in the interior of the austenite grain. Table 5 shows a semi-quantitative analysis of these carbides. All these carbides seem to be of the type M_7C_3 and $M_{23}C_6$. Two groups of carbides can be distinguished. The smallest and brightest (spectrums 2, 3 and 4) are those which present a lower Cr content. These carbides could be associated with mixed carbides of stoichiometry $M_{23}C_6$ Those which are a little bigger, with a

slightly darker colouring, present a greater quantity of chrome (spectrum 5). These carbides could be associated with mixed carbides of stoichiometry M_7C_3. The latter have more similarity to eutectic carbides (spectrum 1). Both types of carbides, with a greater content of Cr, also contain Mo (spectrums 1 and 5). Figure 1e shows the presence of eutectic carbides that could be associated with mixed carbides of stoichiometry M_2C, associated with the Mo. These carbides show a more elongated and narrow morphology than the previous carbides. Due to the high hardenability of these cast irons, the austenite will be transformed into martensite by simple air cooling. This slow cooling favours the presence of retained austenite after hardening. High tempering, at around 500 °C, could favour a second destabilisation of the austenite and its later transformation into martensite after cooling [15].

Table 5. Semi-quantitative analysis of the carbides highlighted in Figure 1. This analysis was carried out through an energy dispersive X-ray microanalysis (EDX). (% atomic).

Spectrum	C	Cr	Fe	Mo	Si
1	38	38	23	0.8	-
2	30	9	61	-	-
3	40	9	51	-	-
4	33	7	60	-	-
5	36	37	26	0.7	-
6	27	6	67	0.2	2
7	26	10	48	16	-
8	28	9	47	16	-

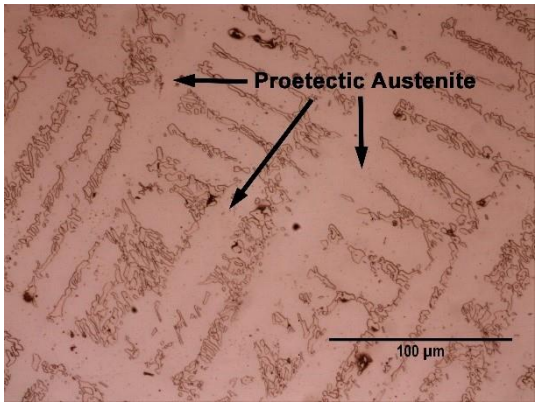

(a)

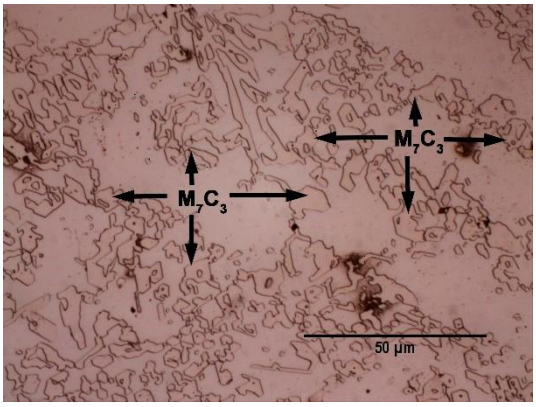

(b)

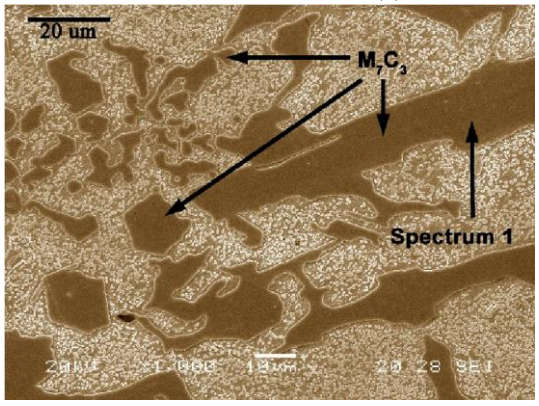

(c)

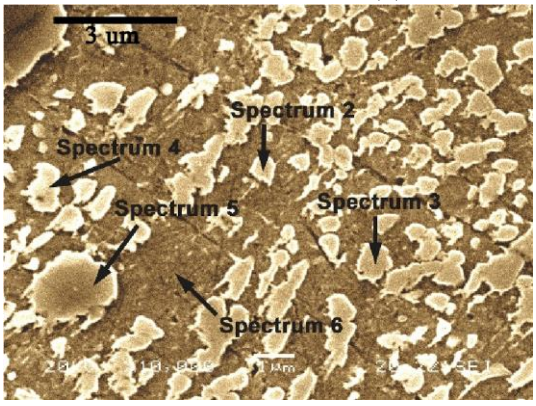

(d)

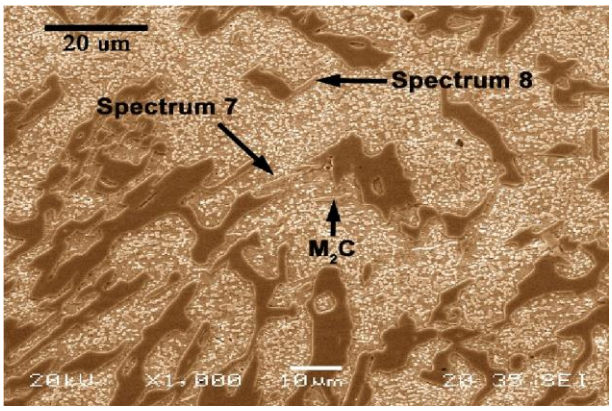

(**e**)

Figure 1. Microstructure as-cast. (**a**) The dendritic growth of pro-eutectic austenite can be seen. Micrograph obtained by optical microscope (magnification of 500×); (**b**) eutectic carbides M_7C_3.can be seen. Micrograph obtained by optical microscope (magnification of 1000×); (**c**) eutectic carbides of the type M_7C_3 can be seen. Micrograph obtained by scanning electron microscope (magnification of 1000×); (**d**) presence of secondary carbides of the type M_7C_3 and $M_{23}C_6$. Micrographic obtained by scanning electron microscopy (magnification of 10,000×); (**e**) presence of mixed eutectic carbides of the type M_2C, associated with the Mo (magnification of 1000×).

Table 6 shows the results obtained from the wear test. Figure 2 shows the representation of the effects in a normal probability plot, highlighting those that present a significant effect on resistance to erosive wear. The C factors (nitriding) and D factors (through cooling during tempering) show a significant effect, in such a way that if factor C is situated at level −1 (without nitriding) and D at level +1 (tempered in oil), an increase in wear is produced, that is to say, these conditions would be those which offer lower resistance to erosive wear. In previous research, it was concluded that through air-cooling in tempering a greater precipitation of secondary carbides of the type M_7C_3 is produced than if cooling is carried out in oil. This is due to the fact that slower cooling speeds favour the kinetics of precipitation by nucleation and growth of carbides in the interval of temperatures between 600 °C and 400 °C [6]. Also, the significant effect of the interactions of second grade AF + BE + CD can be observed. These interactions are analysed in Figure 3. It can be seen that the interaction which has a more significant effect is CD, given that when factor C is situated at level +1 (with nitriding) and D at level −1 (air cooling), is when the least wear is produced.

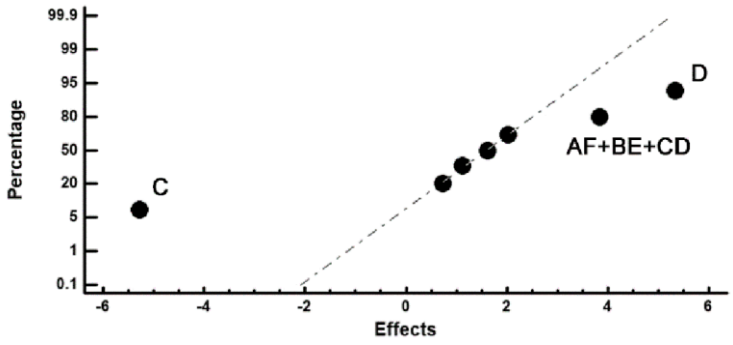

Figure 2. Representation of the effects on a normal probability plot. Those factors with a significant effect on resistance to erosive wear are highlighted.

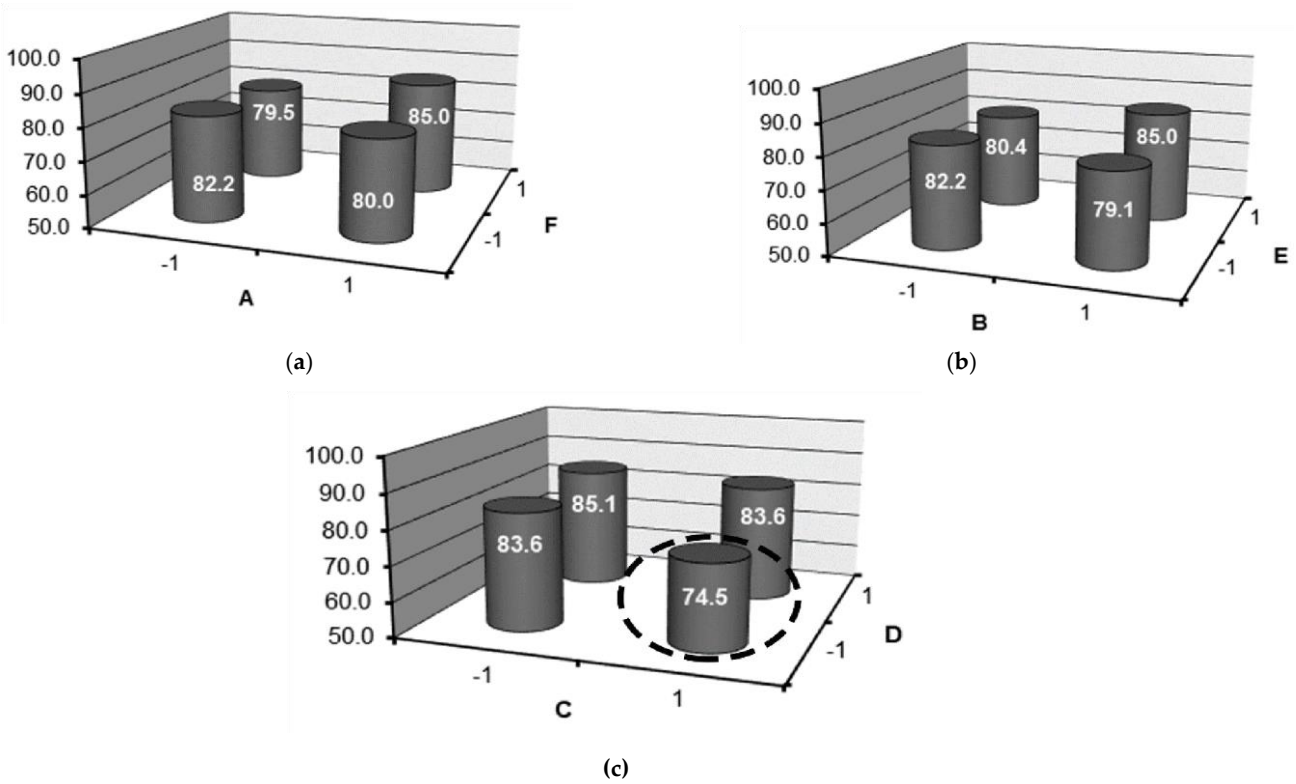

Figure 3. Analysis of the interactions AF + BE + CD. (**a**) interaction AF; (**b**) interaction BE; (**c**) interaction CD.

Table 6. Weight loss in the erosive wear (mg) test. The effects refer to the confounding pattern highlighted in the right-hand column. The average values refer to the average value of the 8 experiments.

Experiment	Erosive Wear		Confounding Pattern
	mg	Effect	
1	85.5	81.712	Average
2	83.6	1.62	A + BD + CE
3	83.6	0.72	B + AD + CF
4	84.7	-5.27	C + AE + BF
5	80.9	5.32	D +AB + EF
6	75.4	2.02	E + AC + DF
7	73.6	1.12	F + BC + DE
8	86.4	3.82	AF + BE + CD

Figure 4 shows an example of the morphology of signs of wear. Figure 4a–c shows the morphology of the signs of wear corresponding to experiment 1, and Figure 4d–f shows the morphology of the signs of wear corresponding to experiment 7. In all of the 8 experiments, the depth of profile of the signs of wear never reached more than 2.2 mm.

In all of those samples subjected to a nitriding treatment, experiments 5 to 8, the thickness of the nitride layer was very small, never reaching 20 microns and resulting in an average thickness of less than 10 microns in all cases. Figure 5a shows an example of the thickness of the nitride layer, in this case corresponding to experiments 5. Figure 5b–d highlight areas, which were analysed through an energy dispersive X-ray microanalysis (EDX). The EDX analysis was

performed on metallographic samples in the polished state, without etching with a chemical reagent. Table 7 shows the results obtained. It should be pointed out that the eutectic carbides of the type M_7C_3 included in the thickness of the nitrided layer were not affected by N (spectrums 1,4 and 6). However, the constituent matrix presents increasing quantities of N from the interior of the layer to its outer edge. See spectra 2, 3 and 6. It must be pointed out that the greater part of the nitrogen is concentrated on the extreme outer edge of the nitride layer, which entails only a few microns (see the "mapping" of elements in Figure 5b).

Table 7. Semi-quantitative analysis of phases shown in Figure 5b. This analysis was carried out through an energy dispersive X-ray microanalysis (EDX). (% atomic).

Spectrum	C	N	Cr	Fe
1	32	–	49	19
2	26	2	14	58
3	30	10	42	18
4	32	–	48	20
5	32	30	18	20
6	32	–	50	18

Figure 6 shows the diffractogram obtained on the surface of the sample corresponding to experiment 8, showing the main phases identified. It must be highlighted that the presence of CrN and Fe_4N has been detected. These precipitates are so fine that they are not detected by SEM. The presence of fine carbides of the M_3C type, precipitated during the tempering of the martensite, has also been detected.

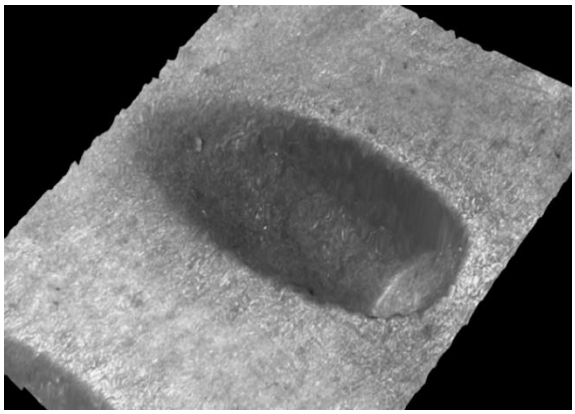

(**a**)

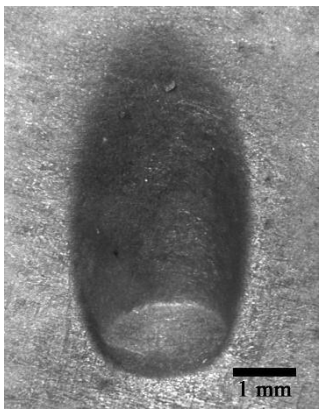

(**b**)

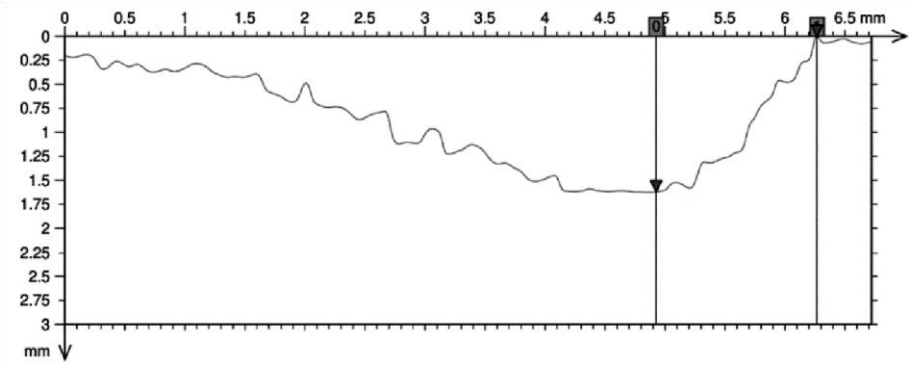

(c)

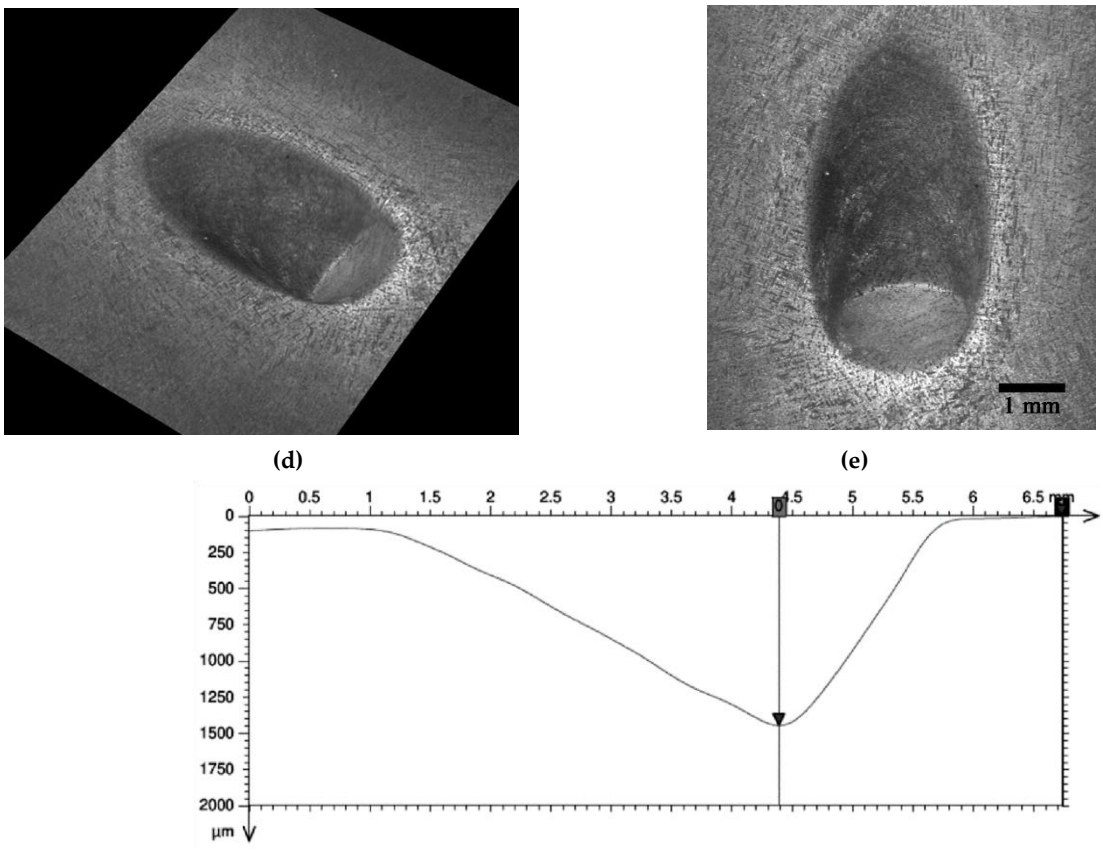

(**d**) (**e**) (**f**)

Figure 4. Morphology of the signs of erosive wear. (**a–c**) corresponding to experiment 1; (**d–f**) corresponding to experiment 7.

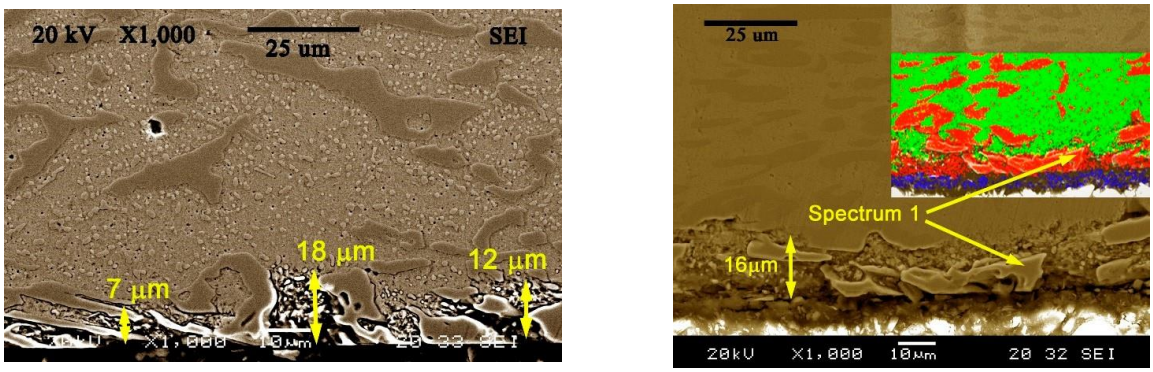

(**a**) (**b**)

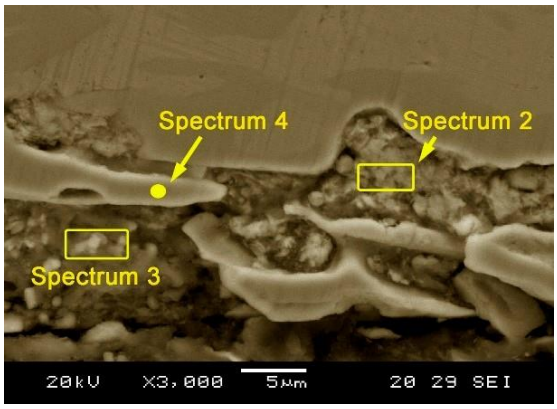

(**c**)

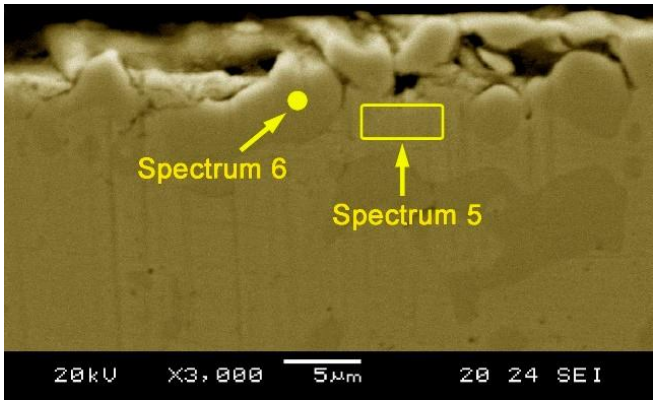

(**d**)

Figure 5. Thickness of the nitrided layer (SEM). (**a**) Experiment 5. Magnification of 1000×; (**b**) Mapping of elements by means of energy dispersive X-ray (EDX) microanalysis, corresponding to experiment 5. Blue: N; Red: Cr; Green Fe. Magnification of 1000×; (**c**) EDX analysis of the nitrided layer corresponding to experiment 7. Magnification of 3000×; (**b**) EDX analysis of the nitrided layer corresponding to experiment 8. Magnification of 3000×.

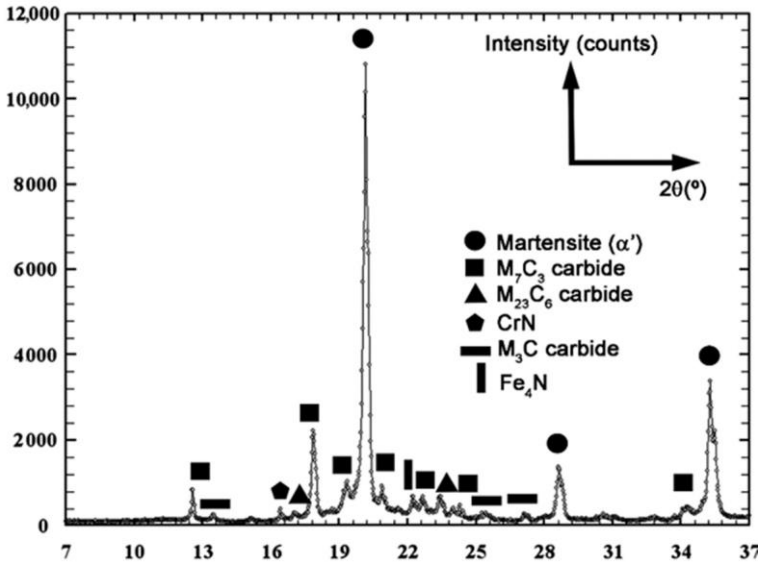

Figure 6. Diffractogram of the nitrided surface of sample corresponding to experiment 8.

Table 8. shows the results of the average values obtained on the hardness of the inside area adjacent to the nitride layer. At the same time, it shows the results of the effects, referring to the confounding pattern that is shown in the matrix of the experiments.

Figure 7a shows the representation of the effects on a normal probability plot, highlighting those that present a significant effect on overall hardness, and Figure 7b shows the representation of the effects on a normal probability plot, highlighting those that present a significant effect on hardness in the constituent matrix (micro-hardness). In both cases, factor C (nitriding) has a significant effect on hardening, in such a way that, if this factor is situated in its level-1 (without nitriding), an increase is produced in the overall hardness and the constituent matrix. So, nitriding treatment entails great softening of the alloy in inside areas adjacent to the nitrided layer. It must also be pointed out that factors A and B (A= destabilisation temperature of austenite and B= time of permanence at the destabilisation temperature) have a significant effect on both hardnesses. From this, nitriding treatment has a less negative effect on hardness in the interior of the nitrided layer when the destabilisation treatment of austenite is carried out at 1100

°C, for prolonged periods of time, around 8 hours. In a preliminary study, it was confirmed that in these conditions, greater dissolution was produced of those primary carbides that precipitated as a consequence of a non-balanced solidification, thus increasing the content of C dissolved in the austenite. This means that, after quenching, the microstructure showed a greater quantity of retained austenite. Through tempering at 500 °C a second destabilisation of austenite was produced, with the precipitation of new secondary carbides and the transformation of this austenite into martensite [7]. This appears to reduce the 'softening' of the material during the nitriding treatment.

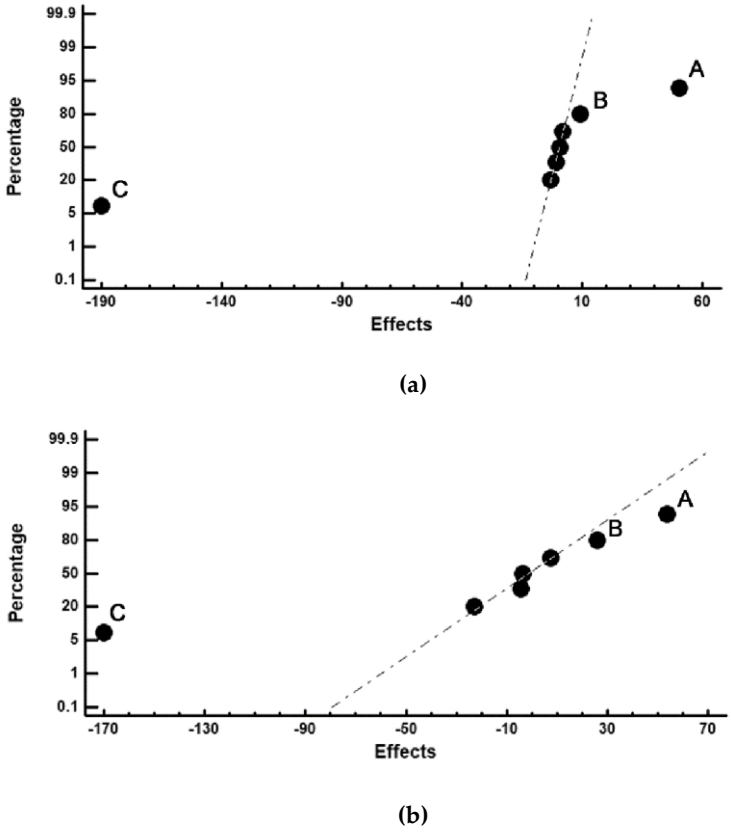

Figure 7. Representation of the effects on a normal probability plot. Those factors are highlighted which have a significant effect on hardness at an approximate distance of 2 mm from the termination of the nitrided layer. (**a**) Vickers hardness with a load of 300 N; (**b**) Vickers hardness with a load of 0.5 N applied to the constituent matrix.

Table 8. Average hardness measures to an interior distance of 2 mm from the end of the nitride layer.

Experiment	Hardness (HV)		Micro-Hardness (HV)		Confounding Pattern
	F = 10 N	Effect	F = 0.5 N	Effect	
1	699	633.87	645	619.00	Average
2	746	50.2	714	53.5	A + BD + CE
3	710	9.2	706	26.0	B + AD + CF
4	760	−189.7	751	−170.0	C + AE + BF
5	510	0.75	509	−4.5	D + AB + EF
6	562	1.75	556	−3.5	E + AC + DF
7	516	−3.25	509	−23.0	F + BC + DE
8	568	−0.75	562	7.5	AF + BE + CD

4. Conclusions

In this study, through the application of an experimental design, the joint effects are analysed of an ionic nitriding treatment and the variation of different thermal parameters associated with the destabilisation of austenite, on the resistance to wear of white cast irons with 25% Cr. The main conclusions are the following:

1. The thickness of the nitrided layer is much smaller in white cast irons with lower percentages of Cr, not reaching 20 microns in any of the experiments carried out. N has been detected forming very fine nitrides of the type CrN and Fe_4N.
2. The nitriding treatment entailed a considerable softening of the material, once the nitrided layer was passed. This softening is 'reduced' when the temperature of destabilisation of the austenite is at 1100 °C. This temperature accelerates the dissolution of eutectic carbides, precipitated as a consequence of non-equilibrium solidification. The nitriding treatment entails an additional tempering which favours a second destabilisation of the austenite with an additional precipitation of secondary carbides and the transformation of the possible retained austenite into martensite.
3. Despite this, the nitriding treatment, together with air-cooling, after the destabilisation of austenite, allows a considerable increase in resistance to erosive wear.

Author Contributions: J.A.-L. Conceived and designed the investigation; A.G.-P. Performed all laboratory work; F.A.-A. Led the investigation, analysed the data and wrote the paper. All authors have read and agreed to the published version of the manuscript.

Funding: This research received no external funding.

Institutional Review Board Statement: Not applicable.

Informed Consent Statement: Not applicable.

Data Availability Statement: Data is contained within the article.

Conflicts of Interest: The authors declare no conflict of interest.

References

1. Chung, R.J.; Tang, X.; Li, D.Y.; Hinckley, B.; Dolman, K. Effects of titanium addition on microstructure and wear resistance of hypereutectic high chromium cast iron Fe-25wt.%Cr-4wt.%C. *Wear* **2009**, *267*, 356–361. [CrossRef]
2. Zhang, Y.; Shimizu, K.; Yaer, X.; Kusumoto, K.; Efremenko, V.G. Erosive wear performance of heat treated multi-component cast iron containing Cr, V, Mn and Ni eroded by alumina spheres at elevated temperatures. *Wear* **2017**, *390–391*, 135–145. [CrossRef]
3. Guitar, M.A.; Suarez, S.; Prat, O.; Guigou, M.D.; Gari, V.; Pereira, G.; Mucklich, F. High Chromium Cast Irons: Destabilized-Subcritical Secondary Carbide Precipitation and Its Effect on Hardness and Wear Properties. *J. Mater. Eng. Perform.***2018**, *27*, 3877–3885. [CrossRef]
4. Karantzalis, A.E.; Lekatou, A.; Diavati, E. Effect of Destabilization Heat Treatments on the Microstructure of High-Chromium Cast Iron: A Microscopy Examination Approach. *J. Mater. Eng. Perform.* **2009**, *18*, 1078–1085. [CrossRef]
5. Gasan, H.; Erturk, F. Effects of a Destabilization Heat Treatment on the Microstructure and Abrasive Wear Behavior of HighChromium White Cast Iron Investigated Using Different Characterization Techniques. *Metall. Mater. Trans. A Phys. Metall. Mater. Sci.* **2013**, *44A*, 4993–5005. [CrossRef]
6. Gonzalez-Pociño, A.; Alvarez-Antolin, F.; Asensio-Lozano, J. Erosive Wear Resistance Regarding Diferent Destabilization Heat

Treatments of Austenite in High Chromium White Cast Iron, Alloyed with Mo. *Metals* **2019**, *9*, 522. [CrossRef]
7. Gonzalez-Pocino, A.; Alvarez-Antolin, F.; Asensio-Lozano, J. Optimization of Thermal Processes Applied to Hypoeutectic White Cast Iron containing 25% Cr Aimed at Increasing Erosive Wear Resistance. *Metals* **2020**, *10*, 359. [CrossRef]
8. Ortega-Cubillos, P.; Nannetti-Bernardini, P.A.; Celso-Fredel, M.; Antonio Campos, R. Wear resistance of high chromium white cast iron for coal grinding rolls. *Revista Facultad de Ingeniería* **2015**, *0*, 134–142. [CrossRef]
9. Bedolla-Jacuinde, A.; Guerra, F.V.; Mejia, I.; Zuno-Silva, J.; Rainforth, M. Abrasive wear of V-Nb-Ti alloyed high-chromium white irons. *Wear* **2015**, *332*, 1006–1011. [CrossRef]
10. Gonzalez-Pocino, A.; Alvarez-Antolin, F.; Asensio-Lozano, J. Optimization, by Means of a Design of Experiments, of Heat Processes to Increase the Erosive Wear Resistance of White Hypoeutectic Cast Irons Alloyed with Cr and Mo. *Metals* **2019**, *9*, 403. [CrossRef]
11. Guitar, M.A.; Nayak, U.P.; Britz, D.; Mucklich, F. The Effect of Thermal Processing and Chemical Composition on Secondary Carbide Precipitation and Hardness in High-Chromium Cast Irons. *Int. J. Met.* **2020**, *14*, 755–765. [CrossRef]
12. Yang, H.S.; Wang, J.; Shen, B.L.; Liu, H.H.; Gao, S.J.; Huang, S.J. Effect of cryogenic treatment on the matrix structure and abrasion resistance of white cast iron subjected to destabilization treatment. *Wear* **2006**, *261*, 1150–1154. [CrossRef]
13. Gonzalez-Pocino, A.; Alvarez-Antolin, F.; Asensio-Lozano, J.; Alvarez-Perez, H. Influence of Thermal Processing Factors, Linked to the Destabilisation of Austenite, on the Microstructural Variation of a White Cast Iron Containing 25% Cr and 0.6% Mo. *Metals* **2020**, *10*, 832. [CrossRef]
14. Antolin, J.F.A.; Garrote, L.F.; Lozano, J.A. Application of Rietveld Refinement to the correlation of the microstructure evolution of white cast irons with 18 and 25 %-wt. Cr after oil quench and successive temper treatments, with abrasive wear and bending testing. *Revista de Metalurgia* **2018**, *54*, 11. [CrossRef]
15. Pero-Sanz, J.A. *Aceros*; Dossat, Ed.; Dossat: Madrid, Spain, 2004; p. 558.
16. Selte, A.; Ozkal, B.; Arslan, K.; Ulker, S.; Hatman, A. Effect of Nitriding on the Wear Resistance of Tool Powder Steels with Different Contents of V, Cr and Mo. *Met. Sci. Heat Treat.* **2018**, *59*, 729–734. [CrossRef]
17. Binder, C.; Bendo, T.; Hammes, G.; Klein, A.N.; de Mello, J.D.B. Effect of nature of nitride phases on sliding wear of plasma nitrided sintered iron. *Wear* **2015**, *332*, 995–1005. [CrossRef]
18. Gonzalez-Pocino, A.; Alvarez-Antolin, F.; Asensio-Lozano, J. Improvement of Adhesive Wear Behavior by Variable Heat Treatment of a Tool Steel for Sheet Metal Forming. *Materials* **2019**, *12*, 2831. [CrossRef]
19. Garzon, C.M.; Franco, A.R.; Tschiptschin, A.P. Thermodynamic Analysis of M7C3 Carbide Dissolution during Plasma Nitriding of an AISI D2 Tool Steel. *ISIJ Int.* **2017**, *57*, 737–745. [CrossRef]
20. Kallel, M.; Zouch, F.; Antar, Z.; Bahri, A.; Elleuch, K. Hammer premature wear in mineral crushing process. *Tribol. Int.* **2017**, *115*, 493–505. [CrossRef]
21. Al-Bukhaiti, M.A.; Abouel-Kasem, A.; Emara, K.M.; Ahmed, S.M. A Study on Slurry Erosion Behavior of High Chromium White Cast Iron. *J. Tribol. Trans. ASME* **2017**, 139. [CrossRef]
22. Atapek, S.H.; Fidan, S. Solid-particle erosion behavior of cast alloys used in the mining industry. *Int. J. Miner. Metall. Mater.* **2015**, *22*, 1283–1292. [CrossRef]
23. Prat-Bartés, A.; Tort-Martorell, X.; Grima-Cintas, P.; Pozueta-Fernández, L.; Solé-Vidal, I. *Métodos Estadísticos*, 2nd ed.; UPC: Barcelona, Spain, 2004; p. 376.

metals

MDPI

Article

Improvement of Impact Toughness and Abrasion Resistance of a 3C-25Cr-0.5Mo Alloy Using a Design of Experiment Statistical Technique: Microstructural Correlations after Heat Treatments

Alejandro González-Pociño [1,*], Juan Asensio-Lozano [1], Florentino Álvarez-Antolín [1] and Ana García-Diez [2,*]

[1]Materials Pro Group, Departamento de Ciencia de los Materiales e Ingeniería Metalúrgica, Universidad de Oviedo, Independencia 13, 33004 Oviedo, Spain; jasensio@uniovi.es (J.A.-L.);alvarezflorentino@uniovi.es (F.Á.-A.)

[2]Departamento de Ingeniería Naval e Industrial, Escuela Politécnica Superior, Universidad de A Coruña, 15403 Ferrol, Spain

*Correspondence: gonzalezpalejandro@uniovi.es (A.G.-P.); ana.gdiez@udc.es (A.G.-D.)

Citation: González-Pociño, A.; Asensio-Lozano, J.; Álvarez-Antolín, F.; García-Diez, A. Improvement of Impact Toughness and Abrasion Resistance of a 3C-25Cr-0.5Mo Alloy Using a Design of Experiment Statistical Technique: MicrostructuralCorrelations after Heat Treatments. *Metals* **2021**, *11*, 595. https:// doi.org/10.3390/met11040595

Received: 9 March 2021 Accepted: 2 April 2021 Published: 6 April 2021

Publisher's Note: MDPI stays neutralwith regard to jurisdictional claims in published maps and institutional affil-iations.

Abstract: Hypoeutectic high chromium white cast irons are commonly used in the mining and cement industries, where high resistance to abrasive wear is demanded. Through the application of a Design of Experiment technique (DoE), different factors related to thermal industrial treatments are analysed with regard to resistance to abrasive wear and impact response. Abrasion tests were carried out in accordance with the ASTM G065-16 standard. The provisional results show that to increase wear resistance, high destabilisation temperatures (1050 °C) followed by slow cooling to room temperature (RT) and subsequent tempering at 400 °C are most favourable. This is because these conditions are favourable to maintaining a certain tetragonality of the martensite after tempering and also, because of the presence of a high density of mixed carbides M_7C_3, through a secondary precipitation during cooling. Oil quenching and a high tempering temperature (550 °C) with long dwell times of 6 h were found to increase impact toughness. These conditions favour a lack of retained austenite. The presence of retained austenite was found unfavourable for both wear resistance and toughness,whereas tempering at 400 °C has been shown to be insufficient to transform martensite on tempering, which in turn seemed to increase the hardness of the matrix constituent.

Keywords: white cast irons with 25% Cr; resistance to abrasive wear; impact toughness; microstruc-ture correlation; destabilisation of austenite; secondary carbides

1. Introduction

White cast irons with a high chrome content and which have a composition defined by ASTM A532 111A [1] are widely used in the crushing and grinding of rocks and mineralsin the mining and construction industries [2–4]. Resistance to abrasive and erosive wear, as well as resistance to corrosion, are critical properties for such aggressive applications [5,6].It is also necessary for these cast irons to show a good balance between wear resistance and impact toughness, given that in the mining industry they are used, for example, as inner linings of tumble mills used for grinding. The repetitive conditions to which they are exposed include continuous sliding and frequent low impact falls of the ores being treated [7].

The chemical composition for these abrasion resistant alloys yields a hypoeutectic microstructure in the as-cast condition, where the solidification temperature is around 1265 °C [8]. Solidification starts with the formation of primary austenite dendrites and to the conclusion of the eutectic solidification becomes the primary isolated constituent. On reaching room temperature this remained as a dispersed constituent, partially transformed in the solid state, surrounded by a eutectic matrix. Such an eutectic phase is composed of a mixture of austenite and M_7C_3 carbides of the mixed type $(Cr, Fe)_7C_3$ [9]. The hardness values of these types of cast irons vary between 500 and 520 HV in the as-cast state [10]. The abrasion resistance of white cast irons with a high chrome content depends, among otherfactors, on the Cr:C ratio, the thermal treatment history and the type of carbides present, as well as on the hardness, morphology, distribution and its volume fraction [11–13]. Other factors which influence wear resistance include the size and shape of the abrasive ore particles [14], the orientation of the carbide in relation to the direction of wear [15] and the context of wear itself [16]. It is essential to take into account that carbides of the type M_7C_3 are more preferable to any other type, like M_3C, $M_{23}C_6$ and M_6C, because they tend to be coarse and continuous. Ideally, the primary austenite should be uniformly surrounded by the eutectic phase. Within the eutectic, $(Cr, Fe)_7C_3$ carbides represent the discontinuous constituent. The other types of carbides have been found to develop at higher M:C ratios [17]. On the other hand, manganese plays an important role in refiningthe austenite dendrites, and it has been shown to prevent pearlite formation on cooling [18].

Resistance to abrasion also arises from the possibility of austenite hardening when itis subjected to plastic deformation, as is often the case when the surface of the componentsreacts to repeated impacts on their surface with ores in the mining industry. Moreover, in mining operations with low impact requirements, this type of high Cr cast iron exhibitsa satisfactory performance in the as-cast condition due to a relatively high presence of retained austenite at room temperature, capable of plastically absorbing this energy, as reported in certain applications [19,20]. However, excessive energy impacts may cause complete breaking of the components and thus, it explains why they are not suitable for high impact loading [10]. In line with the former, it is a common practice to design coolingpaths after destabilization and tempering with the aim of ensuring the maintenance ofa minimum percentage of retained austenite so as to avoid harmful effects like surface spalling whilst the main focus is set on the increase of wear resistance [21].

In abrasive wear processes, the hardest phases of the microstructure are normally prone to easy fracture, whereas the softer ones could be either cracked or plastically deformed. Thus, chips of the material could break off from the surface therefore resultingin a measurable volume loss of material [22]. The role of the matrix constituent in the microstructure surrounding isolated eutectic carbides is to provide enough mechanical endurance to suppress or minimize cracking, deformation and chip detachments from the surface. Field observations confirmed that the variations in wear resistance are mainly caused by the changes in hardness that fine carbide precipitation from destabilisation confers, in combination with the possibility of a refined microstructure presence for the other phases [23].

In view of the above, the present research aimed to find a destabilisation treatment of austenite designed to maximize the formation of Cr-rich secondary carbide. Such a target is

generally accomplished at temperatures comprised of between 900 and 1100 °C with dwell times of up to 6 h, depending on the degree of transformation required [24,25].Heat treatment guides recommend 1 h of soaking at temperature for each 25 mm of thickness of the cross section. During the destabilisation treatment of the austenite, two complementary kinetics compete. On one hand, the precipitation of secondary carbides is produced. On the other hand, the dissolution of precipitated eutectic carbides is produced in non-equilibrium solidification. The predominance of one over the other depends on the temperature and dwell time [26]. When the dwell period finishes, cooling in air at room temperature (RT) follows, where a depleted austenite in Cr and C partially transforms into martensite [27]. A small fraction of residual austenite could remain at RT along with secondary Cr-rich carbides from destabilisation embedded in it. Such a microstructure could lead to a significant increase in hardness.

Following the above, a tempering heat treatment at temperatures comprised of be- tween 450 and 650 °C for up to 12 h is recommended, with the primary objective of ageingmartensite and obtaining conditioned austenite [28]. By means of a second tempering treatment, conditioned austenite transforms. During the first tempering treatment residual stresses from quenching are removed, thus increasing its toughness [29,30]. Caution should be exercised to avoid coarsening of secondary carbides [9] which may occur if excessive tempering times are used, resulting in a substantial reduction in hardness. The Cr atoms occupy substitutional positions, and their diffusion is not effective until reaching500 °C [31,32].

Through the application of a Design of Experiment (DoE for short) technique based on statistics, the influence on microstructure of the destabilisation temperature at a constantdwell time of 5 h has been studied. Two different temperatures are analysed, one of 950 °C and the other of 1050 °C, in order to analyse the influence of precipitation kinetics and the dissolution of eutectic carbides, previously described. Sample cooling with the use ofdifferent cooling media and the role of tempering were the other factors evaluated. Two different tempering temperatures are analysed, one under 500 °C and the other above thistemperature. There are two objectives: firstly, to study the influence of the precipitation ofcarbides $(Cr, Fe)_7C_3$ during tempering, and secondly, to analyse the adjustment and the following transformation of the retained austenite present. All of the above was done withthe objective of maximising the resistance to abrasive wear, without impairing toughness.

2. Materials and Methods

Based on DoE statistical technique, the thermal treatments of destabilisation and tempering at levels set in a Factorial Fractional study was planned to monitor the effects of the variation of four factors simultaneously. Such factors are related in agreement withthe results based on previous studies by the authors. The application of this statistical technique aims to deliberately modify normal working conditions in order to produce changes in some of the studied responses, as would be the case of resistance to wear and toughness. These changes are carried out on certain production factors. The effect of a factor on the variation in the response function is defined as a consequence of the variation of that factor. The main effects are defined as those derived from each separate factor. Occasionally, the value which one factor takes depends on another factor. When this happens, the factors are said to interact. On an industrial level, the importance of the maineffects tends to be much greater than the importance of the interactions of two factors, andthese, at the same time, greater than the interactions of three factors, and so on. This allows for the simplification of the experimental design and reduces the number of

experiments.A complete factorial design needs a total of 2^4 = 16 experiments. In this study, a factorial design fractioned by half has been used with a total of 2^{3-1} = 8 experiments [33].

The samples used in this study come from the Spanish company Fundiciones del Estanda S.A. (Beasain, Guipúzcoa, Spain). Table 1 shows the basic chemistry of the experi-mental material, a high chrome cast iron micro-alloyed with molybdenum. The chemical analysis was supplied by the company Fundiciones del Estanda, S.A. Table 2 shows the combination of factors and levels chosen for the study. Table 3 shows the matrix of the experiments corresponding to this study.

Table 1. Chemical Composition (% in weight).

C	Si	Mn	Cr	Mo
2.7	1.2	0.8	25.1	0.5

Table 2. Factors and levels.

Factors		Levels	
Code	**Metallurgical Parameter (Factors)**	**Level -1**	**Level +1**
A	Destabilisation temperature of austenite (°C) for 5h	950	1050
B	Cooling media from austenite destabilizing	Air convection within a furnace set @150 0C	Gently stirred oil at R.T.
C	Tempering temperature (0C)	400	550
D	Dwell time at tempering temperature (h)	2	6

Table 3. Matrix of Experiments.

No	A	B	C	D	Restricted Confounding Patterns
1	-1	-1	-1	-1	A
2	+1	-1	-1	+1	B
3	-1	+1	-1	+1	C
4	+1	+1	-1	-1	D
5	-1	-1	+1	+1	AB + CD
6	+1	-1	+1	-1	AC + BD
7	-1	+1	+1	-1	AD + BC
8	+1	+1	+1	+1	

The "Restricted Confounding Patterns" column shows the main effects of the factors and the interactions of two factors whose effects are confounded with the main effects. The effects are linear combinations of the analysed responses and, based on the central limit theorem, they follow a normal law distribution. Each main effect may be considered as a random variable, where the value obtained is an estimation of its mean μ, which is accompanied by its standard deviation σ, noted as: N(μ,σ). When the effects are not significant, they will follow the normal law N(0,σ), that is to say, with μ equals zero. When plotting the standardised effects on a normal probability graph, they will appear aligned. However, if one or more effects are significant, they follow a normal law given by N(μ,σ), with μ6= 0, and will easily be identified as they would not appear aligned with regard to the non-significant ones [33].

The standardised effect is the quotient between the difference between the variable and its mean over the standard deviation of said variable. This value not only represents whether the variable is above or below the mean, but most important, how big this difference is, i.e., how distant the value of the variable is from the value of the mean. When the significant factors deviate from the straight line to the left side, it shows that at its "−1" level, the response function increases with respect to its "+1" level. Conversely, those significant factors which deviate from the straight

line to the right side, show that their "+1" level increases the response function with respect to its "−1" level.

The analysed responses in the present experimentation were structured in two categories: microstructural characteristics and mechanical properties. They are listed herein after:

- Microstructural features being evaluated:
  - Percentage in weight of retained austenite and tempered martensite.
  - Cell unit volume of tempered martensite
  - Percentage in weight of the carbides of the following types M_7C_3, $M_{23}C_6$ and M_2C.
- Mechanical properties tested:
  - The Vickers microhardness of the matrix constituent, with 50gf (0.49N), averaging the results of 24 indentations.
  - The abrasive wear resistance by means of the dry sand/rubber wheel abrasion test, executed in accordance with the ASTM G065-16 standard, with the following test parameters: Rubber wheel diameter: 228.6 mm; Shore A hardness of rubber: 60 ± 2; Silica sand (AF50/70); Sand flow: 300–400 g/min; Rate of revolution: 200 rpm; Test time: 30 min.
  - High strain-rate impact test in a Hounsfield pendulum on un-notched round bars of 8 mm in diameter. The test was conducted on 3 un-notched specs typical for brittle materials for each experiment, and its average value reported.

Scanning Electron Microscope (SEM) images were obtained in a JEOL JSM-5600 (JEOL Ltd., Tokyo, Japan) electron microscope and semi-quantitative spectrum analysis of phases were conducted with an energy dispersive X-ray (EDX) microanalyzer connected to the microscope. The microstructural characteristics were quantitatively assessed by X-ray diffraction in a SEIFERT XRD 3000 T/T (KU Leuven, Leuven, Belgium) diffractometer. Radiation was emitted through a fine focus located after a Mo emitting tube, operating at a working voltage and intensity of 40 kV × 40 mA, with monochromatizing to the Kα: λ1 = 0.709316 Å and λ2 = 0.713607 Å. The diffraction intensity was determined at an angle interval 2θ varying from 7 to 57°.The Rietveld refinement method was used to obtain a more precise determination of the percentage of crystalline phases through the adjustment of the formerly obtained diffractograms. This was carried out using the crystallographic information archives pertaining to the Inorganic Crystal Structure Database (ICSD) by FIZKarlsruhe, Germany. The software package used to perform the Rietveld enhancement was FullProf.2k, version 6.20 (2018). The increase in width observed for the peaks of the main phases, was modelled using the formulation after Stephens [34], which was implemented prior to running the software program for Rietveld enhancement of crystalline phase peaks.

3. Results

Figure 1 shows the diffractograms obtained after Rietveld structural refinement. The intensities are highlighted in red, the calculated intensity, according to the Rietveld model, is presented in black, and the difference between the two intensities are drawn in blue. The vertical segments indicate the angular positions of the different phases being identified.

Table 4 shows the percentages in weight of the main crystalline phases detected by X-ray diffraction. The goodness of the fit is assessed by the Rwp agreement factor, the Rexp index, and

its squared ratio, $Chi^2 = (Rwp/Rexp)^2$. The volume of the unaged martensite cell after specific tempering expressed in cubic Armstrong has also been quoted.

Table 4. Distribution in weight of carbides, martensite and austenite, and cell volume of austenite. Statistical error is indicated in parenthesis.

Experiment	Rietveld Refinement	Phases	Lattice Volume of Martensite (Å³)	wt. %
1	Rwp = 11.6 Rexp = 7.40 Chi^2 = 2.46	Martensite	23.58(±0.006)	54.64 (±1.99)
		Austenite	-	5.61 (±0.62)
		M_7C_3 carbide	-	38.86 (±1.45)
		M_2C carbide	-	0.90 (±0.13)
2	Rwp = 15.6 Rexp = 7.15 Chi^2 = 4.79	Martensite	23.67(±0.05)	20.99 (±0.66)
		Austenite	-	9.70 (±0.8)
		M_7C_3 carbide	-	68.83 (±1.82)
		M_2C carbide	-	0.48 (±0.09)
3	Rwp = 10.5 Rexp = 7.84 Chi^2 = 1.81	Martensite	23.61(±0.006)	68.07 (±2.53)
		Austenite	-	6.22 (±0.34)
		M_7C_3 carbide	-	25.06 (±0.94)
		M_2C carbide	-	0.65 (±0.07)
4	Rwp = 11.3 Rexp = 7.19 Chi^2 = 2.48	Martensite	23.64(±0.01)	53.85 (±2.30)
		Austenite	-	18.16 (±0.89)
		M_7C_3 carbide	-	27.40 (±1.15)
		M_2C carbide	-	0.58 (±0.11)
5	Rwp = 14.4 Rexp = 8.63 Chi^2 = 2.78	Martensite	23.53(±0.003)	69.47 (±3.05)
		Austenite	-	0.040 (±0.32)
		M_7C_3 carbide	-	29.50 (±1.26)
		M_2C carbide	-	0.63 (±0.13)
6	Rwp = 11.9 Rexp = 7.35 Chi^2 = 2.60	Martensite	23.61(±0.005)	46.36 (±1.78)
		Austenite	-	1.12 (±0.39)
		M_7C_3 carbide	-	52.09 (±1.45)
		M_2C carbide	-	0.43 (±0.09)
7	Rwp = 20.7 Rexp = 9.96 Chi^2 = 4.33	Martensite	23.56(±0.001)	23.69 (±0.38)
		Austenite	-	0.1 (±0.08)
		M_7C_3 carbide	-	76.11 (±1.68)
		M_2C carbide	-	0.10 (±0.02)
8	Rwp = 11.8 Rexp = 8.34 Chi^2 = 2.00	Martensite	23.53(±0.005)	64.73 (±2.51)
		Austenite	-	0.99 (±0.18)
		M_7C_3 carbide	-	34.03 (±1.14)
		M_2C carbide	-	0.24 (±0.09)

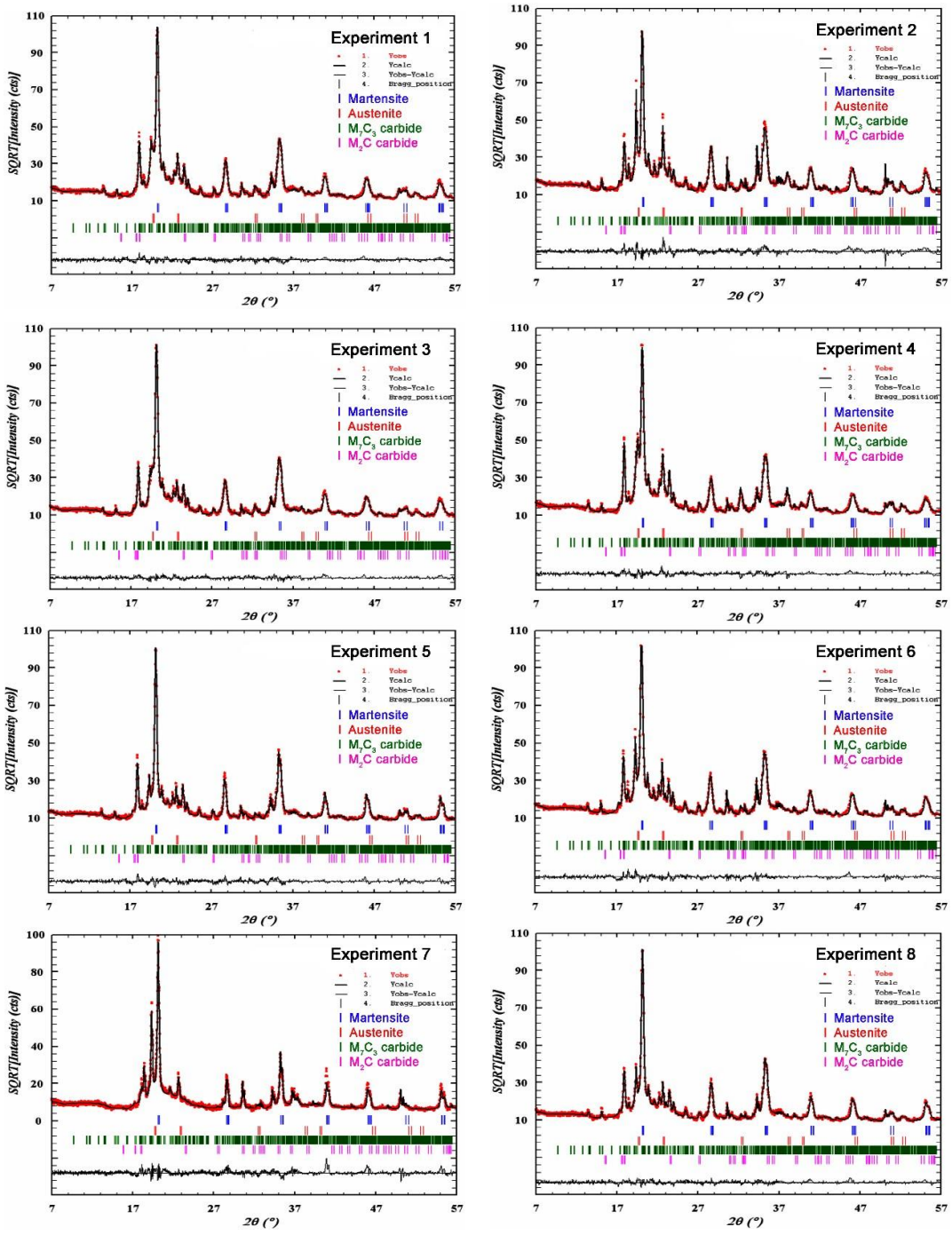

Figure 1. Diffractograms of the experiments after Rietveld refinement.

Table 5 shows a last column entitled "confounding pattern" for which each line (row) corresponds one to one with the numerical values in the columns of the standardised effects. In such fashion, the first numerical value in the column of the standardised effects is always the average of the responses. Values in parenthesis represent the error of the mean given by its standard deviation. Figure 2 depicts the representation of the standardised effects on a normal probability graph, and following the usual practice, for reasons of simplicity, only the factors with a significant effect on the responses are labelled.

Table 5. Average values and obtained effects for the precipitated phases.

(a) Weight percentage of tempered martensite and retained austenite							
Experiment Number	Austenite		Martensite				Confounding Pattern
	wt.%	Effects	wt.%	Effects	vol.%	Effects	
1	5.61	5.29	54.64	50.23	23.58	23.58	Average
2	9.70	4.41	20.99	−7.49	23.67	0.04	A
3	6.22	2.16	68.07	4.72	23.60	−0.01	B
4	18.16	−9.27	53.85	1.68	23.64	−0.07	C
5	0.40	−1.92	69.47	11.18	23.53	−0.01	D
6	1.12	2.01	46.36	20.90	23.6	−0.04	AB + CD
7	0.10	−3.61	23.69	16.45	23.56	−0.02	AD + BC
8	1.00	−2.38	64.73	−18.43	23.53	−0.01	AC + BD

(b) Weight percentage of M_7C_3 and M_2C carbides					
Experiment Number	M_7C_3 Carbide		M_2C Carbide		Confounding Pattern
	wt.%	Effects	wt.%	Effects	
1	38.86	44.00	0.89	0.50	Average
2	68.83	3.21	0.48	−0.14	A
3	25.06	−6.67	0.65	−0.22	B
4	27.40	7.90	0.59	−0.30	C
5	29.50	−9.26	0.63	0.00	D
6	52.09	−23.08	0.43	0.17	AB + CD
7	76.11	−12.95	0.10	0.11	AD + BC
8	34.03	20.95	0.24	−0.14	AC + BD

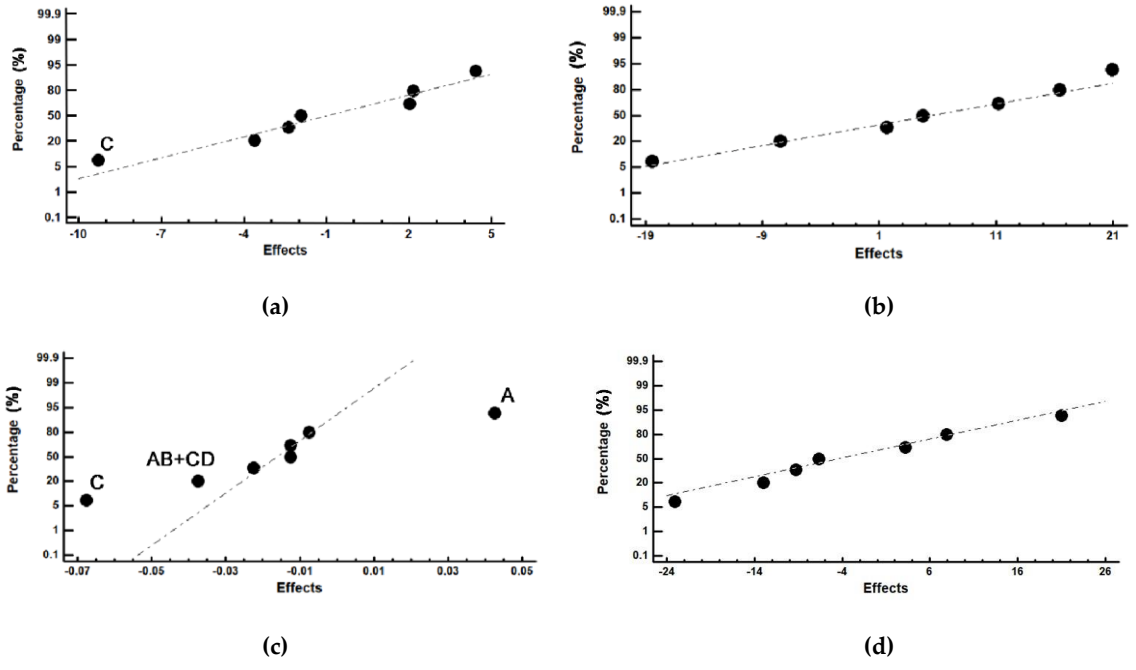

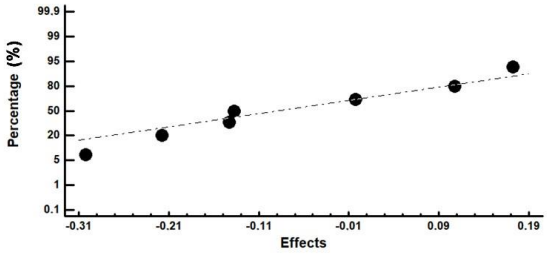

(e)

Figure 2. Representation of the standardized effects for the weight percentages of the different phases plotted on a normal probability graph. Factors with a significant effect have been labelled. A (destabilisation temperature); B (cooling media); C (tempering temperature); D (tempering time): (**a**) wt.% austenite; (**b**) wt.% tempered martensite; (**c**) cell volume of tempered martensite; (**d**) wt.% carbides M_7C_3 (K_2); (**e**) wt.% carbides M_2C.

Figure 2a shows that when factor C (tempering temperature) is at its −1 level (400 °C), the percentage of retained austenite increases. Therefore, such a low ageing temperature seems insufficient for completing the transformation of residual gamma from quenching into martensite. A possible explanation may lie in the fact that a highly alloyed austenite is less prone to transformation during tempering, probably due to low C diffusivity at such a temperature [32]. This is because the thermal gap is lower than if tempering is carried out at 500 °C. The thermal gap makes it possible to decrease free energy for the transformation of the austenite into martensite. This decrease should compensate for the increase of energy which crystalline distortion supposes due to the tetragonality of the martensite [31]. So, the more alloyed this austenite is, the greater the crystalline distortion will be and, because of this, the greater the required thermal gap must be. Figure 2b shows that none of the factors have a significant effect on the weight percent of tempered martensite. However, Figure 2c illustrates that when factor C (tempering temperature) is at its −1 level (400 °C) and factor A (destabilization temperature) is set at its +1 level (1050 °C), an increase in the cell volume of unaged martensite follows. A possible explanation might be given by the fact that higher austenitising temperatures enable the austenite cell to admit more C atoms in solid solution, and on quenching, the resulting martensite should show a more tetragonal cell [31,32]. On the other hand, this martensite would be highly alloyed, and would show a low decomposition rate on tempering because of low C diffusion at low tempering temperatures. Furthermore, the precipitation of chrome carbides of the type M_7C_3 does not begin until temperatures are higher than 500 °C. Moreover, because of the low number of free interstitial sites in martensite effective C diffusion may be restrained too. On the same plot the interaction given by AB + CD has been labelled since it appears to provide a significant effect. Figure 3 presents the results of the calculations made so as to conduct the analysis of the former interactions. It can be seen that those products of A × B yielding a −1 value, as well as the product of C × D yielding also −1 value, should provide a meaningful interaction. In the first case the higher value (tallest column) corresponds to factor A at its +1 level and factor B to its −1 level (+1 × (−1) = −1). For the CD interaction, the highest value corresponds to factor C at its −1 level, and factor D at its +1 (−1 × (+1) = −1). Comparing both interactions, the most representative, i.e., the one with the highest value is the interaction CD: factor C (tempering temperature) at its −1 level (400 °C) and factor D at its +1 level (6 h). The value found for the cell volume of martensite when D factor is at its −1 level (550 °C) provides a somewhat similar value for the cell volume of unaged martensite, thus limiting the effect of factor D in the interaction given by CD. In summary, what seems relevant to obtaining a high-volume cell of martensite after tempering is the use of low tempering temperature, making the dwell time at tempering less relevant when it is comprised of between 2 and 6 h.

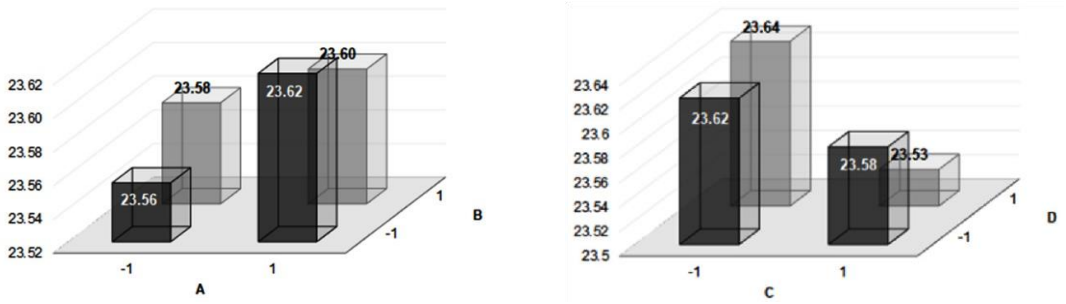

Figure 3. Analysis of interactions with a significant effect with respect to the cell volume of unaged martensite. X-axis represents the two levels of A-factor (figure (**a**)) and the two levels of C-factor (figure (**b**)). Y-axis represents the two levels of B-factor (figure (**a**)) and the two levels of D-factor (figure (b)). Z-axis represents the effect of each possible combination of the factors: (**a**) interaction AB; (**b**) interaction CD.

Table 6 shows the loss of material (in mg.) during the wear test of the specimens against a rubber wheel with ungrounded dry silica sand acting as an abrasive interface. It also shows the corresponding standardised effects and their correspondence with the confounding patterns.

Table 6. Loss of material (mg.) after 30 min of a continuous abrasive wear test conducted in accordance with the ASTM G40-92 standard.

Experiment Number	Wear Loss (30 min)		Effects	Confounding Patterns
	mg	CL (95%)		
1	97.08	±0.75	130.02	Average
2	120.30	±1.45	−29.415	A
3	92.35	±2.10	3.03	B
4	113.00	±0.20	48.675	C
5	194.33	±1.47	6.27	D
6	102.31	±1.75	4.985	AB + CD
7	195.15	±0.37	−51.35	AC + BD
8	125.64	±1.16	9.045	AD + BC

Figure 4 shows the main factors which have a significant effect with respect to an increase in the abrasive wear rate measured by the loss of weight of samples for each experiment. Such factors are: Factor A (temperature of destabilisation of austenite) at its −1 level (950 °C), and factor C (tempering temperature) at its +1 level (550 °C), increase the wear rate. Conversely, a destabilisation treatment of austenite at 1050 °C and a tempering treatment at 400 °C increase the resistance to abrasive wear. The result is in agreement with the factors which also increase the hardness of the matrix constituent, as will be shown later. The results obtained in this manner could be explained by the higher volume fraction of secondary carbides formed in the matrix constituent at a high destabilisation temperature, as well as by the presence of unaged martensite at low tempering temperatures [26,35].

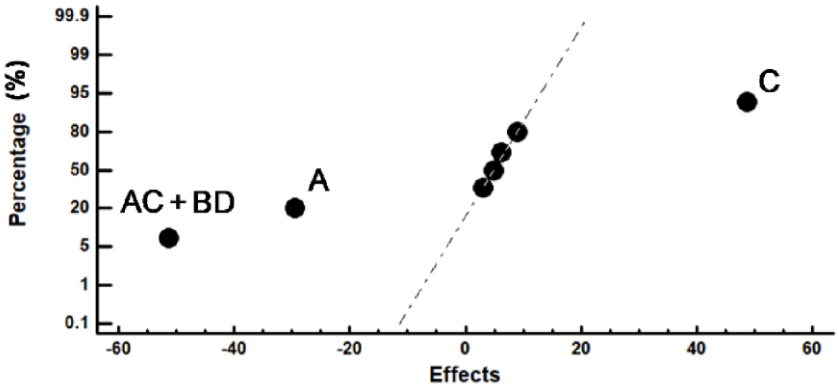

Figure 4. Representation of the standardized effects on the weight loss by abrasive wear in a test of 30 min duration, plotted on a normal probability graph. A (destabilisation temperature); B (cooling media); C (tempering temperature); D (tempering time).

The significant effect of the interactions AC and BD are also shown in Figure 5. The result of the analysis is depicted in the block diagram in Figure 5. It can also be observed how the combination of factors A and C, at their respective −1 and +1 levels (destabilisation of the austenite at 950 °C and tempering at 550 °C), lead to an increase in the wear rate. Thus, this combination yields a more deleterious behaviour for abrasive wear resistance when those main factors operate at those levels than when they are selected individually. These suggest a synergic interrelation of these factors and corresponding levels.

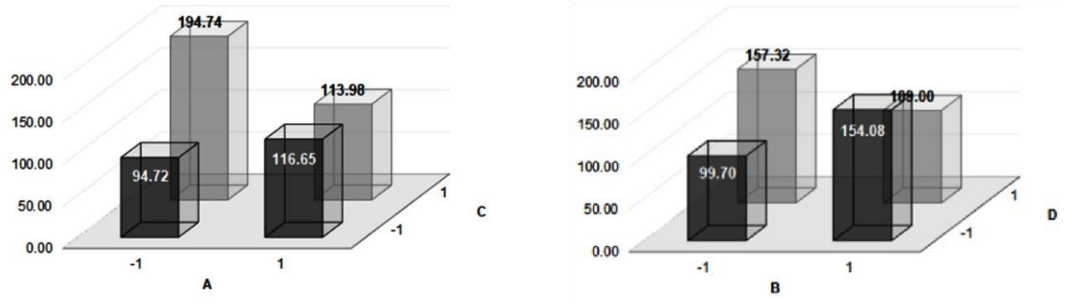

Figure 5. Analysis of interactions with significant effects with respect to abrasive wear. X-axis represents the two levels of A-factor (figure (**a**)) and the two levels of B-factor (figure (**b**)). Y-axis represents the two levels of C-factor (figure (**a**)) and the two levels of D-factor (figure (**b**)). Z-axis represents the effect of each possible combination: (**a**) interaction AC; (**b**) interaction BD.

Figure 6 shows SEI (Secondary Electron Image) SEM micrographs of the wear surface in experiments 1 and 3 once the abrasive test was concluded. Scratches may be observed on the surface of the K_2 eutectic carbides which are less evident on the matrix, suggesting different mechanisms of degradation for both of them. K_2 eutectic carbides, with HV values in the range of 1500–1800 have been lightly scratched by AFS 50/70 ungrounded silica sand which has a lower hardness, but should these carbides become repeatedly abraded, shallow grooves would form. The wear mechanism in the matrix shows uniform wear with occasional tearing and decohesion between carbides and matrix constituents. It is possible to distinguish what seems to be occasional detachment of small broken pieces of K_2 carbides, leaving a hole in the matrix after particle release.

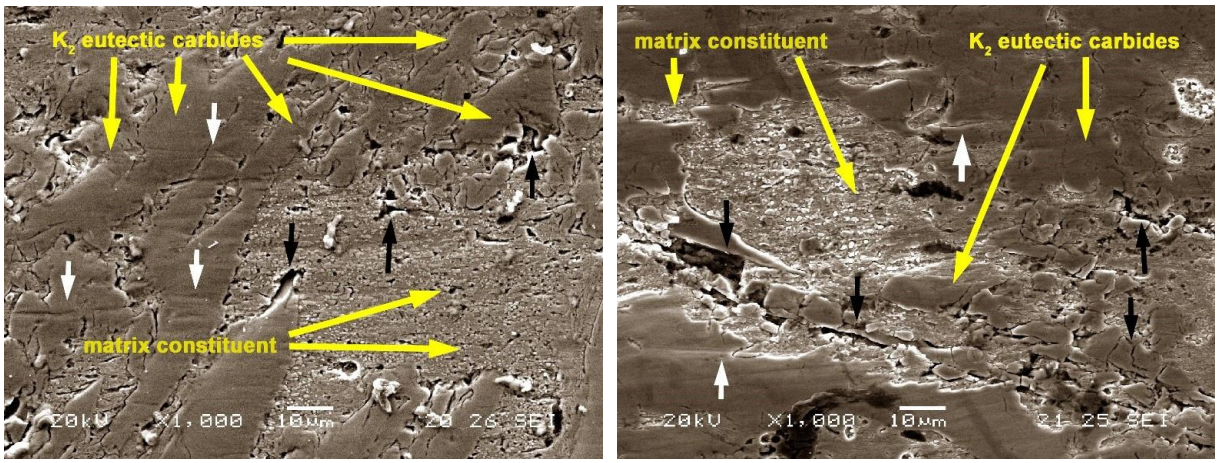

(**a**) (**b**)

Figure 6. Abrasive wear surface in Scanning Electron Microscope (SEM) (**a**) experiment 1; (**b**) experiment 3. Black arrows show the areas of decohesion of broken eutectic carbides from the matrix constituent. White arrows show shallow scratches on the surface of bulk K_2 eutectic carbides [36,37].

Table 7 shows the average values and the standardised effects obtained for the microhardness of the matrix constituent as well as the normalised energy absorbed in the fracture of unnotched cylindrical specimens obtained after impact testing in a Hounsfield balanced machine. Figure 7 show the standardised effects for the matrix microhardness. Once represented on normal probability graphs, and those factors with significant effects were correspondingly labelled.

Table 7. Average values and standardised effects obtained for the microhardness of the matrix constituent and the impact toughness measured in a Hounsfield balanced impact machine.

Experiment	Microhardness			Impact Toughness			Confounding
Number	HV	CL (95%)	Effect	J/cm²	CL (95%)	Effect	Pattern
1	732	±15	667.0	8.85	±1	6.8	Average
2	764	±17	129.2	3.12	±0.27	-1.8	A
3	664	±30	-51.2	1.66	±0.18	0.5	B
4	756	±23	-123.2	4.73	±0.5	4.4	C
5	527	±7	-27.7	10.41	±1.5	0.0	D
6	749	±20	2.2	3.79	±0.4	4.4	AB + CD
7	488	±14	67-2	9.89	±1	-0.5	AD + BC
8	659	±10	-13.2	12.03	±1.7	3.3	AC + BD

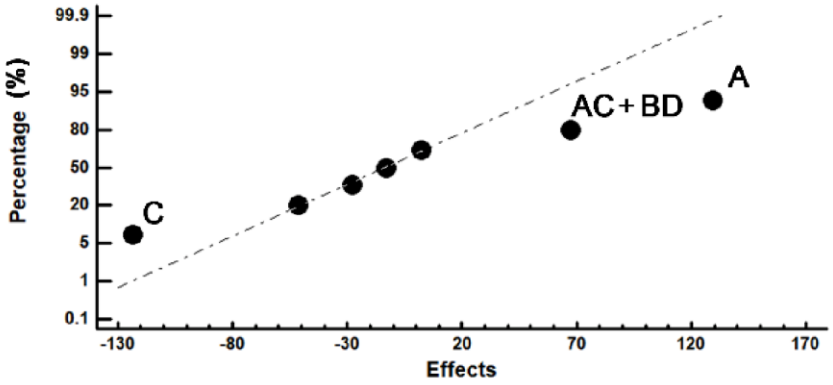

Figure 7. Representation of the factors with significant effect on the hardness of the matrix constituent on a normal probability graph. A (destabilisation temperature); B (cooling media); C (tempering temperature); D (tempering time).

In Figure 7 it can be seen that the hardness of the matrix constituent increases when factor A (temperature of destabilisation) is at its +1 level (1050 °C), and factor C (tempering temperature) is at its −1 level (450 °C). At high temperatures of destabilisation and a sufficient dwell time at temperature, supersaturated austenite from quenching starts gaining equilibrium by precipitating alloy carbides from the excess of C and Cr in the γ cells. At a lower rate, non-equilibrium eutectic, formed at high solidification rates typical of industrial practice, gradually disappears as it approaches equilibrium. As a result of this microstructural change, a new high maximum solubility of carbon for austenite is reached, which, on quenching, yields a more slender tetragonal martensite cell, which the X-ray diffraction analyses have confirmed. This, along with a low tempering temperature could be insufficient for alloyed martensite to age during tempering, and this is thought to entail an increase in the hardness of the matrix phase [31,32].

A sum of interactions AC + BD, with a significant effect in the matrix microhardness, can also be observed in Figure 7. The detailed analysis of the interaction of the effects is presented in Figure 8a, which shows that for the interaction AC, with factor A at its +1 level and factor C at its −1 level, shows more prominent results than the rest. However, such levels yield a negative value for the interaction itself: A × C ∝ (+1 level) × (−1 level) = −1. Such an interaction AC, in order to be considered correct, should have appeared to the left and at the low end of the straight line in the normal probability plot in Figure 7, and thus, it explains why such interaction is dismissed. In summary, each separate factor has a significant effect on the increase in the matrix hardness but, if the two factors perform together at the levels dictated by the interaction no significant effect is appreciated. Figure 8b also shows the interaction BD to have a significant effect when both factors are at level −1, that is to say, when the cooling rate is slower (in a current of hot air at 150 °C), and the time of tempering is shorter (2 h). This could be interpreted as the possibility of further precipitation of K2 carbides between 400 and 600 °C at slow cooling rates, and thus its contribution to the structural hardening of austenite, as has been reported by these authors in an earlier work [26]. Regarding the role of tempering for shorter times and its contribution to the increase in hardness of the matrix, it is thought that such an increase could perhaps be attributed to the presence of unaged hard martensite after treatment.

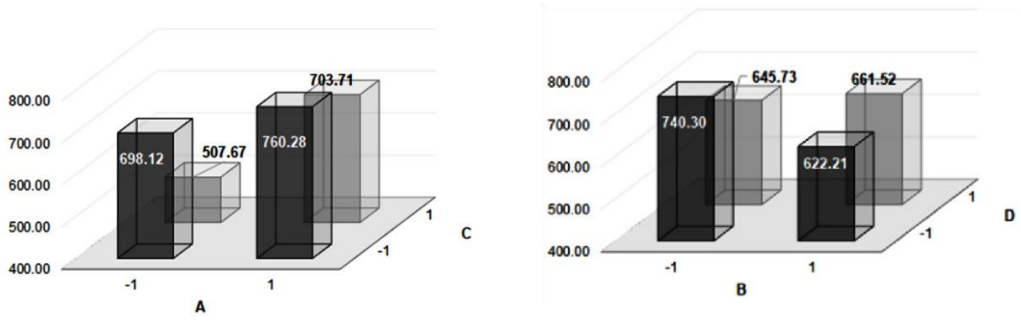

(a) **(b)**

Figure 8. Analysis of interactions with a significant effect with respect to the hardness of the constituent matrix. X-axis represents the two levels of A-factor (figure (**a**)) and the two levels of B-factor (figure (**b**)). Y-axis represents the two levels of C-factor (figure (**a**)) and the two levels of D-factor (figure (**b**)). Z-axis represents the effect of each possible combination: (**a**) interaction AC; (**b**) interaction BD.

Figure 9 shows selected SEM micrographs for experiments 4 and 5, chosen because of great differences in the matrix constituent hardness. In the micrograph corresponding to experiment 4 the abundant presence of retained austenite is highlighted. This can be distinguished from the M_7C_3 carbides since these have a rounded morphology and a slightly darker colouring. The material corresponding to experiment 4 resulted in greater hardness of the matrix constituent along with a greater resistance to abrasive wear. On the other hand, the material corresponding to experiment 5 gave lower values for identical responses, as shown in the results of Tables 6 and 7. Experiment 4 with high matrix hardness and high wear resistance, corresponded to a specimen being tempered at 550 °C for 6 h. It seems that this specific ageing at high temperature and for a long time could have favoured structural hardening by partial ageing of retained austenite from quenching. Moreover, the tempering of martensite at 550 °C could have contributed to structural hardening through the precipitation of M_7C_3 carbides. It can be observed how the matrix constituent in experiment 4 presents a lower density of carbides compared to the matrix constituent in experiment 5.

Figure 10 shows the effects on the toughness of the material, characterised with the Hounsfield test, represented on a normal probability plot. Factor C (tempering temperature) is significant at its +1 level (550 °C). Moreover, the effects of the interactions AB + CD and AD + BC are significant when the product of their respective levels yield a +1. These interactions are analysed in Figure 11. It is concluded that the higher toughness is obtained when Factor B stands at its +1 level (oil quenching) thus maximizing the volume fraction of martensite ensuring a minimal fraction of austenite. Moreover, when both Factor C (tempering temperature) and Factor D, both standing at their +1 level (550 °C and 6 h dwell respectively). In conclusion, the way to gain a good impact response would be by firstly ensuring the maximum conversion of austenite into martensite on quenching, which would be obtained with high severity media: oil at RT with very gentle stirring, preferable to stirred hot air at 150 °C. Highly alloyed austenite usually requires two tempering treatments to age, unlike martensite which tempers with just one, on condition that the temperature and time are high enough (550 °C and 6 h) to promote diffusion and the possibility of reaching the solubility product to allow the formation of high temperature alloyed carbides.

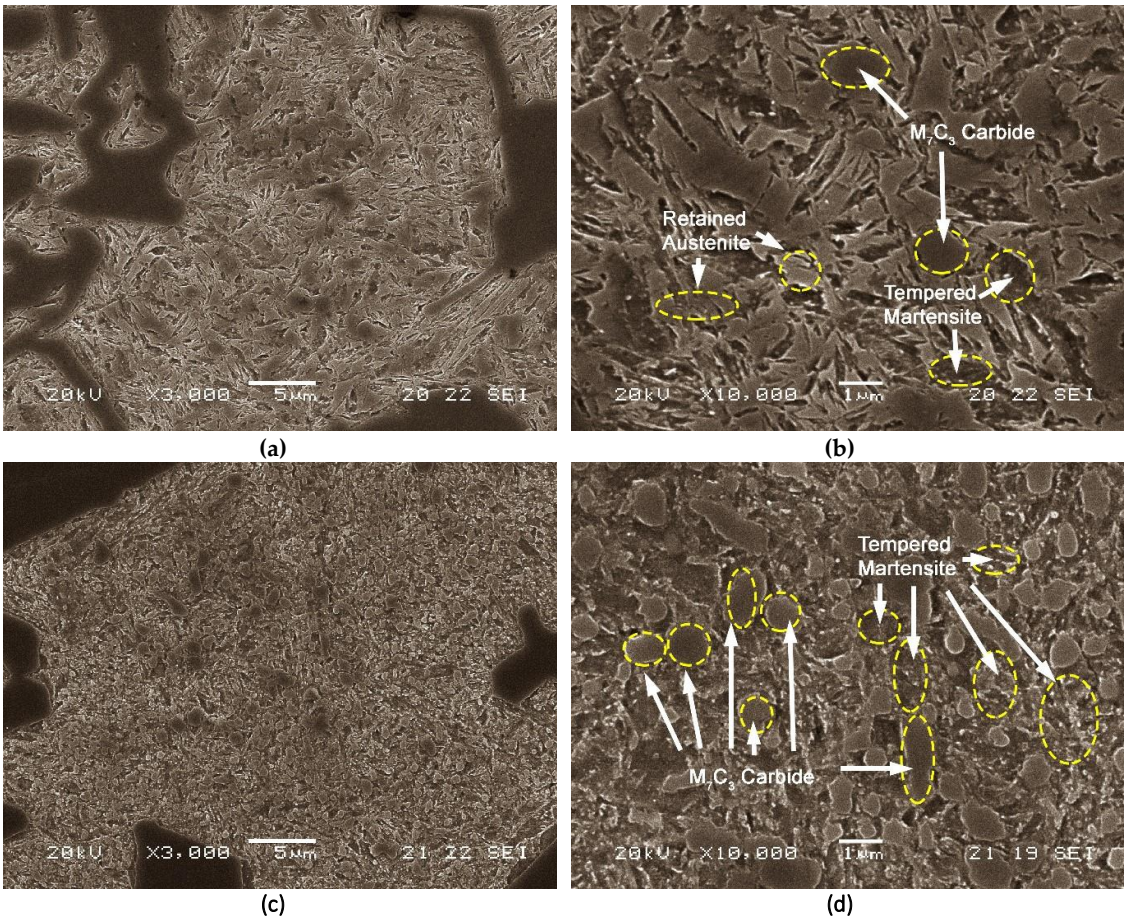

Figure 9. Selected SEM micrographs for experiments 4 and 5. (**a**,**b**) correspond to experiment 4; (**c**,**d**) correspond to experiment 5.

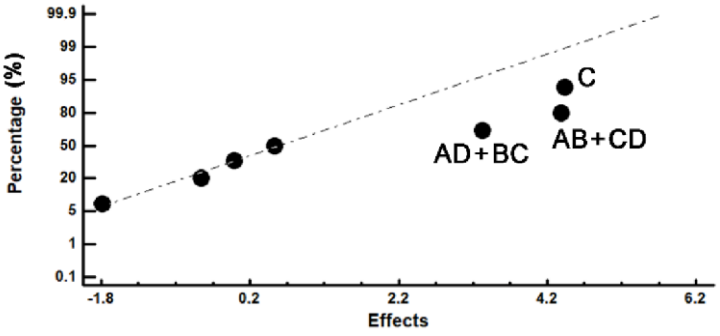

Figure 10. Representation on a normal probability plot of the factors with a significant effect on the response to impact. A (destabilisation temperature); B (cooling media); C (tempering temperature); D (tempering time).

Experiment 8 showed the value for highest energy absorbed, and with regard to the factors with significant effect in the improvement of impact toughness, this experiment corresponds to a high destabilisation temperature. An increase in the temperature prior to quenching ensures a depleted austenite in alloy elements because of the intrinsic nature of destabilisation, consisting of the formation of alloy carbides. This leads to a higher Ms and Mf temperatures and thus, a higher volume fraction of martensite formed. Figure 12 shows the microstructure of this experiment which corresponds to austenitising at 1050 °C for 5 h, followed

by oil cooling and tempering at 550 °C for 6 h. Its matrix constituent does not show the presence of austenite but illustrates an elevated density of carbides.

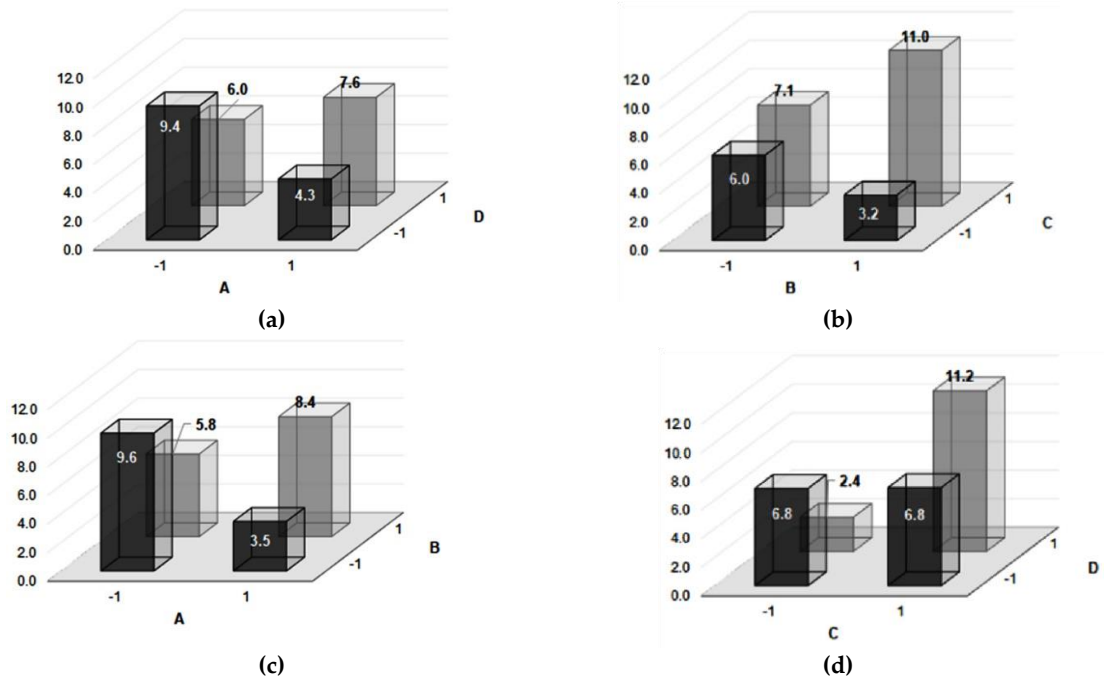

Figure 11. Analysis of the interactions with a significant effect on toughness of material, characterised with the Hounsfield test. X-axis represents the two levels of A-factor (figure (**a**)), of B-factor (figure (**b**)), of A-factor (figure (**c**)), and C-factor (figure (**d**)). Y-axis represents the two levels of D-factor (figure (**a**)) of C-factor (figure (**b**)), of B-factor (figure (**c**)), of D-factor (figure (**d**)). Z-axis represents the effect of each possible combination: (**a**) interaction AB; (**b**) interaction CD; (**c**) interaction AD; (**d**) interaction BC.

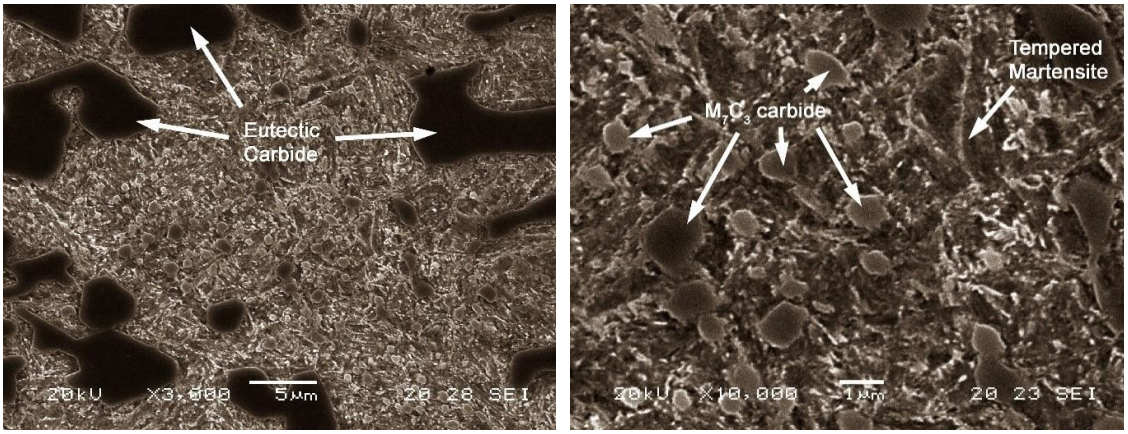

Figure 12. Microstructure corresponding to experiment 8. A high density of carbides in the matrix can be observed.

With regard to the values in Table 4, the presence of carbides of the M_2C type, associated with Mo is confirmed for Table 8. Figure 13 shows a BEI image confirming the presence of this carbide with skeletal morphology which is nucleated from the eutectic M_7C_3 [38].

Table 8. Semi-quantitative analysis of phases shown in Figure 13a,b. This analysis was carried out through an energy dispersive X-ray microanalysis (EDX). (% atomic).

Spectrum	C	Cr	Fe	Mo
1	45.24	4.88	23.70	26.18
2	34.27	39.12	26.61	-
3	40.62	11.51	24.18	23.69
4	31.56	40.43	28.01	-

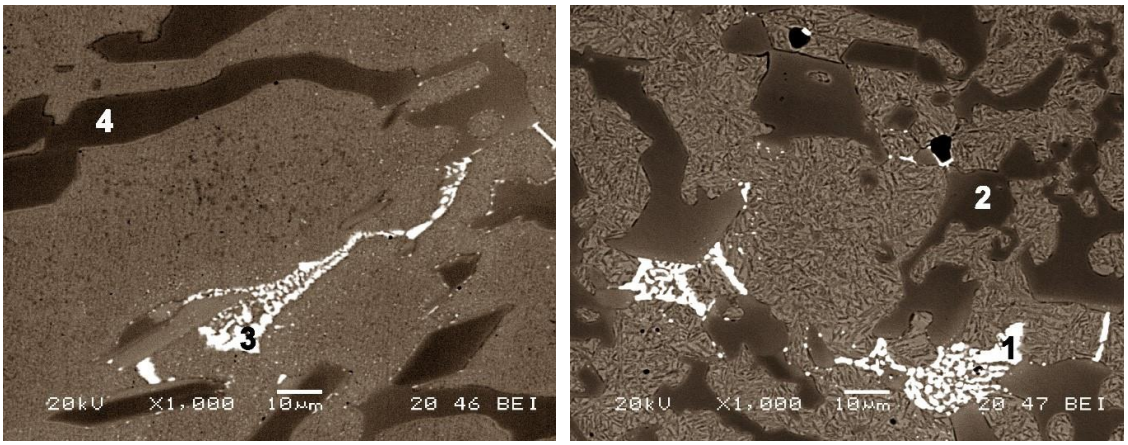

(a) **(b)**

Figure 13. Presence of carbides M_2C, associated with Mo. The numbers 1–4 correspond to the spectra in Table 8: (**a**) experiment 2; (**b**) experiment 7. Images obtained in a back scattered electron detector.

4. Conclusions

The application of Fractional Factorial Design of Experiments with minimum fractioning has allowed the analysis of the effect of four metallurgical factors at two fixed levels to assess both microstructural features and selected mechanical properties in just eight experiments. The factors and their levels are related to the heat treatments to apply to as-cast components made in high chromium cast irons prior to commissioning. These factors are: the destabilisation of austenite for 5 h at two temperatures (950 °C or 1050 °C), the quenching media (agitated air at 150 °C or oil gently stirred at 20 °C); and finally, the tempering temperature (400 and 500 °C) at two dwell times (2 h and 6 h), the latter with the purpose of increasing abrasive wear resistance while modestly improving its impact toughness to fracture. A summary of the findings of this experimental work follows below.

To increase the resistance to abrasive wear the following is recommended:

1. The use of high destabilisation temperatures, around 1050 °C, followed by cooling in hot air at 150 °C. Destabilisation at 1050 °C allows secondary M_7C_3 carbide precipitation from supersaturated austenite accompanied by partial solubilisation of non-equilibrium eutectic carbides which form during solidification. The after cooling that follows if taking place within an air convection furnace set at 150 °C, seemed to favour further carbide formation in the range of 400–600 °C.
2. Abrasion resistance is also favoured by low tempering temperatures (400 °C) and shorter tempering times (2 h). They both seem to favour a fine and dispersed precipitation. From X-ray diffraction analysis, the tempering conditions seemed insufficient for complete ageing of martensite as has been shown by the lattice results which indicate the existence of slender tetragonal lattice remaining after treatment. Thus, its possible contribution to the matrix hardness.

To increase the dynamic impact energy absorbed the following is advised:

1. Quenching in gently stirred oil at ambient temperature has been checked to promote full conversion of destabilised austenite into martensite i.e., to favour the absence of retained austenite after quench. This retained austenite is found to be highly alloyed and with accumulated plastic deformation due to the adjacent presence of tetragonal martensite, thus the need for the absence of residual austenite for better impact response.
2. Tempering at 550 °C and long dwell tempering times of around 6 h, helped to complete full ageing of martensite thus the increase of overall toughness.

Author Contributions: J.A.-L. Conceived and designed the investigation; A.G.-P. and A.G.-D. Performed all laboratory work; F.Á.-A. led the investigation, analysed the data and wrote the paper. All authors have read and agreed to the published version of the manuscript.

Funding: This research received no external funding.

Data Availability Statement: Data is contained within the article.

Conflicts of Interest: The authors declare no conflict of interest.

References

1. *Standard Specification for Abrasion-Resistant Cast Irons*; A532/A532M-10; ASM International: West Conshohocken, PA, USA, 2019. [CrossRef]
2. Amorim, P.; Santos, H.; Santos, J.; Coimbra, S.; Sá, C. Soft Annealing of High Chromium White Cast Iron. *Mater. Sci. Forum* **2004**, *455–456*, 290–294. [CrossRef]
3. Abdel-Aziz, K.; El-Shennawy, M.; Omar, A.A. Microstructural characteristics and mechanical properties of heat treated high-cr white cast iron alloys. *Int. J. Appl. Eng. Res.* **2017**, *12*, 4675–4686.
4. Nayak, U.P.; Guitar, M.A.; Mücklich, F. A comparative study on the influence of chromium on the phase fraction and elemental distribution in as-cast high chromium cast irons: Simulation vs. experimentation. *Metals* **2020**, *10*, 30. [CrossRef]
5. Jones, M.; Llewellyn, R.J. Erosion-corrosion assessment of materials for use in the resources industry. *Wear* **2009**, *267*, 2003–2009. [CrossRef]
6. Llewellyn, R.J.; Yick, S.K.; Dolman, K.F. Scouring erosion resistance of metallic materials used in slurry pump service. *Wear* **2004**, *256*, 592–599. [CrossRef]
7. Zhang, J.-C.; Zhang, T.; Yang, Y.T. Microstructure and properties evolution of Nb-bearing medium Cr wear-resistant cast steel during heat treatment. *J. Iron Steel Res. Int.* **2020**. [CrossRef]
8. Poolthong, N.; Nomura, H.; Takita, M. Effect of heat treatment on microstructure and properties of semi-solid chromium cast iron. *Mater. Trans.* **2004**, *45*, 880–887. [CrossRef]
9. Karantzalis, A.E.; Lekatou, A.; Mavros, H. Microstructural Modifications of As-Cast High-Chromium White Iron by Heat Treatment. *J. Mater. Eng. Perform.* **2009**, *18*, 174–181. [CrossRef]
10. Pero-Sanz, J.A. *Fundiciones Férreas*; Dossat: Madrid, Spain, 1994; pp. 123, 129.
11. Tang, X.H.; Chung, R.; Li, D.Y.; Hinckley, B.; Dolman, K. Variations in microstructure of high chromium cast irons and resultant changes in resistance to wear, corrosion and corrosive wear. *Wear* **2009**, *267*, 116–121. [CrossRef]
12. Hanlon, D.N.; Rainforth, W.M.; Sellars, C.M. The rolling/sliding wear response of conventionally processed and spray formed high chromium content cast iron at ambient and elevated temperature. *Wear* **1999**, *225–229*, 587–599. [CrossRef]
13. Kopycin´ski, D.; Guzik, E.; Szcze¸sny, A. Equiaxed and oriented microstructure in high chromium cast iron. *Arch. Metall. Mater.* **2014**, *59*, 723–726. [CrossRef]
14. Walker, C.I.; Hambe, M. Influence of particle shape on slurry wear of white iron. *Wear* **2015**, *332–333*, 1021–1027. [CrossRef]

15. Dogan, Ö.N.; Hawk, J.A. Effect of carbide orientation on abrasion of high Cr white cast iron.˘ *Wear* **1995**, *189*, 136–142. [CrossRef]
16. Zum Gahr, K.H.; Eldis, G.T. Abrasive wear of white cast irons. *Wear* **1980**, *64*, 175–194. [CrossRef]
17. Thorpe, W.R.; Chicco, B. The Fe-rich corner of the metastable C-Cr-Fe liquidus surface. *Metall. Trans. A* **1985**, *16*, 1541–1549. [CrossRef]
18. Kadhim, M.J.; Abood, A.N.; Yaseen, R.S. The role of manganese on microstructure of high chromium white cast iron. *Mod. Appl. Sci.* **2011**, *5*, 179–185. [CrossRef]
19. Pearce, J.T.H. The use of transmission electron microscopy to study the effects of abrasive wear on the matrix structure of a high chromium cast iron. *Wear* **1983**, *89*, 333–344. [CrossRef]
20. Sinatora, A.; Pohl, M.; Waldherr, E.U. Wear induced martensite in high chromium cast iron. *Scr. Metall. Mater.* **1995**, *32*, 857–861. [CrossRef]
21. Zhang, M.X.; Kelly, P.M.; Gates, J.D. The effect of heat treatment on the toughness, hardness and microstructure of low carbon white cast irons. *J. Mater. Sci.* **2001**, *36*, 3865–3875. [CrossRef]
22. Davis, J.R. *Metallurgy and properties of high alloy white irons. ASM Specially Hand Book, Cast Irons*; ASM International: Materials Park, OH, USA, 1996; pp. 107–130.
23. Chung, R.J.; Tang, X.; Li, D.Y.; Hinckley, B.; Dolman, K. Microstructure refinement of hypereutectic high Cr cast irons using hard carbide-forming elements for improved wear resistance. *Wear* **2013**, *301*, 695–706. [CrossRef]
24. Karantzalis, A.E.; Lekatou, A.; Diavati, E. Effect of destabilization heat treatments on the microstructure of high-chromium cast iron: A microscopy examination approach. *J. Mater. Eng. Perform.* **2009**, *18*, 1078–1085. [CrossRef]
25. Tabrett, C.P.; Sare, I.R. Fracture toughness of high-chromium white irons: Influence of cast structure. *J. Mater. Sci.* **2000**, *35*, 2069–2077. [CrossRef]
26. Gonzalez-Pociño, A.; Alvarez-Antolin, F.; Asensio-Lozano, J. Erosive wear resistance regarding different destabilization heat treatments of austenite in high chromium white cast iron, alloyed with Mo. *Metals* **2019**, *9*, 522. [CrossRef]
27. Powell, G. Improved Wear-Resistant High-Alloyed White Irons-a Historical Perspective. In Proceedings of the International Congress on Abrasion Wear Resistance Alloyed White Cast Iron for Rolling and Pulverizing Mills, Fukuoka, Japan, 16–20 August 2002; pp. 1–10.
28. Wang, J.; Li, C.; Liu, H.; Yang, H.; Shen, B.; Gao, S.; Huang, S. The precipitation and transformation of secondary carbides in a high chromium cast iron. *Mater. Charact.* **2006**, *56*, 73–78. [CrossRef]
29. Oanh, N.T.H.; Viet, N.H. Precipitation of M23C6 secondary carbide particles in Fe-Cr-Mn-C alloy during heat treatment process. *Metals* **2020**, *10*, 157. [CrossRef]
30. Tabrett, C.P.; Sare, I.R.; Ghomashchi, M.R. Microstructure-property relationships in high chromium white iron alloys. *Int. Mater. Rev.* **2014**, *41*, 59–82. [CrossRef]
31. Pero-Sanz, J.A. *Aceros. Metalurgia Física, Selección y Diseño*; Dossat: Madrid, Spain, 2004; pp. 70–71, 128–142.
32. Bhadeshia, H.K.D.H.; Honeycombe, R.W.K. *Steels: Microstructure and Properties*; Butterworth-Heinemann (Elsevier): London, UK, 2006; pp. 101, 193–195.
33. Prat-Bartés, A.; Tort-Martorell, X.; Grima-Cintas, P.; Pozueta-Fernández, L.; Solé-Vidal, I. *Métodos Estadísticos*, 2nd ed.; UPC: Barcelona, Spain, 2004; p. 376.
34. Stephens, P.W. Phenomenological model of anisotropic peak broadening in powder diffraction. *J. Appl. Crystallogr.* **1999**. [CrossRef]
35. Pero-Sanz Elorz, J.A. *Ciencia e Ingeniería de Materiales*, 5th ed.; Cie-Dossat: Madrid, Spain, 2006; p. 237.
36. González-Pociño, A.; Alvarez-Antolin, F.; Asensio-Lozano, J. The joint effects of nitriding and parameters related to the destabilisation of austenite on wear resistance in white cast iron with 25% cr. *Metals* **2021**, *11*, 85. [CrossRef]
37. Gonzalez-Pociño, A.; Alvarez-Antolin, F.; Asensio-Lozano, J. Optimization, by means of a design of experiments, of heat processes to increase the erosive wear resistance of white hypoeutectic cast irons alloyed with Cr and Mo. *Metals* **2019**, *9*, 403. [CrossRef]

38. Zhou, X.; Fang, F.; Gang, L.I.; Jiang, J. Morphology and properties of M2C eutectic carbides in AISI M2 steel. *ISIJ Int.* **2010**, *50*, 1151–1157. [CrossRef]

metals

MDPI

Article

Evaluation of Hardness, Sliding Wear and Strength of a Hypoeutectic White Iron with 25%Cr after Heat Treatments

Alejandro González-Pociño [1,*], Juan Asensio-Lozano [1], Florentino Álvarez-Antolín [1] and Ana García-Diez [2,*]

[1]Materials Pro Group, Departamento de Ciencia de los Materiales e Ingeniería Metalúrgica, Universidad de Oviedo, Independencia 13, 33004 Oviedo, Spain; jasensio@uniovi.es (J.A.-L.); alvarezflorentino@uniovi.es (F.Á.-A.)
[2]Departamento de Ingeniería Naval e Industrial, Escuela Politécnica Superior, Universidad de A Coruña, 15403 Ferrol, Spain
*Correspondence: gonzalezpalejandro@uniovi.es (A.G.-P.); ana.gdiez@udc.es (A.G.-D.)

Citation: González-Pociño, A.; Asensio-Lozano, J.; Álvarez-Antolín, F.; García-Diez, A. Evaluation of Hardness, Sliding Wear and Strength of a Hypoeutectic White Iron with 25%Cr after Heat Treatments. *Metals* **2021**, *11*, x. https://doi.org/10.3390/xxxxx

Academic Editors: Paolo Ferro and Pavel Krakhmalev
Received: 27 April 2021
Accepted: 7 June 2021

Abstract: Hypoeutectic white cast irons with a high chrome content are commonly used in the industrial mining sector where there is a demand for both high resistance to adhesive wear and an acceptable toughness for the absorption of impacts and falls of diverse materials. Through the application of a design of experiment (DoE) technique, factors related to thermal treatment are analyzed with respect to resistance to sliding wear, maximum rupture stress and toughness. The results show that, in order to increase resistance to adhesive wear, it is convenient to use destabilization temperatures of 1050 °C and tempering of two hours at 400 °C. This foments a very hard martensite and a high proportion of highly alloyed retained austenite, which, with low tempering, achieves a precipitation of carbides from this austenite with hardly any loss of hardness of the martensite. In order to increase the energy which this material is capable of absorbing until breakage, furnace cooling set at 150 °C followed by tempering at 550 °C would be favorable. Slower cooling implies a greater quantity of conditioned retained austenite, so that, following this, it may be transformed into lower bainite with a high density of finely dispersed precipitated carbides. Furthermore, this tempering also allows the transformation of martensite into ferrite with finely dispersed carbides.

Keywords: high Cr–Mo white irons; hardness; adhesive wear testing; 3p-bend test; heat treatment; microstructure–properties correlation

1. Introduction

Currently, there are a large number of abrasion-resistant alloys, of which high-chromium Nihard cast irons and Cr–Mo steels are considered materials with excellent resistance to wear [1,2]. Such applications are typical of but not exclusive to the metallurgy and mining industries (waste disposal of by-products, mining excavations, etc.), and they can also be found in coal power plants, management of residues, etc. A few examples of components made of high-Cr cast irons would be jaw crusher liners, mill inner shields, balls for milling, etc. [3–5]. Owing to the very expensive price of nickel as a key alloy element in traditional wear-resistant cast irons such as in Ni-hard abrasive resistance (A.R.) alloys, with the passing of time and the ever-increasing price of Ni, their cost has made them unaffordable.

With the toughness, abrasion and occasional corrosion resistance typically sought in mining applications, it is hard to surpass the high-Cr family of A.R. irons. They are often used as liners for ore processing machine components where the prerequisites are not only limited to wear resistance but also to moderate–low toughness conditions. Components are required to deal with frequent impacts during ore processing, as well as from those grinding and crushing elements which also strike armor-plated components [6,7].

In all these applications, a need is specified for high resistance to abrasive wear. However, behind the term 'abrasive' is often hidden a combination of abrasive and erosive wear, or abrasive and adhesive wear.

When corrosion resistance is added as a prerequisite to wear and toughness, as is the case with slurry impellers and pump cases, white cast irons with higher Cr content must be used. However, in other ferrous alloys, which are alloyed with Cr, it has been confirmed that this resistance to corrosion could also be influenced by the severity of quenching rate [8–11]. Once the mechanical and functional properties are known, the next step will be to focus on how to accomplish those targets at the lowest possible energy and manufacturing costs [12–14].

Other applications require a high resistance to the adhesive wear mechanism, or a combination of both types of wear mechanisms [15,16]. An example of the principal mechanism of adhesive wear would be the equipment used in the cold forming of materials [17]. In this case, apart from high resistance to wear, toughness of the material in service is also required. The steels of tools normally used in these applications are ledeburitic steels [18]. Depending on the wear mechanisms required, these cast irons could be used for similar requirements or in situations which combine mechanisms of both abrasive and adhesive wear, assuming that the toughness is acceptable. An example of this application could be the interior lining of uniaxial presses for the manufacturing of pieces of refractory material. It was found that both a refined microstructure and less interconnected carbides can improve the fracture toughness and wear resistance of high-Cr cast irons [3,19,20].

In the solidification of commercial hypoeutectic high-chromium cast irons, the first phase to nucleate and increase is that of the austenite forming isolated dendrites in the liquid. Further freezing will cause the eutectic liquid to solidify, giving a non-ledeburitic matrix if the Cr content exceeds 15 %-wt. The eutectic matrix consists of austenite as the continuous constituent and M_7C_3 carbides (K_2 carbides), the latter being the dispersed constituent in the eutectic. In the as-cast state, these highly alloyed white irons exhibit a certain toughness level owing to the presence of high percentages of both pro-eutectic and eutectic retained austenite [21]. This highly alloyed austenite phase in the as-cast state is highly supersaturated in carbon and alloy elements, with values in excess of equilibrium solute contents due to non-equilibrium cooling in the foundry cooling yards. As a result, low Ms and Mf values for austenite will be expected, and thus a high-volume fraction of retained austenite present at room temperature (R.T.). It is to be highlighted that the great hardness found in these high alloy white irons due to the contribution of the hardness of eutectic K_2 carbides (1000–1800 HV) is highly significant. These K_2 carbides are much harder than the K_C (M_3C) cementitic carbides (1060–1240 HV) [22].

It is commonly considered that an increase in the weight percent of C in hypoeutectic white irons conveys an increase in the volume fraction of eutectic carbides, which are responsible for an increase in hardness and wear resistance [23–26]. The volume fraction and size of eutectic carbides seem to play a role in the pro-eutectic austenitic grain size while at high temperature, by inhibiting grain growth. This growth constraint on austenite grains is also of interest in the subsequent destabilization heat treatment of austenite which enables secondary carbide formation. The refinement of the microstructure leads to a homogeneity of mechanical properties and an improvement thereof [27–29].

Austenite contains an excess of dissolved carbon with respect to that corresponding to equilibrium which, together with chromium, stabilizes austenite in the as-cast state. The principal objective of a heat treatment applied to the austenite is to destabilize this, by reducing the carbon content through the precipitation of secondary carbides. The precipitation leaves a depleted austenite of excess C and alloy elements in solution, thus raising Ms and Mf temperatures. Therefore, a lower fraction of retained austenite would be expected after destabilization compared to the parent as-cast microstructure [30]. The technical literature indicates that destabilization temperatures vary from 800 °C to 1100 °C, and the usual holding times are between 1 h and 6 h [20,31–35].

Destabilization temperature and time, as well as the cooling rate used after treatment, not only determine the amount of carbide formed, but also its distribution, size and, in some cases, (e.g., for very long holding times) its nature, as well as the relative proportions of martensite to retained austenite [36]. Hardness depends on the amount of martensite and its C content, whereas abrasion resistance depends on the martensite as well as on the fraction and fineness of secondary carbides [37]. When the hardness increases, matrix wear occurs first, and then carbide flakes are formed under alternating stress. The mass loss of the contact surface decreases with increasing hardness for the same sample [15].

Minimizing the amount of retained austenite after treatment and subsequent cooling has been observed to slightly favor impact toughness [38,39]. This is due to the fact that after a destabilization treatment, the austenite is highly alloyed and heavily dislocated by the formation of martensite (α') as the latter induces plastic deformation due to a volume increase in $\gamma \rightarrow \alpha'$, leaving a highly distorted austenite at the γ/α' interface [40].

Wear resistance is closely related, on one hand, to the type, morphology, orientation and properties of secondary carbides, and on the other hand to the matrix type that acts as a binder for these carbides [41]. The type of secondary carbides formed during destabilization treatment depends on composition and destabilization temperature. For instance, the presence of molybdenum in the chemistry of the alloy promotes the formation of other hard carbides in addition to the typical M_7C_3, including $M_{23}C_6$, M_6C and M_2C, depending on the Cr:C ratio [37,42–44]. Some researchers have shown that excellent resistance to abrasive wear of Fe–Cr–C alloys with optimum toughness was obtained when a high- volume fraction of M_7C_3 carbides was achieved within a martensitic matrix [45,46]. This microstructure can be observed in hypoeutectic and with the Cr:C ratio between 5 and 8 [45,47].

Production casting is generally in one of two conditions: (1) as-cast in the austenitic state or (2) heat treated by destabilization with secondary carbides in a matrix which is mostly martensitic with little retained austenite. They can be used directly in either of both states, yet a tempering treatment of martensite is recommended in order to gain toughness as well as to relieve residual stresses from quenching [45,48–50]. Tempering treatment has the additional objective of transforming retained austenite into lower bainite. Usual tempering temperatures for high-Cr white irons vary in the range of 400–600 °C while the tempering time could last between 2 and 6 h [51–53].

The purpose of this work consists of the evaluation of the destabilization treatment, the cooling media and the tempering treatment with the aim of optimizing adhesive wear resistance and hardness. At the same time, the stress and the energy absorbed prior to fracture in a three-

point bend test were maximized. To achieve this aim, a methodology based on statistical methodology, design of experiments (DoE), was used and the correlation of mechanical properties and microstructure established.

2. Materials and Methods

The objective of the present research was to determine the role that selected heat treatment variables applied to a high-chromium as-cast white iron have on evaluated mechanical responses. In order to do this, the research method followed was that of the application of a fractional design of experiments (DoE) with 4 factors and 8 experiments. The basic chemistry of the alloy is presented in Table 1. These alloys are selected when a combination of hardness and resistance to corrosion are sought.

Table 1. Basic chemistry of the experimental high-chromium cast iron (%-wt.).

C	Si	Mn	Cr	Mo	Cr:C
2.7	1.2	0.8	25.1	0.5	9.3

The analyzed factors relate to the destabilization of the austenite, the severity of the cooling media and the tempering treatment as well. In the statistical analysis, two levels were chosen for each factor. Table 2 shows the factors and levels selected for such factors.

Table 2. Factors and levels.

Factors		Levels	
Code	**Heat Treatment Parameters**	**Level –1**	**Level +1**
A	Destabilization temperature (°C) for 5 h	950	1050
B	Cooling media after gamma destabilizing	Air convection within a furnace set @150 °C	Gently stirred in oil at RT
C	Tempering temperature (°C)	400	550
D	Dwell time at tempering temperature (h)	2	6

This DoE is framed in the context of former published work by the authors within a sequential research strategy [54]. The application of a design of experiments statistical technique aims to deliberately modify normal working conditions to produce changes in studied responses, for example, resistance to adhesive wear or the toughness of the material. These deliberate changes are applied to certain productive factors, like, for example, destabilization temperature, means of cooling or the tempering temperature. Table 2 shows the factors considered in this study and the deliberate changes applied to these factors. By planning with a design of experiments, a matrix is generated with the experiments to be carried out.

Often in industrial processes, very few factors are responsible for most of the response variations, with the remaining factors being responsible for variations in the responses of lesser importance, often confused with experimental noise. A complete factorial design of experiments requires a large number of experiments to be performed, and when designed at two levels per factor, the number of experiments is equal to 2^k, where 'k' is the number of factors being analyzed and '2' is the number of levels selected for the variations of each factor. In the present study, 4 factors were studied in eight experiments (Table 2), which is half of the full factorial design. In

this simplification, an information loss is assumed owing to ignoring the interaction of more than two factors, which, in industrial practice, is seldom significant. The effect of a factor is defined as the variation of the response function as a consequence of the variation of said factor. The main effects are defined as those effects on the response function derived from each principal factor taken separately, that is to say, the change in the response when said factor varies from its lowest level, −1, to its highest level, +1. Interactions between 2 factors are defined as the variation between the mean effect of one factor with the other factor at its lowest level, −1, and the mean effect of the same factor with the other factor at the highest level, +1, and then dividing the difference by 2. Similarly, the interactions between three or more factors can be defined. The relevance of the principal effects tends to be higher than the interaction of two factors, and the latter higher than the interaction of three factors, etc. This allows for the simplification of a complete factorial analysis into fractions of this analysis.

Table 3 shows the matrix of experiments generated. The last column in the table labelled as 'Restricted Confounding Patterns' indicates those second order interactions whose effects are confounded with the main effects. The confounding pattern should include all the effects confounded with each other. However, Table 3 shows a restricted confounding pattern in which only the main effects and 2-factor interactions are represented.

Table 3. Matrix of experiments.

No.	A	B	C	D	Restricted Confounding Patterns
1	−1	−1	−1	−1	
2	+1	−1	−1	+1	A
3	−1	+1	−1	+1	B
4	+1	+1	−1	−1	C
5	−1	−1	+1	+1	D
6	+1	−1	+1	−1	AB+CD
7	−1	+1	+1	−1	AC+BD
8	+1	+1	+1	+1	AD+BC

The experimental response is subjected to random variation. This variation follows a normal law, where its standard deviation reflects the experimental error. The effects are linear combinations of the responses, therefore, by application of the central limit theorem, they follow a normal law. It must be taken into account that the linear combination of two normal independent random variables follow a normal law. Each main effect can be considered a random variable where the value obtained is an estimate of its mean μ. If the effects are not significant, they follow a normal law distribution of mean equals zero: N(0, σ), indicating that the sought effects oscillate around zero. From this law of distribution, the associated distribution function can be graphically represented. If this is represented on the scale of a normal probabilistic graph, it appears as a straight line. It appears aligned on a normal probabilistic plot in a representation of the pairs given by the effect and its probability [55]. However, those factors whose representation moves away from the straight line ($\mu \neq 0$) will be considered significant under two possible scenarios. When they appear to the left side of the straight line, its level −1 increases the response function with respect to its level +1. The other possibility for a factor to be significant is that the point moves away from the straight line to its right side and that its level +1 increases the response function with respect to its level −1.

The analyzed responses were:

- Volume fraction of eutectic carbides by quantitative metallography by manual point counting on a total of 30 micrographs at a magnification of 400×.
- Vickers hardness with a load of 30 kgf (~294 N), averaging the results of 12 indentations per experiment.
- Sliding wear resistance evaluated through a reciprocating pin on disk wear test performed according to the ASTM G133-05 standard, with the following characteristics: ball characteristics: WC 4/7%Co, 4 mm diameter, 1550–1780 HV; applied load: 30 N; stroke length: 40 mm; rotating speed: 250 rev·min^{-1} (equivalent to a linear average speed of 20 m·min^{-1}); total distance tested: 10 km.
- Where the mass loss at the end of testing was weighted and registered.
- Three-point flexural bending test with the following characteristics: support span, L = 30 mm; width (w) and thickness (t) of tested beams, 14 mm and 3.5 mm, respectively; center roll diameter for load application and support roll diameters: 10 mm; center roll linear speed: 5 mm·min^{-1}.

The evolution of the material's microstructure following these heat treatments was analyzed by means of optical microscopy (Nikon, Tokyo, Japan) and scanning electron microscopy (JEOL, Nieuw-Vennep, the Netherlands). Grinding was carried out with 60, 120, 240, 400 and 600 grit size SiC paper. Subsequently, the samples were polished in two consecutive stages with 6 μm and 1 μm diamond paste, respectively. Fry was used as the chemical reagent to reveal the microstructure of the material.

3. Results

Figure 1 shows SEM micrographs of the most representative microstructural features for the eight experiments. The higher proportion of retained austenite in experiments 2 and 4 can be appreciated. In addition, the typical needle morphology of the already tempered former martensite phase can be distinguished. This is also found in experiments 1 and 3, though less pronounced. These observations seem to coincide when the highest value of the tempering temperature (550 °C) was applied. Dwell times beyond 2 h do not appear to affect the amount of retained austenite being converted, nor the coarsening of carbides.

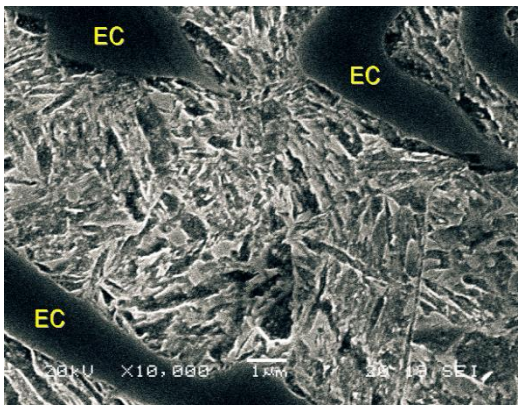

Experiment 1

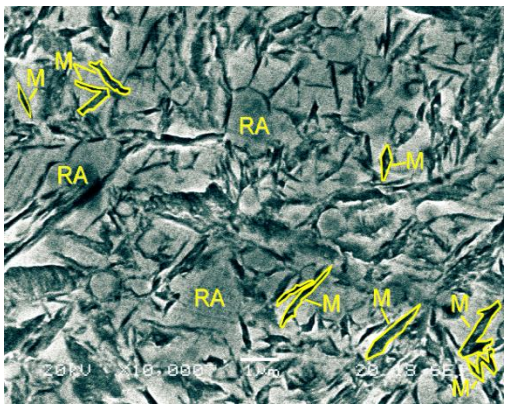

Experiment 2

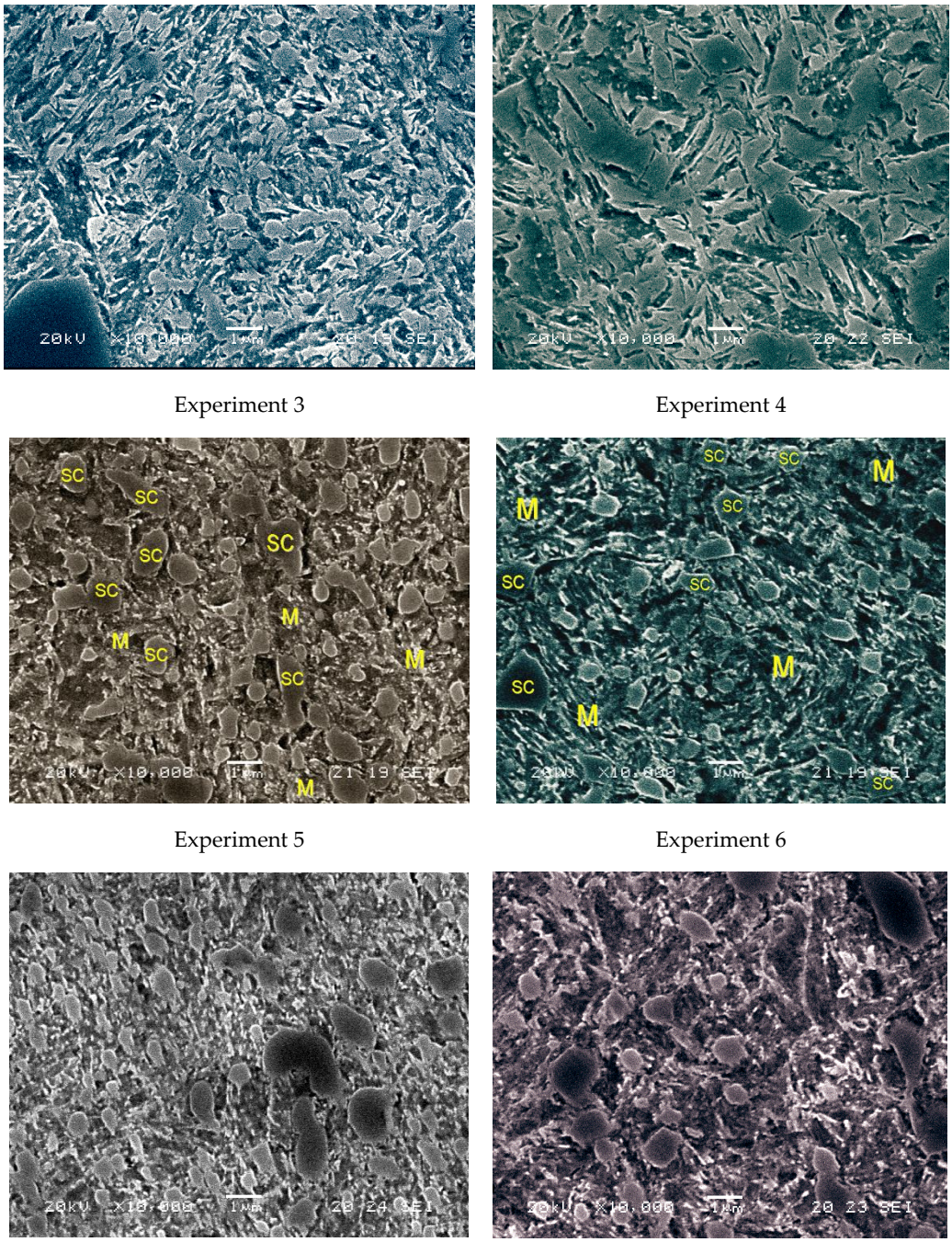

Figure 1. SEI-SEM micrographs illustrating the microstructure of all experiments. The magnification is 10,000×. M: tempered martensite; EC: eutectic carbide; SC: secondary carbide.

Figure 2 shows three secondary electron SEM micrographs depicting the microstructure of precipitated carbides, typical of this highly alloyed white iron. Selected carbides were chosen for EDX semiquantitative analysis, identified with arrows and labeled with the spectrum number, whose composition and most probable carbide type are listed in Table 4.

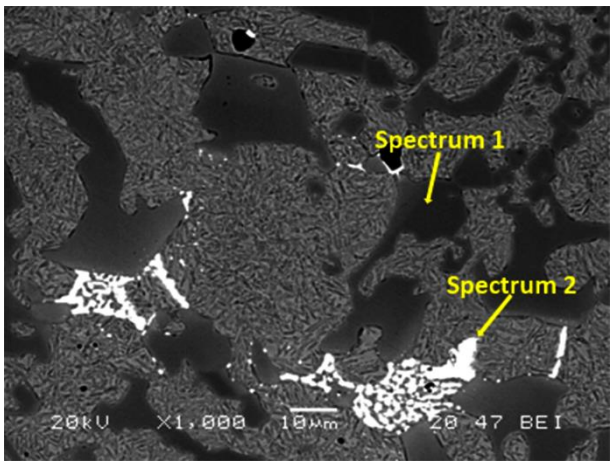

(**a**)

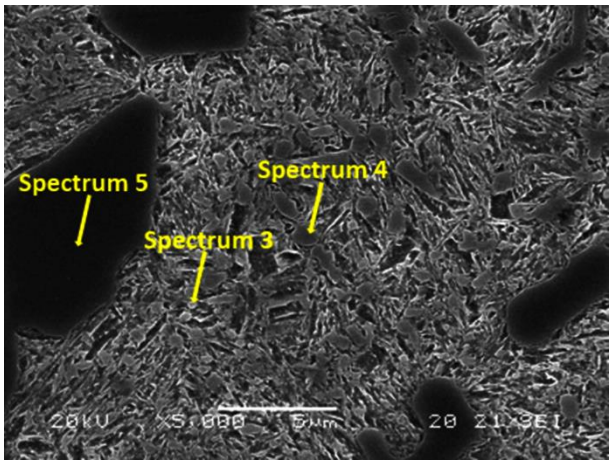

(**b**)

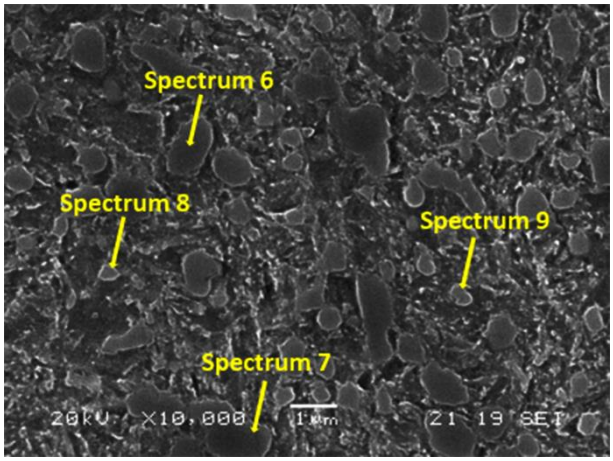

(**c**)

Figure 2. SEM micrographs of increasing magnification, showing the main type and morphology of carbides in selected experiments: (**a**) experiment 2 (1000×) [54]; (**b**) experiment 3 (5000×); and (**c**) experiment 5 (10,000×).

Table 4. Semiquantitative analysis of the carbides indicated with arrows in Figure 2. Semiquantitative compositions determined by EDX microprobe analysis, expressed in atomic percent. The most likely stoichiometry type is shown.

Carbide Spectrum	C	Fe	Cr	Si	Mo	Most Likely Stoichiometry
1	34.27	26.61	39.12	-	-	M_7C_3
2	45.24	23.70	4.88	5.34	20.84	M_2C
3	52.89	38.81	7.01	1.29	-	$M_{23}C_6$
4	62.08	19.71	18.21	-	-	M_7C_3
5	64.56	14.59	20.85	-	-	M_7C_3
6	51.57	32.31	16.12	-	-	M_7C_3
7	52.72	32.11	15.17	-	-	M_7C_3
8	16.12	44.73	5.00	1.29	-	$M_{23}C_6$
9	15.17	35.91	6.29	1.14	-	$M_{23}C_6$

Figure 3 shows the volume fraction of eutectic carbides obtained by manual point counting in a total of 30 micrographs at 400×. The results presented are the average of the experiments after oil quenching and after furnace cooling. A small fraction of the volume of eutectic carbides is confirmed when destabilization is carried out at 950 °C. Given that the destabilization of the austenite begins first at a temperature of 950 °C rather than at 1050 °C, it could be the case that the dwell time (5 hrs) was greater than the time necessary for complete destabilization at 950 °C and lower than the time necessary for complete destabilization at 1050 °C. In this case, a greater density of precipitated secondary carbides would be generated at 950 °C. These carbides could again partially dissolve once the necessary time has passed, until reaching 5 h. This would allow its precipitation through 'coarsening' the eutectic carbides. Figure 3 shows that the volume fraction of eutectic carbides is lower in the as-cast state than after destabilization of the austenite, which justifies the coarsening of the eutectic carbides.

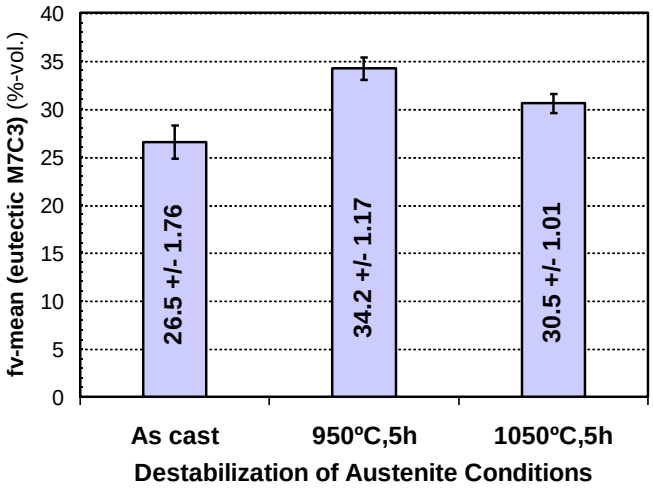

Figure 3. Volume fraction of eutectic carbides after destabilization at the two studied temperatures (%-vol.) and its limit of confidence at 95%.

Table 5 shows the results obtained for hardness and adhesive wear by reciprocating testing and its effects. This relates to the restricted confounding pattern presented in the last column, coinciding with the notation and correspondence indicated in Table 3 for the DoE matrix. Figure 4 shows the representation of those effects represented in normal probability paper, highlighting, in the graph, those with a significant factor in the response function.

It must be pointed out that the WC-Co ball is much harder than the material, so, during the experiment, fracturing of some of the eutectic carbides or detachment of secondary carbides could occur. Thus, some abrasive particles could remain trapped between the two bodies of wear. This could transform an initial wear mechanism of two bodies into another of three bodies during the tests. Therefore, the loss of mass might be due to a combination of factors which are not directly related to the hardness of the material.

Table 5. Average values and effects obtained for Vickers hardness and for the loss of material in a reciprocating sliding wear test against a WC-Co ball.

Experiment No.	Hardness		Mass Loss		Confounding Pattern
	HV30	Effect	mg	Effect	
1	741	668.25	103.1	102.288	Average
2	707	75.5	41.3	−21.025	A
3	746	−42.0	88.9	4.675	B
4	726	−123.5	58.3	58.775	C
5	567	−2.0	195.5	62.075	D
6	742	5.0	59.9	77.675	AB+CD
7	468	102.5	63.7	25.175	AC+BD
8	649	−54.0	207.6	3.275	AD+BC

Figure 4a shows that the principal factors with a significant effect on material hardness are factor A (austenite destabilizing temperature) and factor C (tempering temperature). Additionally, if we aim to increase the hardness, factor A should be placed at its +1 level (1050 °C), and factor C at its −1 level (400 °C). The former could be interpreted as the high destabilizing temperature allowing for high C and Cr in the solution of austenite, leading to high C and hardness of martensite on quenching. Tempering at 400 °C seems insufficient to decompose martensite ($\alpha' \rightarrow \alpha$) [50] and, thus, a high hardness value should be expected.

Table 6 shows the interaction AC+BD. The interaction that produces a greater increase in hardness is A×C, with both factors at −1 level, that is to say, when the austenite destabilizing temperature is 950 °C and tempering treatment is carried out at 400 °C. A possible explanation could be that, at 950 °C, it is possible to reach equilibrium from supersaturated austenite in the as-cast state, since this temperature corresponds approximately to the nose of the C curve for secondary M_7C_3 carbide precipitation [56]. The time chosen of 5 h at the destabilizing of austenite will suffice to complete the precipitation process, after which a depleted austenite in both C and Cr will be left prior to quenching. On quenching, the martensite formation will occur at higher temperatures with the obvious consequence of a higher volume fraction of martensite. The former helps to provide a high hardness in this highly alloyed white iron, despite being a martensite of lower C. Tempering at 400 °C will allow martensite transformation ($\alpha' \rightarrow$ α+carbides), and the formation of these carbides shall contribute to structural hardening of the matrix, and thus to a further increase in the total hardness of the alloy.

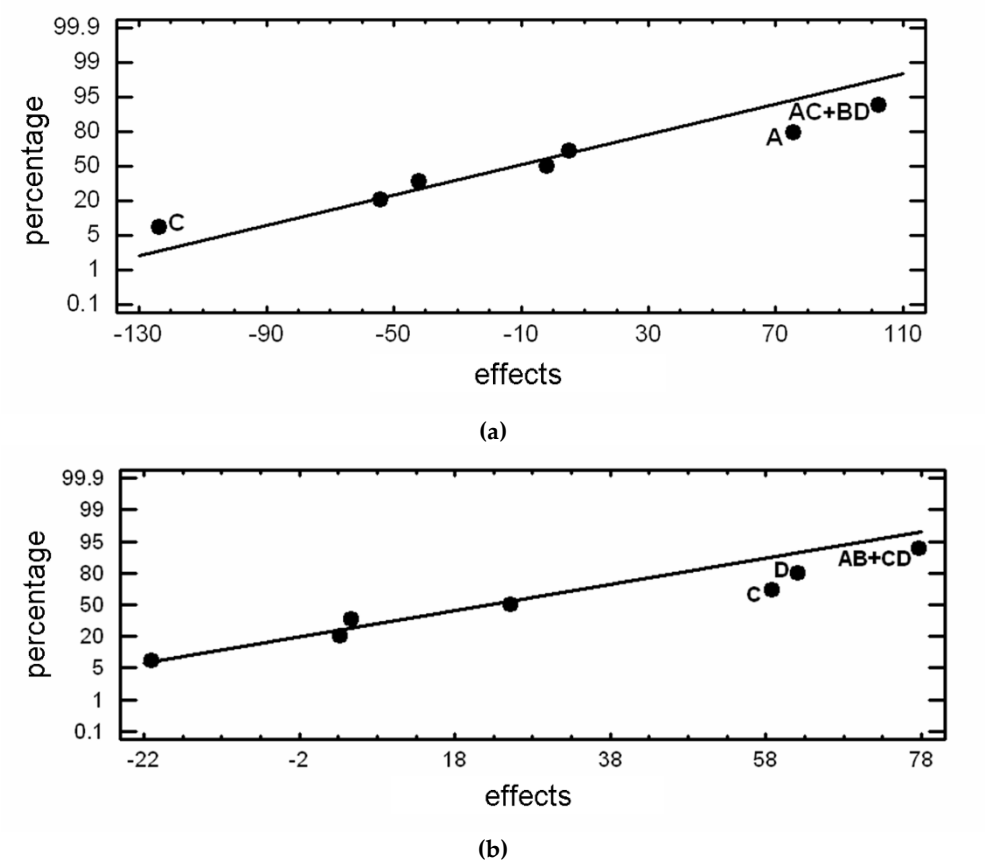

Figure 4. Normal probability plot showing the factors with significant effect on: (**a**) Vickers hardness (HV30), and (**b**) wear resistance measured by the weight loss of high-alloy treated white iron in a sliding test.

Table 6. Effect of the interactions AC and BD for hardness analysis.

A(↓)×C(→)	**−1**	**+1**	**B(↓)×D(→)**	**−1**	**+1**
−1	**743.5**	517.5	**−1**	741.5	637
+1	716.5	695	**+1**	597	697.5

Figure 4b shows the effects of the factors on sliding wear resistance conducted in a reciprocating wear test. Factors C and D appear to have a significant effect on the increase in weight loss (diminution of wear resistance) when both of them are at its +1 level, that is to say, when tempering temperature is at the higher chosen level (550 °C) and the longest tempering time is chosen (6 h). This shows that high temperatures and high tempering times will first result in a complete precipitation of tempering carbides dispersed in a ferrite matrix. Under these conditions, these will coarsen, giving rise to a phenomenon of coalescence among them. All of this implies a reduction in hardness and an increase in the rate of wear of the material. In the same figure, the interaction given by AC+BD also has a significant effect on the response function when they both operate at their +1 level. The analysis of this interaction is provided in Table 7. They both appeared under identical conditions as individual factors, but here, it may be seen that when both factors operate at their +1 level simultaneously, there is a synergistic role whereby an increase in the wear rate is achieved. Conversely, adhesive wear resistance will be maximized with parameters related to tempering: 400 °C and 2 h.

Table 7. Effect of the interactions AB and CD on the increase in weight loss evaluated by means of an adhesive wear test.

A(↓)×B(→)	**−1**	**+1**	**C(↓)×D(→)**	**−1**	**+1**
−1	149.3	76.3	**−1**	80.7	65.1
+1	50.6	133	**+1**	61.8	**201.6**

Table 8 shows the results obtained from a three-point bend test, together with the restricted confounding pattern, previously stated in the DoE matrix. The selected responses for the present test were the maximum flexural strength or fracture strength, and the total area under the load–deflection curve, which represents the total work that the material is capable of absorbing prior to fracture. Figure 5 shows the representation of the significant effects in a normal probability paper.

Table 8. Mean values and effects obtained for maximum flexural strength and the energy absorbed to fracture.

No.	**Maximum Flexural Strength (σ_{max})**		**Absorbed Energy to Fracture (W)**		**Confounding Pattern**
	MPa	**Effect**	**mJ**	**Effect**	
1	945.9	1054.05	489.85	670.433	Average
2	1286.1	−7.4	780.86	15.99	A
3	1114.4	−238.9	749.11	−115.465	B
4	602.6	133.6	352.92	154.495	C
5	1117.7	135.2	629.85	22.96	D
6	1344.3	−290.8	1012.1	−320.64	AB+CD
7	1053	78.4	780.94	68.58	AC+BD
8	968.4	18.6	567.83	−31.125	AD+BC

Figure 5a shows the factors with a significant effect on the increase in flexural strength. It should be noted that all test specimens broke in the elastic domain as it corresponds to a brittle material. In this analysis, it is concluded that factor B (quenching medium) significantly increases the maximum flexural strength at break for its −1 level (cooling from austenitizing temperature in a furnace set at 150 °C). The former suggests that a low-severity medium in quenching helps to minimize the volume fraction of brittle martensite, thus increasing the amount of retained austenite. This austenite will provide a favorable toughness behavior to the matrix, due to the stress relief treatment that such slow cooling represents with regard to the plastic deformation induced by martensite formation.

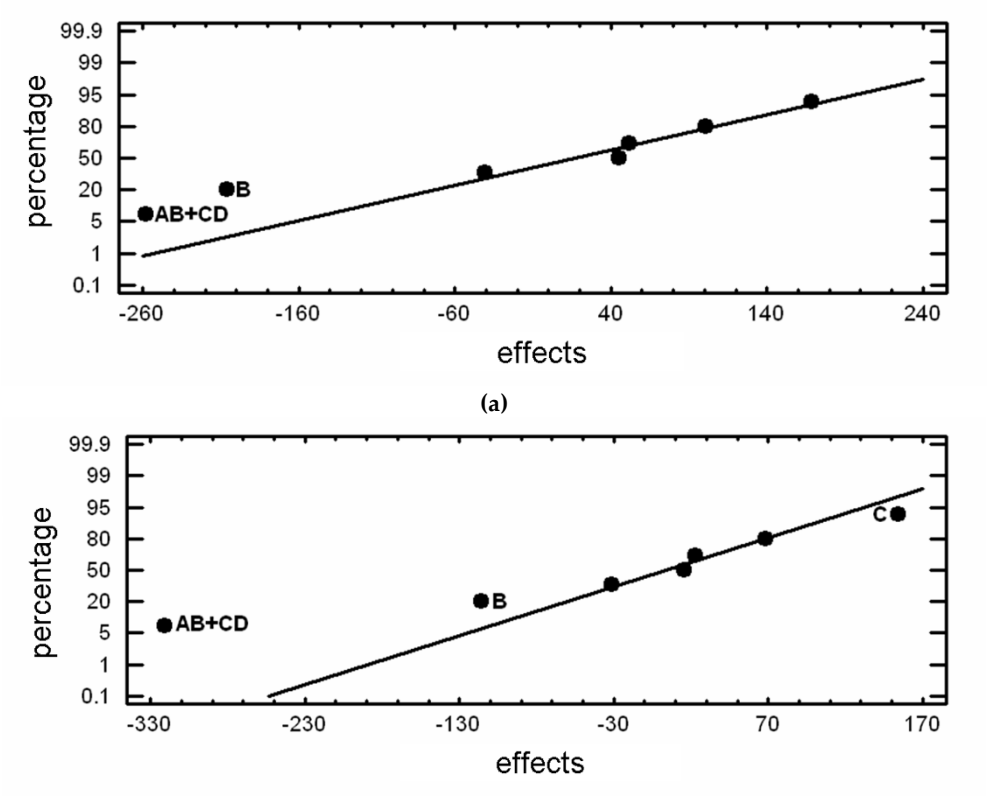

Figure 5. Normal probability plot showing the factors with significant effect on: (**a**) flexural strength to failure (MPa) and (**b**) absorbed energy to fracture (mJ).

The analysis of the interactions A×B+C×D is shown in Table 9, and it can be observed that the highest effect corresponds to factor A at its +1 level (1050 °C for the destabilization temperature), while factor B is at its −1 level (cooling in a furnace set at 150 °C). The novelty here is the role played by factor A, since factor B was seen to be individually significant at the same level. The result seems congruent with higher destabilization temperatures, as a temperature increase during destabilization favors an increase in C in the solution of austenite. Thus, a lower MS temperature will be expected and a higher fraction of residual austenite at RT available. The selected AB interaction has a stronger effect on the increase in flexural strength at fracture than factor A individually, thus suggesting a synergic effect of both factors.

Table 9. Effect of the interactions AB and CD in the analysis of fracture strength at failure in a 3-point bend testing.

A(↓)×B(→)	**−1**	**+1**	**C(↓)×D(→)**	**−1**	**+1**
−1	1031.8	1083.7	**−1**	774.3	1200.3
+1	**1315.2**	785.5	**+1**	1198.7	1043.1

Figure 5b shows the principal factors (B and C) and the interaction (AB + CD) with a significant effect on increasing the response function, i.e., the energy absorbed prior to fracture in a three-point bend test. The principal factors with significant effects are B at its −1 level (cooling in an air convection furnace set at 150 °C), and C at its +1 level (tempering temperature of 550 °C). The interpretation of these results could be as follows: slow cooling rates on quenching following the destabilization process serve to homogenize austenite and thus to considerably reduce the martensitic transformation since martensite nucleates at heterogeneities in austenite. As a result, the volume of stress-relieved austenite at RT would be higher and thus the matrix ductility will be increased.

By means of a high tempering temperature, it is possible to further increase ductility and toughness because brittle martensite (α') will transform into tough ferrite (α) plus alloy carbides. Since alloy carbides do not coarsen easily and tend to remain fine, ductility is not compromised. The austenite, devoid of carbon and alloy elements, is found in favorable conditions for its transformation during this tempering in inferior bainite. This phase contributes to a greater increase in ductility for the matrix than for the martensite.

The interactions A×B and C×D are analyzed in Table 10. It can be seen that the most significant interaction for A×B is obtained with factor A at its +1 level (1050 °C for the destabilization temperature) and with factor B at its −1 level (cooling in a furnace set at 150 °C). Apart from the effect of the low cooling rate on quenching, which was previously discussed, a high destabilization temperature increases the amount of C in austenite, the M_S temperature diminishes and the volume fraction of austenite increases. Considering the effect of a higher fraction of retained austenite with high C and alloy elements at RT, prior to its transformation on tempering, the main difference will be favorable for toughness since a very small amount of martensite will form. The austenite will probably remain as 'conditioned' austenite, and, because of the higher alloy content, it will develop very finely precipitated high-temperature alloy carbides. At higher temperatures, there is a higher chance for SC dissolution, especially of those that have just reached their critical radius. The combination of both factors in this AB interaction considerably increases the energy absorbed to fracture in a three-point bend test.

Table 10. Analysis of the interactions AB and CD towards an increase in the energy absorbed to fracture.

A(↓)×B(→)	**−1**	**+1**	**C(↓)×D(→)**	**−1**	**+1**
−1	559.9	765	**−1**	421.4	764.9
+1	**896.5**	460.4	**+1**	895.5	598.8

4. Conclusions

With regard to the hardness and the resistance to adhesive wear in a reciprocating wear test, the following could be found:

1. Vickers hardness increases when destabilization of austenite takes place at 1050 °C and tempering is conducted at 400 °C. High destabilization temperatures yield a high-C austenite and, on further quenching, provide hard martensite and a high fraction of retained austenite. Low tempering temperature is insufficient to decompose the hard martensite but allows structural strengthening by alloy carbide precipitation from residual austenite.
2. For improved adhesive wear resistance, tempering treatment parameters are critical, the best results being obtained at 400 °C and 2 h. The technical literature underlines the relevance of a high fraction and fineness of secondary carbides from destabilization. Low temperature and short tempering times impede secondary carbide coarsening. Such tempering conditions are also favorable for increased wear resistance of the matrix due to minimal conversion of martensite ($\alpha'\rightarrow\alpha$) and possible conditioning of retained austenite giving alloy carbides from tempering.

With regard to the three-point bending test conducted, the following conclusions can be drawn:

1. Maximum flexural strength could be obtained with high destabilization temperatures (1050 °C) and slow quenching rates (samples introduced in an air convection furnace set at 150 °C). These conditions are favorable for maximizing the volume fraction of ductile retained austenite which allows the deflection required for the high strengths registered.

2. The energy absorbed to fracture in bending, measured as the total area below the force–displacement curve in a bend test curve, is a valuable source of information of combined strength and ductility. It has been seen that this energy could be enhanced by slow cooling quenching (an air convection furnace set at 150 °C) followed by a tempering treatment at 550 °C. The novelty here is that high-temperature tempering favors: (a) total conversion of martensite ($\alpha' \rightarrow \alpha$ + alloy carbides), (b) conditioning of austenite (γ rich in C and alloy elements) → alloy carbides + depleted-γ); and (c) the possibility of transformation of depleted austenite (depleted-γ → lower bainite). In summary, this provides a ductile matrix.

Author Contributions: J.A.-L. conceived and designed the investigation; A.G.-P. and A.G.-D. performed all laboratory work; F.A.-A. led the investigation, analyzed the data and wrote the paper. All authors have read and agreed to the published version of the manuscript.

Funding: This research received no external funding.

Acknowledgments: We want to thank to José María Lobo-Manrique, a master's student in his second year, for his valuable assistance in the execution of the wear testing while compatibilizing these experiments with his master's thesis experimental work.

Conflicts of Interest: The authors declare no conflict of interest.

References

1. Zeytin, H.K.; Yildirim, H.; Berme, B.; Duduoĝlu, S.; Kazdal, G.; Deniz, A. Effect of boron and heat treatment on mechanical properties of white cast iron for mining application. *J. Iron Steel Res. Int.* **2011**, *18*, 31–39, doi:10.1016/S1006-706X(11)60114-3.
2. Fu, H.; Xiao, Q.; Fu, H. Heat treatment of multi-element low alloy wear-resistant steel. *Mater. Sci. Eng. A* **2005**, *396*, 206–212, doi:10.1016/j.msea.2005.01.023.
3. Gasan, H.; Erturk, F. Effects of a Destabilization Heat Treatment on the Microstructure and Abrasive Wear Behavior of High-Chromium White Cast Iron Investigated Using Different Characterization Techniques. *Metall. Mater. Trans. A* **2013**, *44*, 4993–5005, doi:10.1007/s11661-013-1851-3.
4. Wieczerzak, K.; Bała, P.; Stępień, M.; Cios, G.; KozieŁ, T. The characterization of cast Fe-Cr-C alloy. *Arch Metall. Mater.* **2015**, *60*, 779–782, doi:10.1515/amm-2015-0206.
5. Jia, X.; Huang, Y.; Zuo, X.; Liu, Y.; Chen, N.; Rong, Y. High hardness-toughness and wear resistance of white cast iron treated by a multicycle quenching-partitioning-tempering process. *Heat Treat Surf. Eng.* **2019**, *1*, 57–62, doi:10.1080/25787616.2018.1560148.
6. Lindroos, M.; Apostol, M.; Heino, V.; Valtonen, K.; Laukkanen, A.; Holmberg, K.; Kuokkala, V.T. The deformation, strain hardening, and wear behavior of chromium-alloyed hadfield steel in abrasive and impact conditions. *Tribol. Lett.* **2015**, *57*, 1–11, doi:10.1007/s11249-015-0477-6.
7. Lindroos, M.; Ratia, V.; Apostol, M.; Valtonen, K.; Laukkanen, A.; Molnar, W.; Holmberg, K.; Kuokkala, V.T. The effect of impact conditions on the wear and deformation behavior of wear resistant steels. *Wear* **2015**, *328–329*, 197–205, doi:10.1016/j.wear.2015.02.032.
8. Uygura, I.; Gerengib, H.; Arslanc, Y.; Kurtayb, M. The Effects of Cryogenic Treatment on the Corrosion of AISI D3 Steel. *Mater. Res.* **2015**, *18*, 569–574, doi:10.1590/1516-1439.349914.
9. Amini, K.; Akhbarizadeh, A.; Javadpour, S. Effect of Carbide Distribution on Corrosion Behavior of the Deep Cryogenically Treated 1.2080 Steel. *J. Mater. Eng. Perform.* **2016**, *25*, 365–373, doi:10.1007/s11665-015-1858-6.
10. Hill, H.; Huth, S.; Weber, S.; Theisen, W. Corrosion properties of a plastic mould steel with special focus on the processing route. *Werkst. Korros.* **2011**, *62*, 436–443, doi:10.1002/maco.200905570.
11. Hudakova, M.; Bartkowska, A.; Jurci, P. The effect of conventional heat treatment and sub-zero treatment in liquid nitrogen on corrosion resistance of vanadis 6 steel. In Proceedings of the 28th International Conference on Metallurgy and Materials 2019, Brno, Czech Republic, 22 May 2019; pp. 867–873.
12. Qu, Y.; Xing, J.; Zhi, X.; Peng, J.; Fu, H. Effect of cerium on the as-cast microstructure of a hypereutectic high chromium cast iron. *Mater. Lett.* **2008**, *62*, 3024–3027, doi:10.1016/j.matlet.2008.01.129.
13. Wang, J.; Xiong, J.; Fan, H.; Yang, H.S.; Liu, H.H.; Shen, B.L. Effects of high temperature and cryogenic

treatment on the microstructure and abrasion resistance of a high chromium cast iron. *J. Mater. Process Technol.* **2009**, *209*, 3236–3240, doi:10.1016/j.jmatprotec.2008.07.035.
14. Ding, H.; Liu, S.; Zhang, H.; Guo, J. Improving impact toughness of a high chromium cast iron regarding joint additive of nitrogen and titanium. *Mater. Des.* **2016**, *90*, 958–968, doi:10.1016/j.matdes.2015.11.055.
15. Guo, Z.H.; Xiao, F.R.; Lu, S.L.; Liu, R.L.; Liao, B. Effects of heat treatment and counterface on the wear behaviour of Cr21 cast iron. *Ironmak. Steelmak.* **2018**, *45*, 257–263, doi:10.1080/03019233.2016.1259870.
16. Zheng, B.C.; Xing, J.D.; Liu, Y.Z.; Li, W. Two-Body Abrasion Behaviors Characterization of White Cast Iron with Various Chromium Concentrations. *Tribol. Trans.* **2020**, *63*, 519–527, doi:10.1080/10402004.2020.1725204.
17. Groche, P.; Moeller, N.; Hoffmann, H.; Suh, J. Influence of gliding speed and contact pressure on the wear of forming tools. *Wear* **2011**, *271*, 2570–2578, doi:10.1016/j.wear.2010.12.076.
18. Jurci, P. Cr-V Ledeburitic cold-work tool steels. *Mater. Tehnol.* **2011**, *45*, 383–394.
19. Gao, X.J.; Jiang, Z.Y.; Wei, D.B.; Kosasih, B. Effect of thermomechanical treatment on sliding wear of high-Cr cast iron with large plastic deformation. *Tribol. Int.* **2015**, *92*, 117–125, doi:10.1016/j.triboint.2015.06.002.
20. Efremenko, V.; Shimizu, K.; Chabak, Y. Effect of Destabilizing Heat Treatment on Solid-State Phase Transformation in High-Chromium Cast Irons. *Metall. Mater. Trans.* **2013**, *44*, 5434–5446, doi:10.1007/s11661-013-1890-9.
21. Kishore, K.; Kumar, U.; Dinesh, N.; Adhikary, M. Effect of Soaking Temperature on Carbide Precipitation, Hardness, and Wear Resistance of High-Chromium Cast Iron. *J. Fail. Anal. Prev*. **2020**, *20*, 249–260, doi:10.1007/s11668-020-00836-7.
22. Pero-Sanz, J.A.; Plaza, D.; Verdeja, J.I.; Asensio, J. Metallographic Characterization of Hypoeutectic Martensitic White Cast Irons: Fe-C-Cr System Experimental procedure and results composition and microstructural development. *Mater. Charact.* **1999**, *43*, 33–39.
23. Mandal, S.S.; Ghosh, K.S.; Mondal, D.K. Correlation between microstructure, hardness, wear and electrochemical behaviour in 8.0%, 16.0% and 20.0% (by wt) chromium white irons. *Mater. Chem. Phys.* **2017**, *193*, 401–412, doi:10.1016/j.matchemphys.2017.02.041.
24. Wiengmoon, A.; Pearce, J.T.H.; Chairuangsri, T. Relationship between microstructure, hardness and corrosion resistance in 20 wt.%Cr, 27 wt.%Cr and 36 wt.%Cr high chromium cast irons. *Mater. Chem. Phys.* **2011**, *125*, 739–748, doi:10.1016/j.matchemphys.2010.09.064.
25. Zumelzu, E.; Goyos, I.; Cabezas, C.; Opitz, O.; Parada, A. Wear and corrosion behaviour of high-chromium (14–30% Cr) cast iron alloys. *J Mater Process Technol* **2002**, *128*, 250–255, doi:10.1016/S0924-0136(02)00458-2.
26. Tang, X.H.; Chung, R.; Li, D.Y.; Hinckley, B.; Dolman, K. Variations in microstructure of high chromium cast irons and resultant changes in resistance to wear, corrosion and corrosive wear. *Wear* **2009**, *267*, 116–121, doi:10.1016/j.wear.2008.11.025.
27. Pawlak, K.; Białobrzeska, B.; Konat, Ł. The influence of austenitizing temperature on prior austenite grain size and resistance to abrasion wear of selected low-alloy boron steel. *Arch. Civ. Mech. Eng.* **2016**, *16*, 913–926, doi:10.1016/j.acme.2016.07.003.
28. Wang, C.C.; Shen, C.G.; Zhang, Z.; Xu, W. Simulation and verification of core–shell MC carbide design in Fe–C–Ni–V–Ti steel. *J. Iron Steel Res. Int.* **2021**, *28*, 58–65, doi:10.1007/s42243-020-00451-8.
29. Karantzalis, A.E.; Lekatou, A.; Mavros, H. Microstructural Modifications of As-Cast High-Chromium White Iron by Heat Treatment. *J. Mater. Eng. Perform* **2009**, *18*, 174–181, doi:10.1007/s11665-008-9285-6.
30. Bedolla-Jacuinde, A.; Arias, L.; Hernández, B. Kinetics of secondary carbides precipitation in a hiqh-chromium white iron. *J. Mater. Eng. Perform* **2003**, *12*, 371–382, doi:10.1361/105994903770342881.
31. Çöl, M.; Koç, F.G.; Öktem, H.; Kir, D. The role of boron content in high alloy white cast iron (Ni-Hard 4) on microstructure, mechanical properties and wear resistance. *Wear* **2016**, *348–349*, 158–165, doi:10.1016/j.wear.2015.12.007.
32. Gelfi, M.; Pola, A.; Girelli, L.; Zacco, A.; Masotti, M.; La Vecchia, G.M. Effect of heat treatment on microstructure and erosion resistance of white cast irons for slurry pumping applications. *Wear* **2019**, *428–429*, 438–448, doi:10.1016/j.wear.2019.03.011.
33. Guitar, M.A.; Nayak, U.P.; Britz, D.; Mücklich, F. The effect of thermal processing and chemical composition on secondary carbide precipitation and hardness in high-chromium cast irons. *Int. J. Metalcast.* **2020**, *14*, 755–465, doi:10.1007/s40962-020-00407-4.
34. Karantzalis, A.E.; Lekatou, A.; Diavati, E. Effect of Destabilization Heat Treatments on the Microstructure of High-Chromium Cast Iron: A Microscopy Examination Approach. *J. Mater. Eng. Perform*. **2009**, *18*, 1078–1085, doi:10.1007/s11665-009-9353-6.
35. Powell, G.L.F.; Laird, G. Structure, nucleation, growth and morphology of secondary carbides in high

chromium and Cr-Ni white cast irons. *J. Mater. Sci.* **1992**, *27*, 29–35.
36. Yang, J.R.; Tsai, M.C.; Du, J.S.; Chiou, C.S. Phase transformations in AISI 410 stainless steel. *Jpn. Inst. Met. Proc.* **1999**, *332*, 1605–1608.
37. Kusumoto, K.; Shimizu, K.; Yaer, X.; Zhang, Y.; Ota, Y.; Ito, J. Abrasive wear characteristics of Fe-2C-5Cr-5Mo-5W-5Nb multi-component white cast iron. *Wear* **2017**, *376–377*, 22–29, doi:10.1016/j.wear.2017.01.096.
38. Wang, M.Q.; Dong, H.; Hui, W.J.; Shi, J. Effect of heat treatment on microstructure and mechanical properties of Cr-Ni-Mo-Nb steel. *Mater. Sci. Technol.* **2007**, *23*, 963–969, doi:10.1179/174328407X192796.
39. Morito, S.; Saito, H.; Maki, T.; Furuhara, T. Effect of PAGS on crystallography and morphology of lath martensite in low carbon steels. *ISIJ Int.* **2004**, *45*, 91–94.
40. Shaeri, M.H.; Saghafian, H.; Shabestari, S.G. Effect of heat treatment on microstructure and mechanical properties of Cr-Mo steels (FMU-226) used in mills liner. *Mater. Des.* **2012**, *34*, 192–200, doi:10.1016/j.matdes.2011.07.042.
41. Coronado, J.J. Effect of load and carbide orientation on abrasive wear resistance of white cast iron. *Wear* **2011**, *270*, 823–827, doi:10.1016/j.wear.2011.02.009.
42. Tabrett, C.P.; Sare, I.R.; Ghomashchi, M.R. Microstructure-property relationships in high chromium white iron alloys. *Int. Mater. Rev.* **2014**, *41*, 59–82, doi:10.1179/imr.1996.41.2.59.
43. Imurai, S.; Thanachayanont, C.; Pearce, J.T.H.; Tsuda, K.; Chairuangsri, T. Effects of Mo on microstructure of as-cast 28 wt.% Cr-2.6 wt.% C-(0-10) wt.% Mo irons. *Mater. Charact.* **2014**, *90*, 99–112, doi:10.1016/j.matchar.2014.01.014.
44. Wieczerzak, K.; Bala, P.; Dziurka, R.; Tokarski, T.; Cios, G.; Koziel, T.; Gondek, L. The effect of temperature on the evolution of eutectic carbides and M7C3 → M23C6carbides reaction in the rapidly solidified Fe-Cr-C alloy. *J. Alloys. Compd.* **2017**, *698*, 673–684, doi:10.1016/j.jallcom.2016.12.252.
45. Karantzalis, E.; Lekatou, A.; Mavros, H. Microstructure and properties of high chromium cast irons: Effect of heat treatments and alloying additions. *Int. J. Cast. Met. Res.* **2009**, *22*, 448–456, doi:10.1179/174313309X436637.
46. Sabet, H.; Khierandish, S.; Mirdamadi, S.; Goodarzi, M. The microstructure and abrasive wear resistance of Fe-Cr-C hardfacing alloys with the composition of hypoeutectic, eutectic, and hypereutectic at Cr/C 6. *Tribol. Lett.* **2011**, *44*, 237–245, doi:10.1007/s11249-011-9842-2.
47. Taşgin, Y.; Kaplan, M.; Yaz, M. Investigation of effects of boron additives and heat treatment on carbides and phase transition of highly alloyed duplex cast iron. *Mater. Des.* **2009**, *30*, 3174–3179, doi:10.1016/j.matdes.2008.11.015.
48. Filipovic, M.; Kamberovic, Z.; Korac, M.; Gavrilovski, M. Microstructure and mechanical properties of Fe-Cr-C-Nb white cast irons. *Mater. Des.* **2013**, *47*, 41–48, doi:10.1016/j.matdes.2012.12.034.
49. Li, D.; Liu, L.; Zhang, Y.; Ye, C.; Ren, X.; Yang, Y.; Yang, Q. Phase diagram calculation of high chromium cast irons and influence of its chemical composition. *Mater. Des.* **2009**, *30*, 340–345, doi:10.1016/j.matdes.2008.04.061.
50. Kim, C.K.; Lee, S.; Jung, J.Y. Effects of heat treatment on wear resistance and fracture toughness of duo-cast materials composed of high-chromium white cast iron and low-chromium steel. *Metall. Mater. Trans. A Phys. Metall. Mater. Sci.* **2006**, *37*, 633–643, doi:10.1007/s11661-006-0035-9.
51. Doğan, Ö.N.; Hawk, J.A.; Laird, G. Solidification structure and abrasion resistance of high chromium white irons. *Metall. Mater. Trans. A Phys. Metall. Mater. Sci.* **1997**, *28*, 1315–1328, doi:10.1007/s11661-997-0267-3.
52. Carpenter, S.D.; Carpenter, D.; Pearce, J.T.H. XRD and electron microscope study of a heat treated 26.6% chromium white iron microstructure. *Mater. Chem. Phys.* **2007**, *101*, 49–55, doi:10.1016/j.matchemphys.2006.02.013.
53. Lai, J.P.; Pan, Q.L.; Wang, Z.B.; Cui, H.R.; Wang, X.D.; Gao, Z.Z. Effects of Destabilization Temperature on the Microstructure and Mechanical Properties of High Chromium Cast Iron. *J. Mater. Eng. Perform.* **2017**, *26*, 4667–4675, doi:10.1007/s11665-017-2943-9.
54. González-Pociño, A.; Asensio-Lozano, J.; Álvarez-Antolín, F.; García-Diez, A. Improvement of impact toughness and abrasion resistance of a 3C-25Cr-0.5Mo alloy using a design of experiment statistical technique: Microstructural correlations after heat treatments. *Metals* **2021**, *11*, 595, doi:10.3390/met11040595.
55. Prat-Bartés, A.; Tort-Martorell, X.; Grima-Cintas, P.; Pozueta-Fernández, L.; Solé-Vidal, I. *Métodos Estadísticos*, 2nd ed.; UPC: Barcelona, Spain, 2004; p. 376.
56. Maratray, F.; Usseglio-Nanot, R. *Transformation Characteristics of Cr and Cr-Mo White Irons*; Climax Molybdenum S.A.: Paris, France, 1969; p. 150.

4. CONCLUSIONES

4.1- Generales

1. Se ha constatado que en estas fundiciones se produce solidificación de inequilibrio, dando como resultado una mayor proporción de carburos eutécticos K_2, respecto a la teórica solidificación de equilibrio. Cuanto mayor sea la temperatura de desestabilización, mayor es la proporción de eutéctica de no equilibrio disuelta. Esto da como resultado la competición de tres cinéticas a esta temperatura. Por un lado, la redisolución de carburos eutécticos de inequilibrio, por otro lado, el enriquecimiento de la austenita en elementos de aleación y, por último, la precipitación de carburos secundarios de desestabilización.

2. Las bajas velocidades de enfriamiento pueden compensar esta disolución de carburos a través de la precipitación adicional de carburos secundarios en el rango de temperatura de 600-400°C.

3. En el revenido se pueden diferenciar tres aspectos diferentes:

    a. El revenido de la martensita comienza a bajas temperaturas del orden de 200°C, precipitando carburos cuasi-cementíticos.
    b. A pesar de la gran afinidad del Cr por el C, los carburos M_7C_3 no llegan a formarse hasta temperaturas del rango de 500°C o superiores. Estos átomos de Cr sustituyen al Fe en la red cristalina y, por tanto, su difusión es más lenta que la de los átomos de C, que están en solución sólida de inserción. En el rango de 500°C la ferrita con el Cr en solución sólida de sustitución tiene poca cantidad de C puesto que ha precipitado como Fe_3C. Por tanto, para precipitar carburos M_7C_3 de revenido, se requiere de una redisolución previa de la cementita para luego precipitar los carburos mixtos de Cr por nucleación y crecimiento que, siendo finos y homogéneamente dispersos en la matriz, provocan un aumento de la dureza. Se ha constatado que una temperatura de revenido a 500°C aumenta la dureza del material. A mayores temperaturas de revenido, se acelera el proceso, pero se produce el engrosamiento de estos precipitados, pudiendo llegar a producirse la coalescencia de los mismos que, sumada a la pérdida total de la tetragonalidad de la martensita, produce un decaimiento de la dureza.
    c. La desestabilización de la austenita retenida, a las temperaturas de revenido, tiene dos fases. Una primera que consiste en acomodar la austenita, provocando una segunda desestabilización y la disminución de la densidad de dislocaciones en la interfase austenita-martensita, provocadas por el cambio brusco de volumen que implica la transformación en martensita, tanto mayor cuanto más distorsionada sea la martensita generada tras el temple. La segunda fase consiste en que la austenita ya acomodada es susceptible de transformarse en martensita o en bainita inferior.

4. El espesor de la capa nitrurada es mucho menor en las fundiciones de 25%Cr respecto a las de 18% Cr, no llegando a 20 micras en ninguno de los experimentos realizados. Se han detectado la formación de nitruros muy finos del tipo CrN y Fe_4N.

5. Se constata que microestructuras que favorezcan un incremento de la tenacidad favorecen la resistencia al desgaste erosivo. Sin embargo, para aumentar la resistencia al desgaste abrasivo convienen microestructuras que, al contrario, eleven la dureza de la fase matriz. En ambos tipos de desgastes la presencia de carburos secundarios aumenta la resistencia al desgaste.

6. Como se ha explicado anteriormente, la tetragonalidad de la martensita y, en consecuencia, la dureza de esta fase se consigue en ambas aleaciones a elevadas temperaturas de austenización. La diferencia que se ha constatado entre ambas es que en la fundición con 18%Cr queda un mayor porcentaje de austenita retenida que en la fundición de 25%Cr. Esto se debe a que la fundición de 18%Cr, al presentar un mayor contenido en C y Mo, presenta una temperatura Ms más baja.

7. Para contenidos de 25%Cr se recomienda aumentar la temperatura de austenización para obtener una martensita de elevada dureza con poca austenita residual, que posteriormente se eliminará junto con una precipitación homogénea y dispersa de precipitados secundarios durante el revenido. Si durante el revenido no se logra la pérdida completa de tetragonalidad de la martensita revenida, la resistencia al desgaste abrasivo se ve incrementada.

8. Sin embargo, dada la tendencia a formarse una mayor cantidad de austenita retenida en las fundiciones con 18% Cr es preferible conseguir una completa desestabilización de la austenita a 1000°C, para minimizar al máximo la presencia de austenita retenida.

4.2- Fundición Blanca 18%Cr

Se constata que la resistencia al desgaste por erosión depende principalmente de la fracción de volumen de los carburos secundarios precipitados durante la desestabilización de la austenita. A su vez, resulta que:

1. La severidad del medio de enfriamiento no influye de manera significativa en la dureza del material.

2. La temperatura de desestabilización juega un papel fundamental para disminuir la cantidad de austenita retenida y, por tanto, favorecer la transformación martensítica. Para ello, se requieren temperaturas de desestabilización de 1000°C en lugar de 1100°C, puesto que el inicio de la precipitación de carburos durante la desestabilización se encuentra lo más cercana al origen de tiempos a la temperatura aproximada de 1000°C.

3. La dureza del material se ve incrementada con temperaturas de desestabilización a 1100°C respecto a la que se consigue a 1000°C. Esto es debido a una mayor cantidad de martensita como constituyente matriz.

4. La nitruración aumenta la dureza en la superficie del material, pero ello no supone un aumento significativo de la resistencia al desgaste erosivo.

5. Las altas temperaturas de revenido consiguen la desestabilización de la austenita retenida y favorecen su transformación en martensita y/o bainita inferior.

6. Los tiempos de revenido prolongados (6h), aumentan la resistencia al desgaste erosivo. Esto se debe a que una mayor precipitación de carburos mixtos de Cr durante el revenido retrasa el deterioro del constituyente de la matriz, los cuales actúan complementariamente a los carburos secundarios previamente precipitados durante la desestabilización. Además de esto, se genera una matriz con mayor tenacidad, resultando una mejor propiedad ante un desgaste erosivo por impactos con partículas de corindón.

7. El desgaste erosivo comienza en el constituyente de la matriz sin afectar inicialmente a los carburos eutécticos. Una vez que se produce el deterioro del constituyente de la matriz que rodea a estos carburos, estos pierden la base que les sustenta y son arrancados.

4.3- Fundición blanca 25%Cr

1. La mayor dureza del material se consigue con una temperatura de austenización de 1100°C. Altas temperaturas implican tener una austenita más sobresaturada en elementos de aleación. Tras el enfriamiento se obtendrá una martensita cuya red BCT es muy tetragonal y, por tanto, de alta dureza. Esto a su vez implica mayor cantidad de austenita retenida que a temperaturas de desestabilización más bajas.

2. El mayor grado de desestabilización y, por tanto, empobrecimiento de elementos de aleación de la austenita se encuentra a temperaturas del entorno de 950°C.

3. Esta austenita se consigue eliminar con revenidos de 500°C durante 6h favoreciendo una precipitación de los elementos que la saturan y su posterior transformación en martensita o bainita inferior. La martensita formada tras el temple se reviene provocando mayor cantidad de precipitados finamente dispersos en la matriz.

4. La resistencia al desgaste erosivo se ve incrementada con revenidos altos. De esta manera se completa el revenido total de la martensita y se favorece la transformación de la austenita en bainita inferior. Todo ello contribuye a un aumento significativo de la tenacidad del constituyente matriz.

5. La resistencia al desgaste abrasivo se ve incrementada con revenidos bajos, temperaturas de desestabilización altas y enfriamientos lentos. A altas temperaturas de desestabilización, no se consigue completar la precipitación de carburos secundarios, aunque se ve compensado con un enfriamiento lento, el cual conlleva una segunda desestabilización. A pesar de esto, esa austenita dará lugar a una martensita de gran tetragonalidad y, por tanto, dureza tras el temple. Con revenidos bajos se consigue formar mayor cantidad de carburos de revenido sin mermar mucho la tetragonalidad de la martensita, obteniendo un constituyente matriz de gran dureza.

6. El tratamiento de nitruración supuso un ablandamiento considerable del material, una vez superada dicha capa. Este ablandamiento se reduce cuando las temperaturas de desestabilización son altas (1050°C-1100°C) debido a la martensita tan dura formada tras el temple y también debido a que la nitruración actúa como un revenido adicional "acomodando" una austenita residual muy tensionada para facilitar su posterior transformación en martensita y/o bainita inferior.

7. A pesar de esto, el tratamiento de nitruración permite un aumento considerable de la resistencia al desgaste erosivo, aumentando la tenacidad de la fase matriz al actuar como un revenido adicional.

8. Para incrementar la tenacidad al impacto se precisa de temples con enfriamiento rápido, seguido de largos tiempos de revenido a 550°C. El enfriamiento enérgico en aceite reduce la presencia de austenita retenida. La austenita retenida se encuentra con excesiva densidad de dislocaciones debido a la presencia adyacente de martensita tetragonal, de ahí la necesidad eliminar al máximo esta austenita. A continuación, tiempos de permanencia de 6h a 550°C completan el tratamiento de revenido de la martensita.

9. En la fundición 25%Cr se constata que, aunque a altas temperaturas de desestabilización tengamos mucha cantidad de austenita residual (Ms está muy baja), la martensita que conseguimos transformar es extraordinariamente dura debido a la elevada distorsión de la celda BCT. Por tanto, es deseable acomodar esa austenita tan tensionada sin que llegue a perder completamente la tetragonalidad de la martensita generada tras el temple. De esta manera, se consigue una martensita muy dura y una elevada densidad de carburos tras el proceso térmico completo.

Referencias bibliográficas

1. Norman, T.E.; Abrasive wear of ferrous materials in climax operations. *Materials research and standards* **1968**, *8*, 65.
2. Maja, M.E.; Maruma, M.G.; Mampuru, L.A.; Moema, S.J. Effect of niobium on the solidification structure and properties of hypoeutectic high-chromium white cast irons. **2016**, *116*, 981–986.
3. Tabrett, C.P.; Sare, I.R.; Ghomashchi, M.R. Microstructure-property relationships in high chromium white iron alloys. *Int Mater Rev* **2014**, *41*, 59–82, doi:10.1179/imr.1996.41.2.59.
4. Pearce, J.T.H. Structural characterisation of high chromium cast irons. *International conference on solidification science and processing: outlook for the 21st century, Bangalore, India* **2001**, 241–247.
5. Hadji, A.; Bouhamla, K.; Maouche, H. Improving wear properties of high-chromium cast iron by manganese alloying. *Int J Met* **2016**, *10*, 43–55, doi:10.1007/s40962-015-0003-5.
6. Zhou, S.; Shen, Y.; Zhang, H.; Chen, D. Heat treatment effect on microstructure, hardness and wear resistance of Cr26 white cast iron. *Chinese J Mech Eng* **2015**, doi:10.3901/CJME.2014.0620.116.
7. Tabrett, C.P.; Sare, L.R. The effect of heat treatment on the abrasion resistance of alloy white irons. *Wear* **1997**, *203–204*, 206–219, doi:10.1016/S0043-1648(96)07390-5.
8. Powell, G.L.F. Morphology of eutectic M_3C and M_7C_3 in white iron castings. *Metals Forum* **1980**, *3*, 37-46, ISSN: 0160-7952.
9. Powell, G.L.F.; Lloyd, P.G. A deep etching technique for the examination of the carbide of high chromium cast iron in a scanning electron microscope. *Metallography* **1981**, *14*, 271–274, doi:10.1016/0026-0800(81)90032-X.
10. Powell, G.L.F.; Carlson, R.A.; Randle, V. The morphology and microtexture of M_7C_3 carbides in Fe-Cr-C and Fe-Cr-C-Si alloys of near eutectic composition. *Journal of Materials Science* **1994**, *68*, doi: 10.1007/BF00356539.
11. Laird, G.; Gundlach, R.; Röhrig, K. Abrasion-resistant cast iron handbook. *American Foundry Society Illinois USA* **1990**, 14, *68-81*, ISBN:0-87433-224-19.

12. Laird, G.; Powell, G. Solidification and solid-state transformation mechanisms in Si alloyed high-chromium white cast irons. *Metallurgical and Materials Transactions A* **1993**, *24*, 981–988, doi: 10.1007/BF02656520.

13. Benz, R.; Elliott, J.; Chipman, J. Thermodynamics of the carbides in the system Fe-Cr-C. *Metallurgical and Materials Transactions B* **1974**, *5*, 2235–2240, doi:10.1007/BF02643938.

14. Kagawa, A.; Kawashima, S.; Ohta, Y. Wear Properties of $(Fe, Cr)_7C_3$ Carbide Bulk Alloys. *Mater Trans JIM* **1992**, *33*, 1171–1177, doi:10.2320/matertrans1989.33.1171.

15. Maratray, F.; Usseglio-Nanot, R. Atlas. Transformation characteristics of chromium and chromium-molybdenum white irons. Experimental procedure. *Climax molybdenum CO* **1970**, ASIN:B000UG6M1U.

16. Grobe, A.H.; Roberts, G.A. Effect of carbon content on 18-4-1 high speed steel. *Transactions of the american society for metals* **1953**, *45*, 475–497, ISSN: 0096-7416.

17. Thorpe, W.; Chicco, B. The Fe-rich corner of the metastable C-Cr-Fe liquidus surface. *Metallurgical and Materials Transactions A* **1985**, 16, 1541-1549, doi: 10.1007/BF02663011.

18. Babu, S.; Bhadeshia, H. Diffusion of carbon in substitutionally alloyed austenite. *Journal of Materials Science Letters* **1995**, *14*, 314–316, doi: 10.1007/BF00592135.

19. Radcliffe, S.V.; Cohen, M.; Kaufman, L. Thermodynamics of martensite transformation. *Acta metallurgica* **1962**, *10*, 1110, doi:10.1016/0001-6160(62)90081-0.

20. Shipway, P.H.; Bhadeshia, H. Mechanical stabilisation of bainite. *Materials science and technology* **1995**, 11, 1116–1128, doi: 10.1179/mst.1995.11.11.1116.

21. Stark, P.; Lement, B.S.; Effect of tempering on the hardness of retained austenite. *Transactions of the american institute of mining and metallurgical engineers* **1954**, *200*, 1074–1075.

22. Shimizu, K.; Purba, R.H.; Kusumoto, K.; Yaer, X.; Ito, J.; Kasuga, H.; Gaqi, Y. Microstructural evaluation and high-temperature erosion characteristics of high chromium cast irons. *Wear* **2019**, *426*, 420–427, doi:10.1016/j.wear.2019.01.043.

23. Liu, Z.L.; Chen, X.; Hu, K.H. Microstructure and mechanical properties of high boron white cast iron. *Mater. Sci. Eng. A-Struct. Mater. Prop. Microstruct. Process* **2008**, *486*, 112–116, doi:10.1016/j.msea.2007.10.017.

24. Fairhust, W.; Rohrig, K. Abrasion resistant high chromium cast irons. *Foundry Trade J* **1974**, *136*, 685–698, ISSN：0015-9042.

25. Filipovic, M.M. Iron-chromium-carbon-vanadium white cast irons. *The microstructure and properties. Hem. Ind.* **2014**, *68*, 413–427, doi: 10.2298/hemind130615064f.

26. Pero-Sanz, J.A. Fundiciones Férreas; Dossat: Madrid, Spain, 1994; p. 154.

27. Bedolla-Jacuinde, A.; Arias, L.; Hernández, B. Kinetics of secondary carbides precipitation in a hiqh-chromium white iron. *J Mater Eng Perform* **2003**, *12*, 371–382, doi:10.1361/105994903770342881.

28. Ju, J.; Fu, D.; M Fu, D.; Z. Wei, S.; Sang, P.; Wu, W.; Tang, Z.; Lei, Y.P. Effects of Cr and V additions on the microstructure and properties of high-vanadium wear-resistant alloy steel. *Ironmaking & Steelmaking* **2018**, *45*, 176–186, doi:10.1080/03019233.2016.1250491.

29. Álvarez Antolín, J.F.; Francos Garrote, L.; Asensio Lozano, J. Aplicación del ajuste de Rietveld para correlacionar la evolución microestructural de fundiciones blancas con 18 y 25% en Cromo, templadas en aceite y sucesivos revenidos, con el comportamiento frente al desgaste abrasivo y esfuerzos de flexión. *Rev Metal* **2018**, *54*, 113, doi:10.3989/revmetalm.113.

30. Pero-Sanz Elorz, J.A. *Ciencia e Ingeniería de Materiales*, 5th ed.; Cie-Dossat: Madrid, Spain, 2006; p. 673.

31. Pero-Sanz, J.A. *Fundiciones Férreas*; Dossat: Madrid, Spain, 1994; p. 124.

32. Gonzalez-Pociño, A.; Alvarez-Antolin, F.; Asensio-Lozano, J. Influence of thermal parameters related to destabilization treatments on erosive wear resistance and microstructural variation of white cast iron containing 18% Cr. application of design of experiments and rietveld structural analysis. *Materials (Basel)* **2019**, *12*, doi:10.3390/ma12193252.

33. Wiengmoon, A.; Pearce, J.T.H.; Chairuangsri, T. Relationship between microstructure, hardness and corrosion resistance in 20 wt.%Cr, 27 wt.%Cr and 36 wt.%Cr high chromium cast irons. *Mater Chem Phys* **2011**, *125*, 739–748, doi:10.1016/j.matchemphys.2010.09.064.

34. Heino, V.; Kallio, M.; Valtonen, K.; Kuokkala, V.T. The role of microstructure in high stress abrasion of white cast irons. *Wear* **2017**, *388–389*, 119–125, doi:10.1016/j.wear.2017.04.029.

35. Pero-Sanz Elorz, J.A. *Ciencia e Ingeniería de Materiales*, 5th ed.; Cie-Dossat: Madrid, Spain, 2006; p. 360

36. Gasan, H.; Erturk, F. Effects of a Destabilization Heat Treatment on the Microstructure and Abrasive Wear Behavior of High-Chromium White Cast Iron Investigated Using Different Characterization Techniques. *Metall Mater Trans A* **2013**, doi:10.1007/s11661-013-1851-3.

37. Guitar, M.A.; Suárez, S.; Prat, O.; Duarte Guigou, M.; Gari, V.; Pereira, G.; Mücklich, F. High Chromium Cast Irons: Destabilized-Subcritical Secondary Carbide Precipitation and Its Effect on Hardness and Wear Properties. *J Mater Eng Perform* **2018**, *27*, 3877–3885, doi:10.1007/s11665-018-3347-1.

38. Kootsookos, A.; Gates, J.D. The role of secondary carbide precipitation on the fracture toughness of a reduced carbon white iron. *Mater Sci Eng A* **2008**, *490*, 313–318, doi:10.1016/j.msea.2008.01.036.

39. Carpenter, S.D.; Carpenter, D.; Pearce, J.T.H. XRD and electron microscope study of a heat treated 26.6% chromium white iron microstructure. *Mater. Chem. Phys*. **2007**, 101, 49–55, doi:10.1016/j.matchemphys.2006.02.013.

40. Wang, J.; Sun, Z.; Zuo, R.; Li, C.; Shen, B.; Gao, S.; Huang, S. Effects of secondary carbide precipitation and transformation on abrasion resistance of the 16Cr-1Mo-1Cu white iron. *J Mater Eng Perform* **2006**, *15*, 316–319, doi:10.1361/105994906X108602.

41. Lai, J.P.; Pan, Q.L.; Sun, Y.W.; Xiao, C.A. Effect of Si content on the microstructure and wear resistance of high chromium cast iron. *ISIJ Int* **2018**, *58*, 1532–1537, doi:10.2355/isijinternational.ISIJINT-2018-099.

42. Efremenko, V.; Shimizu, K.; Chabak, Y. Effect of destabilizing heat treatment on solid-state phase transformation in high-chromium cast irons. In Proceedings of the Metallurgical and Materials Transactions A: Physical Metallurgy and Materials Science; 2013; Vol. 44, pp. 5434–5446.

43. Liu, Q.; Shibata, H.; Hedström, P.; Jönsson, P.G.; Nakajima, K. Dynamic precipitation behavior of secondary M7C3 carbides in ti-alloyed high chromium cast iron. *ISIJ Int* **2013**, *53*, 1237–1244, doi:10.2355/isijinternational.53.1237.

44. Karantzalis, A.E.; Lekatou, A.; Diavati, E. Effect of destabilization heat treatments on the microstructure of high-chromium cast iron: A microscopy examination approach. *J Mater Eng Perform* **2009**, *18*, 1078–1085, doi:10.1007/s11665-009-9353-6.

45. Powell, G.L.F.; Bee, J.V. Secondary carbide precipitation in an 18 wt.% Cr-1 wt.% Mo white iron. *J. Mater. Sci*. **1996**, 31, 707–711, doi:10.1007/BF00367889

46. Zhi, X.H.; Xing, J.D.; Gao, Y.M.; Fu, H.G.; Peng, J.Y.; Xiao, B. Effect of heat treatment on microstructure and mechanical properties of a Ti-bearing hypereutectic high chromium white cast iron. *Mater. Sci. Eng. A* **2008**, 487, 171–179, doi:10.1016/j.msea.2007.10.009.

47. Bedolla-Jacuinde, A.; Guerra, F.V.; Mejia, I.; Zuno-Silva, J.; Rainforth, M. Abrasive wear of V-Nb-Ti alloyed high-chromium white irons. *Wear* **2015**, 332, 1006–1011, doi:10.1016/j.wear.2015.01.049.

48. Wang, J.; Xiong, J.; Fan, H.; Yang, H.S.; Liu, H.H.; Shen, B.L. Effects of high temperature and cryogenic treatment on the microstructure and abrasion resistance of a high chromium cast iron. *J Mater Process Technol* **2009**, *209*, 3236–3240, doi:10.1016/j.jmatprotec.2008.07.035.

49. Liu, H.H.; Wang, J.; Yang, H.S.; Shen, B.L. Effects of cryogenic treatment on microstructure and abrasion resistance of CrMnB high-chromium cast iron subjected to sub-critical treatment. *Mater. Sci. Eng. A* **2008**, 478, 324–328, doi:10.1016/j.msea.2007.06.012

50. Jia, X.; Hao, Q.; Zuo, X.; Chen, N.; Rong, Y. High hardness and toughness of white cast iron: The proposal of a novel process. *Mater Sci Eng A* **2014**, *618*, 96–103, doi:10.1016/j.msea.2014.08.075.

51. Yang, H.S.; Jun, W.; Bao-Luo, S.; Hao-Huai, L.; Sheng-Ji, G.; Si-Jiu, H. Effect of cryogenic treatment on the matrix structure and abrasion resistance of white cast iron subjected to destabilization treatment. *Wear* **2006**, *261*, 1150–1154, doi:10.1016/j.wear.2006.03.021.

52. Wang, J.; Xiong, J.; Fan, H.; Yang, H.S.; Liu, H.H.; Shen, B.L. Effects of high temperature and cryogenic treatment on the microstructure and abrasion resistance of a high chromium cast iron. *J Mater Process Technol* **2009**, *209*, 3236–3240, doi:10.1016/j.jmatprotec.2008.07.035.

53. Liu, H. huai; Wang, J.; Shen, B. luo; Yang, H. shan; Gao, S. ji; Huang, S. jiu Effects of deep cryogenic treatment on property of 3Cr13Mo1V1.5 high chromium cast iron. *Mater Des* **2007**, *28*, 1059–1064, doi:10.1016/j.matdes.2005.09.007.

54. Inthidech, S.; Sricharoenchai, P.; Matsubara, Y. Effect of molybdenum content on subcritical heat treatment behaviour of hypoeutectic 16 and 26 wt-% chromium cast irons. *Int J Cast Met Res* **2012**, *25*, 257–263, doi:10.1179/1743133612y.0000000009.

55. Çetinkaya, C. An investigation of the wear behaviours of white cast irons under different compositions. *Mater Des* **2006**, *27*, 437–445, doi:10.1016/j.matdes.2004.11.021.

56. Li, Y.; Li, P.; Wang, K.; Li, H.; Gong, M.; Tong, W. Microstructure and mechanical properties of a Mo alloyed high chromium cast iron after different heat treatments. *Vacuum* **2018**, *156*, 59–67, doi:10.1016/j.vacuum.2018.07.013.

57. Oh, H.; Lee, S.; Jung, J.Y.; Ahn, S. Correlation of microstructure with the wear resistance and fracture toughness of duocast materials composed of high-chromium white cast iron and low-chromium steel. *Metall. Mater. Trans. A* **2001**, 32, 515–524, doi:10.1007/s11661-001-0068-z.

58. Scandian, C.; Boher, C.; de Mello, J.D.B.; Rézaï-Aria, F. Effect of molybdenum and chromium contents in sliding wear of high-chromium white cast iron: The relationship between microstructure and wear. *Wear* **2009**, doi:10.1016/j.wear.2008.12.095.

59. Bedolla-Jacuinde, A.; Guerra, F. V.; Mejía, I.; Zuno-Silva, J.; Maldonado, C. Boron effect on the precipitation of secondary carbides during destabilization of a high-chromium white iron. *Int J Cast Met Res* **2016**, doi:10.1080/13640461.2016.1142236.

60. Sun, Z.; Zuo, R.; Li, C.; Shen, B.; Yan, J.; Huang, S. TEM study on precipitation and transformation of secondary carbides in 16Cr–1Mo–1Cu white iron subjected to subcritical treatment. *Mater. Charact.* **2004**, 53, 403–409, doi: 10.1016/j.matchar.2004.09.007.

61. Li, Y.; Li, P.; Wang, K.; Li, H.; Gong, M.; Tong, W. Microstructure and mechanical properties of a Mo alloyed high chromium cast iron after different heat treatments. *Vacuum* **2018**, *156*, 59–67, doi:10.1016/j.vacuum.2018.07.013.

62. Guitar, M.A.; Nayak, U.P.; Britz, D.; Mücklich, F. The Effect of Thermal Processing and Chemical Composition on Secondary Carbide Precipitation and Hardness in High-Chromium Cast Irons. *Int J Met* **2020**, *14*, 755–765, doi:10.1007/s40962-020-00407-4.

63. Khanitnantharak, W.; Hashimoto, M.; Shimizu, K.; Yamamoto, K.; Sasaguri, N.; Matsubara, Y.; American Foundry, S. Effects of Carbon and Heat Treatment on the Hardness and Austenite Content of a Multi-Component White Cast Iron. *Trans. Am. Foundry Soc.* **2009**, 117, 435.

64. Matsubara, Y.; Sasaguri, N.; Shimizu, K.; Kon Yu, S. Solidification and abrasion wear of white cast irons alloyed with 20% carbide forming elements. *Wear* **2001**, *250–251*, 502–510, doi:10.1016/S0043-1648(01)00599-3.

65. Hashimoto, M.; Kubo, O.; Matsubara, Y. Analysis of carbides in multi-component white cast iron for hot rolling mill rolls. *ISIJ Int*. **2004**, 44, 372–380, doi:10.2355/isijinternational.44.372.

66. Opapaiboon, J.; Na Ayudhaya, M.S.; Sricharoenchai, P.; Inthidech, S.; Matsubara, Y. Effect of chromium content on heat treatment behavior of multi-alloyed white cast iron for abrasive wear resistance. *Mater Trans* **2019**, *60*, 346–354, doi:10.2320/matertrans.M2018318.

67. Meebupha, T.; Inthidec, S.; Sricharoenchai, P.; Matsubara, Y. Effect of molybdenum content on heat treatment behavior of multi-alloyed white cast iron. *Mater Trans* **2017**, *58*, 655–662, doi:10.2320/matertrans.M2016396.

68. Yamamoto, K.; Inthidech, S.; Sasaguri, N.; Matsubara, Y. Influence of Mo and W on High Temperature Hardness of M_7C_3 Carbide in High Chromium White Cast Iron. *Mater Trans* **2014**, *55*, 684–689, doi:10.2320/matertrans.f-m2014801.

69. Karantzalis, E.; Lekatou, A.; Mavros, H. Microstructure and properties of high chromium cast irons: Effect of heat treatments and alloying additions. *Int. J. Cast Met. Res*. **2009**, 22, 448–456, doi:10.1179/174313309 ×436637. 23.

70. Nurjaman, F.; Sumardi, S.; Shofi, A.; Aryati, M.; Suharno, B. Effect of molybdenum, vanadium, boron on mechanical properties of high chromium white cast iron in as-cast condition. I*n Proceedings of the AIP Conference Proceedings*; **2016**, 1711, doi:10.1063/1.4941614.

71. Opapaiboon, J.; Sricharoenchai, P.; Inthidech, S.; Matsubara, Y. Effect of carbon content on heat treatment behavior of multi-alloyed white cast iron for abrasive wear resistance. *Mater Trans* **2015**, *56*, 720–725, doi:10.2320/matertrans.M2015001.

72. Liu, Z.; Li, Y.; Chen, X. Effect of tempering temperature on microstructure and mechanical properties of high boron white cast iron. *China Foundry* **2012**, *9*, 313–317, ISSN: 1672-6421.

73. Sare, I.R.; Arnold, B.K. The influence of heat-treatment on the high-stress abrasion resistance and fracturetoughness of alloy white cast irons. Metall. Mater. Trans. A-Phys. Metall. Mater. Sci. 1995, 26, 1785–1793, doi:10.1007/bf02670766.

74. Chen, X.; Li, Y. Effect of heat treatment on microstructure and mechanical properties of high boron white cast iron. *Mater Sci Eng A* **2010**, *528*, 770–775, doi:10.1016/j.msea.2010.09.092.

75. Li, D.; Liu, L.; Zhang, Y.; Ye, C.; Ren, X.; Yang, Y.; Yang, Q. Phase diagram calculation of high chromium cast irons and influence of its chemical composition. *Mater Des* **2009**, *30*, 340–345, doi:10.1016/j.matdes.2008.04.061.

76. Wang, J.; Li, C.; Liu, H.; Yang, H.; Shen, B.; Gao, S.; Huang, S. The precipitation and transformation of secondary carbides in a high chromium cast iron. *Mater Charact* **2006**, *56*, 73–78, doi:10.1016/j.matchar.2005.10.002.

77. Fernández-Pariente, I.; Belzunce-Varela, F.J. Influence of different heat treatments on the microstructure of a high chromium white cast iron. *Rev Metal* **2008**, *42*, 279-286, doi:10.3989/revmetalm.2006.v42.i4.27.

78. Gonzalez-Pociño, A.; Alvarez-Antolin, F.; Asensio-Lozano, J. Optimization of thermal processes applied to hypoeutectic white cast iron containing 25% Cr aimed at increasing erosive wear resistance. *Metals (Basel)* **2020**, *10*, doi:10.3390/met10030359.

79. Pero-Sanz, J.A. *Aceros*; Dossat: Madrid, Spain, **2004**; p. 558.

80. Selte, A.; Ozkal, B.; Arslan, K.; Ulker, S.; Hatman, A. Effect of Nitriding on the Wear Resistance of Tool Powder Steels with Different Contents of V, Cr and Mo. Met. Sci. Heat Treat. 2018, 59, 729–734.

81. Binder, C.; Bendo, T.; Hammes, G.; Klein, A.N.; de Mello, J.D.B. Effect of nature of nitride phases on sliding wear of plasma nitrided sintered iron. *Wear* **2015**, *332–333*, 995–1005, doi:10.1016/j.wear.2015.01.083.

82. Steiner, T.; Meka, S.R.; Bischoff, E.; Waldenmaier, T.; Mittemeijer, E.J. Nitriding of ternary Fe-Cr-Mo alloys; role of the Cr/Mo-ratio. *Surf Coatings Technol* **2016**, *291*, 21–33, doi:10.1016/j.surfcoat.2016.02.011.

83. Prat-Bartés, A.; Tort-Martorell, X.; Grima-Cintas, P.; Pozueta-Fernández, L.; Solé-Vidal, I. *Métodos Estadísticos, 2nd ed.*; UPC: Barcelona, Spain, **2004**, p. 376.

84. Efremenko, V.G.; Wu, K.M.; Chabak, Y.G.; Shimizu, K.; Isayev, O.B.; Kudin, V.V. Alternative Heat Treatments for Complex-Alloyed High-Cr Cast Iron Before Machining. *Metall. Mater. Trans. A-Phys. Metall. Mater. Sci* **2018**, 49A, 3430–3440, doi:10.1007/s11661-018-4722-0.

85. Stephens, P.W. Phenomenological model of anisotropic peak broadening in powder diffraction. *J. Appl. Crystallogr*. **1999**, 32, 281–289, doi:10.1107/s0021889898006001.

86. Pero-Sanz, J.A. Fundiciones Férreas; Dossat: Madrid, Spain, 1994; p. 154.